# Errata

## Summary

| | |
|---|---|
| Page iii, para 2, line 2 | sentence now begins 'A need' |
| Page iii, para 2, line 3 | change 'have' to 'has' |

## Chapter 1

| | |
|---|---|
| Page 18, para 3, line 3 | typo corrected to 'bis(diphenylphosphino)' |
| Page 20, fig. 1.10 caption | caption changed to 'Compounds with longer chain length than those in Figure 1.9.' |
| Page 22, para 4, line 1 | insert 'a' between 'as' and 'variable' |
| Page 24, para 1, line 4 | insert 'solvent or' before 'solution' |
| Page 30, para 2, line 1 | change 'electric' to 'electronic' |

## Chapter 2

| | |
|---|---|
| Page 43, para 4, line 3 | change 'optic' to 'optical' |
| Page 43, para 4, line 5 | change 'measurement' to 'measurements' |
| Page 48, para 1, line 2 | change 'lower' to 'higher' |
| Page 54, para 3, line 6 | change 'is' to 'are' |
| Page 55, para 1, line 3 | delete 'may' |
| Page 65, para 2, line 2 | second and third sentences changed to 'Halochromic switching allows for the conversion of the acetylide moiety to a vinylidene (28 to 30 and 29 to 31) and back. Reversible electrochromic switching is only possible on the acetylide compounds (28 and 29, oxidizing them to 32 and 33, respectively) because the oxidized versions of the vinylidene compounds are not stable in the beam of the laser.' |
| Page 65, footnote xiii | change '(27-32)' to '(28-33)' |
| Page 66, para 2, line 2 | change '(27 and 28)' to '(28 and 29)' |
| Page 67, para 2, line 11 | change ‹122-124› to ‹123-125› |
| Page 67, para 3, line 4 | final sentence of paragraph changed to 'The electroltyte $(NBu^n_4)PF_6$ was prepared by Dr. Marie Cifuentes.' |
| Page 68, para 2, line 7 | change ‹125› to ‹126› |
| Page 69, para 1, line 1 | typo corrected to 'dithienylperfluorocyclopentene' |

## Chapter 3

| | |
|---|---|
| Page 73, para 2, line 3 | change ‹126, 127› to ‹127, 128› |
| Page 74, para 2, line 6 | change ‹128› to ‹121› |
| Page 74, para 3, line 3 | change ‹129, 130› to ‹130, 131› |
| Page 75, fig. 3.2 caption | change ‹131› to ‹132› |

# Nonlinear Optical Structure – Property Relationships in Organometallic Compounds

Timothy Christopher Corkery

A thesis submitted for the degree of Doctor of Philosophy

The Australian National University


THE AUSTRALIAN NATIONAL UNIVERSITY

July, 2010

# Declaration

The work described in this thesis is my own unless stated otherwise. I have not submitted this material for any other degree or qualification. Where contributions have been made by others, their efforts have been acknowledged and referenced.

T. Christopher Corkery

July 2010

# Acknowledgements

To begin with, I would like to thank the chair of my supervisory committee, Prof. Mark Humphrey. Without his decision to give me the opportunity to study with him, none of this work would have been possible for me. Throughout the duration of my PhD, he has remained accessible, helpful and supportive. Thank-you Mark.

Many thanks also to the other members of my supervisory committee: Prof. Marek Samoc, Prof. Rob Stranger and Dr. Marie Cifuentes. Your support, patience and guidance definitely helped me through the more difficult parts. I would also like to thank Ann Bell, Geoff Deeble, Prof. Mick Collins and Steph Neulinger for helping me understand and deal with the inevitable bureaucracy that accompanies university degrees.

For everything to do with lasers and NLO measurement I must again thank Marek Samoc, whose patient tutelage, seemingly inexhaustible supply of knowledge and incredible enthusiasm sparked excitement in me and the desire to do better. I would also like to thank Dr. Anna Samoc, Dr. Andrei Rode and Maryla Krolikowska for always being helpful smiling faces and assisting me with anything I needed in the Laser Physics Centre.

In terms of measurements and technical support, there are many many people who have contributed to this work. Thanks go to Dr. Inge Asselberghs and Stijn van Cleuvenbergen, in the laboratory of Prof. Koen Clays, for their measurements of quadratic NLO properties. For cyclic voltammetry and spectro-electrochemistry I am indebted to Marie Cifuentes, Nico Gauthier and Guillaume Grelaud. John Allen, Gordon Lockhart and Anitha Jeyasingham were always prompt and willing to go the extra distance when it came to mass spectrometry. Vicky Withers and Sasha Melnitchenko are so kind that they somehow lessen the pain of microanalyses. Lastly, Peta Simmonds and Chris Blake, of the NMR Centre, always (always) made time for me and helped me get the spectra I needed.

There are many members of the Humphrey Group, past and present who taught me how to do things, listened to me complain about failed reactions and helped to make the daily experience of lab work more enjoyable. I would like to thank Dr. Joe Morrall taking me under his wings and teaching me what I needed to know about the Humphrey

laboratories. Over the years, many have come and gone, but they were wonderful people. Dr. Gull Dalton, Dr. Rachel Roberts, Dr. Luca Rigamonti, Mike Randles, Katy Green, Tim Fondum, Al Watson, Dr. Nico Gauthier, Junior Jennaway, Torsten Schwich, Dr. Sanjay Chavan, Pat West, Bandar Babgi, Junior Jennaway, Samuel Drouet, Adam Barlow, Floriane Malvolti, Guillaume Grelaud and Vivek Gupta have all been enjoyable workmates in the time I've been here.

I also appreciate the opportunities given to me by Dr. Mark Ellison and all of the teaching staff in the Department of Chemistry at the ANU. I really enjoy teaching and providing me with the chance to help students learn had beneficial effects on both my chemistry and my sanity.

The thesis you are holding was written in May, June and July of 2010. In that time, I had advice, assistance, editing, proofreading, image beautification, font management and software assistance. Heartfelt thanks go to Prof. Marek Samoc, Prof. Mark Humphrey, Dr. Marie Cifuentes, Dr. Michelle Weir, Dr. Rowan Martin-Hughes, Dr. Tanya Bradford, Mike Randles, Torsten Schwich, Adam Barlow and Romain Veillard. Everything correct is through their help, the errors are all mine.

On a more personal note, I would like to thank the different people who have lived with me over the years. Everywhere I lived in my time here felt like a home, and I didn't dream to hope for people as good as you. Good memories all around: Rachel Roberts, Luca Rigamonti, Marit Kragt, Catie Flick, Cat Gray, Anna Lehmann, Kathryn Sedgwick, Jason Roberts, Bjorn Bohman and Rowan Martin-Hughes.

I would like to thank the many people who have made living in Canberra the incredibly enjoyable experience that it was. I am filled with good memories. Australia is a wonderful country and I am indebted to everyone who took me out of Canberra to see as much of it as I have. Thank-you also to the all of the people who have been happy to come round to play games, have drinks and share good food. Special thanks go to Michelle, for reminding me what a wonderful place the world can be.

Lastly, and most, I thank my parents and sisters. I've been far away this whole time, but I will see you soon.

# Summary

Nonlinear optical (NLO) effects refer to interactions between matter and electromagnetic radiation that are dependent upon the intensity of the radiation. The interaction of a high intensity light beam with matter may lead to generation of electric field components of different phase, frequency, orientation, etc. This allows for valuable applications in optical devices, including generation of new frequencies of coherent light, optical switching, data storage and computing.

Most devices using NLO processes on the market today use glasses or crystals of inorganic salts to provide the necessary NLO responses. Need to meet the growing technological requirements of devices and processes have caused the field to branch into organic and organometallic materials. The combination of metals and organics has the potential to combine the advantages of organic molecules (design flexibility, fast response) and inorganic salts (ease of fabrication, durability), making organometallic materials increasingly popular in the field of nonlinear optics.

In order to design new compounds with optimal characteristics for applications, it is imperative to understand the structural properties of molecules that lead to enhanced NLO processes. For many years, the NLO responses of different materials were measured at only a handful of different wavelengths (energies of light). By examining NLO processes across a broad spectrum of wavelengths, considerably more information about their optical behaviour can be obtained. Using a measurement technique known as Z-scan, the second chapter of this thesis looks at the nonlinear optical responses of a variety of compounds made by several different researchers. Comparison of these results allows for an expansion of the known NLO structure-property relationships of organometallic materials.

The remaining chapters cover the design, synthesis and measurement of two different series of compounds, with the intention of furthering this knowledge. The third chapter looks at the incorporation of electron withdrawing and donating groups at the termini of molecules known to have good NLO properties. Their role is to alter the polarity of the molecules, which, in turn, should alter their NLO responses. The final chapter contains compounds with varying levels of substitution about a central core. A higher level of substitution has a beneficial effect for organic molecules and the compounds were designed to see if these benefits translate to organometallic molecules.

# Table of Contents

# Abbreviations

| | |
|---|---|
| bpy | bipyridyl |
| $Bu^n$ | normal butyl |
| $Bu^t$ | tertiary butyl |
| c.c. | complex conjugate |
| Cp | cyclopentadienyl |
| CT | charge-transfer |
| CV | cyclic voltammetry |
| Cy | cyclohexyl |
| d | doublet |
| dc | direct current |
| DFWM | degenerate four-wave mixing |
| DMF | N,N-dimethylformamide |
| dmso | dimethyl sulfoxide |
| dppe | 1,2-bis(diphenylphosphino)ethane |
| dppf | 1,1'-bis(diphenylphosphino)ferrocene |
| dppm | bis(diphenylphosphino)methane |
| DTE | 5,5'-dithienylperflurocyclopentene |
| EFISH | electric field-induced second harmonic generation |
| EI | electron impact |
| ESI | electrospray ionization |
| Et | ethyl |
| etet | 2-ethylthioethanethiolate |
| Fc | ferrocenyl |
| fund | fundamental |
| HR MS | high resolution mass spectrometry |
| HRS | hyper-Rayleigh scattering |
| IR | infrared |
| LMCT | ligand to metal charge transfer |
| m | multiplet |
| $[M]^+$ | molecular ion |
| Me | methyl |

| | |
|---|---|
| MLCT | metal to ligand charge transfer |
| MS | mass spectrometry |
| NIR | near infrared |
| NLA | nonlinear absorption |
| NLO | nonlinear optical |
| NLR | nonlinear refraction |
| NMR | nuclear magnetic resonance |
| OPL | optical power limiting |
| OTTLE | optically transparent thin layer electrochemical |
| Ph | phenyl |
| phen | 1,10-phenanthroline |
| $Pr^i$ | isopropyl |
| q | quartet |
| s | singlet |
| SHG | second harmonic generation |
| t | triplet |
| tBAF | tetra-*n*-butylammonium fluoride |
| THF | tetrahydrofuran |
| THG | third harmonic generation |
| TIPS | triisopropylsilyl |
| TPA | two-photon absorption |
| tpy | tripyridyl |
| TMS | trimethylsilyl |
| UV | ultraviolet |
| vis | visible |

# Introduction

## 1.1 Nonlinear Optics

Nonlinear optical (NLO) effects refer to interactions between matter and electromagnetic radiation that are dependent upon the intensity of the radiation. They are typically only observed at high light intensities, such as those available from pulsed lasers. When an intense beam of light interacts with a material, there are potential effects other than the 'normal' refraction, reflection, absorption and emission associated with linear effects. The interaction of a high intensity light beam with matter may lead to generation of electric field components of different phase, frequency, orientation, etc. This allows for valuable applications in optical devices, including (but not limited to) generation of new frequencies of coherent light, optical switching, data storage and computing.

At the end of 1959, Richard Feynman gave a landmark talk at the annual meeting of the American Physical Society, entitled 'There's Plenty of Room at the Bottom'.[1] Feynman was outlining to the audience ideas which have developed into the field of nanotechnology. One of the examples he used was that of storing data at a molecular or atomic level. Nonlinear optical processes (especially two-photon absorption) play an important role in nanofabrication, 3-D imaging and data storage.

With the plethora of applications that nonlinear optics can provide, the search for better NLO materials is a rapidly expanding field.[2] Better materials are those which provide faster responses, have more intense interactions, exhibit effects over a wider electromagnetic frequency (or wavelength) range and demonstrate these effects at lower light intensities (requiring less energy to use). Application considerations also include: ease of fabrication, thermal and photochemical stability, good optical transparency and a general robustness that will keep devices from degrading.

Currently, the materials that are most frequently used in NLO devices are crystals of inorganic salts.[2-4] Lithium and barium borates, potassium phosphates and lithium niobate are examples of crystals that are used in NLO devices utilizing second-order interactions. Second-order NLO effects (Section 1.2) are those which relate to the square of the intensity of incident light. They include properties such as electro-optic modulation and frequency mixing. Crystals of barium borate may be used to split photons from a laser beam (of a particular wavelength) into new photons, giving rise to coherent light beams. This property, called parametric generation (or parametric

amplification, depending upon the design of the device) is used extensively in the work presented in this thesis to generate the different wavelengths of laser light used to examine wavelength-dependent effects.

The materials currently used for so-called third-order NLO effects (Section 1.3) are often glasses, organic dyes or nanoparticles of semiconductors. The refractive index of some glasses is intensity dependent, creating refractive nonlinear effects, useable for optical switching. Organic dyes and semiconductors exhibit two-photon absorption, with applications in 3-D fabrication, data storage and biomedical imaging.

Each of these classes of NLO materials has its strengths and weaknesses. Inorganic salts have lower values of the parameters describing the NLO responses and often slower response times (e.g. in electrooptic modulation applications) than organic materials, but are more robust and easier to fabricate. Organic materials allow for much greater synthetic variety, but tend to have a narrower operational window (in terms of wavelength ranges) due to their absorptive properties.

This introduction is not intended to be a full review of nonlinear optics or the materials which give rise to NLO effects. It deals largely with the cubic NLO properties of organometallic compounds in solutions. There are many books and reviews available concerning nonlinear optical processes and their origins.[2-33]

### 1.1.1 Organometallic Complexes for Nonlinear Optics

The combination of metals and organics has been sought as an avenue for finding ideal NLO active compounds for more than twenty years.[2] Table 1.1 outlines some of the advantages and disadvantages of strictly inorganic and organic materials.

**Table 1.1** A comparison of the advantages and disadvantages of organic and inorganic materials for NLO application.

| | Pros | Cons |
|---|---|---|
| **Organic Materials** | Design flexibility<br>Fast response time<br>Ease of synthesis | Reduced optical transparency<br>Poor stability |
| **Inorganic Materials** | High damage threshold<br>Thermal stability<br>Wide optical transparency range<br>Low optical losses<br>Ease of device fabrication | Slow response time<br>Lower intensity responses |

There are two main advantages of organic materials. The first is that the NLO responses are mainly electronic in nature. This allows for considerably faster effects than seen from inorganic materials, which often include contributions depending upon lattice distortion and have slower (nanosecond) response times. In order for NLO photonic devices to be competitive with electronic devices, the faster responses of organic materials are necessary.

The second advantage is that NLO effects in organic materials are often quite large. This is due (in part) to the design flexibility available to organic compounds. By slightly varying the structure of the molecule, it is possible to 'tweak' the resulting properties and maximize desired effects. This is more difficult to achieve with inorganic materials.

Conversely, the disadvantages of organic materials are often prohibitive. Organic materials have a much narrower optical transparency range and tend to be considerably less stable then their inorganic counterparts, making them unattractive for device fabrication.

Organometallic materials have even greater design flexibility than organics.[34] The potential exists to vary the metal or metals, ligands, coordination geometry and oxidation state. Metals may also be used to stabilize organic fragments with good NLO effects but poor stability. In addition, metal-to-ligand charge transfer (MLCT) bands and the strong electron-donating or withdrawing character of metals are available to exploit. This is important because stronger optical responses often arise from

compounds with large differences between excited state and ground state dipole moments. Following this, compounds with large dipole moments often have stronger nonlinear responses.[35]

The ability of metals to have a range of stable redox states is of great interest. By changing the oxidation state of a metal atom in an organometallic compound, the electronic nature of the compound is changed (often drastically). Because the difference between ground and excited stated dipole moments is so vital to optical character, altering this electronically allows for materials with electrically switchable NLO properties to be created.

Ideally, by combining organic and inorganic materials, the strengths of each may be emphasized with the disadvantages of each being minimized. In practice, new strengths are uncovered and different weaknesses revealed.[2, 4, 15, 17, 19, 29, 31, 36] It is the desire to exploit these new strengths that have caused organometallic materials to become increasingly popular in the field of nonlinear optics.

### 1.1.2 Derivations

The first published observation of a nonlinear optical response was by Franken in 1961, shortly following the invention of the laser.[37] Some of the first theoretical work in the field was as early as 1931, when Maria Goeppert-Mayer presented the theory for two-photon absorption in atoms as part of her doctoral thesis.[38] Honouring her for this, the unit for the two-photon absorption cross section is the Goeppert-Mayer (GM).

Nonlinear optical effects arise from what is called the 'hyperpolarizability' of a compound.[39] This refers to the higher order terms ($\beta$ and $\gamma$) of the expansion of the dipole moment of a molecule in terms of an external electric field (Equation 1.1). $\beta$ is often referred to as second-order (quadratic) nonlinearity or the first hyperpolarizability, while $\gamma$ is the third-order (cubic) nonlinearity or second hyperpolarizability.

Eq. 1.1 $$\boldsymbol{\mu} = \boldsymbol{\mu_0} + \alpha\mathbf{E}_{loc} + \beta\mathbf{E}_{loc}\mathbf{E}_{loc} + \gamma\mathbf{E}_{loc}\mathbf{E}_{loc}\mathbf{E}_{loc} + \ldots$$

$\boldsymbol{\mu_0}$ is the dipole moment at zero field and $\boldsymbol{\mu}$ is the dipole moment in the presence of an electric field with an amplitude of $|\mathbf{E}_{loc}|$. The subscript *loc* is used to denote the local electric field (inside a material) which may be substantially different from the field in a

vacuum. When the localized electromagnetic field is low in amplitude ($|\mathbf{E}_{loc}|$ is small) relative to the internal electric fields of the molecule, only linear optical processes are observed (due to polarizability α). It is with higher amplitude light fields (lasers) that the successively smaller terms which relate to hyperpolarizability effects can be observed.

μ and $\mathbf{E}_{loc}$ are vectors, dependent upon the orientation of the molecule and the incident field. This gives rise to a large number of hyperpolarizability tensor components, many of which interfere with each other because of symmetry reasons.[28] In fact, for centrosymmetric compounds, the value of all components of β is zero.

Equation 1.1 is for microscopic interactions. For examining nonlinear effects in bulk materials, the equation is:

Eq. 1.2 $$\mathbf{P} = \chi^{(1)}\mathbf{E} + \chi^{(2)}\mathbf{EE} + \chi^{(3)}\mathbf{EEE} + \ldots$$

**P** is the polarization of the material, dependent upon the incident field (**E**). This equation defines the macroscopic susceptibilities (χ) of various orders. These are also tensors with many components, but symmetry conditions again allow for simplification, as in the molecular example. The high symmetry of an isotropic material may be reduced by 'poling' the material, a process where an external field is applied, aligning individual molecules within the material. This removes the symmetry and allows for appearance of second-order effects. One issue with poled materials is that they may relax into a more random orientation, reducing their durability in devices.[28]

By modifying Equation 1.1, time dependent effects can be incorporated. An applied electric field is usually not static: the electromagnetic field associated with a light beam oscillates at frequency ω. Equation 1.3 includes a time variable (**E**(t)) and contains a term oscillating at the frequency of light as well as an envelope function ($\mathbf{E}_0$), which may be time dependent.

Eq. 1.3 $$\mathbf{E}(t) = \mathbf{E}_0 \cos(\omega t) = \frac{\mathbf{E}_0}{2}[\exp(i\omega t) + \exp(-i\omega t)]$$

Incorporating Equation 1.3 into Equation 1.1, results in:

Eq. 1.4
$$\begin{aligned}\mu(t) &= \mu_0 + \alpha\mathbf{E}_0\cos(\omega t) + \beta\mathbf{E}_0^2\cos^2(\omega t) + \gamma\mathbf{E}_0^3\cos^3(\omega t) + \ldots \\ &= \mu_0 + \tfrac{1}{2}\alpha\mathbf{E}_0\exp(i\omega t) + \tfrac{1}{2}\beta\mathbf{E}_0^2 + \tfrac{1}{4}\beta\mathbf{E}_0^2\exp(2i\omega t) + \tfrac{3}{8}\gamma\mathbf{E}_0^3\exp(i\omega t) \\ &\quad + \tfrac{1}{8}\gamma\mathbf{E}_0^3\exp(3i\omega t) + \text{c.c.} + \ldots\end{aligned}$$

Where the c.c. term represents coupled conjugate terms in the complex presentation of the field components. This shows how higher order (nonlinear) terms give rise to new frequencies. For example, the β term has the exponent ($2i\omega t$) which is the portion of the equation describing frequency doubling. Frequency doubling is a phenomenon where incident light is halved in wavelength (doubling the frequency). This causes higher energy photons to be created as the beam passes through a material (but less of them – the law of conservation of energy is upheld, giving rise to so-called Manley-Rowe relations).

Even more complication arises when the fact that more than one specific wavelength of light may be incident upon a material at a time is taken into consideration. This leads to wave mixing events, a special case of them being the 'Pockels Effect', where a static field can modify an oscillating field by applying a phase shift. This second-order effect allows information from an electrical signal to be imparted onto a laser beam.

Another matter to be examined is the resonances within the molecules. When an electric field frequency is close to that of a molecular resonance, a damping and/or phase lag effect on the field appears. To account for this, it is convenient to treat frequency dependent polarizabilities as being complex (composed of real and imaginary parts). One can therefore examine the Fourier components of the induced dipoles:

Eq. 1.5 $$\Delta\mu^{(1)}(\omega) = \alpha(\omega)E(\omega)$$

Eq. 1.6 $$\Delta\mu^{(2)}(\omega_3) = \beta(-\omega_3;\omega_1,\omega_2)E(\omega_1)E(\omega_2)$$

Eq. 1.7 $$\Delta\mu^{(3)}(\omega_4) = \gamma(-\omega_4;\omega_1,\omega_2,\omega_3)E(\omega_1)E(\omega_2)E(\omega_3)$$

When the frequency (ω) of incident light (or sometimes generated frequencies, such as 2ω) is close to that of the resonances within the molecules, the NLO effects are often strongest. This is important, because it means that NLO effects are very 'wavelength dependent', as will be demonstrated later in this work. Examining the NLO effects due to the third-order term (Equation 1.7), it is important to include the complex nature of γ. It can be broken into two distinct parts, $\gamma_{real}$ and $\gamma_{imaginary}$ ($\gamma_{imag}$). $\gamma_{real}$ leads to the refractive nonlinearity of a material (how the refractive index of the material changes depending upon intensity of incident radiation) and $\gamma_{imag}$ describes the absorptive

component of the third-order NLO processes. This can be related to what is often called the 'two-photon absorption cross-section', $\sigma_2$.

Two-photon absorption is a process analogous to single photon absorption, but different selection rules apply.[35] One-photon absorption in a centrosymmetric molecule is allowed only between states of different parity (g-u or u-g) while two-photon absorption is allowed only between states of the same parity (g-g or u-u).

One more consideration to examine in this section is that of units. Two different systems are commonly employed: the Gaussian (cgs) and SI (MKS).[4, 29] Conversion between the two systems is outlined in Table 1.2.

**Table 1.2** Conversion between the cgs and SI measurement systems

| **Property** | **SI** | **cgs** | **Conversion factor** |
|---|---|---|---|
| $\mu$ | C m | statC cm = statV $cm^2$ | $\mu_{SI} = 1/3 \times 10^{-11} \mu_{cgs}$ |
| **E** | V $m^{-1}$ | statV $cm^{-1}$ = (erg $cm^2$)$^{1/2}$ | $\mathbf{E}_{SI} = 3 \times 10^4 \mathbf{E}_{cgs}$ |
| $\alpha$ | C $m^2$ $V^{-1}$ | $cm^3$ | $\alpha_{SI} = (1/3)^2 \times 10^{-15} \alpha_{cgs}$ |
| $\chi^{(1)}$ | unitless | unitless | $\chi^{(1)}_{SI} = 4\pi \chi^{(1)}_{cgs}$ |
| $\beta$ | C $m^3$ $V^{-2}$ | $cm^2$ $statV^{-1}$ = esu | $\beta_{SI} = (1/3)^3 \times 10^{-19} \beta_{cgs}$ |
| $\chi^{(2)}$ | m $V^{-1}$ | cm $statV^{-1}$ = ($cm^3$ $erg^{-1}$)$^{1/2}$ = esu | $\chi^{(2)}_{SI} = (4\pi/3) \times 10^{-4} \chi^{(2)}_{cgs}$ |
| $\gamma$ | C $m^4$ $V^{-3}$ | $cm^5$ $statV^{-2}$ = esu | $\gamma_{SI} = (1/3)^4 \times 10^{-23} \gamma_{cgs}$ |
| $\chi^{(3)}$ | $m^2$ $V^{-2}$ | $cm^2$ $statV^{-2}$ = $cm^3$ $erg^{-1}$ = esu | $\chi^{(3)}_{SI} = (4\pi/3^2) \times 10^{-8} \chi^{(3)}_{cgs}$ |

There is sometimes difficulty in comparison of hyperpolarizabilities and susceptibilities between different authors because there is disagreement as to whether the complex field amplitude in Equation 1.3 should include the denominator of 2. There is also disagreement about including the multiplying factor for the degeneracies in Equation 1.4 when reporting hyperpolarizabilities. In all of the work in this thesis, these values *are* included. The unit system used throughout this thesis is the cgs system.

## 1.2 Second-Order Nonlinear Optics

Quadratic NLO processes are most commonly used in laser technology – they were also the first to be observed and are considerably stronger than other NLO effects.[37] One such process is sum frequency generation (SFG). SFG generates new photons that have energy equal to the sum of two incident photons. A special case of this is second harmonic generation (SHG), also called frequency doubling (described after Eq. 4), where two photons of identical energy are 'combined' into one. There are higher order frequency generation effects as well, where the energy of more than two photons is simultaneously combined. Third harmonic generation (THG) is a cubic NLO process combining three photons into one. However, in commercial third harmonic generators (e.g. those used in neodymium lasers to obtain ultraviolet radiation) instead of a THG process two consecutive frequency summation processes are used (SHG followed by SFG).

Another class of second-order NLO effects is difference frequency generation (DFG). This category of processes includes optical parametric effects, where a beam of photons at energy A are split into two distinct beams, of energies B and C, such that the energy of A is the sum of the energies of B and C. These two new beams are termed the signal (higher energy) and idler (lower energy). An example of this is called optical parametric generation (OPG) which was used in much of this work to generate the large variety of wavelengths of laser beam used to probe the compounds for third-order properties.

Other types of quadratic NLO processes include optical rectification, which can be used to generate terahertz radiation, the Pockels (electrooptic) effect, and more. The multiplicity of applications of NLO effects plays a large part in why there is so much interest in nonlinear optics.

### 1.2.1 Measurement Methods

There are a variety of techniques used to measure quadratic nonlinear optical processes. Two of them are outlined here: electric field induced second harmonic generation (EFISH) and hyper-Rayleigh scattering (HRS).

### 1.2.1.1 Electric Field Induced Second Harmonic Generation

EFISH is a technique which uses a short electrical pulse to align the molecules of an isotropic solution (generating a short-lived polar solution, analogous to the poling of polymers). This 'polar' solution is then probed with a laser pulse to examine $\chi^{(2)}$ by observing the second harmonic generated by the solution. The current is pulsed (just prior to the laser pulses, to allow the dipoles in solution to orient) to prevent a continuous direct current (dc) voltage from causing electrolysis of the compound.

Because all materials possess some degree of cubic nonlinearity which interferes with the determination of quadratic effects, the method has some complications. Fortunately, for compounds which have non-zero molecular dipoles (and therefore non-zero $\beta$ values), the experimentally observed signals are usually dominated by second-order effects.

One difficulty with EFISH measurements is that there is a complicated relation between the phase of the second harmonic wave that is generated by the solution and that of the fundamental wave. The newly generated wave (at frequency $2\omega$) will travel at a different speed through the solution than the fundamental wave. At certain distances, the locally generated second harmonic has a phase opposite to that of the travelling second harmonic and there is back energy transfer from the second harmonic to the fundamental, causing the amplitude of the second harmonic to oscillate with distance. The problem is solved by using a wedge-shaped cell to hold the sample solution (common solvents are chloroform and dichloromethane) and translating it across the fundamental beam. So-called Maker fringes are recorded as a function of the position of the wedge with a periodicity dependent upon the geometry of the cell and the coherence length (related to the difference of the refractive indices for the fundamental and second harmonic waves). Reference measurements, either on the pure solvent or a known reference compound, need to be taken to calibrate the instrument.

The knowledge of relative amplitudes of the Maker fringes allows for the calculation of the product $\mu\beta_{EFISH}$. The product involves a vectorial component of $\beta$ (not all tensorial components contribute equally). Unfortunately, it can often be difficult to obtain the dipole moment, so values are sometimes reported as $\mu\beta_{EFISH}$, instead of $\beta$. Another limitation of this technique is that it cannot be used on highly conducting solutions, such as those of ionic salts.

### 1.2.1.2 Hyper-Rayleigh Scattering

For these reasons, since roughly twenty years ago, the majority of second-order measurements have been carried out using a technique known as hyper-Rayleigh scattering.[28, 40, 41] This method is considerably simpler than EFISH, but requires more sensitive measurement equipment. It involves the collection of the scattered second-harmonic generated light from isotropic solutions. A schematic for the HRS experiment is shown in Figure 1.1.

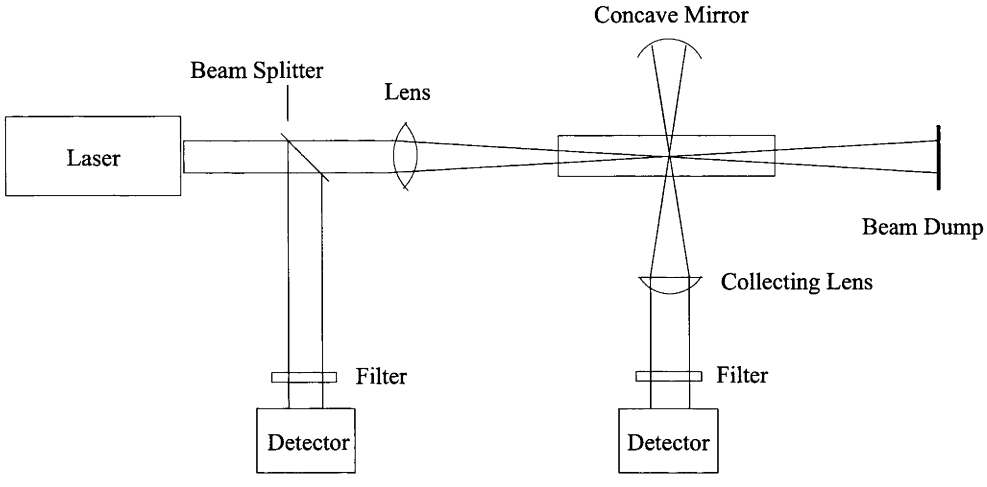


**Figure 1.1** A schematic of the Hyper-Rayleigh Scattering (HRS) technique.

The scattered light has a component at the second harmonic frequency that depends on the first hyperpolarizability of the solute molecules. The intensity of the generated light varies quadratically with the intensity of the incident light. The difficulty with this form of measurement is in capturing enough of the emitted light to obtain accurate measurements. The scattered light is weak, so as much as possible is collected by a back-mirror and collimating lens to focus into the detector.

The initial detector is used to monitor the intensity of the incident beam (at frequency $\omega$) and the final detector measures the collected light (at frequency $2\omega$). This light going into the second detector (usually a photomultiplier tube, which is very sensitive) is filtered to ensure that only light of the wavelength corresponding to $2\omega$ is detected.

This technique also allows for the measurement of compounds (with no net dipole moment) that have multiple internal dipoles (e.g. octupolar compounds). The electric field used for EFISH experiments does not align nonpolar materials, therefore they

cannot be measured by EFISH. However, the internal dipoles of these compounds do give rise to second-order effects.

HRS has several advantages over EFISH: no electric field is needed, allowing for the measurement of ionic or centrosymmetric species. Knowledge of the dipole moment ($\mu$) or the second hyperpolarizability ($\gamma$) is not required. The main disadvantage is that very intense light is required to generate enough $2\omega$ photons to measure. This can lead to decomposition of the material in the beam. Fluorescent compounds present the difficulty of distinguishing between the SHG light (at $2\omega$) and fluorescence light from multiphoton absorption. HRS is still the most widely used form of measuring second-order NLO effects today.[41-47]

### 1.2.2 Second-order NLO Response of Selected Compounds

With the development of methods to analyze NLO properties, many compounds were tested in order to determine what made a good second-order NLO material. Several important structure-property relationships have been determined.[7, 8, 17, 23, 25, 28] Chief among these is a large difference between the ground and excited state dipoles. As described by perturbation approaches, or the two-level model, the larger the difference, the higher the magnitude of the second order NLO properties.[48-50]

The two level model (Equation 1.8) describes how it is possible to maximize the value of $\beta$:

Eq. 1.8 $$\beta \propto (\mu_{ee} - \mu_{gg}) \frac{\mu_{eg}^2}{E_{eg}^2}$$

where $\mu_{(gg)}$ and are $\mu_{(ee)}$ permanent dipole moments of the molecule in the ground and the excited state, respectively, $\mu_{(eg)}$ is a transition moment between the ground and the excited state and $E_{(eg)}$ is transition energy. From this equation, the importance of the magnitude of the transition moment is also apparent. A large transition moment, and the transition occurring at a lowest possible energy, will also contribute to the maximization of $\beta$.[48] These are the principles upon which a large number of studies attempting to maximize $\beta$ have been based.[51]

The two-level model is a simplification – it assumes that only one excited state contributes to the hyperpolarizability. In reality the hyperpolarizability depends on many transitions and thus is a function of a large number of parameters – knowledge of a large number of dipole moments and excited state energies are required to accurately predict it theoretically for any given system. Some solution to this problem can be derived from so-called sum rules discussed by Kuzyk that relate the hyperpolarizabilities to the number of electrons which contribute to optical excitations.[52]

For organometallic molecules, this includes the outer shell of the metal atoms and the π electrons from the organic portions of the molecule. This approach allows one to find the upper limits of the hyperpolarizabilities in systems with many excited states. Good tutorial reviews on the origin of nonlinear interactions are available.[33, 53] Returning to the two-level approximation, the first characteristic that makes a good molecule for quadratic NLO application is a large difference in the ground state and excited state dipoles. This type of molecule can be achieved with donor-bridge-acceptor arrangements:


A strong electron donor at one end and a strong acceptor at the other will increase the magnitude of the molecular dipole of the molecule and, provided that electrons are free to travel along the bridge, the excited state dipole will often be quite different. The reason for the use of metals as becomes apparent: they often have strong donor/acceptor character. Towards this end, considerable work has been done with organometallic 'molecular wires', which can easily transfer electrons from a donating metal to an accepting organic (or metal) moiety.[54-60]

A large ground state dipole does not guarantee good second-order NLO properties. It is the difference in the magnitude of the ground and excited state dipoles that produce good values of β. Thus there must be good electronic delocalization throughout the molecule, to facilitate a change in dipole with the change to the excited state. The conjugative (or π-delocalization) properties of π-bonded atoms (aromatic rings, double and triple bonds) fulfill the requirements of electron delocalization. Marder and Perry's

'bond-length alternation theory' hypothesized and then confirmed the structures of good π-delocalized bridges.[61, 62]

If the bridge compound has a series of single and double bonds in the ground state that change to double and single bonds, respectively, in the excited state (Figure 1.2), the compound will (according to the theory) have high magnitude values of β. Note that both the ground and the excited states of a molecule can be considered a combination of the neutral and ionic structures. It has been found that compounds in which all of the bonds are of similar length (there is little difference in C-C length and C=C length) have β values of increased magnitude. These compounds are referred to as 'cyanine-like' compounds. Conversely, when the bond alternation is more pronounced ('polyene-like' compounds), the magnitude of β is less.[62]

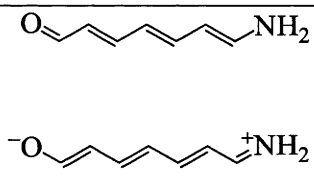


**Figure 1.2** A theoretical bridging molecule in the ground state (top) and excited state (bottom).

Not all types of π-bonded bridges are equally good in the respect of their ability to maintain conjugation when excited – for a bridge containing aromatic units, the aromatization in the ground state impedes aromatization in the excited state (aromatization in the excited state benefits charge delocalization). By contrast, a degenerate π-electron system (as in Figure 1.2) has equivalent resonance energies in both the neutral and polarized forms. Some aromatic bridges (with polarized states that increase aromaticity) actually assist charge polarization; increasing the magnitude of the polarization and, hence, the magnitude of the NLO response.[61]

The remainder of this section outlines (with organometallic examples) the known, experimentally determined, structure-property relationships for quadratic NLO properties. Looking at the difference in the nonlinearities of the two ferrocenyl compounds in Figure 1.3, the importance of an electron acceptor is obvious. The iron is acting as a moderate strength donor, the addition of a conjugated acceptor gives rise to a hundredfold increase in β.[17, 55]

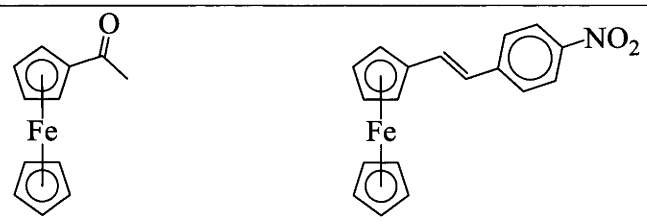


$\beta = 0.3 \times 10^{-30}$ esu

$\lambda_{fund} = 1.91$ μm

$\beta = 31 \times 10^{-30}$ esu

$\lambda_{max} = 536$ nm

$\lambda_{fund} = 1.91$ μm

**Figure 1.3** Compounds with (right) and without (left) an electron accepting group.

In this introduction, groupings are such that (except for Figure 1.3) the materials within a figure were measured by the same research group, at the same wavelength ($\lambda_{fund}$) and in identical solvents. Experimental error has been left out of the nonlinear values reported in this chapter. These error values tend to be between 15 and 20% for second-order measurements and 10 to 30% for third-order measurements.

Looking further into this series of ferrocenyl compounds, it can be seen that nitro groups are better acceptors than cyano groups and that the (*E*) conformation of the -ene group allows for better transfer of charge (Figure 1.4). It has also been shown that nitro groups are better acceptors than aldehydes.[63]

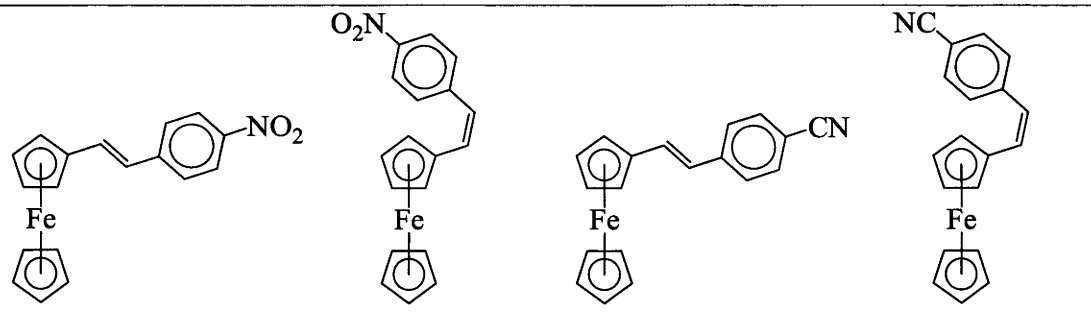


$\beta = 31 \times 10^{-30}$ esu
$\lambda_{max} = 536$ nm
$\lambda_{fund} = 1.91$ μm

$\beta = 13 \times 10^{-30}$ esu
$\lambda_{max} = 480$ nm
$\lambda_{fund} = 1.91$ μm

$\beta = 10 \times 10^{-30}$ esu
$\lambda_{max} = 466$ nm
$\lambda_{fund} = 1.91$ μm

$\beta = 4 \times 10^{-30}$ esu
$\lambda_{max} = 460$ nm
$\lambda_{fund} = 1.91$ μm

**Figure 1.4** A comparison of acceptor groups and C=C bond conformation.

Each of the above compounds has values which have been measured at different wavelengths. This is a frustrating problem relating to nonlinear optical data. Similar to

linear spectra, compounds have very different NLO responses at different wavelengths; it was only recently that compounds began to be measured across a broad spectrum of wavelengths.[64, 65] Compounds also exhibit solvatochromism, having different values of $\lambda_{max}$ and giving different values of $\beta$ when dissolved in different solvents.[66]

The donating strength of the ligand is important. In Figure 1.5, the cyclopentadienyl (Cp) group on the ruthenium is replaced with a pentamethylcyclopentadienly ($Cp^*$) moiety, causing the ruthenium to be more electron rich. This creates a stronger electron donor, which also has a beneficial effect on the $\beta$ value.[67]

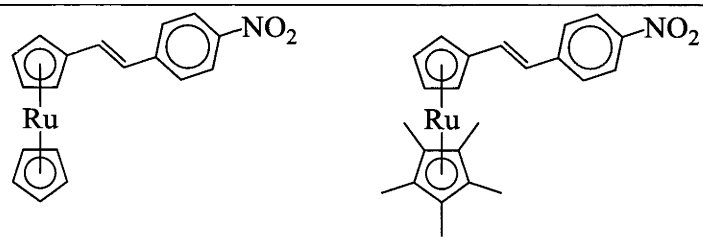


$\beta = 16 \times 10^{-30}$ esu
$\lambda_{max} = 390$ nm
$\lambda_{fund} = 1.91$ μm

$\beta = 24 \times 10^{-30}$ esu
$\lambda_{max} = 424$ nm
$\lambda_{fund} = 1.91$ μm

**Figure 1.5** Compounds with weaker (left) and stronger (right) electron donating groups.

Replacing a double bond with a triple bond increases the degree of π-delocalization in a compound. Bond alternation theory supports this, with the triple bond creating an 'island' of conjugation that reduces the overall π-delocalization of the molecule. The reduced π-delocalization normally has a detrimental effect on the intensity of $\beta$ (Figure 1.6).[68]

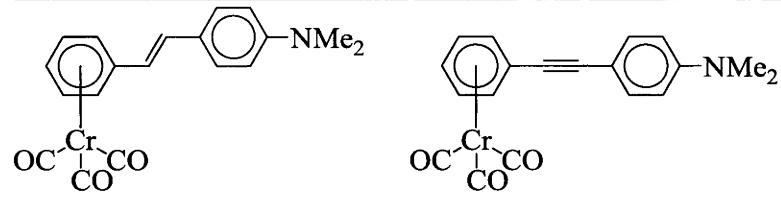


$\beta = 20 \times 10^{-30}$ esu
$\lambda_{max} = 418$ nm
$\lambda_{fund} = 1.5$ μm

$\beta = 11 \times 10^{-30}$ esu
$\lambda_{max} = 405$ nm
$\lambda_{fund} = 1.5$ μm

**Figure 1.6** The effect of varying the bond order.

Figure 1.7 shows a mixed metal system.[69] The use of metals in both the donor and acceptor position allow for additional increase in the benefits of using metals in these materials. Notice that the wavelength of measurement is different than that used for the compounds shown in Figure 1.6. Despite similarity in the molecules, this difference precludes comparison between the compounds to examine the effect of the second metal versus the electron-donating 4-dimethylaminophenyl moiety (the size of the complexing ring has relatively minimal effect).

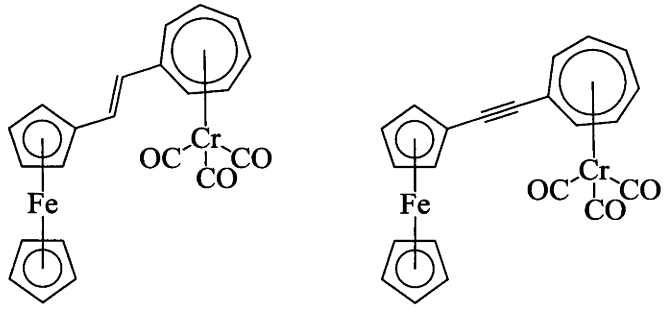


$\beta = 320 \times 10^{-30}$ esu
$\lambda_{max} = 670$ nm
$\lambda_{fund} = 1.06$ μm

$\beta = 570 \times 10^{-30}$ esu
$\lambda_{max} = 600$ nm
$\lambda_{fund} = 1.06$ μm

**Figure 1.7** Metals in both the donor and acceptor positions.

This example (Figure 1.7) demonstrates that these properties are not absolute. The double bond connectivity between the metals results in a lower β value than the triple bond. This could be because the measurement is at an absorbance maxima for the triple-bond compound and not for the double-bond compound. However, all of these

properties are generalizations and exceptions to the rules are always possible. Bond alternation theory posits that, in most cases, double-bond-containing bridges are better for NLO properties than triple-bond-containing bridges.[53, 62, 70]

All of the systems so far have had the metal moiety bonded to the face of a conjugated ring. This format places the metal orbitals orthogonal to the plane of the 'bridge'. By using metal acetylides, the metal atom is in the plane (Figure 1.8). This can have a striking effect on the quadratic nonlinearities of compounds.

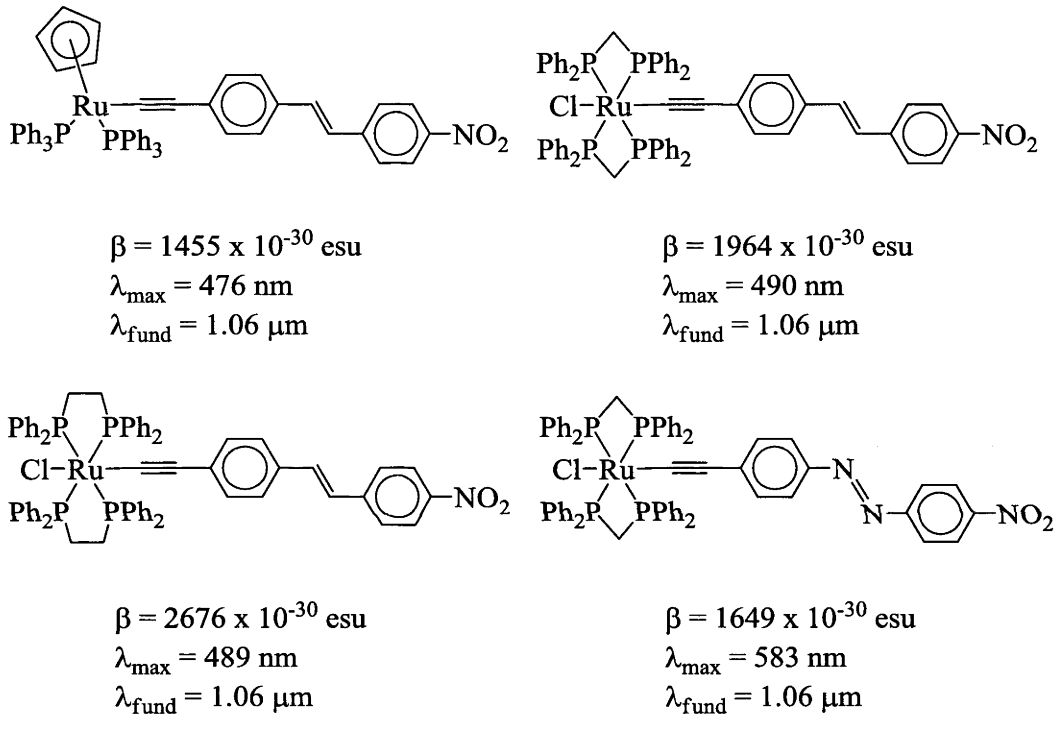


**Figure 1.8** The effects of placing the metal in the plane and ligand variation.

Changing from the triphenylphosphine / cyclopentadiene ligand combination to the more electron-donating bis(diphenylphosphino)methane (dppm) / chloride or 1,2-bis(dihpenylphosphino)ethane (dppe) / chloride ligand combinations causes the ruthenium centre to be even more electron rich and a stronger donor. This leads to the increase in values for the compounds with the bidentate ligands. The increased electron density of the azo-linkage appears to have the effect of blocking some of the electron withdrawing capability of the nitro group.[63]

Having multiple metal centres in the plane of electron transfer gives rise to similar improvements to mixing metals in compounds where the metals are bound to the faces of conjugated rings (Figure 1.9).[71]

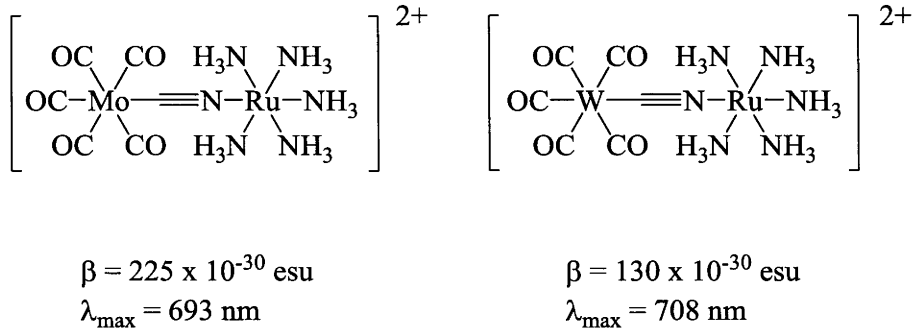


$\beta = 225 \times 10^{-30}$ esu
$\lambda_{max} = 693$ nm

$\beta = 130 \times 10^{-30}$ esu
$\lambda_{max} = 708$ nm

**Figure 1.9** Examples of some mixed-metal acetylides.

There is a danger in comparing the compounds in Figure 1.10 with each other.[42] Despite being mixed-metal alkynyl compounds, there are many differences. The ligands, formal charge of the species and type of metals all vary, making direct comparison suspect. What these indicate is that increasing the distance between the acceptor and donor group also causes the value of β to increase. This property is examined more fully in Chapter 2.

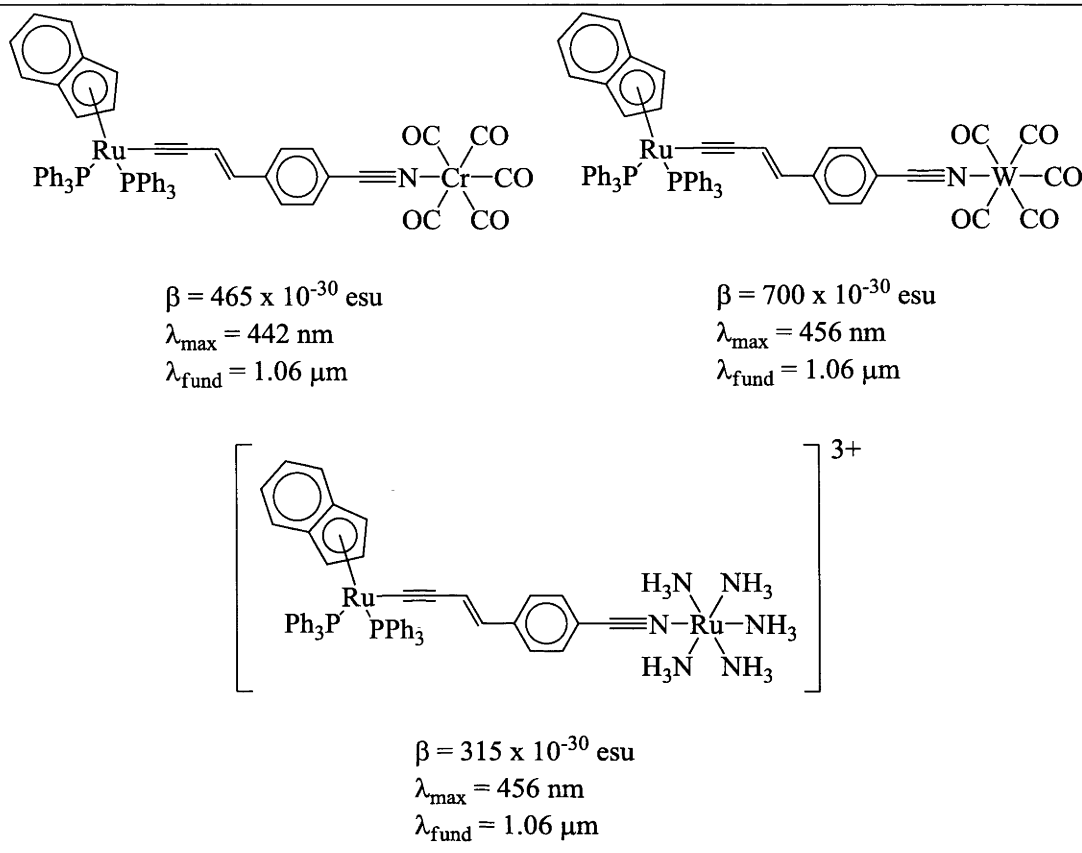


**Figure 1.10** The effect of varying the chain length.

Several methods to increase the value of quadratic nonlinearities have been outlined. Strong donors and acceptors are important, to give a strong ground state dipole. A good conjugated or π-delocalized bridge allows for ease of electron movement through the system, maximizing the potential difference in ground and excited state dipoles. If the metal is located in the same plane as the π-delocalization, as opposed to orthogonal to it, the influence of the metal centre on the system increases. Finally, existence of multiple metal centres gives rise to even further design flexibility than a single metal centre allows.

## 1.3 Third-Order Nonlinear Optics

The development of materials in which cubic NLO processes are optimized is in a more experimental stage. Third-order materials have not yet found application in devices to the same extent as those using second-order processes. This is partly because the effects are often too weak to easily induce unless ultrashort (femtosecond or picoseconds) laser pulses are used. The processes are different from quadratic processes but equally enticing in the opportunities they present.

Perhaps the most potential to revolutionize optical technology is in application of optical Kerr effects. These are the refractive (due to the real part of the nonlinear susceptibility) nonlinear processes (NLR) whereby the refractive index of a material depends upon the intensity of the incident beam. This would allow for a laser beam carrying information (e.g. in terms of intensity variation) to be redirected and processed. One application is in Kerr lens mode locking, used in short-pulse lasers. Another potential application is optical data manipulation, which could lead to optical computing.

A property that has found numerous applications is that of two-photon absorption. This is the absorptive (due to the imaginary part of the nonlinear susceptibility) nonlinear process (NLA) where two photons are absorbed simultaneously to generate an excited state, as first described by Maria Goeppert-Mayer.[38] This creates the possibility of developing methods of storing three-dimensional images, 3-D nanofabrication, etc. Other cubic NLO effects include wave-mixing phenomena, supercontinuum generation, optical power limiting and some modulation effects, among others.

### 1.3.1 Measurement Methods

It is the search for materials with better cubic responses that drives most of the research in this thesis. Three methods of measuring third-order nonlinear effects are outlined here: Z-scan, degenerate four-wave mixing (DWFM) and optical Kerr gate (OKG) experiments.

### 1.3.1.1 Z-Scan

Z-Scan is a simple and elegant technique for determining cubic nonlinearities and has been the most popular method since the early nineties.[24] It involves moving a sample (which can be an isotropic solution in a cell) along the path of a focussed beam. This allows for the solution to encounter different intensities of electromagnetic radiation as it is moved down the beam in the Z direction (Figure 1.11).[72]

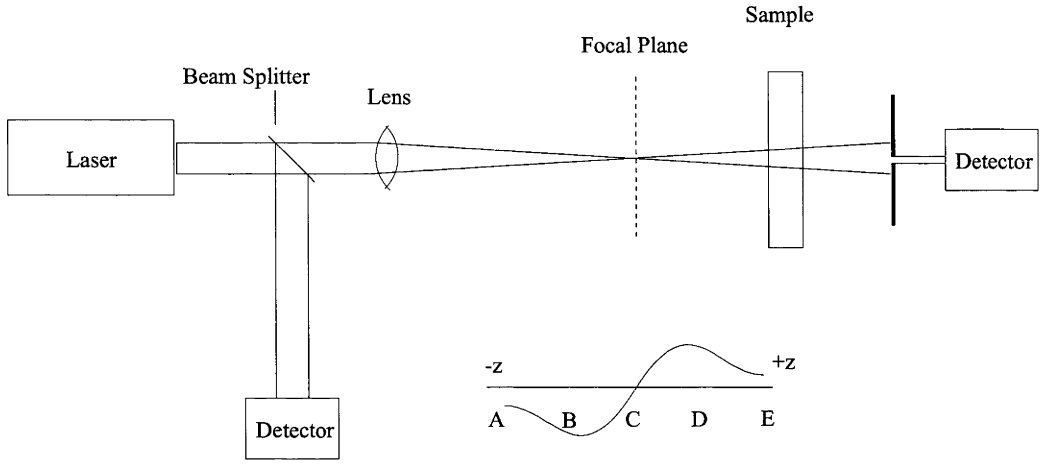


**Figure 1.11** A schematic of a Z-Scan setup.

The beam is focussed through a lens, such that the narrowest part of the beam (the beam waist) is at Z = 0. The beam waist (of radius $w_0$) is the position where the material is subjected to the most intense radiation. The sample is then moved from –Z to +Z, ideally through several Rayleigh lengths. A Rayleigh length is described by:

Eq. 1.10 $$Z_R = \pi w_0^2/\lambda$$

To obtain accurate Z-scan measurements, it is important that the sample width be narrow (less than a Rayleigh length) and that the sample pass through several Rayleigh lengths. The intensity of the beam on the sample varies as it moves, such that:

Eq. 1.11 $$I_{(Z)} = I_{max}/[1 + (Z/Z_R)^2]$$

As the intensity of light reacting with the sample changes, the sample acts as variable strength lens, changing the path of the beam. As the sample moves from A to B (in Figure 1.11), the solution will act as a virtual lens to either focus the beam (bring the focal point in the –Z direction) or defocus the beam (moving the focal point in the +Z

direction). Materials are said to either be self-focussing (positive value of the nonlinear index $n_2$, related to the cubic susceptibility $\chi^{(3)}$) or self-defocussing (negative value of $n_2$). Due to the pinhole prior to the detector, a focussing solution (in position B) will cause less light to hit the detector – the reverse is true for a defocussing solution.

As the sample then moves through the focal plane (C), these focussing effects are lost. When it continues on to the D position, they are measureable again, but with reverse effects (focussing materials increase the amount of light that hits the detector and vice versa). This allows for the comparative measurement of the refractive nonlinearity of a solution.

This sort of setup does not compensate for any absorptive effects which the investigated compound may show. In order to determine the absorptive (third-order) nonlinearity of a material, the experiment must be repeated, without the pinhole in front of the detector. This provides data to determine the imaginary (absorptive) component of $\gamma$. By dividing the data from the original run (with pinhole) by the data obtained without a pinhole, it is possible to isolate only the real (refractive) portion of $\gamma$.

Another alternative (Figure 1.12) is to split the beam prior to the pinhole. Passing one of the two beams through a collimating lens and then collecting it allows for the simultaneous collection of refractive and imaginary data.

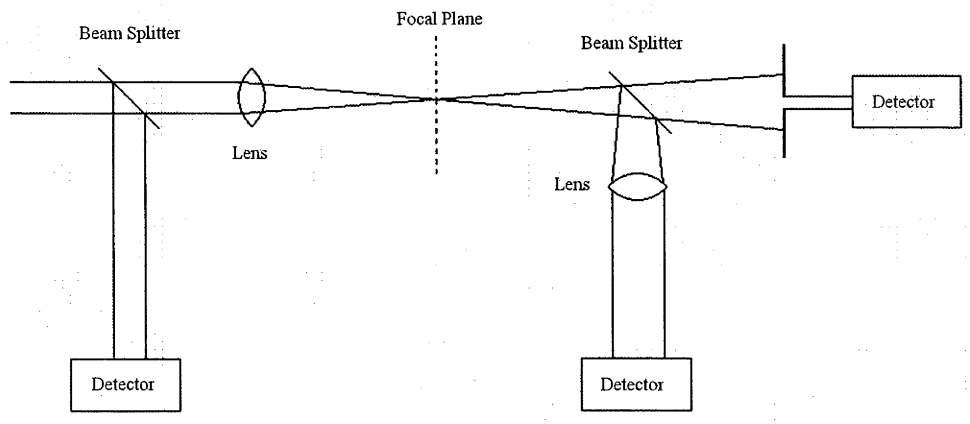


**Figure 1.12** Three Z-scan detectors measuring real and imaginary components.

Z-Scan can be used as a comparative technique. As all materials exhibit some degree of third-order nonlinearity, it is important to exclude the nonlinear behavior of the cell (optical glass or silica), as well as the solvent from the final data. This can be done by measuring silica and a reference cell containing pure solution and subtracting their effects. Another option is to repeat the experiment at several concentrations, extrapolating to determine the non-linear contributions of the pure solute.

The advantage of Z-scan as compared to other techniques of measuring the cubic nonlinearity is that only one laser beam is required (as opposed to DFWM or pump-probe type experiments, below). The sign and magnitude of $\gamma_{real}$ and $\gamma_{imag}$ are both obtained in a single experimental run, making Z-scan a very popular technique. The main drawback is that the sample is in the beam continuously for the duration of the experiment, allowing for thermal- or photo-degradation, as well as interference due to excited state effects. For this reason, it is crucial to use very short pulses (minimizing excited state absorption within the pulse duration) at a low repetition rate (so that the material can entirely relax prior to the next pulse).

Several modifications to the basic Z-Scan experiment are also possible. Chapter 2 deals entirely with Z-Scan experiments and the determination of cubic nonlinearities of materials. The use of multiple wavelengths, photoswitching and electrochemical switching of the sample while in the path of the beam all allow for the obtaining of additional information. These ideas will be discussed there.

#### 1.3.1.2 Degenerate Four Wave Mixing

Z-Scan does not have the capability to provide information needed to determine the origin of the nonlinearity observed. Degenerate four wave mixing (DFWM) is a time-resolved experiment that allows the experimenter to determine if the origin of the nonlinearity is electronic. It works by the interaction of three beams at the same wavelength to produce a fourth beam (also at the same wavelength).

Two coherent beams (pump beams) interacting with a material at a small angle produce a transient diffraction grating in that material. This grating is actually an interference pattern of varying light intensity. Through modulation of the refractive index and the absorption coefficient of the material this leads to the appearance of the complex index grating. When a third beam of light (probe beam) is introduced, it is diffracted at the

grating. This diffraction produces a fourth (phase conjugate) beam, the intensity of which is measured. It is proportional in intensity to the product of the pump beams intensities and $|\chi^{(3)}|^2$.[25]

Normally, only one laser is used, with the initial beam being split into three separate beams (one of which is delayed by increasing the path length). In the case of long (nanosecond) laser pulses, the third beam may be obtained by reflecting one of the pump beams back into the material (Figure 1.13).[73] Setup of the experiment is more difficult with a shorter pulse laser. This changes the setup into a 'folded-BOXCARS' geometry, in which all three beams enter the sample from the same side.

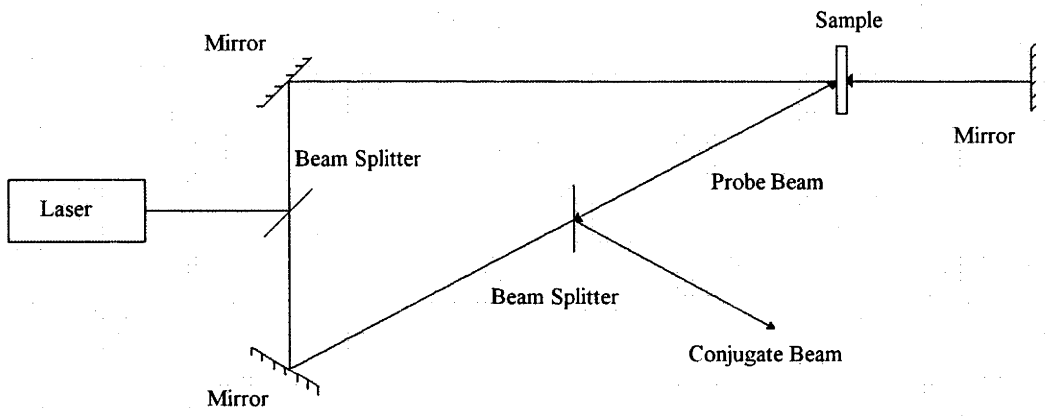


**Figure 1.13** A schematic of a Degenerate Four-wave Mixing (DWFM) experiment in the 'backward' geometry.

DFWM allows for the measuring of different $\chi^{(3)}$ tensor components separately through various combinations of polarization of the beams. Similarly to Z-scan, the measurements of $\chi^{(3)}$ are often carried out in a relative manner, older work typically using $CS_2$ as a reference sample. The most important information which can be gained is the time dependence of the transient grating decay, which allows one to separate various timescales of nonlinear effects (not possible with Z-scan).[25] With the classical DFWM experiment, it is not easy to separate the contributions of the nonlinear absorption and refraction of a material, although phase-sensitive DFWM techniques have been introduced.

### 1.3.1.3 Optical Kerr Gate

DFWM is an example of a class of experiments which are pump-probe experiments. In general, they require multiple laser beams, a strong 'pump' beam which causes a change in the optical properties of a material and (after a delay) a probe beam, which detects the change. The probe beam may be at the same or at a different frequency from the pump beam. Continuum probing (using white light supercontinuum generated through nonlinear interactions (e.g. in a photonic crystal fibre) is becoming very popular as it provides information on the spectral dependence of the photoinduced change in the material.

An optical Kerr gate (OKG) experiment is a specific type of pump-probe experiment that uses a polarized probe beam incident at a small angle to the pump beam. The (also polarized) pump beam induces birefringence in the NLO material and the differently polarized probe beam then passes through. Its polarization is perturbed by the induced birefringence in the material (Figure 1.14).[74] In the presence of the pump-induced effect, the probe beam is able to partly pass through a crossed polarizer.

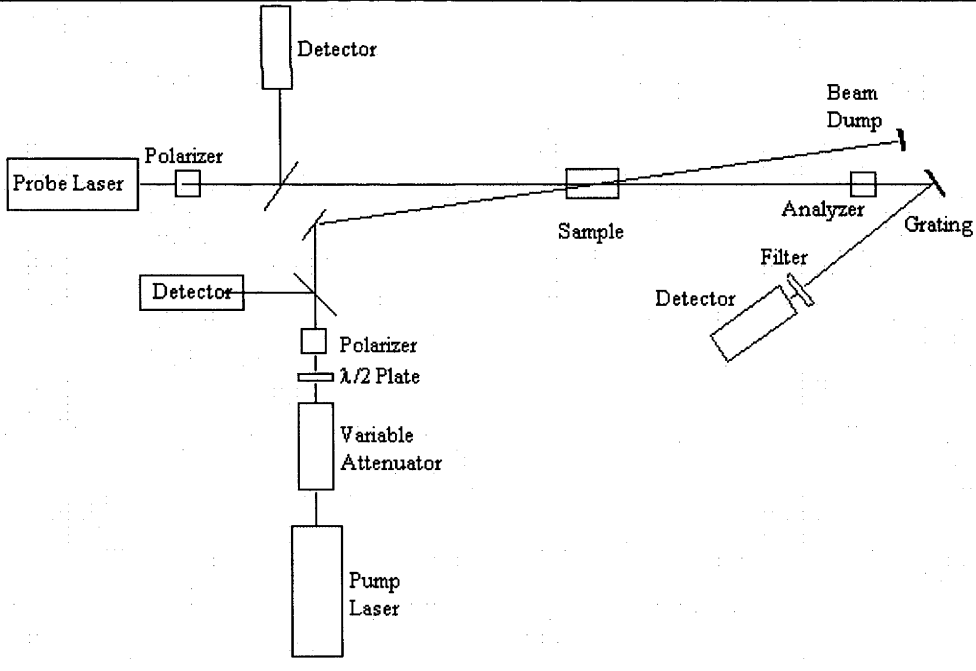


**Figure 1.14** A schematic of an Optical Kerr Gate (OKG) experiment.

The Kerr gate transmittance is proportional to the square of the induced birefringence. This allows for the determination of specific combinations of the tensor components of

$\chi^{(3)}$. One drawback of OKG experiments is that it is necessary to run multiple experiments (at different polarizations) to determine tensor components. Matching the timing and geometry of the beam is of a similar difficulty to other wave mixing experiments. Using a so-called heterodyne Kerr gate experiment, one is able to measure both the real and imaginary components of the cubic nonlinearity.

### 1.3.2 NLO Response of Selected Compounds

The molecular properties that give rise to good second-order NLO responses also give rise to good third-order responses. and a 'three-level model' exists, similar to the 'two-level model'.[75, 76] The major difference between the two is a symmetry effect; cubic effects are stronger when there are several dipoles within a molecule with a larger π-delocalizable area. The two-level model used for the second-order NLO effects is insufficient in the case of third-order effects. The three-level model (Equation 1.12), that also allows for the calculation of cubic NLO effects:[75, 76]

Eq. 1.12 $$\gamma \propto -\frac{\mu_{eg}^4}{E_{eg}^3} + \frac{\mu_{e'e}^2 \mu_{eg}^2}{E_{eg}^2 E_{e'g}} + \frac{\mu_{eg}^2 (\mu_{ee} - \mu_{gg})}{E_{eg}^3}$$

In this equation the symbols *e* and *e'* denote two different excited states. Since terms can have different signs, they can partly cancel each other, thus the usefulness of the three-level model for obtaining chemical intuition concerning the second hyperpolarizability is quite limited.

From this model, it is in principle possible to calculate formulae that attempt to describe the nonlinear refraction (NLR) and nonlinear absorption (NLA) of a molecule at a given frequency w (Eq.1.12 is for static γ, i.e. at ω = 0). For example, by assuming only one resonant frequency ($\omega_{10}$), i.e. limiting to only the first term of the model in Eq.1.12, approximate formulae for dispersion of the nonlinear parameters can be obtained.[53]

Eq. 1.13 $$n_{2,el} \cong -\frac{1}{4n_x^2 \varepsilon_0 c} \frac{N}{\varepsilon_0 \hbar^3} f^{(3)} |\bar{\mu}_{10}|^4 \frac{2(\bar{\omega}_{10} - \omega)\left[(\bar{\omega}_{10} - \omega)^2 - \frac{\bar{\Gamma}_{10}^2}{4}\right]}{\left[(\bar{\omega}_{10} - \omega)^2 + \frac{\bar{\Gamma}_{10}^2}{4}\right]^3}$$

Eq. 1.14 $$\alpha_{2,el} \cong -\frac{\omega}{2n_x^2 \varepsilon_0 c^2} \frac{N}{\varepsilon_0 \hbar^3} f^{(3)} |\bar{\mu}_{10}|^4 \frac{\bar{\Gamma}_{10}(\bar{\omega}_{10} - \omega)\left[2\bar{\omega}_{10}(\bar{\omega}_{10} - \omega) + \frac{\bar{\Gamma}_{10}^2}{4}\right]}{\bar{\omega}_{10}\left[(\bar{\omega}_{10} - \omega)^2 + \frac{\bar{\Gamma}_{10}^2}{4}\right]^3}$$

Equations 1.13 and 1.14 describe approximations of the electronic nonlinear refractive index coefficient ($n_{2,el}$) and an electronic intensity-dependent change in absorption ($\alpha_{2,el}$) for a one-photon resonance system. $\Gamma$ is a quenching parameter[77] and $f^{(3)}$ is a local field correction. Properties that apply to individual molecules are represented with an overbar.

The bond-alternation theories may also be useful for second hyperpolarizabilities – in this case, the nature of the linking bridge in the ground and excited states is more important than the magnitude of the dipoles.[62] The previously mentioned issue with aromatic rings is still present in cubic NLO studies: the aromatic ring does not allow for π-delocalizations as effectively as a polyene. However, phenylenevinylene or phenyleneethynylene bridges allow for considerably better excited-state π-delocalization than do purely polyphenylene bridges. For this reason, and because the structural benefits of aromatic rings outweigh the polarizability deficits, these types of linkers are used frequently.

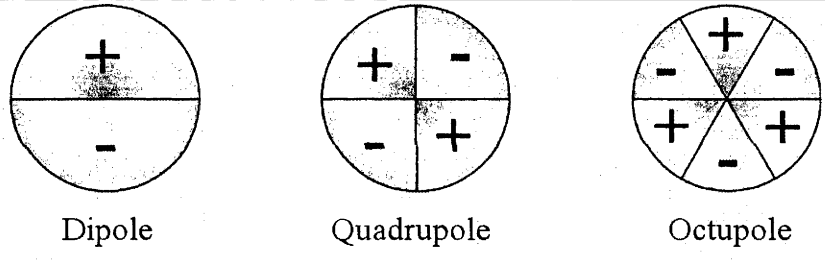


**Figure 1.15** Various symmetries of charge distribution in molecules.[44]

As mentioned previously, the symmetry of a molecule, in particular the presence of multipolar charge distribution (Figure 1.15), may also have important influence on both quadratic and cubic NLO properties.[2] Quadratic effects can only be present in molecules which have dipolar or octupolar character.[78] Cubic properties are always present and the multipolar distributions have a positive effect. In particular, it has been proven that quadrupolar distributions of charges, such as those existing in molecules of D-A-D or A-D-A type (A = acceptor, D = donor) are essential in obtaining large values of the two-photon absorption coefficients.[79]

In the case of organometallics, the effect of varying the metal on the cubic NLO properties is apparent. Figure 1.16 shows the measured (by the THG method[i]) $\gamma$ values of a series of small metal acetylides. There is a discrepancy here, with two different reports giving the same values of $\gamma$ but with $\lambda_{max}$ differing by 20-30 nm.[80, 81]

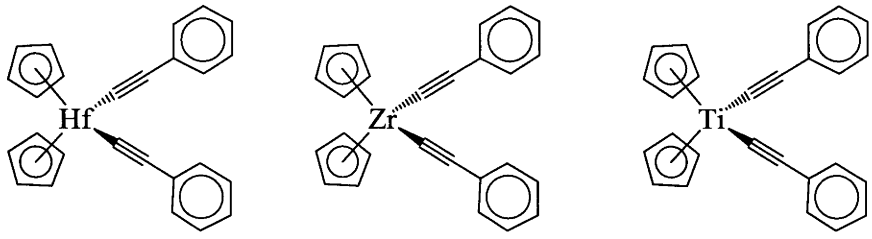


| | | |
|---|---|---|
| $\gamma = 51 \times 10^{-36}$ esu | $\gamma = 58 \times 10^{-36}$ esu | $\gamma = 92 \times 10^{-36}$ esu |
| $\lambda_{max} = 358 / 390$ nm | $\lambda_{max} = 370 / 390$ nm | $\lambda_{max} = 416 / 410$ nm |
| $\lambda_{fund} = 1.91$ μm | $\lambda_{fund} = 1.91$ μm | $\lambda_{fund} = 1.91$ μm |

**Figure 1.16** The effect of changing the metal centre on the second hyperpolarizability.

These compounds exhibit relatively small values for $\gamma$. As molecules get larger and the electrons are more delocalized, their nonlinearity increases. This is illustrated below (Figure 1.17), where the ferrocene oligomer (n = 6-8) has a higher cubic nonlinearity than nonoligomeric molecules.[20]

[i] THG is a useful method for determination of NLO parameters, but it refers to a different hyperpolarizability: $\gamma(-3\omega: \omega,\omega,\omega)$ as opposed to $\gamma(-\omega: \omega,-\omega,\omega)$, which is the degenerate hyperpolarizability relevant for nonlinear refraction and absorption.

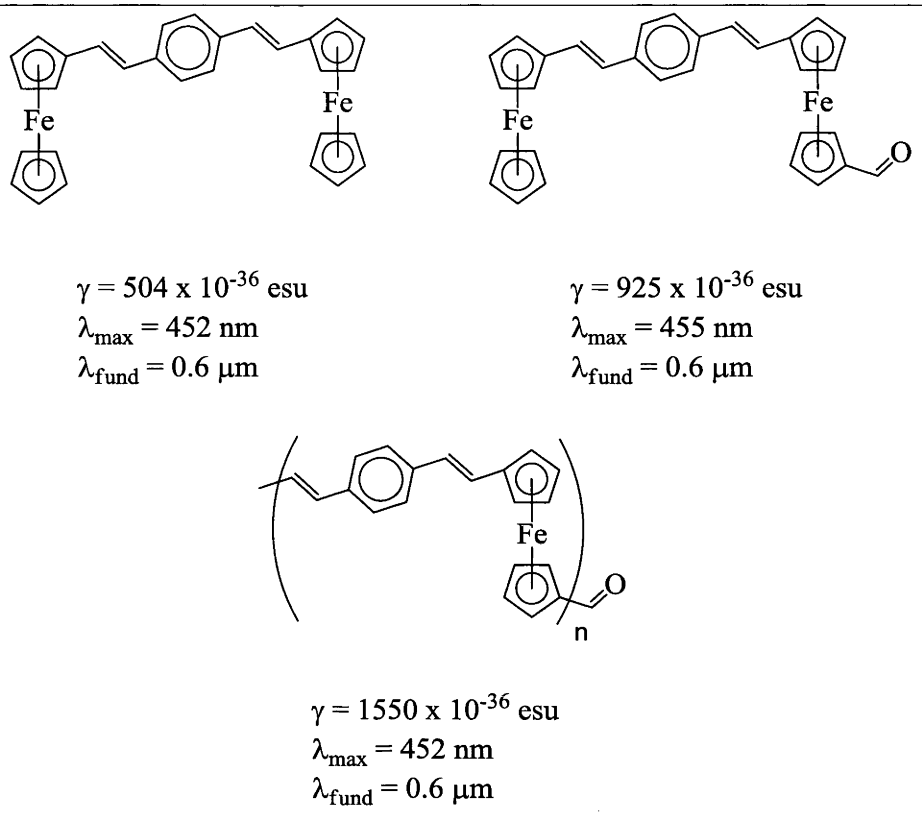


**Figure 1.17** A comparison of molecular size (n = 6-8).

The withdrawing aldehyde group acts to polarize the molecule, probably giving it some quadratic NLO character as well. It has been found that there is a general trend towards increased values of $\gamma$ for metal centres with higher atomic number. Iron compounds tend to have less NLO response than ruthenium compounds, which have less than osmium compounds, provided everything else remains equal.[82] Thus these same metallocenes with ruthenium or osmium would probably have higher values of $\gamma$.

In compounds with multiple metal centres, electric communication between the metals is often examined using cyclic voltammetry (CV). When one metal atom oxidizes, the charge delocalizes through the molecule and (if communication between the metals is present) the second atom is harder to oxidize. The difference in potential between the two oxidations can be indicative of the level of communication and this is reflected in the NLO properties.

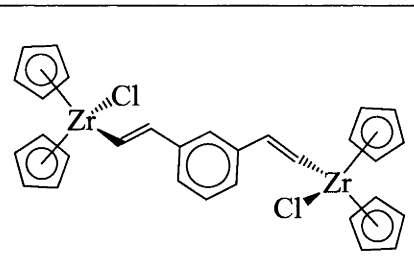


$\gamma = 68 \times 10^{-36}$ esu
$\lambda_{max} = 356$ nm
$\lambda_{fund} = 1.91$ μm

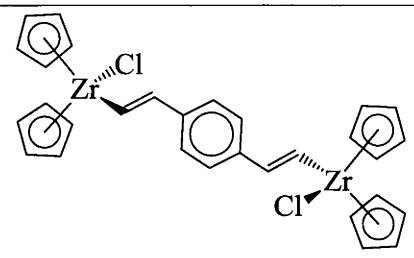


$\gamma = 154 \times 10^{-36}$ esu
$\lambda_{max} = 380$ nm
$\lambda_{fund} = 1.91$ μm

**Figure 1.18** The benefits of *para-* vs. *meta-* communication.

Figure 1.18 demonstrates that π-delocalization occurs better across an aromatic ring when the substituents are in the *para-* position.[81] Comparatively, the π bonds in the *meta-* position hamper communication. Compounds in Figure 1.16 and Figure 1.18 were all measured by third-harmonic generation.[25]

Properties that give rise to better cubic nonlinearities are found in large (often centrosymmetric) molecules containing metal or mixed metal centres (lower on the periodic table is better) with good communication between them.

Figure 1.19 marks the first of the compounds measured by Z-Scan in this introduction.[34, 83] Z-Scan allows for the separation of $\gamma$ into $\gamma_{real}$ and $\gamma_{imag}$, the refractive and absorptive components. Negative values of $\gamma_{real}$ indicate that the compound is self-defocussing and positive values refer to self-focussing compounds. Positive values of $\gamma_{imag}$ indicate that the compound is a nonlinear absorber, while negative values are for compounds which are saturable absorbers. A compound may be of different character (focussing or defocusing, saturable absorber or nonlinear absorber) at different wavelengths.

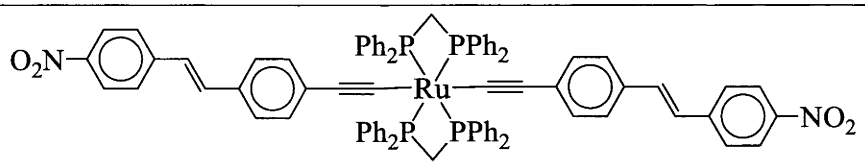


$\gamma_{real} = 1100 \times 10^{-36}$ esu
$\gamma_{imag} = 3400 \times 10^{-36}$ esu
$\lambda_{max} = 367$ nm
$\lambda_{fund} = 0.8$ μm

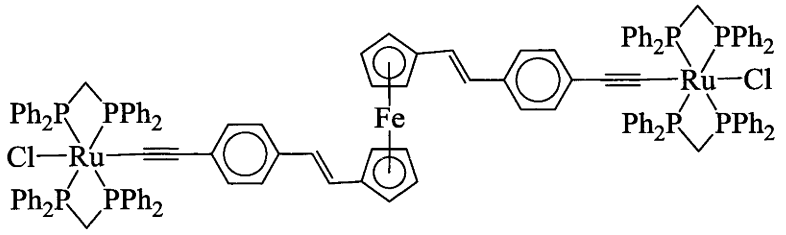


$\gamma_{real} = -7100 \times 10^{-36}$ esu
$\gamma_{imag} = 10600 \times 10^{-36}$ esu
$\lambda_{max} = 396$ nm
$\lambda_{fund} = 0.8$ μm

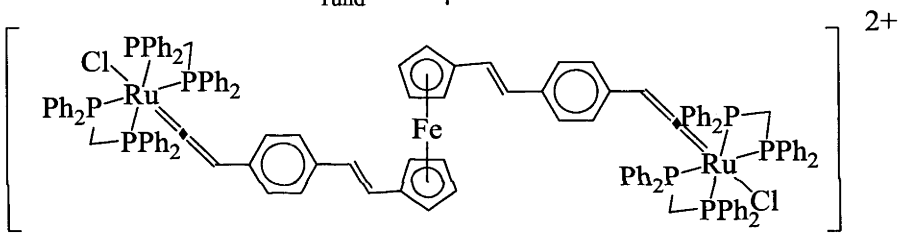


$\gamma_{real} = -3000 \times 10^{-36}$ esu
$\gamma_{imag} = 2300 \times 10^{-36}$ esu
$\lambda_{max} = 383$ nm
$\lambda_{fund} = 0.8$ μm

**Figure 1.19** The influence of the nature of the carbon-metal bond.

When forming a ruthenium acetylide complex, the metal-carbon bond may be isolated as the intermediate vinylidene.[84] Abstraction of the vinylidene proton (by a weak base) gives the acetylide. It is possible to isolate the vinylidene complex, allowing comparison between the nonlinearity of both materials. Figure 1.19 shows that this variation can have a marked influence on the strength of the cubic NLO effects.

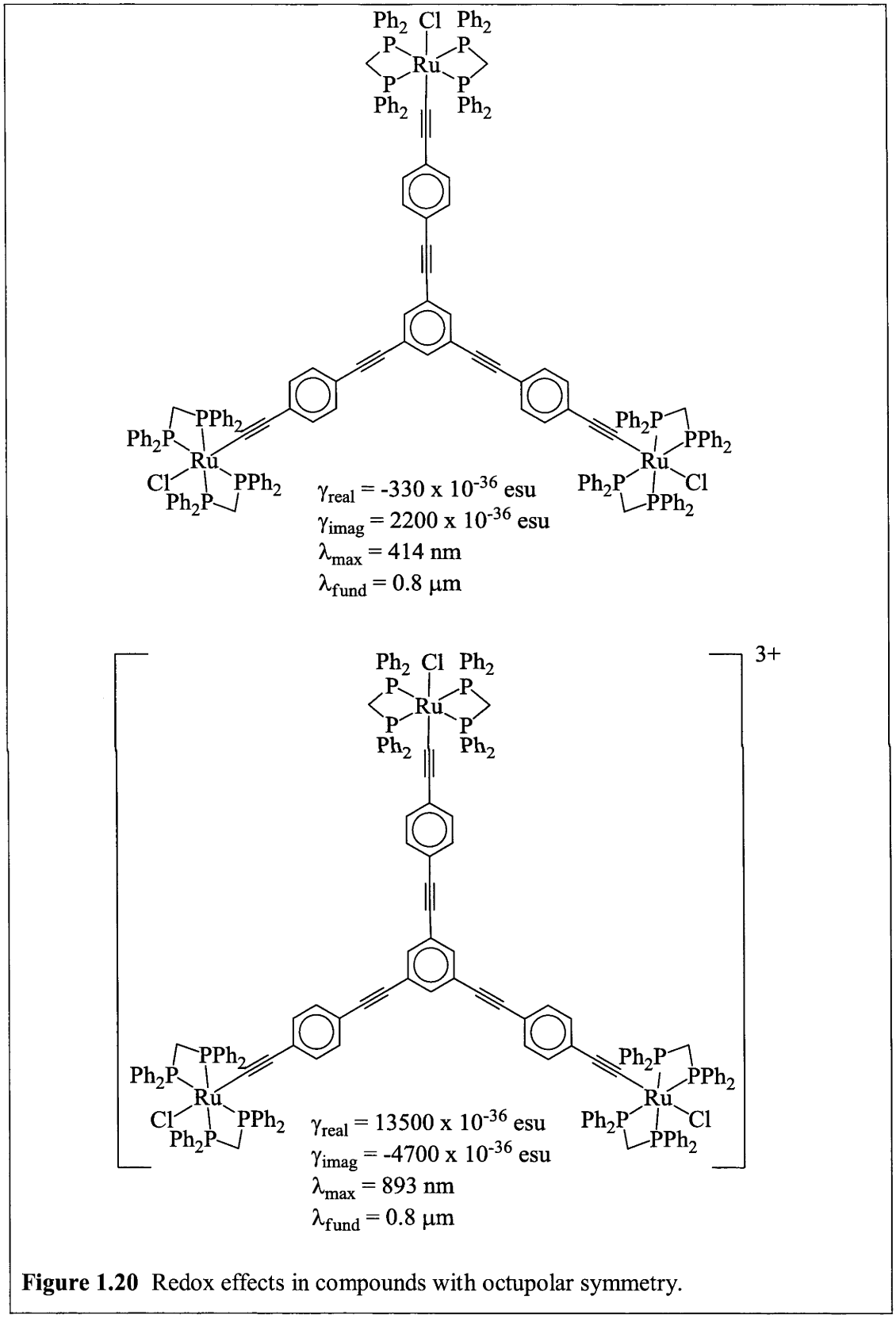


**Figure 1.20** Redox effects in compounds with octupolar symmetry.

Figure 1.20 shows a molecule with all the ruthenium centres in the +2 state and the same molecule where all of the ruthenium atoms have been oxidized to the +3 state.[85, 86] Both the NLR and NLA experience a change in character as well as significant magnitude changes. These compounds have octupolar symmetry and noticeably higher values of γ than previous examples in this chapter.[87] Although not directly comparable, they are an example of how an increase in symmetry tends to lead to increases in the absolute values of γ. A detailed study of the importance of symmetry is the subject of Chapter 4.

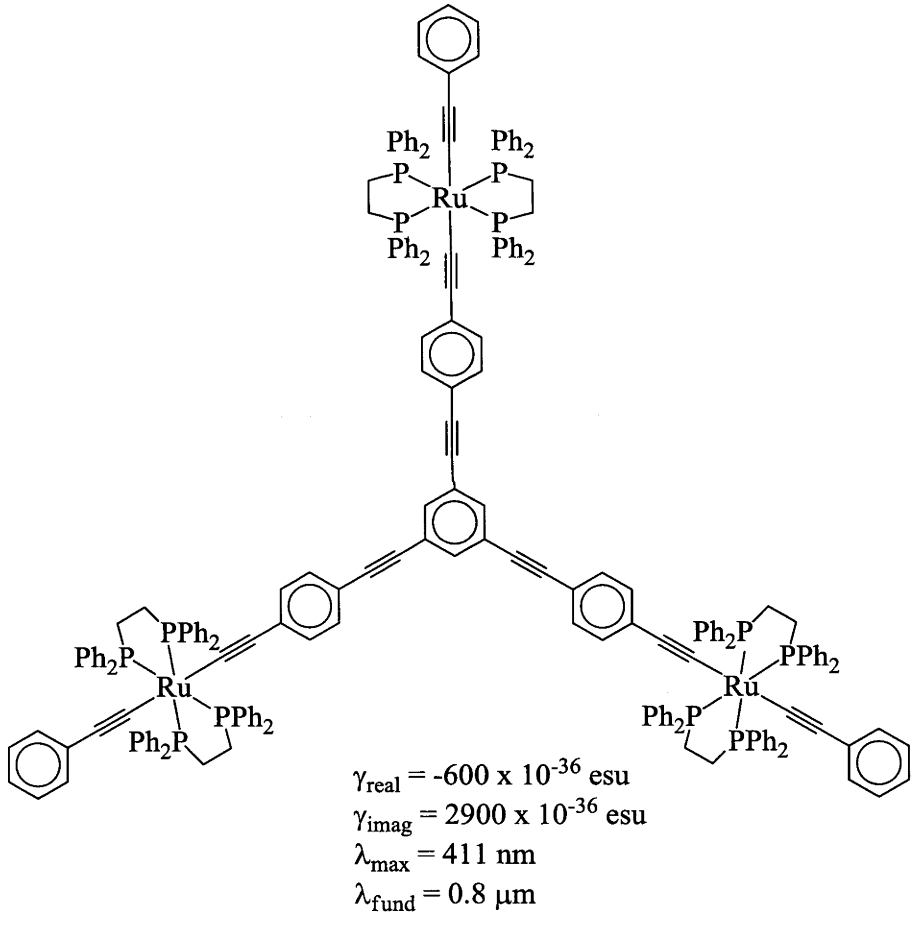


**Figure 1.21** A ruthenium bis-acetylide complex with octupolar symmetry.

By forming ruthenium bis-acetylide complexes, the NLO character of the compounds is not changed (Figure 1.21).[88]

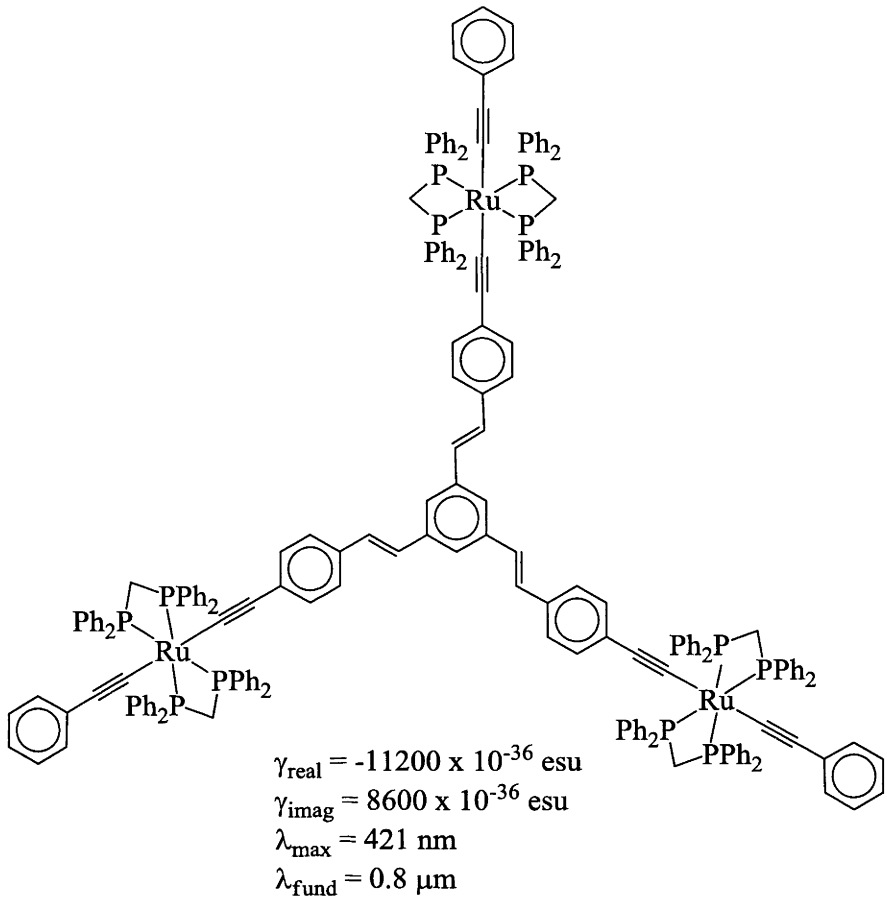


**Figure 1.22** The effect of bond order in compounds with octupolar symmetry (by comparison with Figure 1.21).

As with quadratic nonlinearities, bond order effects are quite important. Figure 1.22 shows a compound analogous to the one in Figure 1.21.[86, 89] The differences are the ligand (dppm vs. dppe) and the order of the linking carbon-carbon bonds about the central ring. The absolute value of $\gamma_{real}$ increases almost twenty-fold and the $\gamma_{imag}$ values more than triple. This occurs without a change in the character (sign) of the responses.

The final effect illustrated here is the so-called 'dendritic effect'. Prasad and coworkers have found that there is a more than linear increase in the magnitude of the TPA when NLO molecules are incorporated into larger dendrimers.[90-93] This 'coherent enhancement' effect applies to organometallic dendrimers as well. By including metal centres in a π-delocalized branching dendrimer, the magnitude of the γ values is increased dramatically (Figure 1.23).[88]

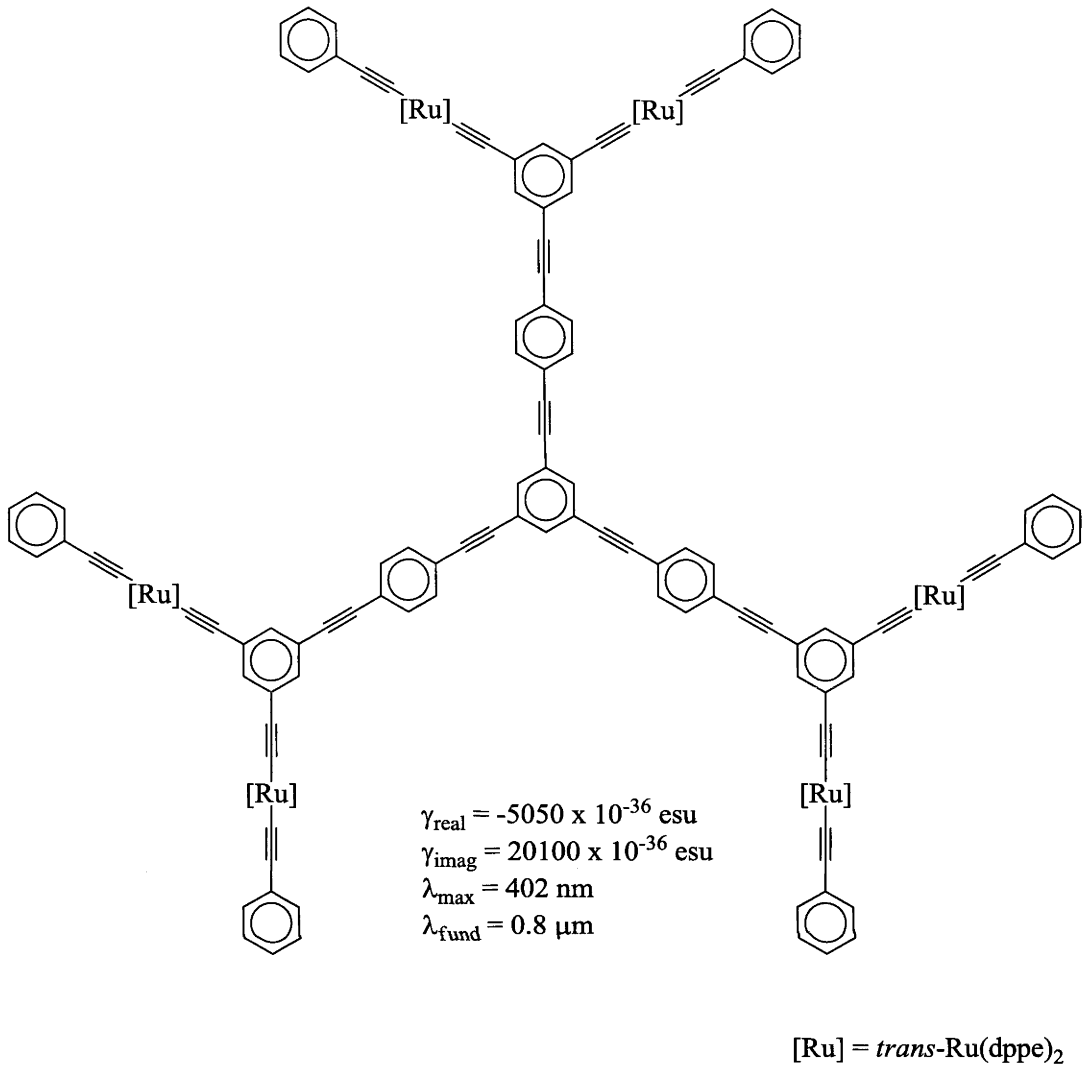


**Figure 1.23** A first generation dendrimer.

This increase in magnitude occurs without changing the sign of the real or imaginary parts of the γ of the compound. The improvement caused by this 'dendritic effect' is often considerably greater than the expected effect for additional metal centres.[94, 95]

With these further properties, even more tools for manipulating the nonlinear behaviour of materials are available. The nature of the metal-carbon bond is important, as is the symmetry of the molecule (this is different than for second-order effects). Incorporation of the dendritic effect allows for the increase of the absolute value of γ without changing the overall shape of the absorbance spectrum. These structure-property relationships can be used to produce better NLO materials.

## 1.4 Conclusions

It is important to be careful when comparing nonlinear optical responses of materials. EFISH and HRS usually give comparable values (within experimental error).[96] The wavelength at which compounds are measured must be identical in order to compare results. For true comparisons, full spectrum wavelength-dependence studies of the complex hyperpolarizability should be done. The first of these (for $\gamma$ of an organometallic compound) was reported in 2004.[97]

All of the comparisons in this chapter involve organometallic compounds. The described structure-property relationships hold true when it comes to organic compounds (except for those relying upon the presence of a metal centre). Organometallic materials tend to have similar NLO merit to the best organic materials, but the expense and difficulty of synthesis is potentially limiting. It will be through exploitation of the properties unique to metal centres that organometallic materials can become useful in functioning devices. One such property is the reversible redox behavior of many metal complexes. This electrochromic switching of NLO effects has commanded great interest in recent years.[2]

By combining all of the structural characteristics which improve nonlinear responses and minimizing those effects known to interfere, it is anticipated that improved devices can be developed. It is also hoped that by providing materials with better NLO responses, previously unavailable applications (due to a lack of sufficiently responding materials) will become available.

The work in this thesis focusses on producing organometallic compounds and materials that have improved NLO properties. Understanding the structural elements that give rise to these properties is required in order to hypothesize what new compounds would have desired characteristics. Vital to this is the ability to properly compare the NLO response of materials with each other. Chapter 2 deals with measurement of compounds and elucidation of these structure-property relations. The subsequent chapters involve the synthesis and measurement of materials designed to further confirm the relationships between structure and property outlined here and in Chapter 2.

# Nonlinear Optical Effects in Organometallic Complexes

## 2.1 Introduction

This chapter presents the cubic NLO behavior of a selection of compounds, both from within the Humphrey group and from our collaborators.[ii] The compounds are chosen with the intention of elucidating the structure-property relationships outlined in the introduction. This chapter also demonstrates the wealth of information available from the Z-scan technique, starting from basic measurements and finishing with more complex measurements at the end of the chapter.

Data for wavelength dependence measurements for compounds can be found as graphs in the appendices. Each compound is represented by a pair of graphs. The first is a plot of the two-photon absorption cross section versus wavelength. The second presents the complex cubic hyperpolarizability of the compounds as a function of the wavelength, with the absorptive (imaginary) component represented as blue diamonds and the refractive (real) component shown as red squares.

This information can provide better understanding of the interrelationships between the structures of compounds and their optical effects. From this understanding, it may become possible to tailor future compounds toward desired effects.

## 2.2 Z-Scan

All of the measurements in this section were done using Z-scan with an amplified femtosecond laser system. The light source was a Clark-MXR CPA-2001 regenerative amplifier, producing a beam at 775 nm. The beam was then passed into a Light Conversion TOPAS optical parametric amplifier. The TOPAS could be used to generate short (150 fs), high energy (μJ) pulses of light at any wavelength between 530 nm and 1600 nm.

The pulse repetition rate was 250 Hz. This means that each pulse was 4 ms apart, therefore the materials being tested were actually only in the laser beam for approximately $3.7 \times 10^{-7}$ % of the time. Another way of looking at this is that the pulse is roughly 0.045 mm long, followed by a 1200 km gap before the next pulse. The short

[ii] Footnotes are used to credit the researchers who prepared the materials. All measurements were done by the author, with the assistance of Prof. Marek Samoc, at the Research School of Physics and Engineering, ANU.

duration of the pulses and the (relatively) extremely long relaxation time means that contributions of excited state effects due to incomplete relaxation between consecutive pulses (e.g. thermal effects) are almost entirely avoided. More detailed specifics of this laser setup are available in Section 2.7.

For each Z-scan run, one hundred points are measured as the sample moves along the Z axis (normally a distance of 50 to 80 mm, depending upon beam geometry). Recalling the full Z-scan setup (Figure 1.11 and Figure 1.12), there are three detectors. The first of them is designed to monitor laser stability. For each point, multiple pulses are measured. Only those that fall within 2% of the desired power (determined by the experimenter over multiple runs by the response of the material which should give signals of certain amplitudes) are used. If a pulse is of appropriate energy, the data from both of the other detectors (closed aperture and open aperture) are taken for the averaging.

When several data points at one position are accumulated to give a reasonable average (typically 10-30 accepted pulses, depending upon laser stability), the electronic stage moves the sample 1/100$^{th}$ of the distance along the Z axis and the process is repeated. This culminates in a series of three lines, representing the traces for the open and closed aperture detectors and the reference detector.

Dividing the closed aperture trace by the open aperture trace, an approximate curve representing only the refractive nonlinearity of the compound is obtained. This curve can be fitted,[iii] as outlined by Sheik-Bahae, et. al., to determine the value of the nonlinear phase shift at z = 0 (the sample at the focal plane), $\Delta\Phi_0$.[24] The phase shift at different positions z is equal to (Equation 2.1):

Eq. 2.1 $$\Delta\phi(z) = \frac{\Delta\Phi_0}{1+z^2/z_0^2} = \frac{kn_2 I_0 L_{eff}}{1+z^2/z_0^2} = \frac{kn_2 I_0 (1-e^{-\alpha L})}{(1+z^2/z_0^2)\alpha}$$

where Z is the position of the sample along the Z axis, $L_{eff}$ is the sample length and $\alpha$ is the linear absorption coefficient and $k$ is the wave vector ($k = 2\pi/\lambda$). Knowing the phase shift one can calculate the nonlinear refractive index $n_2$ of the sample. The nonlinear

[iii] Using a custom program written by Marek Samoc.

absorption coefficient $\alpha^{(2)}$ can be derived from the open aperture trace, which is given by:

Eq. 2.2 $$T(z) = \frac{1}{\sqrt{\pi} q_0(z,0)} \int_{-\infty}^{\infty} \ln\left[1 + q_0(z,0) e^{-\tau^2}\right] d\tau$$

where $q_0 = \alpha^{(2)} I L_{eff.}$

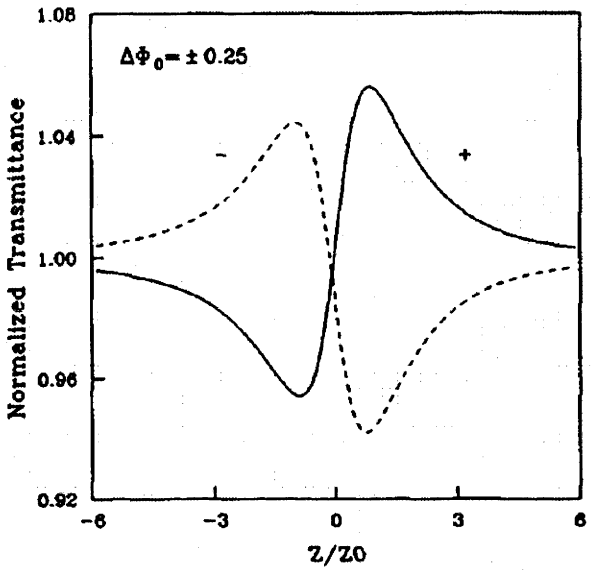


**Figure 2.1** Calculated Z-scan transmittance curves for a cubic nonlinearity of either polarity and a small aperture.[24]

Figure 2.1 shows the calculated closed aperture curves for nonlinear samples with $\Delta\Phi_0$ values of ± 0.25. The trace for a positive $n_2$ (self-focussing) sample is drawn as a solid line and the negative $n_2$ (self-defocussing) sample is the hashed line. Notice that a sample with a positive value of $n_2$ first distorts the beam so that less energy makes it through the aperture and then, once the sample has passed the z = 0 position, the distortion causes more energy to hit the detector.

The open aperture trace may then be fitted (using the custom fitting program) to determine the normalized Z-scan transmittance (T (z)), a value which represents change in absorption of the compound depending upon the intensity of the beam ($\alpha^{(2)}$ is related to $\gamma_{imag}$). These are the experimental data that are required to calculate the nonlinearities

of a sample, using the equations above and in Sheik-Bahae's paper.[24] Figure 2.2 shows a series of theoretical traces for a self-defocussing material.[98]

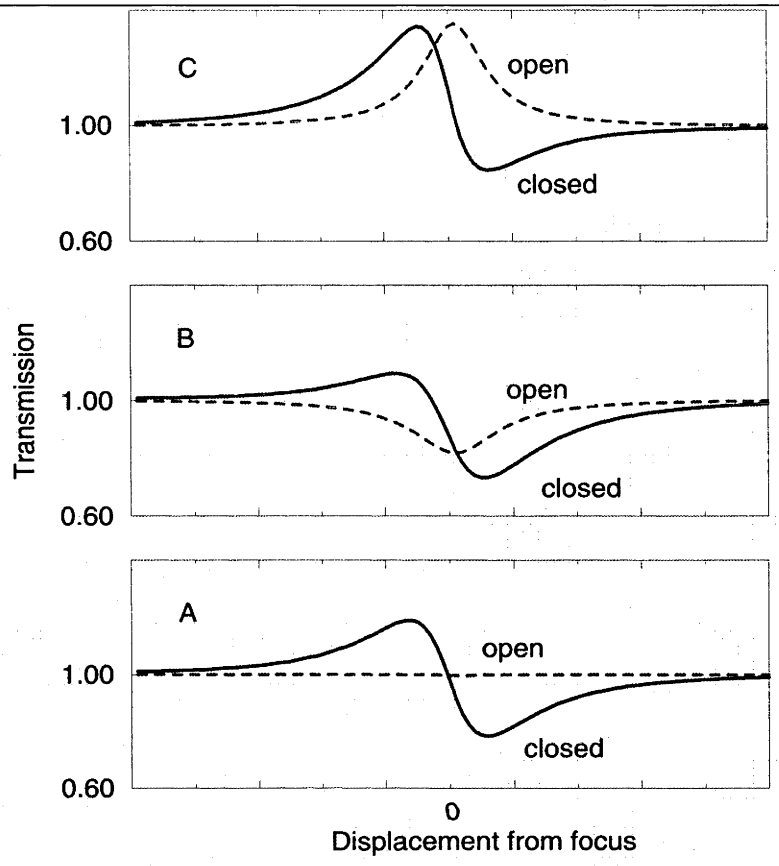


**Figure 2.2** Theoretical Z-Scan traces for a self-defocussing material.[98]

In Trace A, the nonlinear absorption is assumed to be zero and we are seeing a closed aperture trace similar to that in Figure 2.1. When the value of the nonlinear absorption coefficient is positive (Trace B), the nonlinear absorber causes a reduction in the power of light which hits the detector, as more is absorbed at the higher intensity. The reverse is true when the nonlinear absorption coefficient $\alpha^{(2)} < 0$, the case of a saturable absorber (Trace C). Notice that the shape of the open aperture (hashed) curves has a distorting effect on the closed aperture curves. This is why it is convenient to divide the closed aperture curves by the open aperture curves (to isolate the refractive component) prior to curve fitting to determine $\Delta\Phi_0$.

All compounds have some sort of cubic nonlinearity, but not all compounds are two-photon absorbers. Saturable absorbers (Trace C in Figure 2.2) are compounds where

the excited state absorption cross section is smaller than that of the ground state. When this occurs, increasing the input light intensity results in decreasing (saturating) the absorption due to the fact that more and more of the molecules are in the excited state.[99]

At this point, the researcher has obtained the total refractive and absorptive nonlinearities of the sample. This information includes the hyperpolarizability contributions of the solute, solution and the cell holding them. Two methods have been used in this work to isolate the nonlinearity of the solute. The first is to perform measurements of different concentrations of solution.

The second method is to measure the nonlinearities of the material of the cell (silica) and then the cell and solvent, separately. These values are calculated and then removed from the bulk values obtained for the combined sample.[100] This method was preferential for multiple wavelength studies and studies using an OTTLE cell (Sections 2.4 and 2.5) as it involves considerably less measurements.

## 2.3 Single Wavelength Measurements

Two different research groups (Kühn and Che) had previously demonstrated the synthesis of Ru-Re mixed metal materials and suggested that they could have good potential as compounds for nonlinear optic applications.[101-103] Following a prior collaboration,[104] the Hor research group sent a series of novel Ru-Re bimetallic species for measurement.[iv]

The compounds are interesting as the linking bridges between them are pyridylacetylides. This means that both metals are in the plane of conjugation. The pyridylacetylide ligand is directional, giving some polar character to the compounds in addition to that which is imparted by the metal centres. This is a series of seven compounds, as hexafluorophosphate salts, differing only in the nature of the ligands about the metals (Figure 2.3).

[iv] Compounds **1** – **7** were synthesized by Qingchun Ge, working in the research group of Andy Hor at the National University of Singapore, Singapore.

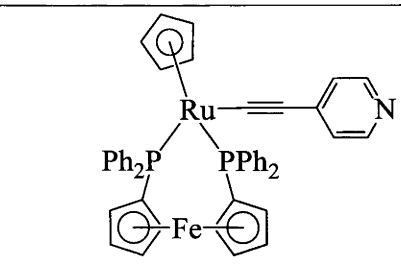


**1**

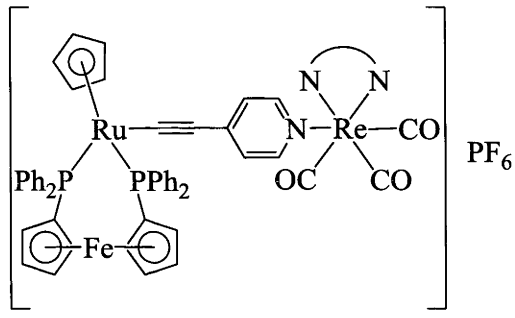


N N = bpy **2**
$Me_2$pby **3**
$Bu^t_2$pby **4**
phen **5**
tpy **6**

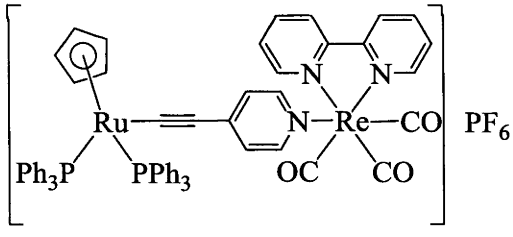


**7**

**Figure 2.3** A series of Ru-Re compounds with pyridylacetylide bridges.

All of compounds (**2-7**) had absorbance maxima at approximately 400 nm, so a wavelength of 750 nm was chosen to do the measurements, as it was expected that this wavelength would provide sizable two-photon absorption effects. This means that each photon would provide roughly half the energy required to excite the molecule.

**Table 2.1** Nonlinear Data Obtained for Ru-Re Complexes

| Compound | $\lambda_{max}$ (nm) | $\gamma_{real}$ ($10^{-36}$ esu) | $\gamma_{imag}$ ($10^{-36}$ esu) | $\sigma_2$ (GM) |
|---|---|---|---|---|
| **1** | 339 | 40 ± 100 | 10 ± 4 | 3 ± 1 |
| **2** | 409 | -590 ± 250 | 230 ± 40 | 65 ± 10 |
| **3** | 407 | -230 ± 60 | 280 ± 20 | 80 ± 6 |
| **4** | 407 | -480 ± 200 | 200 ± 40 | 55 ± 10 |
| **5** | 408 | -460 ± 150 | 280 ± 50 | 80 ± 15 |
| **6** | 407 | -570 ± 250 | 180 ± 30 | 50 ± 6 |
| **7** | 410 | -560 ± 150 | 280 ± 40 | 80 ± 10 |

The compounds were dissolved in dichloromethane at high concentrations (approx. 2 w/w% - the linear absorption spectra are measured at approx. 0.0005 w/w%) and measured at this concentration and two dilutions. Table 2.1 shows the results of these measurements. The major trend seen is that the addition of the rhenium moiety causes a significant increase in both the refractive and absorptive nonlinearities. This is due to the communication between the ruthenium and rhenium centres and is considerably more than the sum of the nonlinearities of the respective components.[34]

Interestingly, the iron appears to have little or no effect on the overall nonlinearity of the compounds. Replacing the dppf ligand with two triphenylphosphine ligands does not give rise to an appreciable change (within experimental error) in the nonlinear refraction (NLR) or nonlinear absorption (NLA) properties of the compounds. Perhaps this is due to the peripheral (out of plane) nature of the metal centre – it appears to be acting only as a ligand in these molecules.

It has been previously reported that effects which change the linear absorption spectrum of a compound also often change the nonlinear absorption.[105, 106] The redshift in the linear spectra when progressing from compound **1** to compounds **2-7** demonstrates this to be true in this case. This study highlights the value of mixed-metal materials, but (in comparison with larger systems) shows the need for larger, more diffuse electron fields to maximize cubic NLO properties.

## 2.4 Multiple Wavelength Measurements

Measuring the cubic nonlinearity of a compound at only one wavelength is no more informative than measuring the linear optical absorption of a compound at a single wavelength. Considerably more information may be obtained by measuring (point by point) a full nonlinear spectrum for a compound.

This has been done (in this work) by measuring the nonlinear response of a compound at several different wavelengths (usually approx. 20). This process is lengthy, taking roughly a week for a single compound, because of the need to retune and realign the laser system for each wavelength. By measuring multiple compounds at once (in the same solvent), it is possible to shorten this time considerably. Measurements were usually carried out in such a way that the laser was tuned to a certain wavelength, the Z-scans were recorded for a 3 mm thick silica sample and a 1 mm cell with the solvent and then consecutively for a number of solutions of several compounds. After completing the measurement at a single wavelength, the laser was tuned to a new wavelength, the system realigned and the measurements for silica, solvent and all of the samples were again carried out.

This procedure assumes that the cell material, solution and solute effects on cubic nonlinearities are additive.[100] Due to the errors in the determination of nonlinear parameters from each Z-scan, this is not as accurate as the concentration dependence method. However, adjacent points on the curve act to support the certainty of any given point. This allows for only one measurement for a compound at a specific wavelength and less frequent measurement of silica and solvent references (at a minimum, one per wavelength, although more in practice).

### 2.4.1 A Toroidal Nickel Cluster

The amount of extra information gained through wavelength dependence studies can be seen in the data obtained for this nickel cluster. The $[Ni(\mu\text{-}SBu^t)(\mu\text{-}etet)]_{12}$ cluster (Figure 2.4, compound **8**) was measured in dimethylformamide (DMF).[v]

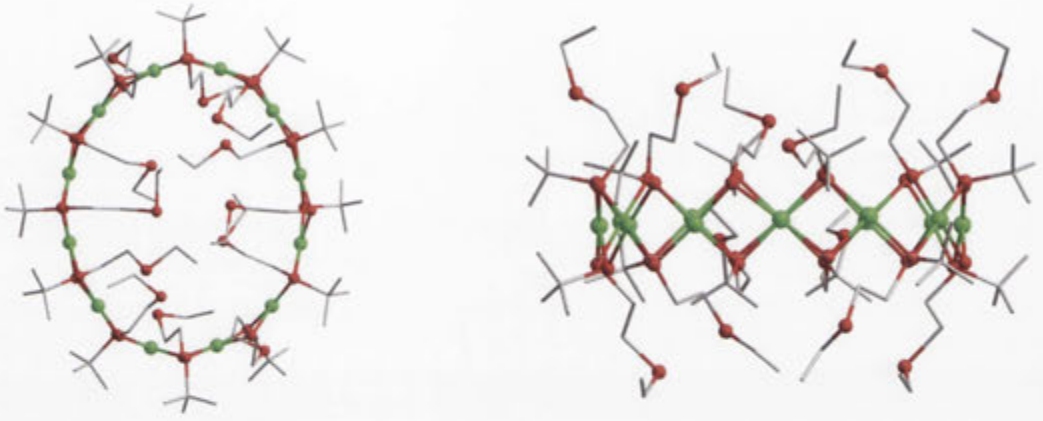

**Figure 2.4** An image of the dodecanuclear nickel cluster (**8**). Nickel atoms are shown in green, sulfur in red and carbon in grey.

Initially, a concentration dependence Z-scan study was done at 530 nm.[107] At this wavelength, the compound has a two-photon absorption cross section of approximately 80 GM, with a large experimental error (Figure 2.5). This error is due in part to linear absorption of the compound, which does not drop off completely until roughly 650 nm.

[v] This cluster (**8**) was synthesized by Chi Zhang, now at Jiangsu University, while working in the laboratory of Kazuyuki Tatsumi at Nagoya University, Japan.

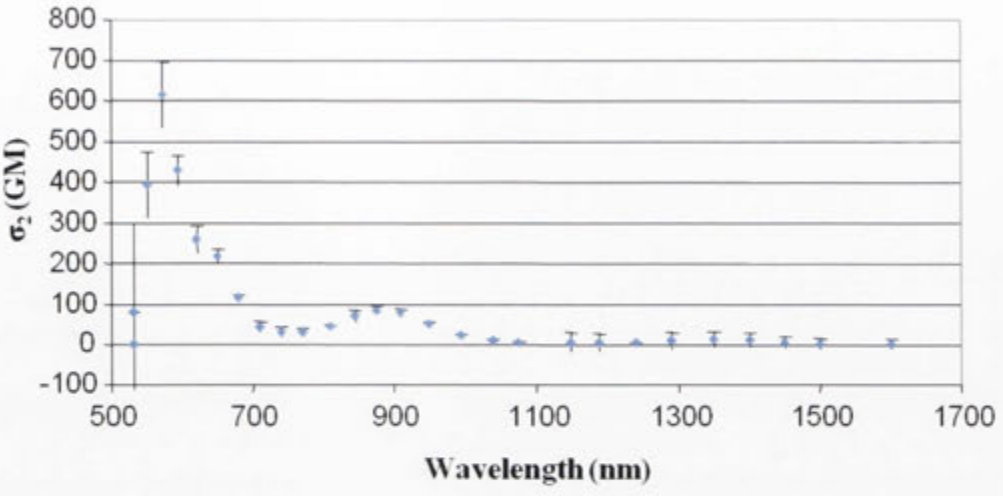


**Figure 2.5** The TPA spectrum of the $Ni_{12}$ cluster (**8**).

Examining Figure 2.5, the two-photon absorbance maximum occurs at 570 nm, with a second smaller peak at roughly 900 nm. The lower energy band is likely due to one-photon resonance enhanced two-photon absorption. The weaker, longer wavelength band (900 nm) is likely due to normal (off-one-photon-resonance) two-photon absorption.[53]

### 2.4.2 Ruthenium Acetylides

The remainder of this section (Section 2.4) examines some wavelength dependence Z-scan experiments. They further elucidate the structure-property relationships specific to ruthenium acetylide complexes and ruthenium acetylide-containing dendrimers. All of the compounds are designed to be compared with each other to elucidate structure-property relations.

### 2.4.2.1 Chain Lengthening Effects

A series of polar, linear ruthenium acetylides were prepared in order to determine the importance of the length of the conjugated linker between the electron donor (ruthenium) and the acceptor (nitro group).[vi] The competing effects are the improvement in the cubic NLO properties gained due to a larger π-delocalized system versus the loss of communication as the ruthenium and nitro groups become farther apart.

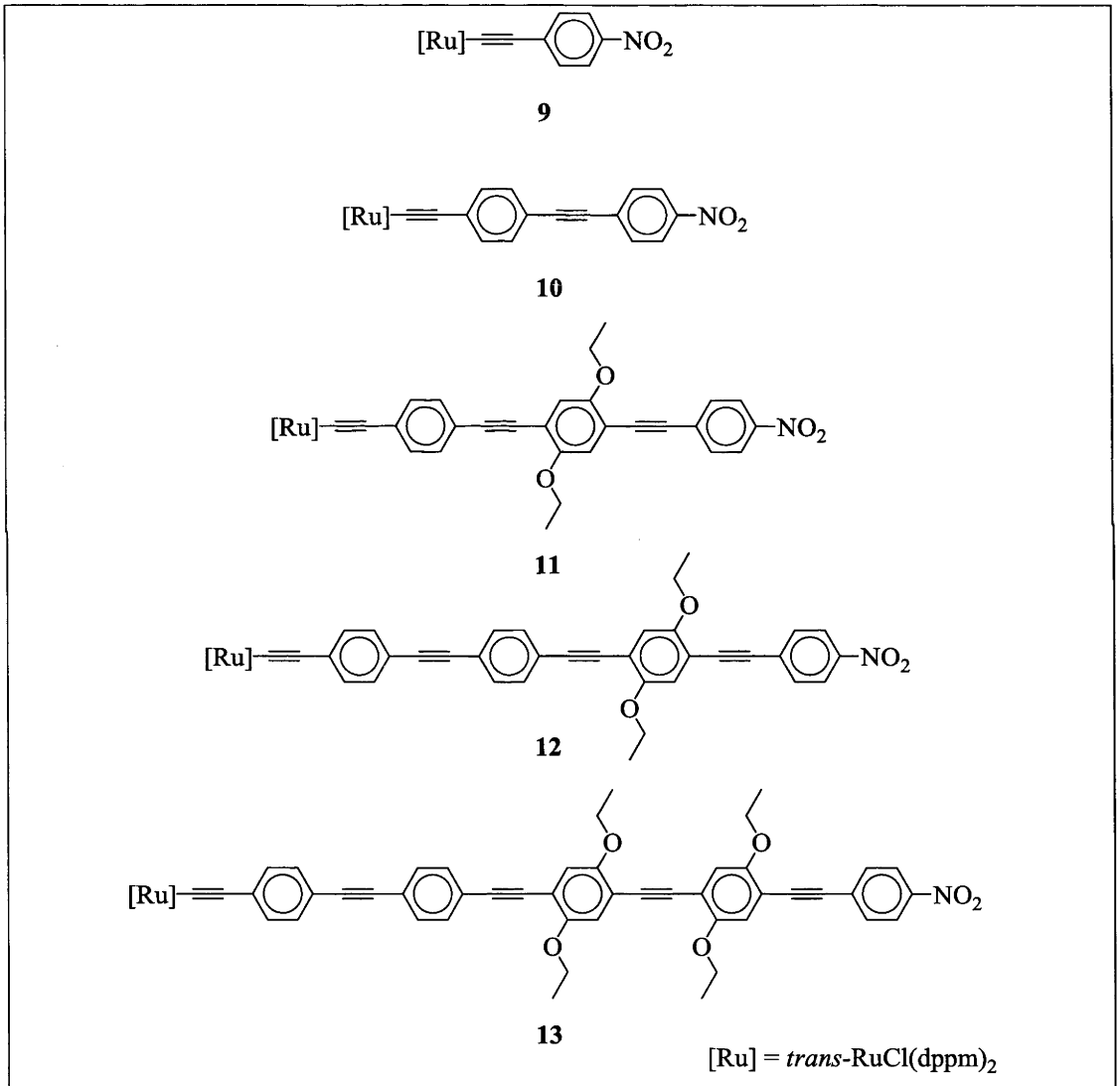


**Figure 2.6** The structure of the molecules synthesized to demonstrate the effect on NLO properties of chain lengthening in ruthenium acetylides.

[vi] Compounds **9** – **13** were synthesized by Bandar Babgi in the laboratory of Mark Humphrey at the Australian National University, Australia

Figure 2.6 shows the variation in structure as successively more phenyleneacetylene moieties are placed between the electron donating and accepting groups. The ethoxy groups are used to increase the solubilities of the molecules. It was found during synthesis (by Babgi) that the compound with three phenyleneethynylene spacers and no ethoxy units (similar to compound **11**) was not soluble enough to work with.

The results of this study (spectra are shown in Appendix 2.4) are that the optimal distance between this sort of donor and acceptor groups is three phenyleneethynylene units (Compound **11**). The intensity of the TPA bands increased from compound **9** to **10** and again between compounds **10** and **11**, where a plateau was reached. The lack of significant increase and the decreasing solubility (potentially making processing more difficult) mean that further increase in the number of 'spacers' is counterproductive.[108]

It was also possible that the presence of the ethoxy moieties had a damping effect on the nonlinearity. Comparisons within the paper showed that compounds without the solubilizing groups had stronger (and blueshifted) linear absorption spectra.[108] This is indicative that the nonlinear absorption would also be stronger. This will be discussed further in Chapter 4.

### 2.4.2.2 Effects of the Bond Order

The influence of the bond order in organometallic dendrimers on their NLO properties is not always as predicted by bond alternation theory, as the compounds in Figure 2.7 show.[109, 110] In these zero generation dendrimers, also called 'stars' (dendrimer generation is counted based upon number of branching points in the arms), the stilbene-containing compound (**14**) has less TPA at 800 nm (200 GM vs. 400 GM) than the tolane-containing counterpart (**15**).[vii]

[vii] Compound **14** was synthesized by Steph Hurst and compound **15** was synthesized by Andrew McDonagh, both while working in the research group of Mark Humphrey at the Australian National University, Australia.

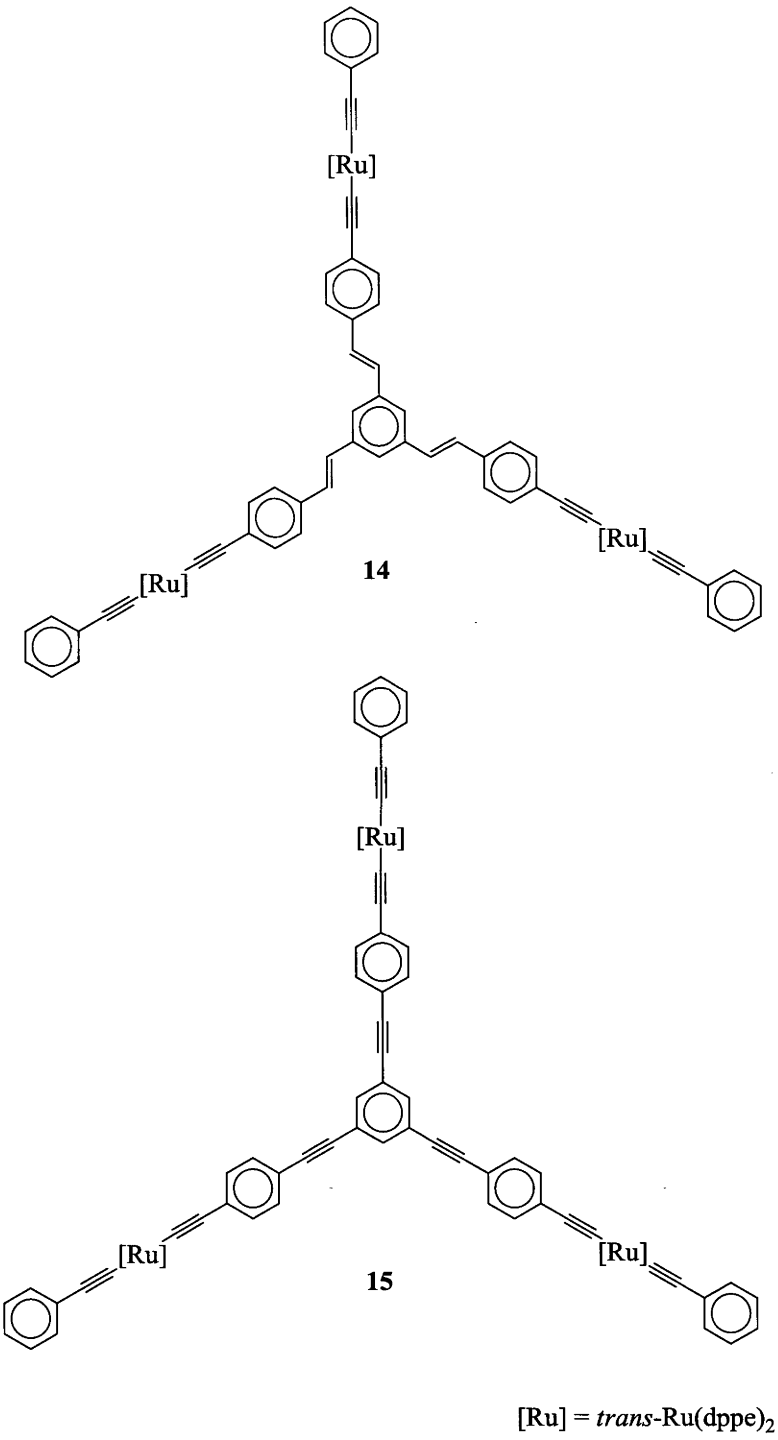


**Figure 2.7** The structures of stilbene- (**14**) and tolane- (**15**) containing 'star' molecules.

Both compounds are two-photon absorbers across the measured spectral range. The fact that the tolane-containing molecule is a stronger absorber does not necessarily mean that it is more useful. The non-linear absorption cross-section spectra of compounds **14** and **15** (Figure 2.8) show that both species have a nonlinear absorption of approximately

100 GM at 1300 nm. This is a 'telecommunication wavelength' (a wavelength at which optical telecommunication signals are transmitted through optical fibres) and both of these compounds (in terms of nonlinear response) would be equally useful for this type of application.

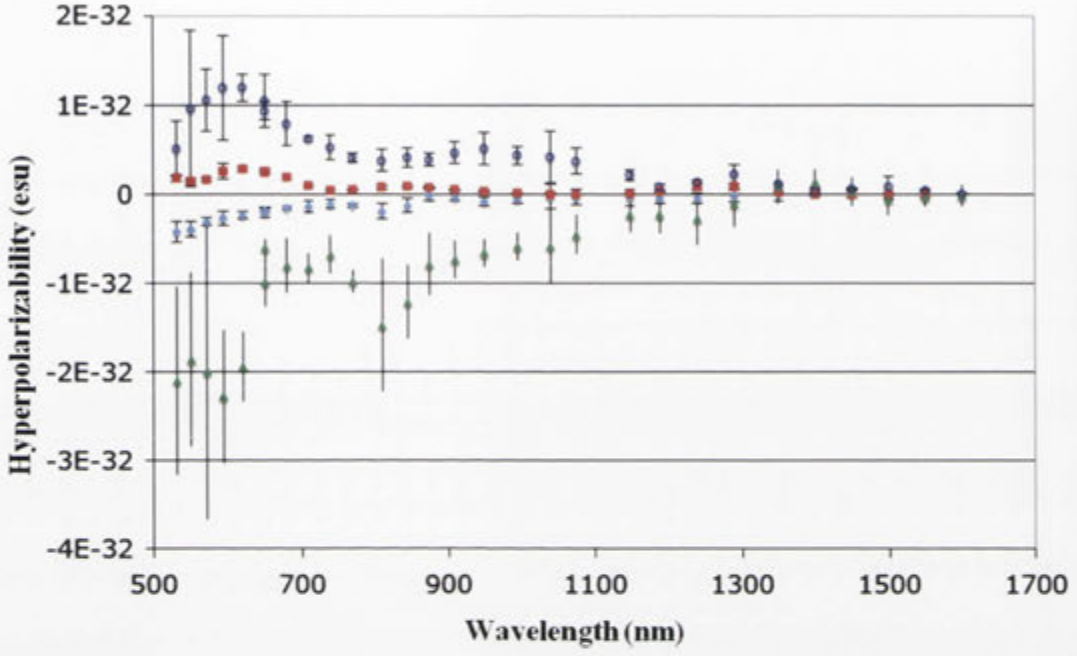


**Figure 2.8** Comparison of the real and imaginary parts of hyperpolarizabilities of compounds **14** ($\gamma_{real}$ = green triangles, $\gamma_{imag}$ = blue circles) and **15** ($\gamma_{real}$ = red squares, $\gamma_{imag}$ = cyan diamonds).

Compounds **14** and **15** are also examples of the importance of full-spectrum measurements. Single wavelength measurements were performed on them at 800 nm previously (Figure 1.21 and Figure 1.22).[88, 89] Comparing the intensity of the TPA spectra of these compounds (**14** and **15**) with those of compounds **9-13**, there is an increase in $\gamma_{imag}$ at most wavelengths. For example, compound **15** has a hyperpolarizability of $4 \times 10^{-33}$ esu at 1000 nm, while compound **11** has only $2 \times 10^{-33}$ esu at the same wavelength. The problem with this sort of comparison is that compound **15** has three times as many metal centres as compound **11.** From an atom economy point of view, compound **11** is better. If the desired result is a single molecule with higher response (as solutions of these compounds require less molecules and are more transparent), then the benefit of increasing the symmetry from dipolar to octupolar is

apparent. This is why these compounds have attracted as much attention as they have.[105, 111-114]

### 2.4.2.3 Communication through the Central Core

In octupolar materials, it is the conjugation or π-delocalization throughout the entire material which contributes to the cubic nonlinear optical properties. The nature of the ease of electron travel about the entire molecule is important. π-Delocalization and electron rich metal centres bonded in the plane of the molecule are important. The central core also plays a role in the π-delocalization. In compounds **14** and **15**, the central core is a 1,3,5-substituted benzene ring. There is greater communication through a benzene ring between groups in an *ortho-* or *para-* relationship than through groups in a *meta-* relationship.

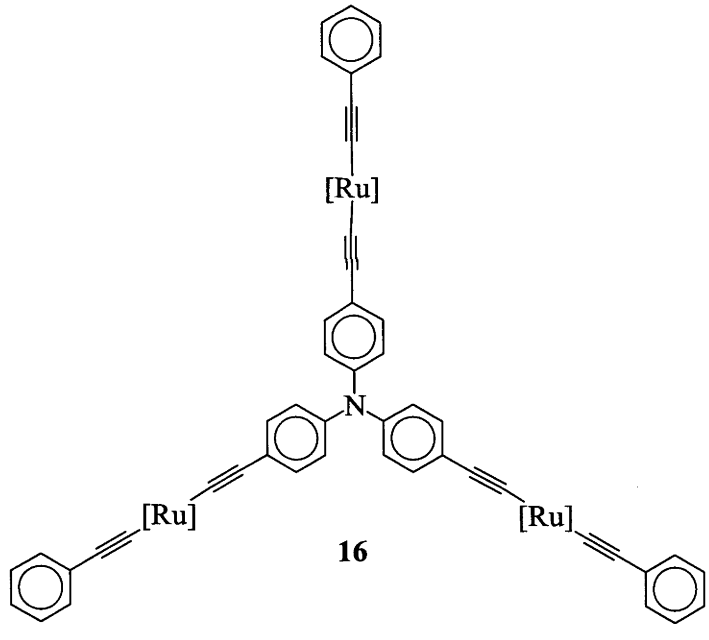


**Figure 2.9** Replacing the core of a dendrimer with a nitrogen atom.

This means that the central ring in the compounds in Figure 2.7 actually has a (comparatively) detrimental effect on the π-delocalization throughout the molecule. The nitrogen-cored compound in Figure 2.9 does not have this problem, but typical

geometry of bonds about a nitrogen atom (due to the lone pair of electrons) would indicate that the arms of the molecule do not all lie in the same plane.[viii]

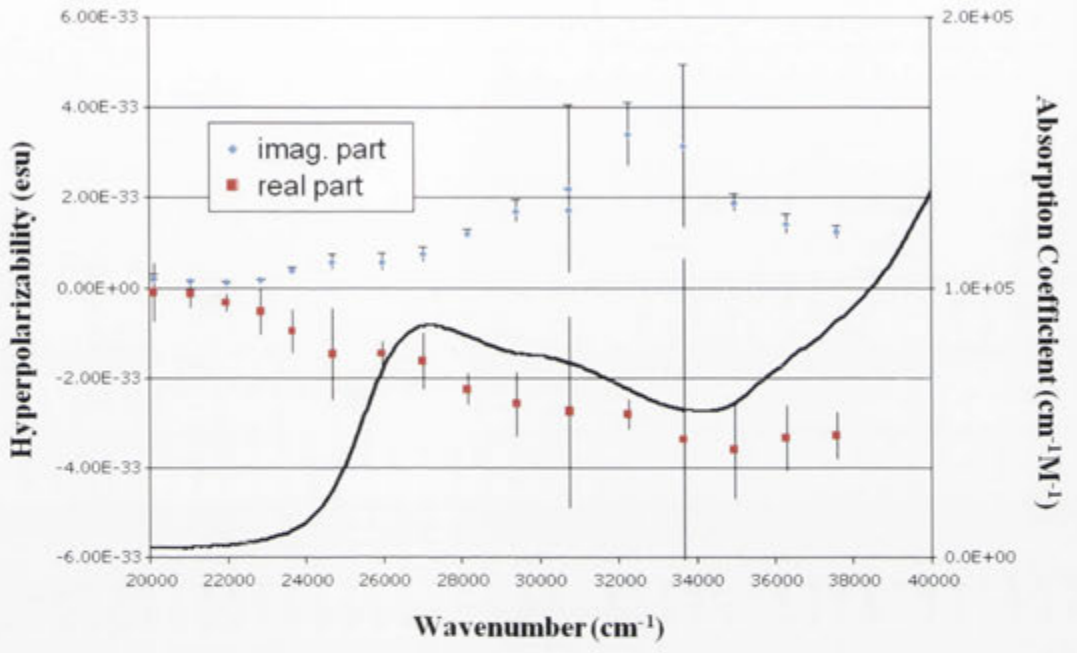


**Figure 2.10** Dispersion of the complex third-order polarizability for an N-cored dendrimer. The black line is the visible absorption spectra. The hyperpolarizabilities are plotted vs. twice the frequency of the laser beam, to allow for comparison.

The nitrogen core molecule (**16**) has weaker NLO responses (γ values) than the corresponding 1,3,5-substituted benzene core molecule (**15**). This would indicate that the loss of planarity results in a reduction in the NLO response of this type of molecule.

Figure 2.10 shows the hyperpolarizability of the compound **16**.[115] When peaks in the imaginary component trace and linear traces align (as plotted in Figure 2.10), it is indicative of the two-photon absorption occurring to the same final states as the ones seen in the standard one-photon absorption spectrum. They do not align very well in this trace (Figure 2.10). This may indicate that the relative contributions of various states to the one-photon and two-photon transitions is markedly different but may also be due to the fact that the origin of the nonlinear absorption is non-standard, perhaps due to contribution from excited state absorption.[53]

[viii] Compound **16** was synthesized by Rachel Roberts, while working in the research group of Mark Humphrey at the Australian National University, Australia.

#### 2.4.2.4 Increasing Dendrimer Size

One very appealing property of organometallic complexes is the 'dendritic effect'. As organometallic dendrimers increase in generation, the magnitude of the NLO response may increases nonlinearly. This means that the first generation dendrimers (meaning that there is one branching point in the 'arms' (dendrons)) in Figure 2.11 and Figure 2.12 would be expected to have a larger than arithmetic increase in the magnitude of the nonlinear response.[ix]

The magnitude of the imaginary and real NLO responses is uniformly greater for these first generation dendrimers than it is for the zero generation dendrimers. Both of the pairings (**14** and **17**, **16** and **18**) have a 1:3 relationship between the number of ruthenium centres in the zero and first generation dendrimers and the first generation analogs have more than three times the NLO response.

Comparing the two-photon absorptions cross section spectra of the ene-linked dendrimers (**14** and **17**), both curves have nonlinear absorbance at 800 nm. The value of $\sigma_2$ for the zero generation molecule is 100 ± 10 GM. The second generation analog has a value of 900 ± 200 GM, almost an order of magnitude increase in NLO response for a threefold increase (in terms of metal centres) in molecular size.[109]

[ix] Compound **17** was synthesized by Chris Jeffery and compound **18** was synthesized by Rachel Roberts, both while working in the research group of Mark Humphrey at the Australian National University, Australia.

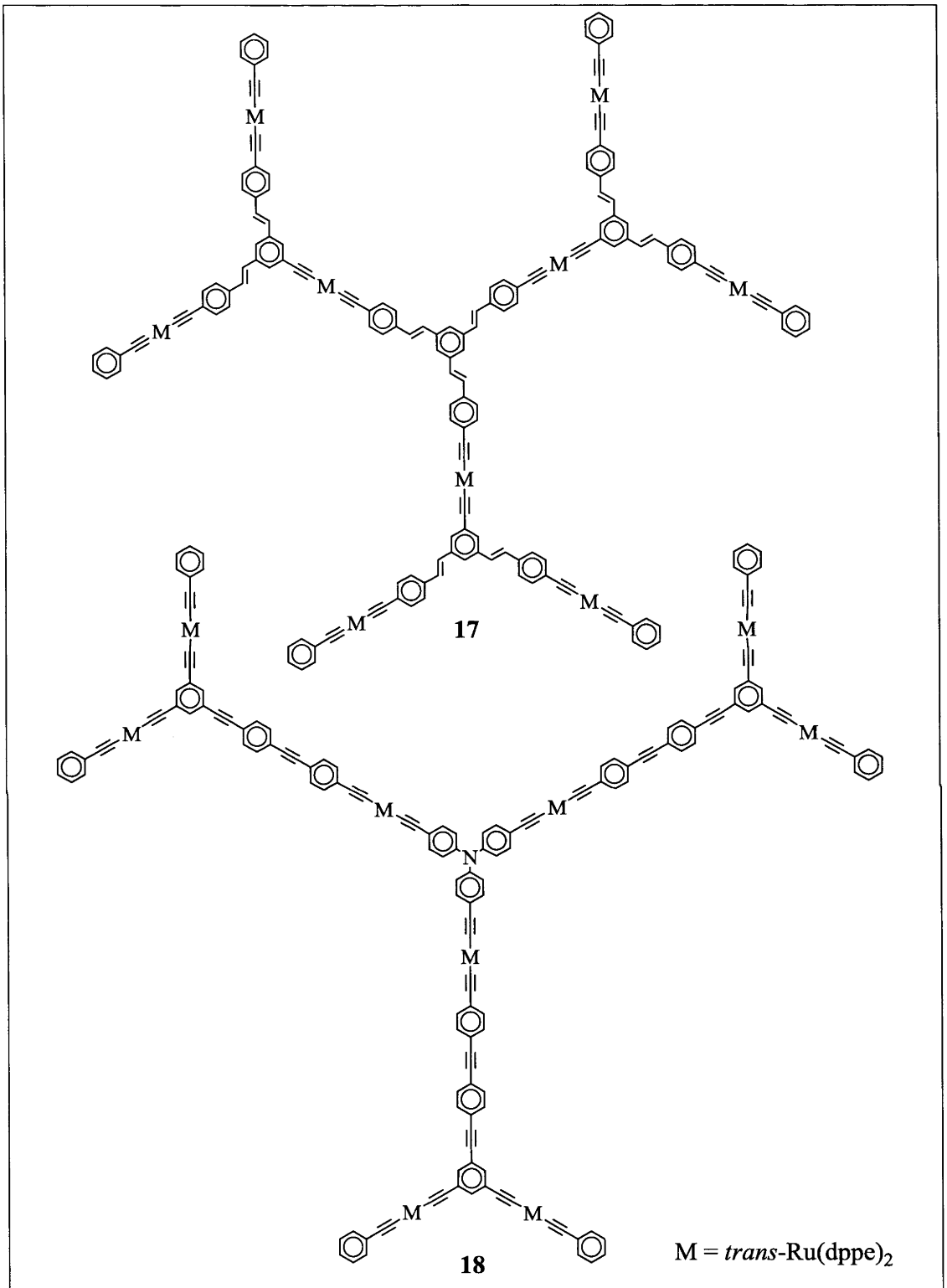


**Figure 2.11** First generation dendrimer analogs of compounds **14** and **16**.

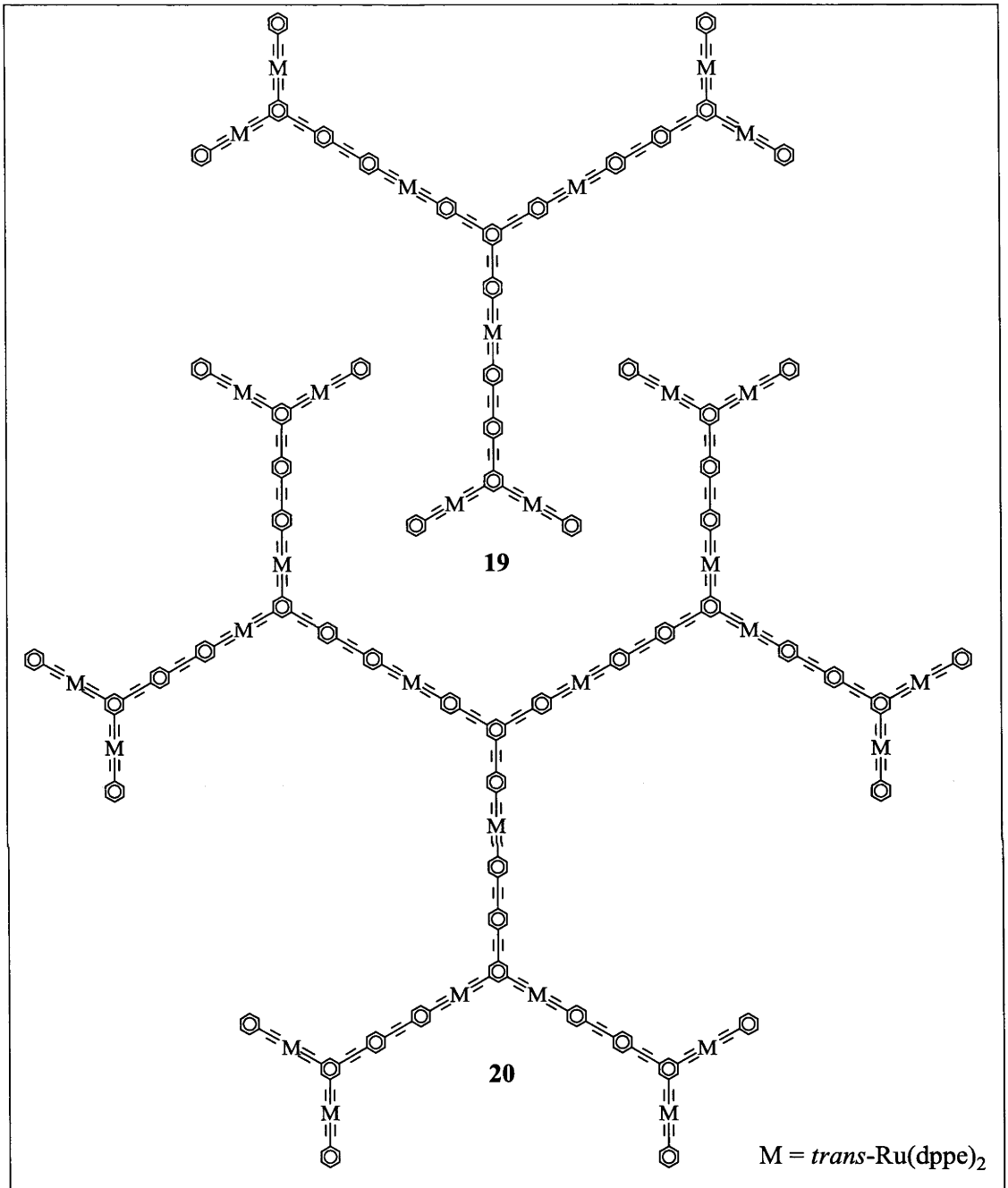


**Figure 2.12** Structures of first and second generation dendrimers.

Figure 2.12 shows a pair of first and second generation dendrimer analogs, synthesized to examine this comparison further (compound **15** is the zero generation analog).[x] The drastic increase in magnitude from compound **15** to compounds **19** and **20** highlight the value of increasing molecular size (Figure 2.13).

[x] Compounds **19** and **20** were synthesized by Katy Green, while working in the research group of Mark Humphrey at the Australian National University, Australia.

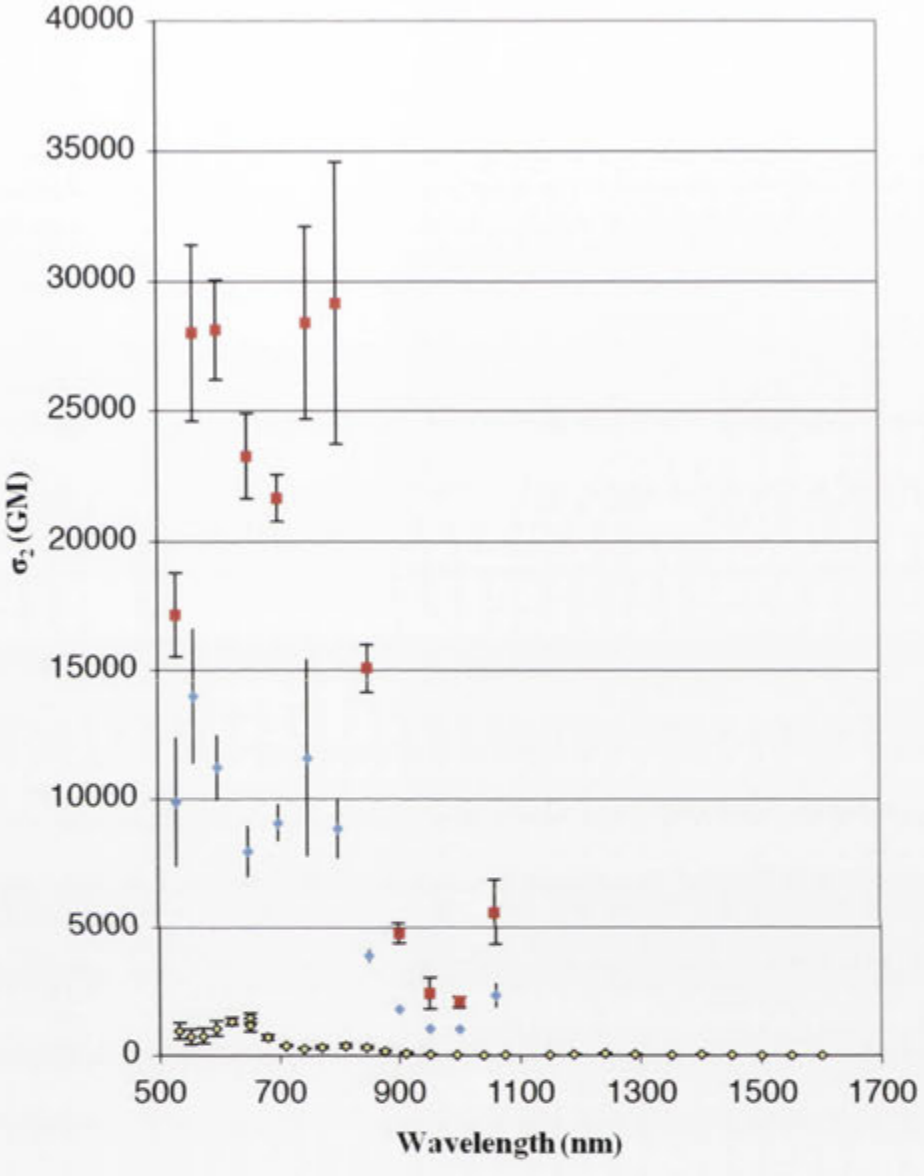


**Figure 2.13** Comparison of the TPA cross sections of compounds **15** (zero gen, yellow diamonds), **19** (1st gen, blue diamonds) and **20** (2nd gen, red squares)

### 2.4.2.5 Varying Capping Groups to Alter Polarity

In addition to varying the core, the linkers and the overall size of the dendrimer, it is also possible to alter the ligands or bonds on terminal ruthenium centres. These changes bring about a change in the electron density of the metal, changing the local polarity within the molecule. This alters the nature of the molecular electric field, which has an impact on both the linear and nonlinear spectra.[25]

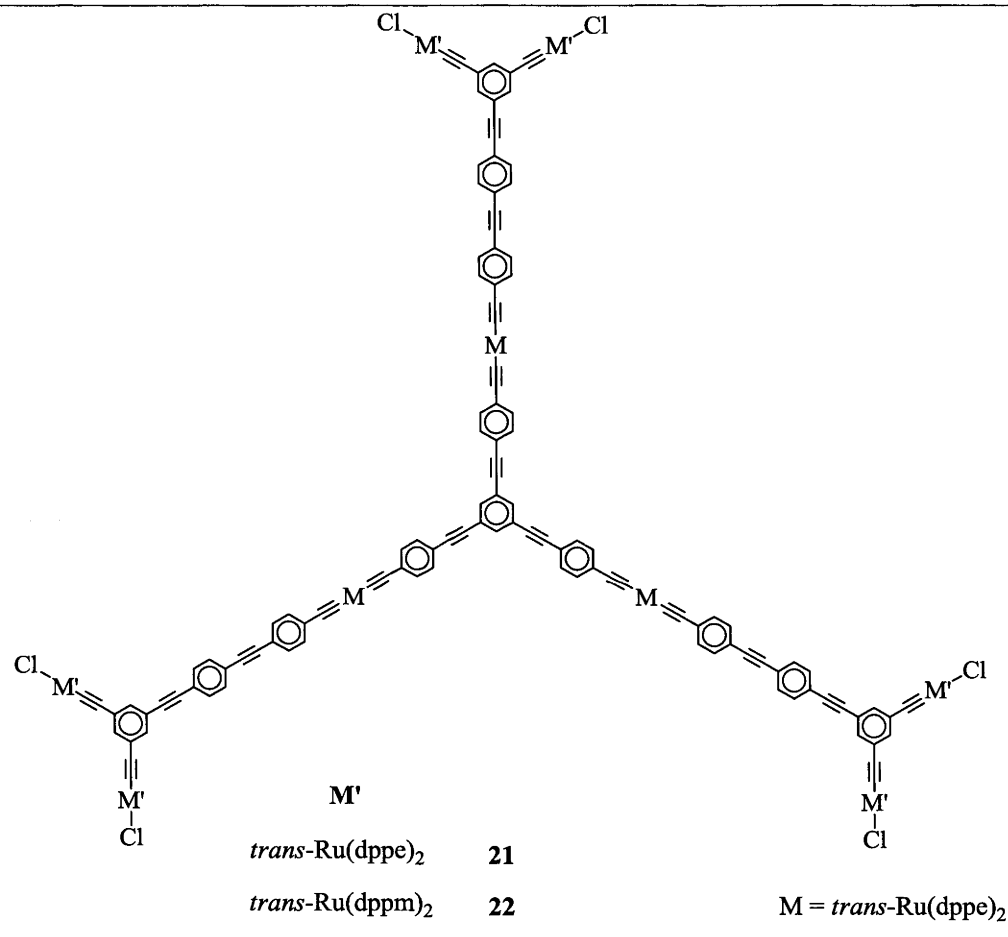


**Figure 2.14** Structures of molecules synthesized to compare dppm vs. dppe ligands in chloro-terminated first generation dendrimers.

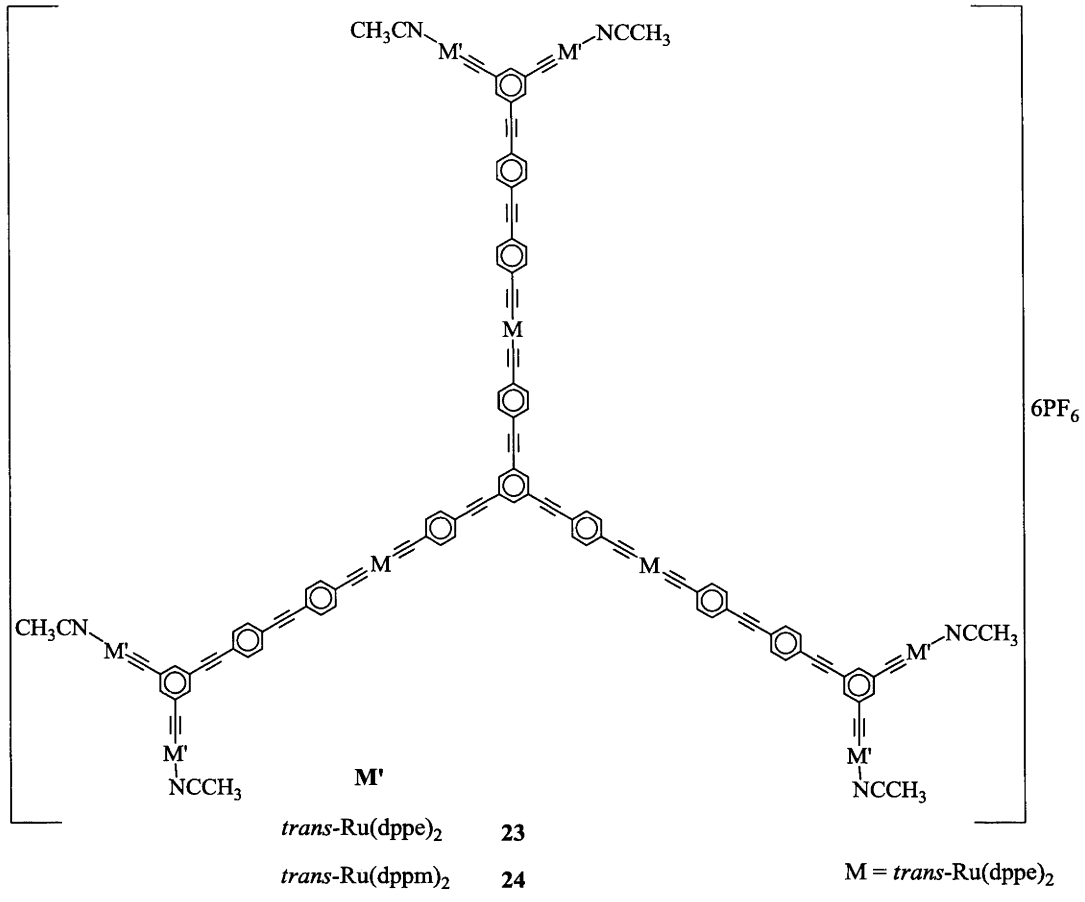


**Figure 2.15** Exchanging the chloride ligand (of compounds **21** and **22**) for an acetonitrile ligand.

Figure 2.14 and Figure 2.15 demonstrate a series of variations of compound **19**. The first is exchanging the phenylacetylide ligand for a chloride bound to the terminal ruthenium (**21**). A variant of this compound is shown as compound **22**, where the 1,2-bis(diphenylphosphino)ethane (dppe) ligands have been replaced with bis(diphenylphosphino)methane (dppm) ligands.[xi] The compounds in Figure 2.15 both have a formal charge of +6, with the chloride ion being replaced by an acetonitrile ligand. The difference between compounds **23** and **24** is also the bidentate ligands (dppe vs. dppm) on the peripheral metal centres, as with compounds **21** and **22**.

[xi] Compound **21** was synthesized by Katy Green, while compounds **22-24** were synthesized by Mark Jennaway, both while working in the research lab of Mark Humphrey at the Australian National University, ANU.

Comparing between the chloro- and phenylacetylide ligands (compounds **21** and **19**, respectively) there is very little change at all in either the linear or nonlinear spectra. It appears that molecule's response is not altered significantly by this ligand exchange.[116] There is a change when moving from the dppe ligands to the dppm ligands. Compound **22** has considerably higher two-photon absorption between 500 and 700 nm than compound **21**. This is accompanied by a reduction in the magnitude of the self defocussing ability of the molecule at these wavelengths. The other regions of the spectra remain identical to each other, within experimental error.

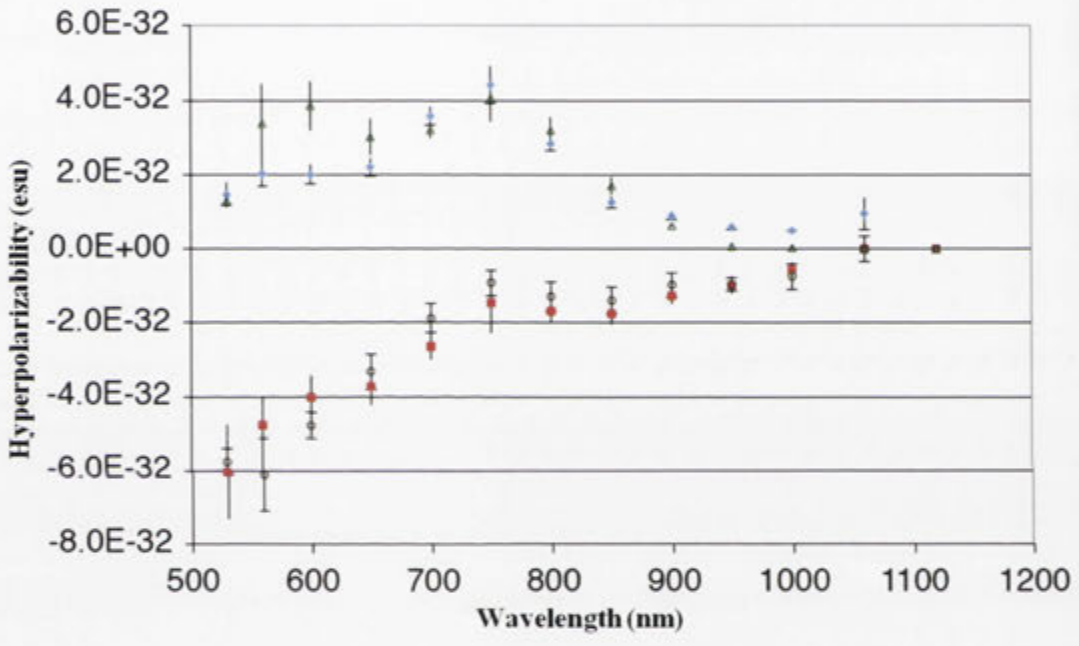


**Figure 2.16** Comparison of the hyperpolarizabilities of compounds **21** (blue diamonds and red squares) and **23** (green triangles and black circles)

It is possible to exchange the chloride ligand for an acetonitrile ligand by boiling the chloro-terminated material in MeCN, creating a charged compound. This change in charge of the molecule has little effect on the NLO response of the compounds (Figure 2.16).

## 2.5 Switching Cubic NLO Properties

Switching of nonlinear responses is perhaps the greatest strength of organometallic materials. The ability of a metal centre to undergo redox processes without the molecule decomposing is an excellent method of altering the distribution of charge and electron density about a molecule. Much more quickly than the change discussed above (chloride to acetonitrile), the oxidation of a ruthenium centre creates a positively charged species, with very differently polarized internal dipoles.

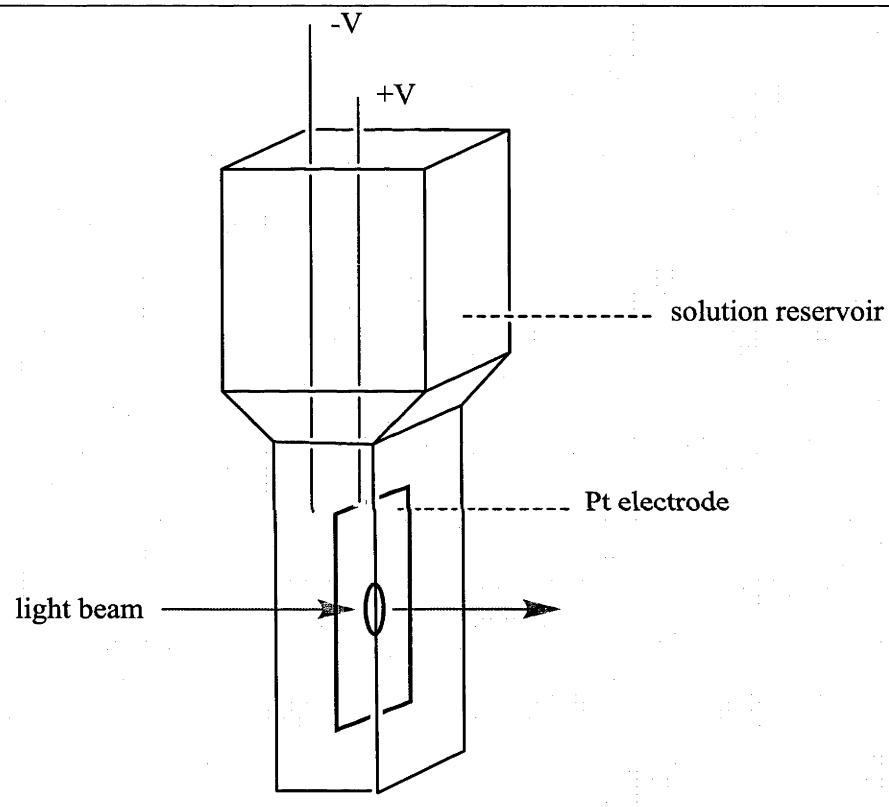


**Figure 2.17** A schematic of the OTTLE cell used for electrochemical switching experiments.[72]

An optically transparent thin layer electrochemistry (OTTLE) cell is used to perform oxidation and reduction Z-scan experiments (Figure 2.17). The beam is aligned through the hole in the electrode plate such that the changes in intensity passing through the hole are related exclusively to the beam geometry and not the shape of the aperture. The beam should not be cropped by the aperture at all positions of the sample as the travelling stage with the cell is scanned along the Z axis. This alignment can be difficult, particularly at longer wavelengths which are invisible to the naked eye.

### 2.5.1 Switching Mixed Metal Compounds

The relative ease of redox switching (compared to chemical switching) makes the potential of electrochemical switching very exciting and adds to the possibilities available to organometallic compounds.[85, 117] Incorporation of diverse metal centres with different oxidation potentials make it possible to switch between more than two states, as demonstrated previously.[106, 118-120] Compounds in Figure 2.18 were designed to examine this hypothesis.[xii]

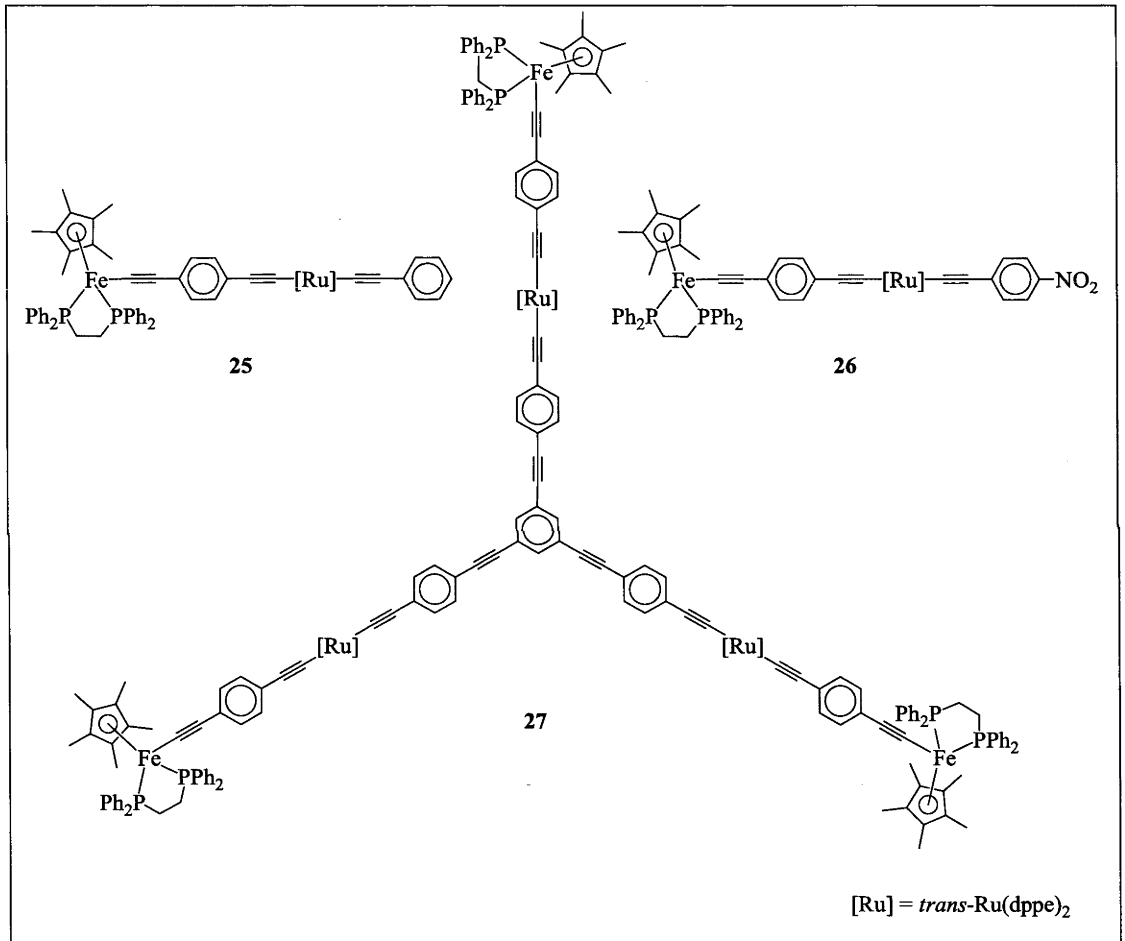


**Figure 2.18** Structures of iron-ruthenium compounds for electrochemical switching.

[xii] The three compounds in Figure 2.18 were synthesized by Nicolas Gauthier while working in the research group of Frederic Paul at the University of Rennes, France.

The nonlinear properties of the compounds were measured at 750 nm and 1250 nm and it was found that the compounds all behaved similarly to each other (Table 2.2). At 750 nm, all of the compounds switch from being two-photon absorbers to saturable absorbers when a potential of +0.6 V is applied. At 1250 nm, the compounds are saturable absorbers in the resting state and become (weak) nonlinear absorbers when a potential of -0.6 V is applied. Although the compounds have only two states (not three) at each wavelength, going from 750 nm to 1250 nm in the ground state also cause them to change character, from nonlinear absorbers to saturable absorbers. The effect of increased size and symmetry (together) is also demonstrated here, with the larger, octupolar compound **27** having stronger responses in all cases.

**Table 2.2** Two-photon absorption cross section values of compounds **25** to **27**

| **Wavelength (nm) / Potential (V)** | **Cmpd 25 $\sigma_2$ (GM)** | **Cmpd 26 $\sigma_2$ (GM)** | **Cmpd 27 $\sigma_2$ (GM)** |
|---|---|---|---|
| **750 / -0.6** | 710 | 1420 | 9500 |
| **750 / 0.0** | 1200 | 2150 | 6200 |
| **750 / 0.6** | -260 | -1300 | -29000 |
| **1250 / -0.6** | 150 | 320 | 650 |
| **1250 / 0.0** | -1900 | -1100 | -2500 |
| **1250 / 0.6** | – | -2500 | -9200 |

### 2.5.2 Optically Switching a Ruthenium Acetylide

The search continues to find materials where the nonlinear optical properties can be switched with enough reversible stability for incorporation into devices. This elegant compound (Figure 2.19) was created in order to determine if multiple switching scenarios can be incorporated into a single molecule.[xiii]

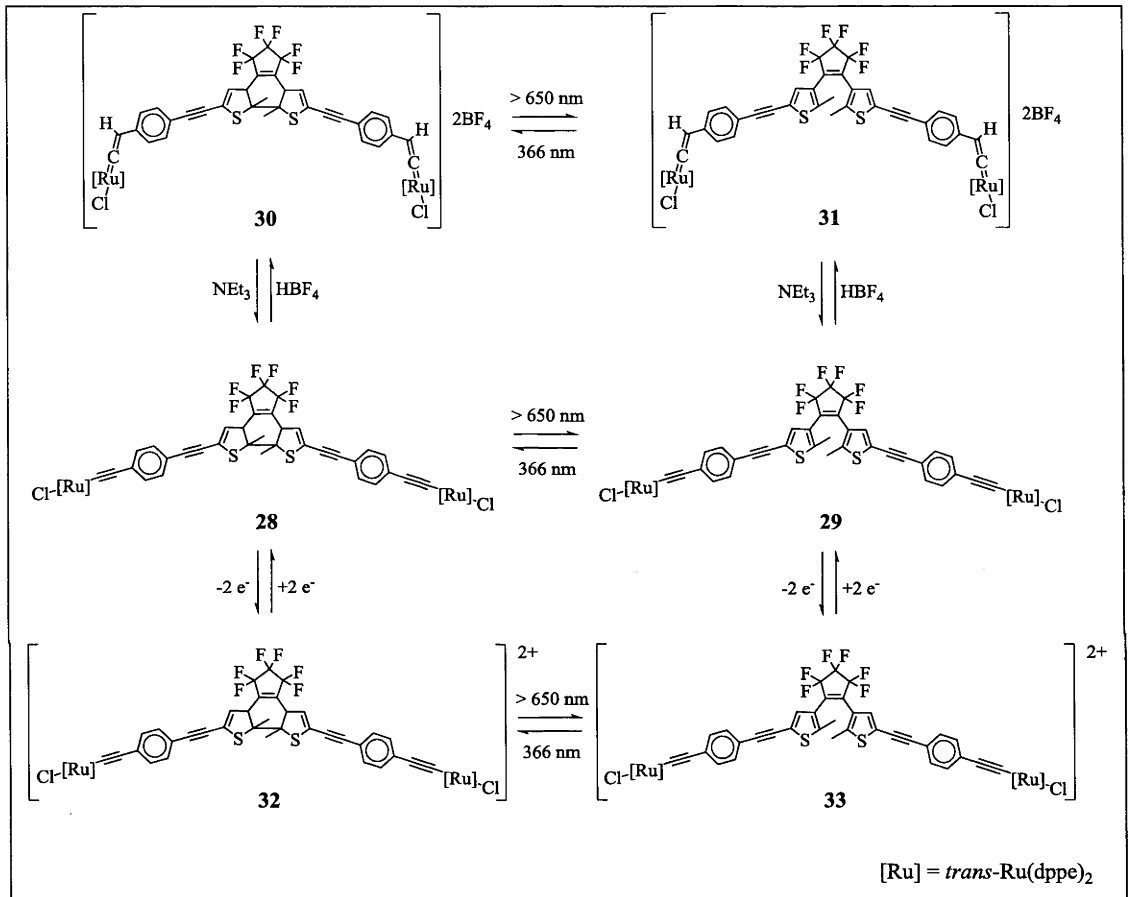


**Figure 2.19** A ruthenium acetylide with six switchable states. The arrows show the conditions required to convert between states (not equilibria).

The compound may be interconverted between six states through three switching modes.[121] Halochromic switching allows for the conversion of the acetylide moiety to a vinylidene (**27** to **29** and **28**-**30**) and back. Reversible electrochromic switching is only possible on the acetylide compounds (**27** and **28**, oxidizing them to **31** and **32**, respectively) because the oxidized versions of the vinylidene compounds are not stable

[xiii] This compound (**27**-**32**) was synthesized by Katy Green while working in the research group of Mark Humphrey, at the Australian National University, Australia.

in the beam of the laser. The final switch is an optic switch, with red light opening the 5,5′-dithienylperflurocyclopentene (DTE) unit and UV light closing it again.[122]

This optical switching is particularly interesting because it affects the degree of π-delocalization through the molecule. When the DTE unit is in the closed position (**28** and **30**), the compound acts as a strong nonlinear absorber across most wavelengths (800 to 1600 nm). When subjected to red light (converting to **29** and **31**), this communication is reduced and the NLA property is effectively 'switched off'.[121]

The oxidative switching process also shows promise. In the wavelength range from approximately 700 to 1000 nm, the ground state compounds (**27** and **28**) are nonlinear absorbers. When oxidized, the character of the absorption property changes, and the compound becomes a saturable absorber (**32** and **33**). The protic switch (acetylide to vinylidene) has a slight reduction in the magnitude of the NLA property, but is not as defined a switching process as the other two switching modes.

## 2.6 Conclusions

Z-scan is a powerful and relatively simple technique for the measurement of nonlinear optical properties of molecules in solutions. It allows the determination of the cubic hyperpolarizability ($\gamma$) of the solute. Since $\gamma$ is complex this means that actually the refractive ($\gamma_{real}$) and absorptive ($\gamma_{imag}$) components are both determined. The sign of these components is also determinable, allowing for differentiation between focussing and defocussing as well as between nonlinear absorbers and saturable absorbers.

Considerably more information is available through the measurement of the compounds at not just one or two discrete wavelengths but across a broad spectrum of wavelengths. The change in character of the nonlinearity of a compound at different wavelengths is often pronounced. This is of particular importance when compounds are being devised with the intention of switching the nonlinear properties. The difficulty with wavelength dependence measurements is that they are very time consuming. Development of techniques such as 'white light continuum Z-scan' (which can measure a broad spectrum of wavelengths at the same time) will drastically reduce the time it takes to obtain NLO spectra. Hopefully, this will cause an increase in the number of NLO spectra of materials and further facilitate the discovery of materials with device-applicable levels of cubic nonlinearity.[122-124]

## 2.7 Experimental

**Materials.** All measured compounds were obtained in crystalline form from the researchers credited. Solvents were obtained commercially, dried and distilled prior to use. The electrolyte $(NBu^n_4)PF_6$ was purchased commercially (Sigma-Aldrich) and recrystallized prior to use.

**Methods and Instrumentation.** Solutions were prepared in air or in a glove box under an $N_2$ atmosphere, where necessary. The solutions were loaded into 1 mm path length Starna glass cells, stoppered and sealed with Teflon tape. The exception to this is the electrochemical solutions, which were prepared differently and measured in 0.5 mm path length OTTLE cells.

The light source was a Clark-MXR CPA-2001 regenerative amplifier pumping a Light Conversion TOPAS optical parametric amplifier. Pulse length was 150 fs (FWHM)

with a repetition rate of 250 Hz. Wavelength ranges used were 530 nm to 1600 nm. The OPA was tuned appropriately and one of four modes of output were selected: second harmonic of the idler, second harmonic of the signal, idler-pump mixing or the signal. Unwanted wavelength components of the beam emitted from the TOPAS were filtered out using polarizing filters, coloured glass filters and spatial filtering.

As previously mentioned, data for single wavelength measurements were obtained using a concentration dependence method, while multiple wavelength measurements were carried out using identical cells containing solvent (or electrolyte solution) as references. A piece of 3 mm silica glass was used for calibration and all measurements were referenced to this, using the rough approximation for $n_{2,silica}$ of $3 \times 10^{-16}$ $cm^2/W$ or the more accurate (wavelength dependent) approximation derived basing on data compiled by Milam:[125]

Eq. 2.3 $$n_{2,silica}(\nu) = 2.82 \times 10^{-16} - 3 \times 10^{-21}\nu + 2 \times 10^{-25}\nu^2$$

where $n_2$ is in $cm^2/W$ and $\nu$ is the wavenumber in $cm^{-1}$. This precluded the need for detailed information about beam geometry and pulse shape. Errors were estimated from the assessed accuracies from the Z-scan fitting parameters and the corresponding solvent scans.

Pulse energy of the laser was adjusted to approximately 1 μJ using neutral density filters. In typical measurements this gave $\Delta\Phi_0$ values between 0.4 and 1 rad. Care was taken after each measurement to ensure that this was the case. If it was not, the power was adjusted, the sample was rerun and the silica reference was also run again. This ensured that the calibration was as accurate as possible for each measurement.

Solutions for electrochemical switching were prepared under argon, loaded into an OTTLE cell and sealed. Electrochemical solutions were prepared at the start of each testing day, to prevent electrochemical decomposition. The supporting electrolyte was approximately 0.5 M $(NBu^n_4)PF_6$ in distilled, deoxygenated (argon) $CH_2Cl_2$. Electrochemical switching measurements were obtained using a MacLab potentiostat from eDAQ Pty Ltd. Measurements were carried out using Pt disc working-, Pt wire auxiliary- and Ag/AgCl reference electrodes.

Optical switching was carried out in the Teflon sealed 1 mm Starna cells. The cell was placed under a UV lamp for 30 minutes, to ensure complete closing of the 5,5'-

dithienylperflurocyclopentene (DTE) switch. Opening of the switch was originally carried out using a red 'party bulb', obtained at the local Dollar Store™, but it was found that a 100 W white light bulb filtered by 10-15 layers of red cellophane for a period not less than 2 hours facilitated a more complete opening of the DTE switch. Care had to be taken that the heat generated by the bulb over long periods of time did not cause the solution to heat up as well. A fan was employed to continually cool the cell as switching was effected.

**Single Wavelength Measurement of Compounds 2-7.** All compounds were used as received and the solutions were prepared in air. The solvent in every case was distilled, deoxygenated dichloromethane and all measurements were taken at 750 nm. Concentrations used (w/w%) are outlined in Table 2.3.

**Table 2.3** Concentrations of solutions for measurement of Ru-Re complexes.

| Compound | Conc 1 (w/w%) | Conc 2 (w/w%) | Conc 3 (w/w%) |
|---|---|---|---|
| **2** | 2.199 | 1.121 | 0.571 |
| **3** | 2.001 | 1.082 | 0.520 |
| **4** | 2.679 | 1.497 | 0.685 |
| **5** | 1.910 | 1.013 | 0.473 |
| **6** | 1.769 | 0.978 | 0.468 |
| **7** | 1.717 | 0.961 | 0.534 |

**Wavelength Dependence of Compound 8.** This compound was measured in N,N-dimethylformamide. 0.00562 g of $[Ni(\mu\text{-}SBu^t)(\mu\text{-}etet)]_{12}$ was dissolved in 1.5047 g of distilled, deoxygenated DMF in a glove box, under a nitrogen atmosphere. The resulting (0.373 w/w%) solution was sealed in a Starna glass cell and measured as outlined above.

**Wavelength Dependences of Compounds 9-24.** The compounds were all measured in dichloromethane. The samples for measurement were all prepared in air, using distilled, deoxygenated dichloromethane, sealed in a Starna cell and measured as outlined above. The concentrations used are outlined in Table 2.4.

**Table 2.4** Solution concentrations for wavelength dependence measurements.

| Compound | Conc (w/w%) |
|---|---|
| **9** | 1.253 |
| **10** | 0.971 |
| **11** | 0.834 |
| **12** | 0.953 |
| **13** | 0.801 |
| **14** | 1.400 |
| **15** | 0.971 |
| **16** | 1.697 |
| **17** | 1.161 |
| **18** | 0.504 |
| **19** | 0.767 |
| **20** | 0.257 |
| **21** | 1.126 |
| **22** | 0.527 |
| **23** | 0.590 |
| **24** | 0.837 |

**Two-Wavelength Switching of Compounds 25-27.** The compounds were all measured in dichloromethane. The solvent was distilled and vigorously degassed with argon prior to use. The electrolyte solution was prepared first (0.5 M). The compound was then dissolved into solution and transferred into a sealing OTTLE cell, all under argon. Argon techniques were used as the iron is very prone to oxidative decomposition. Samples were made at the beginning of each day, and not reused, as a precaution against deterioration. Concentration dependence measurements were performed on the three compounds at 750 nm, prior to redox experiments (Table 2.5).

**Table 2.5** Iron-ruthenium solution concentrations.

| Compound | Conc 1 (w/w%) | Conc 2 (w/w%) | Conc 3 (w/w%) |
|---|---|---|---|
| **25** | 1.053 | 0.649 | 0.324 |
| **26** | 0.865 | 0.488 | 0.202 |
| **27** | 1.191 | 0.634 | 0.306 |

Redox switching was performed at 750 nm and 1250 nm. Concentrations of the successful runs are reported in Table 2.6.

**Table 2.6** Iron-ruthenium solution concentrations for redox switching experiments.

| Compound | Conc at 750 nm (w/w%) | Conc at 1250 nm (w/w%) |
|---|---|---|
| **25** | 1.064 | 1.045 |
| **26** | 0.442 | 0.204 |
| **27** | 0.310 | 0.208 |

**Wavelength Dependence Switching of Compounds 28-33.** Compounds were measured in distilled, deoxygenated dichloromethane. Solutions for oxidative switching were prepared under argon. Solutions for optical switching were prepared under nitrogen. As with compounds **25** to **27**, above, the ground state compounds (**28** and **30**) were measured first using the concentration dependence method at 1200 nm (Table 2.7).

**Table 2.7** Concentrations for measurement of the DTE compound.

| Compound | Conc 1 (w/w%) | Conc 2 (w/w%) | Conc 3 (w/w%) |
|---|---|---|---|
| **28** | 0.790 | 0.385 | 0.198 |
| **30** | 0.873 | 0.469 | 0.222 |

Solutions were then prepared for wavelength dependence measurements. Two cells were filled with 2.250 w/w% solutions of compound **28**. Two other cells were filled with 1.899 w/w% solutions of compound **30**. One of each of these cells was subjected to red-filtered light, converting the molecules in solution to **29** and **31**, respectively. Throughout the wavelength dependence process, these cells were continually subjected to either red-filtered light or ultraviolet light to maintain the molecular configuration.

For the measurements of the oxidized compounds (**32** and **33**), solutions of the ground state compound were made (0.213 w/w% for **28** and 0.271 w/w% for **29**) and loaded into the OTTLE cell. The compound was oxidized while in the path of the laser beam (to measure when oxidation was complete) and a measurement taken. Then the wavelength was adjusted and another measurement taken. This process continued until a full set of wavelengths had been measured.

# Tuning Nonlinear Optical Properties by Altering End-group Polarity

## 3.1 Introduction

The addition of a functional group in the *para-* position of phenylacetylene units bound to ruthenium atoms makes it is possible to alter the electron density of the ligating aromatic ring. Due to π-delocalization, the change in electron density will propagate through the molecule, which will change the molecular polarity in both the ground and excited states. This will alter the NLO properties of the compound.

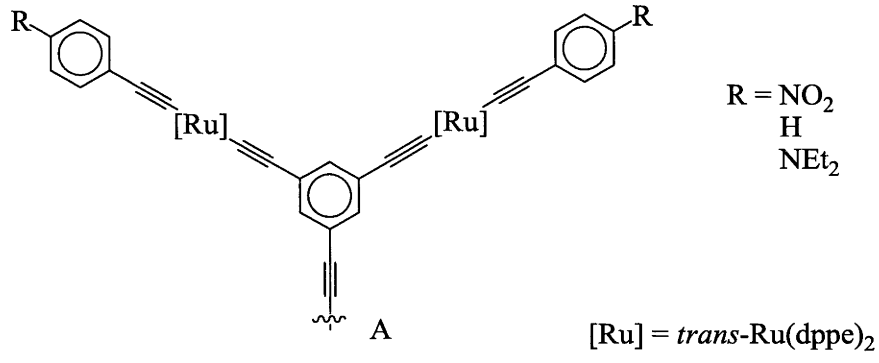


**Figure 3.1** The structure of 'wedge-shaped' dendrimer precursors designed to have altered polarity.

Incorporating electron withdrawing ($NO_2$) and electron donating ($NEt_2$) groups on the terminal branching unit (wedge) of a dendrimer (Figure 3.1) alters the electron density distribution in the molecule and the energetic structure of its excited states.[65, 126, 127] Comparing the changes in the linear and nonlinear optical spectra will demonstrate the degree of control achievable over these optical properties.

The geometry of the wedge molecules reduces the overall dipole due to vector cancellation (opposing portions negate each other). For quadratic NLO studies, substituted phenylacetylene moieties were added to the molecules at position A, to further alter the molecular dipole.

Cubic NLO properties are favorably influenced in structures that are centrosymmetric and have quadrupolar distribution of charges. In order to achieve such structures, the wedges were homocoupled (at position A), making centrosymmetric, quadrupolar compounds. The nonlinear responses for both sets of compounds were measured, determining the degree to which the altered charge distribution symmetry affects the NLO properties of ruthenium alkynyl complexes.

### 3.1.1 Synthetic Tools

The synthesis of compounds presented relies heavily upon a few, crucial reactions. Compounds with terminal alkynes are formed by the reaction of silyl-protected acetylenes (trimethylsilylacetylene or triisopropylsilylacetylene) with aryl halides (see Section 3.1.1.1). The protecting silyl moiety is removed later in the synthetic process, immediately prior to the reaction of the alkynyl group it is protecting.

Two different protecting groups are used, triisopropylsilyl (TIPS) and trimethylsilyl (TMS). Selective removal of TMS groups (with potassium carbonate), keeping TIPS protecting groups in place, allows for greater design flexibility. TIPS moieties are removed using tetra-*n*-butylammonium fluoride (tBAF). The metal centre used in the formation of the metal-containing compounds described in this chapter is *cis*-$RuCl_2(dppe)_2$.[128]

#### 3.1.1.1 Sonogashira Coupling Reaction

The most frequently used reaction in this work is the hetero-coupling of a terminal alkyne and an aryl halide to form an arylacetylene. This reaction (commonly referred to as the Sonogashira reaction) is one of the most valuable tools in acetylenic chemistry.[129, 130] The Sonogashira coupling is catalyzed by a $Pd^0$ complex, which binds the aryl halide in an oxidative addition reaction (Figure 3.2). Transmetallation between a cuprous acetylide and the palladium complex followed by reductive elimination produces an arylacetylene and regenerates the palladium centre. Most frequently, a $Pd^{II}$ species is used as a catalyst ($PdCl_2(PPh_3)_2$) with a cuprous halide as a co-catalyst. This requires the formation of a catalytic amount of homocoupled material, to initially reduce the $Pd^{II}$ to $Pd^0$, activating the catalyst.

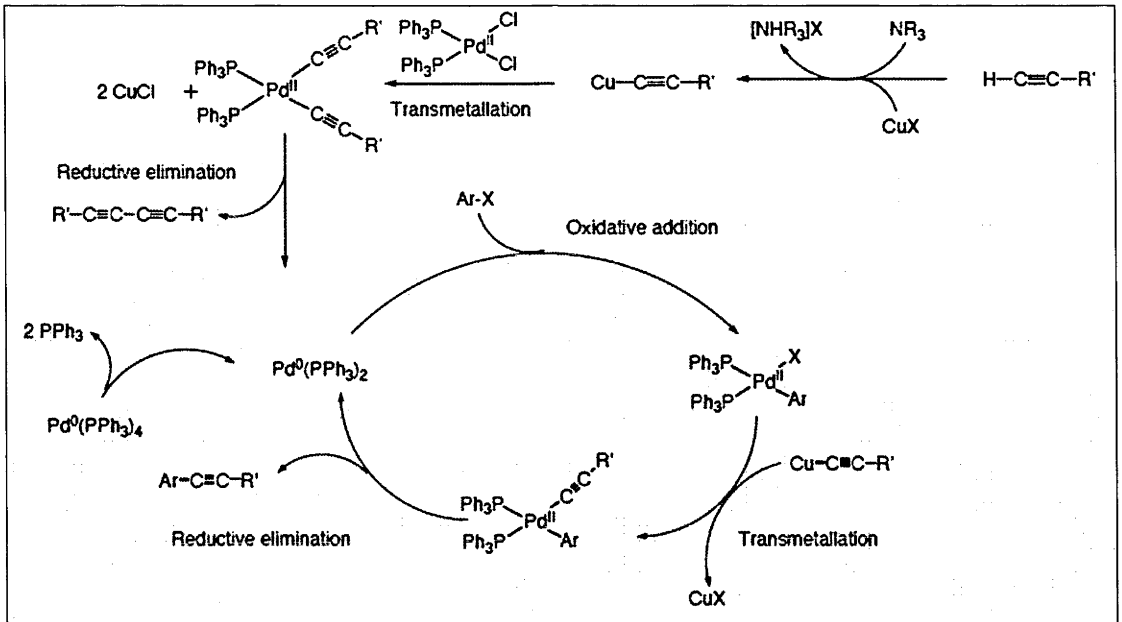


**Figure 3.2** The Sonogashira coupling mechanism.[131]

In cases where this homocoupled material may be difficult to remove, a $Pd^0$ catalyst may be used instead (at greater expense). There is always the danger of oxidation degrading the catalyst, resulting in the formation of greater amounts of homocoupled material as the catalyst is regenerated. It is possible to reduce this by flooding the reaction vessel with hydrogen gas, which helps to prevent the oxidation of the catalyst that leads to homocoupling.[132] Homocoupling (if desired) is facilitated by the addition of an oxidizing agent ($O_2$, $X_2$, etc.) to the catalyst system, as an alternative to the copper catalyzed Glaser-type coupling methods.[133]

### 3.1.1.2 Metal-acetylide Coupling

Ruthenium acetylides are formed through the coupling of arylacetylenes with *cis*-$RuCl_2(dppe)_2$.[134] This reaction proceeds through a vinylidene intermediate, which may be isolated and characterized. Reactions are typically carried out in chlorinated solvents at room temperature, making this a very facile synthesis (Scheme 3.1). The addition of a weak base (amine) abstracts the vinylidene proton and completes the formation of the acetylide.

**Scheme 3.1**[134]

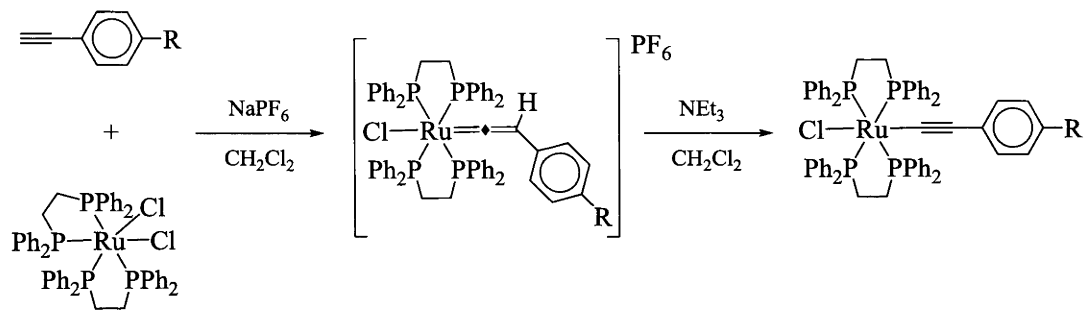


The conformation of the metal complex is important; *trans*-$RuCl_2(dppe)_2$ is unreactive. The metal centre adopts the *trans* configuration as the complex is formed. By heating the mono-acetylide with an excess of a second arylacetylene, the remaining chloride ligand can be replaced, forming a bis-acetylide.

The reaction of *cis*-$RuCl_2(dppe)_2$ with 1,3,5-triethynylbenzene yields only the bis-substituted product (Scheme 3.2).[59] This is due to steric hindrance about the central aromatic ring, the $RuCl(dppe)_2$ moieties are too sterically bulky to allow for threefold substitution. This 'steric control' is synthetically valuable because it is a single-step method of forming a branching point for dendrimer synthesis. From compound **34**, it is possible to perform stepwise metal-acetylide and Sonogashira couplings to build dendrons (dendrimers arms) that may be coupled to a central core to form a dendrimer.[xiv]

[xiv] This assumes the 'convergent synthesis' approach. For information regarding convergent and divergent dendrimer synthesis, the reader is directed towards the following literature.[136-138]

**Scheme 3.2**[59]

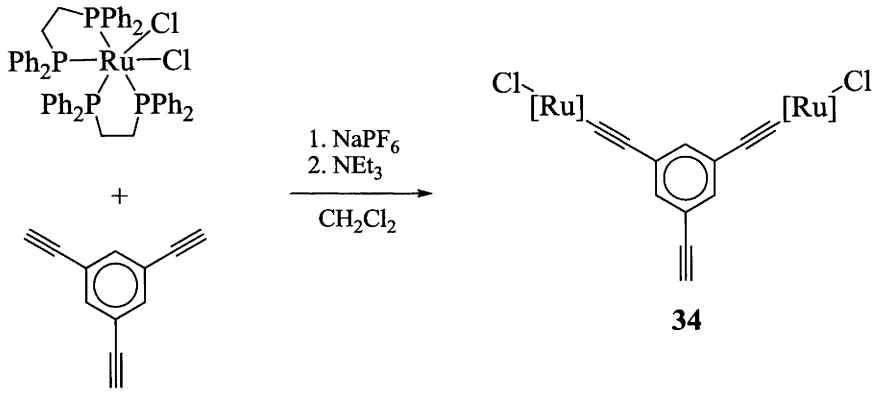


**34**

[Ru] = *trans*-Ru(dppe)$_2$

The 'wedge' compounds in this chapter are treated as precursors to dendrimers. It is hoped that dendrimers with these wedges incorporated at the outer ring will have comparable properties.

## 3.2 Synthesis

Three different phenylacetylenes were chosen to replace the chloride ligands on the chloro-capped wedge-shaped compound (**34**). Phenylacetylene is available commercially; 4-nitrophenylacetylene [135] and 4-N,N-diethylaminophenylacetylene [136, 137] were prepared through literature procedures (Scheme 3.3). The selection was made in order to have neutral, electron withdrawing and electron donating ligands on the metal centre.

**Scheme 3.3**[136-138]

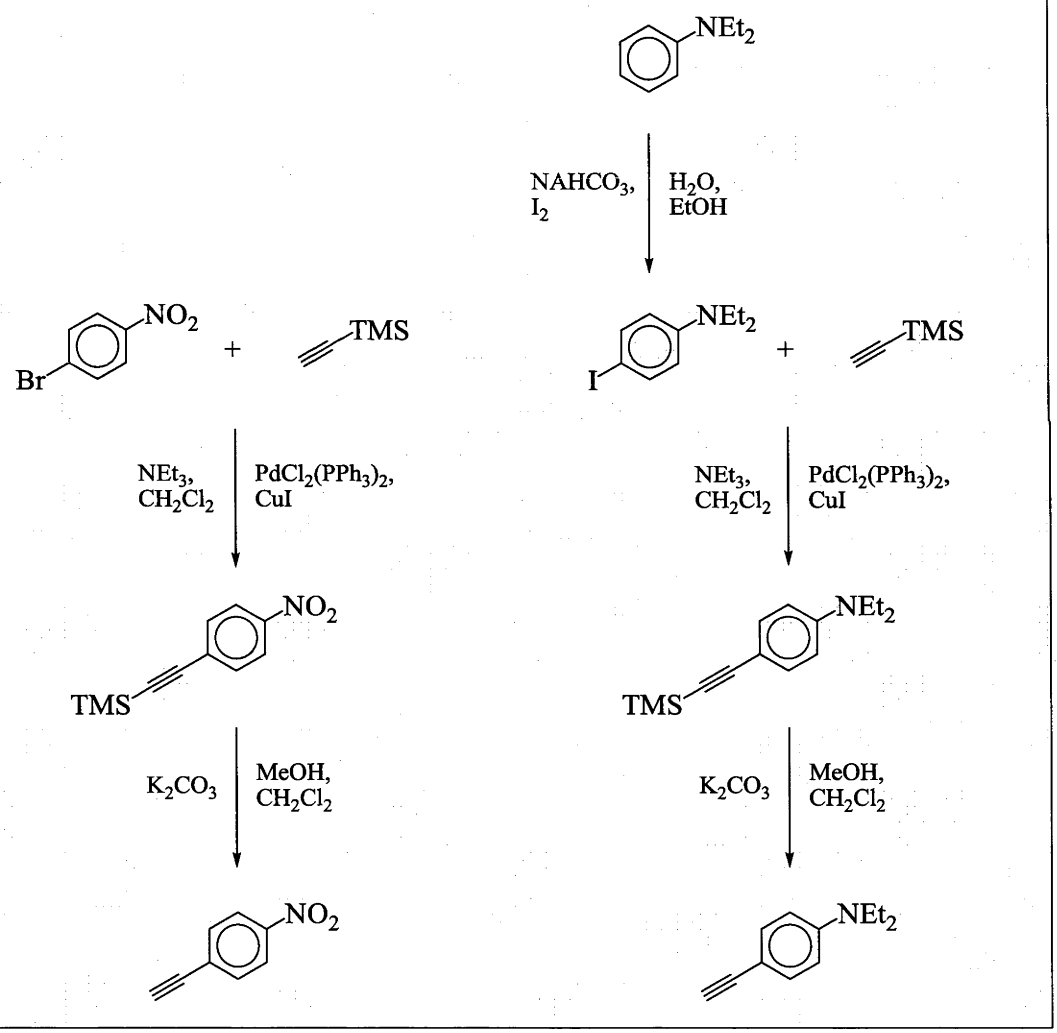


The terminal alkynes were coupled with 1,3-{trans-$[(dppe)_2ClRuC{\equiv}C]\}_2$-5-$C_6H_3C{\equiv}CH$ (**34**) to form three differently terminated 'wedge' complexes (Scheme 3.4).[xv] Formation

[xv] Compounds **35** and **36** had been previously prepared by Steph Hurst and Clem Powell, respectively, and were resynthesized for this work.[65]

of the phenyl (**35**) and diethylaminophenyl (**37**) complexes was straightforward, requiring reflux temperatures for at least twelve hours to proceed to completion (as is normal for bis-acetylide formation).

**Scheme 3.4**

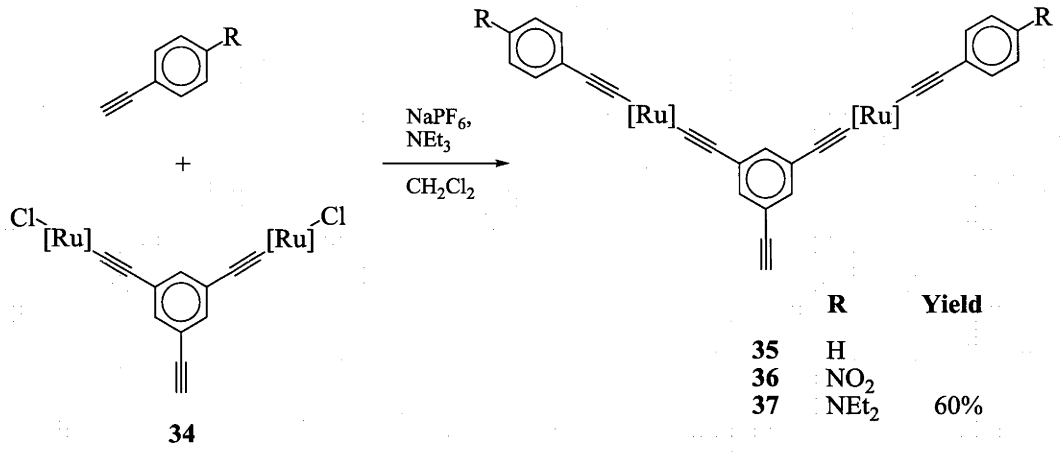


**34**

In contrast, the *p*-nitrophenylacetylene was considerably more reactive towards the ruthenium centre. It was found that compound **36** would form at room temperature. Unfortunately, *p*-nitrophenylacetylene is an active enough ligand to break the pre-existing metal-acetylide bond. Optimal conditions for the reaction were found to be 45 to 75 minutes at reflux. Less than 45 minutes did not allow for complete addition of the terminal alkyne; more than 75 minutes led to the formation of an unknown byproduct, based on $^{31}$P NMR shifts (Table 3.1). Room temperature reactions led to the formation of the possible 'bis-nitro' species prior to complete formation of the intended product.

**Table 3.1** $^{31}$P NMR shifts of ruthenium acetylides with different terminal ligands.

| Compound | Ligand | $^{31}$P (ppm) |
|---|---|---|
| **34** | -Cl | 49.9 |
| **35** | $-C{\equiv}CC_6H_5$ | 54.4 |
| **36** | $-C{\equiv}CC_6H_4NO_2$ | 53.3 |
| **37** | $-C{\equiv}CC_6H_4NEt_2$ | 54.7 |

The synthesis of the mono- and bisacetylides was confirmed by $^{31}P$ NMR. The $^{31}P$ atoms resonate at 49.9 ppm for compound **34**. Formation of bis-acetylides causes the $^{31}P$ resonances to shift downfield. The withdrawing or donating character of the terminal moiety caused the $^{31}P$ atoms to become more deshielded or shielded.

The synthesis of the polar wedges was completed by the addition (by Sonogashira reaction) of an aryl halide to the remaining terminal alkyne of compounds **35** – **37**. 4-bromotoluene was chosen to test reaction conditions as the methyl protons could be used as an NMR marker: the presence of methyl protons in the $^{1}H$ NMR spectrum would indicate reaction success.

**Scheme 3.5**

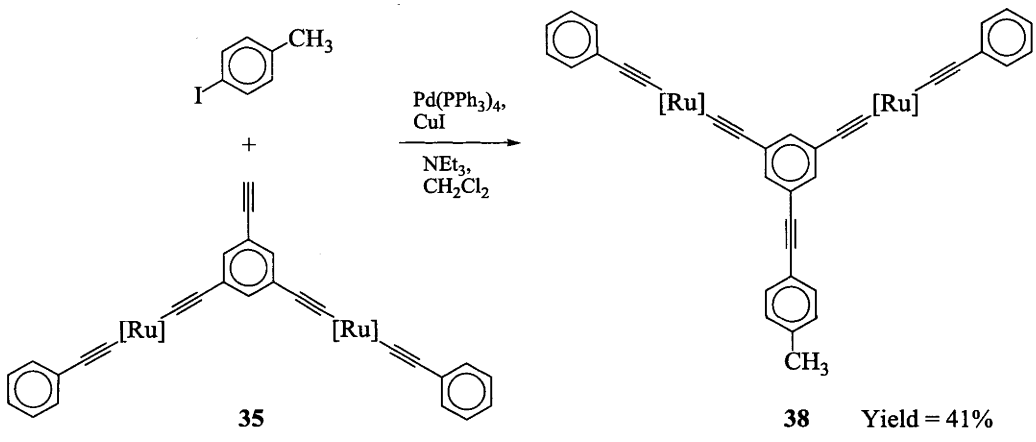


Conditions could not be found to react aryl bromides with compounds **35** – **37**. Aryl iodides are much more reactive under Sonogashira conditions, with the iodine acting as a better leaving group.[135] 4-Iodotoluene was found to be a suitable reagent (Scheme 3.5), giving the desired product with the methyl protons resonating at 2.42 ppm in the $^{1}H$ NMR spectrum.

Compounds **35** – **37** were then reacted with iodobenzene and *p*-iodonitrobenzene to give **39** – **44** as a series of wedge-shaped compounds (Scheme 3.6). The catalyst used was $Pd(PPh_3)_4$, in order to minimize homocoupling. As was later learned (see below), homocoupling did not happen readily with these compounds.

**Scheme 3.6**

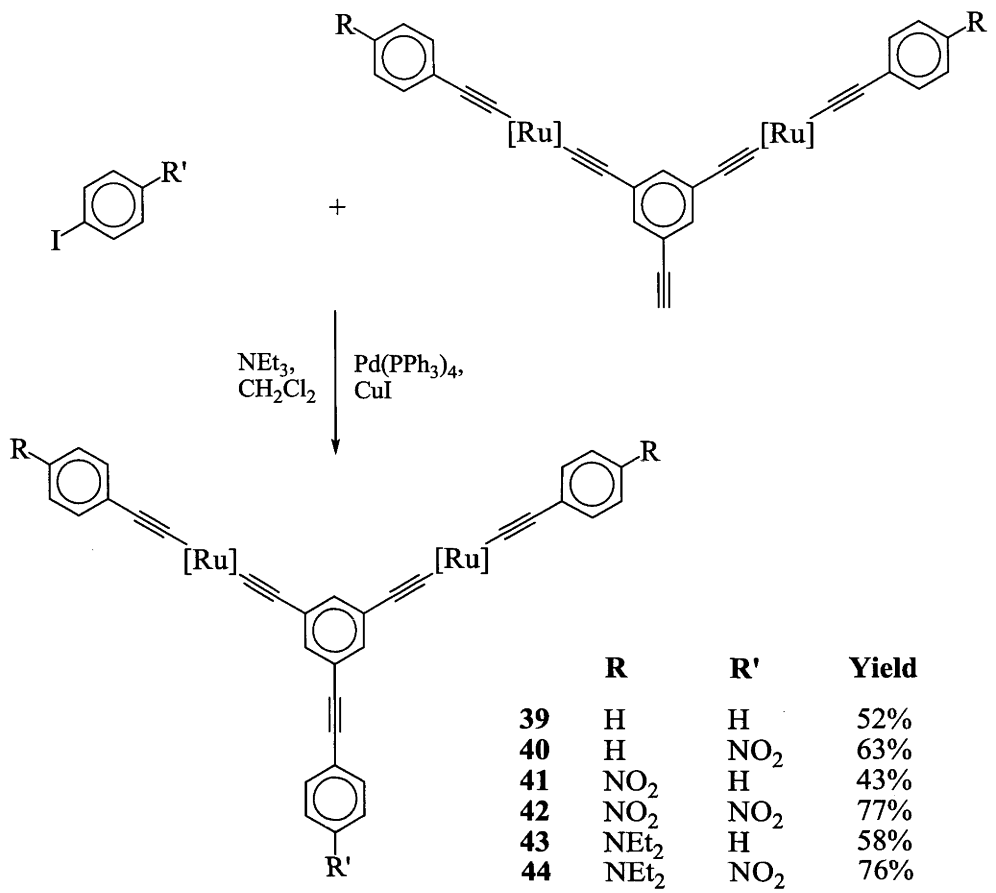


| | R | R' | Yield |
|---|---|---|---|
| **39** | H | H | 52% |
| **40** | H | $NO_2$ | 63% |
| **41** | $NO_2$ | H | 43% |
| **42** | $NO_2$ | $NO_2$ | 77% |
| **43** | $NEt_2$ | H | 58% |
| **44** | $NEt_2$ | $NO_2$ | 76% |

[Ru] = *trans*-Ru(dppe)$_2$

A variety of conditions were attempted to react the electron donating *p*-iodo-N,N-diethylaminobenzene with compounds **35** – **37**, but none were successful. Varying the catalyst system ($PdCl_2(PPh_3)_2$ vs. $Pd(PPh_3)_4$), presence or absence of CuI, solvent ratios of $NEt_3$ / $CH_2Cl_2$, replacing $CH_2Cl_2$ with $CHCl_3$ to allow for higher reaction temperatures and longer reaction times all resulted in no heterocoupling.

As the reaction did proceed with iodobenzene and the electron withdrawing *p*-iodonitrobenzene, it was hypothesized that the electron donating nature of the diethylamino moiety was potentially interfering with progress of the reaction.[135] Electron rich aromatic rings are less reactive under Sonogashira conditions. Reactions were also attempted between compound **35** and a series of *para*-substituted electron-donating iodobenzenes. The heterocoupling was also unsuccessful when 4-iodoaniline, 4-iodoanisole and 4-$IC_6H_4$-N=C-4-$C_6H_4NO_2$ were used as the aryl halides.

Compounds **34** – 37 were homocoupled to form quadrupolar compounds (Scheme 3.7). Ironically, despite the presence of homocoupled material being an unwanted side product in previous reactions, complete homocoupling was difficult to achieve. Exposing the solution mixture to air with Sonogashira catalysts did not result in complete homocoupling, even after 7 days. The Hay method was attempted (using Cu(TMEDA), but this also resulted in incomplete reaction.[139]

**Scheme 3.7**

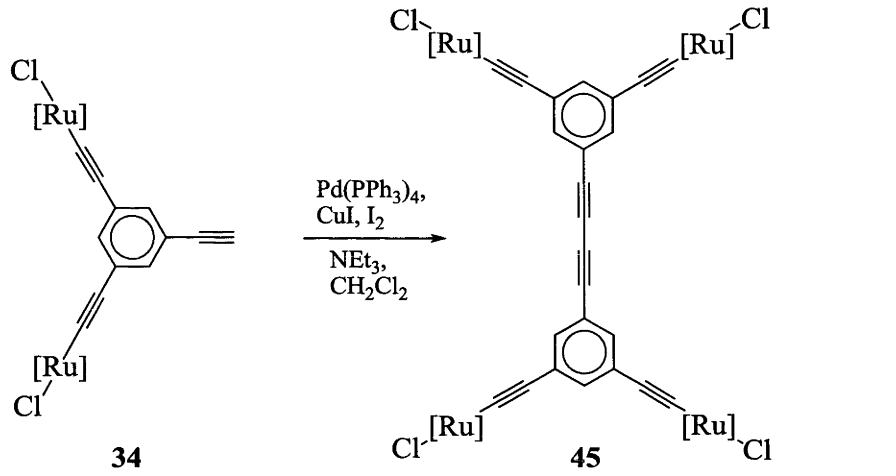


The addition of a stoichiometric amount of iodine to a Sonogashira-type reaction was successful (Scheme 3.7 and Scheme 3.8).[133] The iodine acts as an oxidizing agent and the homocoupling reaction proceeded to completion.

**Scheme 3.8**

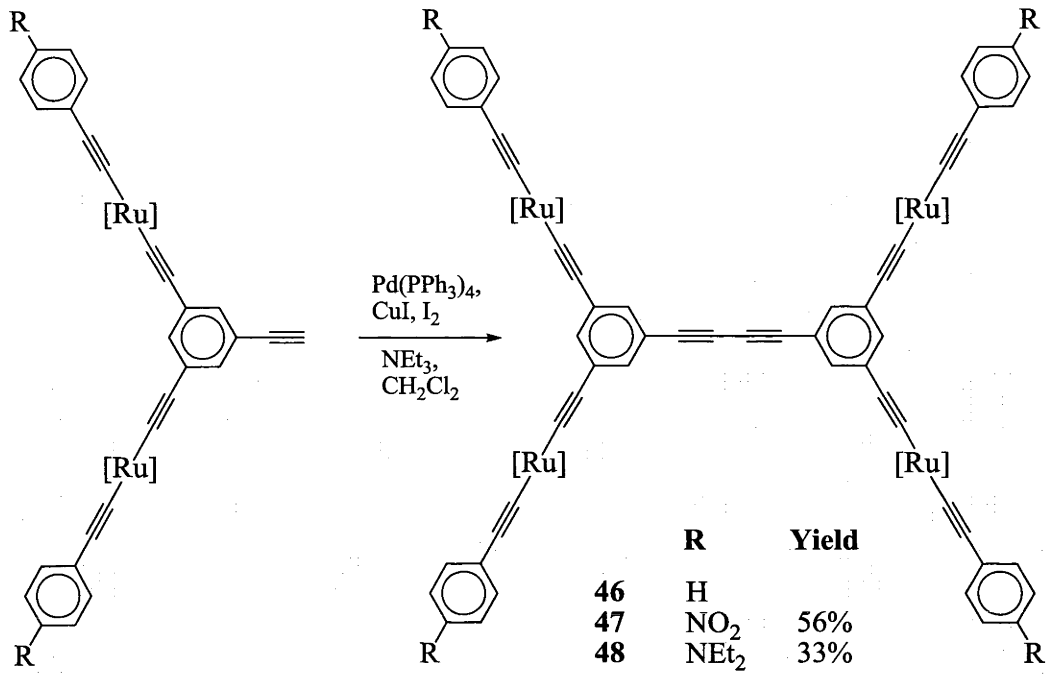


This gave a series of quadrupolar compounds (**45** – **48**)[xvi] with internal dipoles (of varying strength depending upon the terminal moieties), but no overall dipole. These compounds were ideal for testing the dependence of cubic NLO properties upon the electron-donating or withdrawing- character of the end-group.

## 3.3 Characterization

All of the new complexes (**37** – **44**, **47** and **48**) were characterized by a combination of IR, UV-vis, $^{1}H$ and $^{31}P$ NMR spectroscopy, cyclic voltammetry and ESI mass spectrometry. IR bands between 2059 and 2046 $cm^{-1}$ correspond to the $\nu$(C≡C–Ru) energies. Compounds **41**, **42** and **47**, with *p*-nitrophenylethynyl moiety bound to the metal centre, are at the lower energy range (2046 – 2047 $cm^{-1}$); all of the other ligands led to vibrational energies of 2053 – 2059 $cm^{-1}$. ESI mass spectra contain molecular ions, protonated molecular ions or sodium adducts. These characteristics are consistent with previously reported ruthenium acetylides.[2]

[xvi] Compounds **45** and **46** had been previously prepared by Steph Hurst and were resynthesized for this work.

### 3.3.1 Linear Optical Behaviour

The UV-vis spectra demonstrate dependence of the longer wavelength absorption maxima upon the electronic character of the phenylethynyl ligand (Table 3.2). As with the IR vibrational transitions, only compounds with a *p*-nitrophenylethynyl ligand in the R position have experimentally different behavior.

**Table 3.2** UV-vis maxima of compounds **38** – **44** and **46** – **48**.

| Compound | R | R′ | $\lambda_{max}$ (nm) | $\varepsilon$ ($10^4 M^{-1}cm^{-1}$) |
|---|---|---|---|---|
| **38** | H | Me | 330 | 8.9 |
| **39** | H | H | 335 | 7.8 |
| **40** | H | $NO_2$ | 330 | 10.9 |
| **41** | $NO_2$ | H | 484 | 4.7 |
| **42** | $NO_2$ | $NO_2$ | 484 | 3.6 |
| **43** | $NEt_2$ | H | 334 | 5.9 |
| **44** | $NEt_2$ | $NO_2$ | 341 | 7.5 |
| **46** | H | – | 335 | 14.0 |
| **47** | $NO_2$ | – | 481 | 8.1 |
| **48** | $NEt_2$ | – | 342 | 16.2 |

This data shows that the presence of a nitro group in the R position causes a red shift of approximately 150 nm in wavelength. This confirms that these absorption bands are MLCT in nature. The molar absorption coefficient of compounds **46** to **48** is roughly twice that of the compounds they were synthesized from (**39**, **41**, **43**, respectively). This is consistent with the number of chromophores (metal centres) in the molecule.

### 3.3.2 Electrochemistry

Cyclic voltammetry was a good comparative measure of the difference in electron density about the ruthenium atoms, based upon the electron donating or withdrawing character of the terminal group (in the R position). Table 3.3 shows the two different oxidation potentials for each molecule. These represent the oxidation of one ruthenium atom, followed by a more difficult oxidation of the second atom. Compounds containing nitro groups had a reversible reduction process between -1.16 and -0.91 V.

**Table 3.3** The oxidation potentials of ruthenium atoms.[xvii]

| Compound | R | R′ | $E_{1/2}Ru^{II/III}$ (V) | $E_{1/2}Ru^{II/III}$ (V) | $\Delta E_c$ (V) |
|---|---|---|---|---|---|
| **39** | H | H | 0.48 | 0.63 | 0.15 |
| **40** | H | $NO_2$ | 0.53 | 0.66 | 0.14 |
| **41** | $NO_2$ | H | 0.64 | 0.79 | 0.15 |
| **42** | $NO_2$ | $NO_2$ | 0.63 | 0.75 | 0.12 |
| **43** | $NEt_2$ | H | 0.21 | 0.74 | 0.52 |
| **44** | $NEt_2$ | $NO_2$ | 0.25 | 0.76 | 0.49 |
| **45** | – | – | 0.47 | 0.63 | 0.15 |
| **46** | H | – | 0.50 | 0.62 | 0.12 |
| **47** | $NO_2$ | – | 0.67 | 0.77 | 0.10 |
| **48** | $NEt_2$ | – | 0.26 | 0.75 | 0.13 |

Phenylethynyl ligands have roughly the same effect on the oxidation potential of the molecule as chloride ligands. The nitrophenylethynyl ligand pulls electron density away from the ruthenium, making it less easily oxidized. The electron donating

[xvii] Cyclic voltammetry experiments were carried out as outlined in Section 3.7.2

character of the diethylaminophenylethynyl ligand has the most pronounced effect, easing the first oxidation by approximately 0.25 V. The oxidation of the second ruthenium atom in the N,N-diethylamino-containing molecules is not altered compared to the other compounds, making for a larger difference in the two oxidation potentials of compounds **43**, **44** and **48**.

## 3.4 Second-Order Nonlinear Optics

Hyper-Rayleigh scattering measurements of compounds **38** to **44** reiterated the importance of molecular dipoles in quadratic NLO materials. Each of the compounds measured[xviii] could be considered to have three 'internal dipoles', which are components of the total dipole. Two of them are formed by the arms terminated with R and have a 120 degree angle between them and the third is the dipole along the axis of the molecule, in the same direction as the total dipole. For the two dipoles due to the arms (Figure 3.3), they may be broken down into two-dimensional components (red and blue arrows). The red components cancel each other out, while the blue components are additive, giving a contribution to the overall molecular dipole represented by the black arrow.

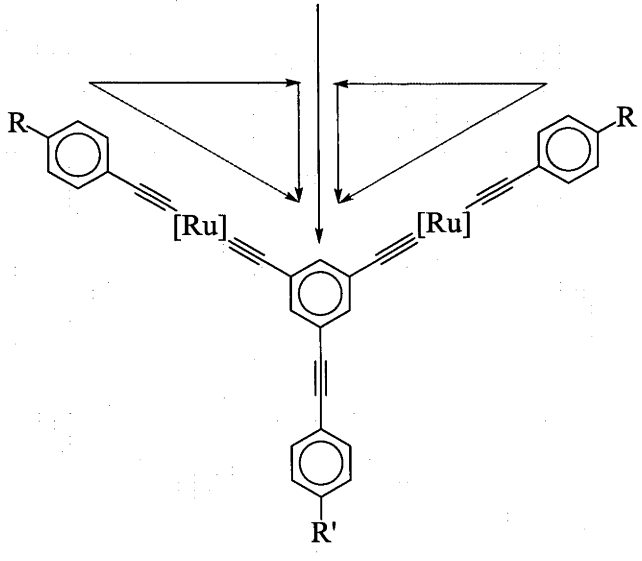


| | R | R' |
|---|---|---|
| **38** | H | Me |
| **39** | H | H |
| **40** | H | $NO_2$ |
| **41** | $NO_2$ | H |
| **42** | $NO_2$ | $NO_2$ |
| **43** | $NEt_2$ | H |
| **44** | $NEt_2$ | $NO_2$ |

Ru = *trans*-Ru(dppe)$_2$

**Figure 3.3** The dipole components due to the 'arms' of the wedge-shaped compounds.

[xviii] HRS measurements on these compounds were performed by Stijn van Cleuvenbergen and Inge Asselberghs in the research laboratory of Koen Clays at the University of Leuven, Belgium.

The moiety in the R position contributes to changes in both of the local dipoles (purple arrows) and the molecular dipole (black arrow). The molecular dipole is also influenced by the group in the R′ position: the electron withdrawing nitrophenyl group would increase the magnitude of the black arrow, while the phenyl and tolyl groups would have less of an effect. The largest molecular dipoles would be obtained from compounds where R and R′ had the greatest electron-donating and withdrawing character, respectively. These larger dipoles could potentially lead to larger values of β, depending upon the nature of the excited state dipole.

**Table 3.4** HRS data for wedge-shaped compounds (**38** – **44**) at 800 nm.

| **Compound** | **R** | **R′** | $\beta_0$ ($10^{-30}$ esu) | σ |
|---|---|---|---|---|
| **38** | H | Me | no signal | no signal |
| **39** | H | H | no signal | no signal |
| **40** | H | $NO_2$ | 49 ± 4 | 2.63 ± 0.04 |
| **41** | $NO_2$ | H | 60 ± 6 | 2.49 ± 0.08 |
| **42** | $NO_2$ | $NO_2$ | 33 ± 2 | 2.29 ± 0.05 |
| **43** | $NEt_2$ | H | 64 ± 12 | 2.13 ± 0.07 |
| **44** | $NEt_2$ | $NO_2$ | 91 ± 17 | 2.64 ± 0.04 |

Table 3.4 summarizes the results of these experiments. Compounds **38** and **39** did not give a strong enough signal to measure. Compound **42**, with the nitro groups in both the R and R′ positions competing for electrons in the molecule, gave the lowest measured response. By contrast, compound **44**, with the most difference in electronic character of the terminal groups, had the highest magnitude response. This indicates that the design of these materials may be altered to adjust the magnitude of the second-order NLO properties.

The final column of Table 3.4 shows the depolarization ratio (σ), which depends on the symmetry of the electronic density distribution of the molecule giving rise to the NLO

response. A value of 1 is characteristic a compound that is entirely octupolar in nature, while a dipolar compound should give a value of 5. The electron density distribution in molecules may be intermediate between that of a pure dipole and that of a pure octupole; molecules may possess both dipole moments and the octupole moments. The values of σ indicate that the NLO effects arise from both types of molecular polarity. Thus, the behaviour of the compounds is a combination of dipolar and octupolar.

## 3.5 Third-Order Nonlinear Optics

Wavelength dependence measurements were carried out on compounds **45** – **48** and two additional compounds (**49** and **50**, Figure 3.4[xix]). The intent of examining these compounds is to show the effect of the terminal moiety (R) on the NLA, as well as compare the chain-lengthening effects of quadrupolar compounds with the previously demonstrated effects for dipolar compounds (**9-13**).[108, 140]

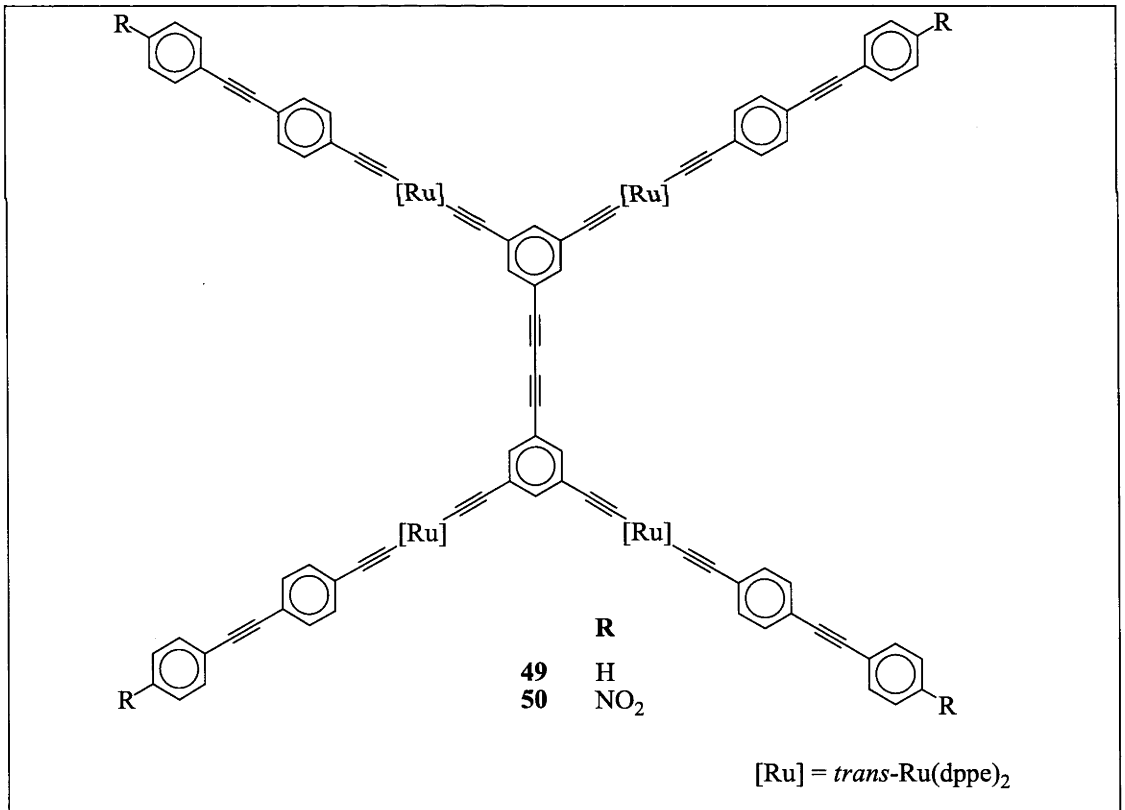


**Figure 3.4** The structure of chain-lengthened analogs of compounds **46** and **47**.[141]

[xix] Compounds **49** and **50** were synthesized by Sanjay Chavan while on sabbatical in the research group of Mark Humphrey, at the Australian National University, Australia.

All of the compounds showed a complex hyperpolarizability dispersion similar to many ruthenium acetylides: negative real part of $\gamma$ (self-defocussing character) with strong effects below 600 nm, which may be due to some influence of nearby single-photon transitions. Neither compound **45** nor **46** showed any appreciable two-photon absorption. The other compounds all showed a TPA maximum around 850 nm (Table 3.5).

**Table 3.5** Two-photon absorption cross section maxima.

| Compound | Ligand | TPA $\lambda_{max}$ (nm) | $\sigma_2$ (GM) |
|---|---|---|---|
| **47** | $C{\equiv}CC_6H_4NO_2$ | 880 | 1400 ± 100 |
| **48** | $C{\equiv}CC_6H_4NEt_2$ | 880 | 900 ± 200 |
| **49** | $(C{\equiv}CC_6H_4)_2H$ | 840 | 1200 ± 300 |
| **50** | $(C{\equiv}CC_6H_4)_2NO_2$ | 880 | 5600 ± 200 |

Both compounds **47** ($NO_2$) and **48** ($NEt_2$) had $\sigma_2$ values relatively close to each other, at the same wavelength. This is contrary to the expectation that a change in wavelength of the linear absorption maxima would result in a similar change in the nonlinear absorption maxima. The additional polarity of the ligand (either electron donating or withdrawing) does appear to have the effect of increasing the magnitude of the TPA, but does not alter the wavelength at which the maximum occurs.

The chain-lengthened compounds **49** (H) and **50** ($NO_2$) possess greater magnitude $\sigma_2$ values than their 'shorter' counterparts (compounds **46** and **47**, respectively). In the specific case between compounds **47** and **50**, there is a fourfold increase in the magnitude of $\sigma_2$ with the insertion of one additional phenylethynyl unit in the ligand. This is indicative that quadrupolar molecules exhibit the same chain-lengthening trends as the dipolar examples (compounds **9** – **13**) in chapter 2.

## 3.6 Conclusions

This work demonstrates that it is possible to vary electron density at the ruthenium centre using substituted phenylethynyl ligands, which has an effect on the molecular polarity. Altering the polarity also has the effect of changing the magnitude of the quadratic NLO response of the materials – the more polar molecules have stronger quadratic responses. It was found that the overall molecular polarity was not the sole factor influencing the NLO response: the local dipoles also play a role, contributing to the strength of the nonlinear interaction. The incorporation of nitro or diethylamino moieties at the terminus of the molecule has the effect of increasing the magnitude of the cubic nonlinearities. While there is not an appreciable NLA difference between compounds with either unit, they both show greater two-photon absorption than the phenylethynyl or chloride ligated ruthenium adducts.

Depending upon the electronic character of the ligand, the linear absorption maxima shift over a range of about 150 nm. This shift does not translate into a shift in the TPA cross-sections, the two-photon spectrum remaining similar for all the materials measured, with maxima between 840 and 880 nm for all measured compounds.

## 3.7 Experimental Section

### 3.7.1 Materials

All reactions were performed under a nitrogen atmosphere with the use of Schlenk techniques. Dichloromethane was dried by distillation over calcium hydride; all other solvents were used as received. Petrol refers to the fraction of petroleum ether with a boiling range of 60-80°C. Chromatography was performed on silica gel (230-400 mesh ASTM) or ungraded basic alumina. The following were prepared by literature procedures: *cis*-[$RuCl_2(dppe)_2$],[128] 1,3,5-triethynylbenzene,[142] 1,3-{*trans*-[$(dppe)_2ClRuC{\equiv}C$]}$_2$-5-$C_6H_3C{\equiv}CH$ (**34**), 4-$HC{\equiv}CC_6H_4NO_2$,[135] 4-iodo-N,N-diethylaniline,[137] 4-$HC{\equiv}CC_6H_4NEt_2$,[136] 1,3-{*trans*-[$(dppe)_2(C_6H_5C{\equiv}C)RuC{\equiv}C$]}$_2$-5-$C_6H_3C{\equiv}CH$ (**35**), 1,3-{*trans*-[$(dppe)_2(O_2NC_6H_4$-4-$C{\equiv}C)RuC{\equiv}C$]}$_2$-5-$C_6H_3C{\equiv}CH$ (**36**).[65] All other reagents were obtained commercially and used as received.

### 3.7.2 Methods and Instrumentation

Microanalyses were carried out at the Australian National University. UV-vis-NIR spectra of solutions in $CH_2Cl_2$ (except where noted) in 1 cm quartz cells were recorded using a Cary 5 spectrophotometer and are reported as $\nu_{max}$ (nm) [$\varepsilon$ $10^4$ $M^{-1}$ $cm^{-1}$)]. Infrared spectra were recorded as $CH_2Cl_2$ solutions (except where noted) using a Perkin-Elmer System 2000 FT-IR. $^1H$ (300 MHz) and $^{31}P$ NMR (121 MHz) spectra were recorded using a Varian Gemini-300 FT NMR spectrometer and are referenced to residual chloroform (7.26 ppm) or external $H_3PO_4$ (0.0 ppm), respectively. Electrospray ionization mass spectra (ESI MS) were recorded using a Bruker Apex3 at the Australian National University. Solutions in MeOH or acetonitrile were ionized with sodium ions; peaks are reported as *m/z* (assignment, relative intensity). Cyclic voltammetry measurements were recorded using a MacLab 400 interface and MacLab potentiostat from eDAQ Pty Ltd. The supporting electrolyte was 0.1 M $(NBu^n_4)PF_6$ in distilled, deoxygenated $CH_2Cl_2$; solutions containing ca 1 x $10^{-3}$ M complex were maintained under nitrogen. Measurements were carried out at room temperature using Pt disc working-, Pt wire auxiliary- and Ag/AgCl reference electrodes, such that the ferrocene/ferrocenium redox couple was located at 0.56 V (peak separation ca 0.08 V). Scan rates were typically 100 mV $s^{-1}$. HRS measurements were performed in $CH_2Cl_2$ at 800 nm, using $\beta_{xxx}$ (CV) = 338 x $10^{-30}$ esu in MeOH as a reference. Local field correction factors were used to correct for solvent differences and $\beta_0$ values were calculated using a 2-level model. Z-scan measurements were performed as described in Chapter 2.

### 3.7.3 Experimental Data for Compounds 37 – 48

**Synthesis of 1,3-{*trans*-[(dppe)$_2$(Et$_2$NC$_6$H$_4$-4-C≡C)RuC≡C]}$_2$-5-(HC≡C)C$_6$H$_3$ (37).** 1,3-{*trans*-[(dppe)$_2$ClRuC≡C]}$_2$-5-HC≡CC$_6$H$_3$ (**34**, 800 mg, 0.397 mmol), $NaPF_6$ (330 mg, 1.96 mmol) and 4-Et$_2$NC$_6$H$_4$C≡CH (300 mg, 1.74 mmol) were added to a mixture of $CH_2Cl_2$ (100 mL) and $NEt_3$ (15 mL) and heated at reflux for 18 h. The solvents were removed under reduced pressure and the residue dissolved in $CH_2Cl_2$ and filtered through a short pad of alumina. The solution was taken to dryness and the residue crystallized from $CH_2Cl_2$/petrol to give a yellow solid (548 mg, 60%). Anal. Calcd for $C_{140}H_{128}N_2P_8Ru_2$: C 73.48, H 5.64, N 1.22. Found: C 72.63, H 5.65, N 1.20 %. IR: $\nu$(RuC≡C) 2054 $cm^{-1}$. UV-vis: 339 [10.7]. $^1H$ NMR: $\delta$ 1.27 (t, $J_{HH}$ = 15 Hz, 12H, Me),

2.58-2.65 (m, 16H, $PCH_2CH_2P$), 3.02 (s, 1H, C≡CH), 3.24-3.46 (q, 8H, $NCH_2$), 6.29-7.83 (m, 91H, Ph). $^{31}P$ NMR: δ 54.7. ESI MS: 2290 ($[M]^+$, 5), 898 ($[Ru(dppe)_2]^+$, 100).

**Synthesis of 1,3-{*trans*-[(dppe)$_2$(PhC≡C)RuC≡C]}$_2$-5-(4-MeC$_6$H$_4$C≡C)C$_6$H$_3$ (38).** 4-Iodotoluene (50 mg, 0.23 mmol), 1,3-{*trans*-[(dppe)$_2$(PhC≡C)RuC≡C]}$_2$-5-HC≡CC$_6$H$_3$ (**35**, 200 mg, 93 μmol), $Pd(PPh_3)_4$ (2.0 mg, 17 μmol) and CuI (0.8 mg, 42 μmol) were added to a mixture of $CH_2Cl_2$ and $NEt_3$ (1:1, 60 mL) and heated at reflux for 24 h. The solution was filtered through a short pad of alumina and the solvent removed under reduced pressure. The residue was crystallized from $CH_2Cl_2$/petrol to give a yellow solid (85 mg, 41%). Anal. Calcd for $C_{139}H_{116}P_8Ru_2$: C 74.65, H 5.23 %. Found: C 74.32, H 5.23 %. IR: ν(RuC≡C) 2059 $cm^{-1}$. UV-vis: 276 [14.3], 330 [8.9]. $^1H$ NMR: δ 2.42 (s, 3H, Me), 2.54-2.73 (m, 16H, $PCH_2CH_2P$), 6.71-7.96 (m, 97H, Ph). $^{31}P$ NMR: δ 54.5. ESI MS: 2236 ($[M + 2H]^+$, 5).

**Synthesis of 1,3-{*trans*-[(dppe)$_2$(PhC≡C)RuC≡C]}$_2$-5-(PhC≡C)C$_6$H$_3$ (39).** Iodobenzene (1 mL, 9 mmol), 1,3-{*trans*-[(dppe)$_2$(PhC≡C)RuC≡C]}$_2$-5-HC≡CC$_6$H$_3$ (**35**, 187 mg, 79 μmol) and $Pd(PPh_3)_4$ (2.1 mg, 1.8 μmol) were added to a mixture of $CH_2Cl_2$ and $NEt_3$ (4:1, 100 mL) and heated at reflux for 21 h. The solution was filtered through a short pad of alumina and the solvent removed under reduced pressure. The residue was crystallized from $CH_2Cl_2$/petrol to give a yellow solid (93 mg, 53 %). Anal. Calcd $C_{138}H_{114}P_8Ru_2$: C 74.58, H 5.17 %. Found: C 74.13, H 5.38 %. IR: ν(RuC≡C) 2055 $cm^{-1}$. UV-vis: 276 [14.0], 335 [7.8]. $^1H$ NMR: δ 2.58-2.73 (m, 16H, $PCH_2CH_2P$), 6.51-7.96 (m, 98H, Ph). $^{31}P$ NMR: δ 54.5. ESI MS: 2245 ($[M + Na]^+$, 5), 898 ($[Ru(dppe)_2]^+$, 100).

**Synthesis of 1,3-{*trans*-[(dppe)$_2$(PhC≡C)RuC≡C]}$_2$-5-(O$_2$N-4-C$_6$H$_4$C≡C)C$_6$H$_3$ (40).** 4-Iodonitrobenzene (25 mg, 0.10 mmol), 1,3-{*trans*-[(dppe)$_2$(PhC≡C)RuC≡C]}$_2$-5-HC≡CC$_6$H$_3$ (**35**, 144 mg, 0.067 mmol) and $Pd(PPh_3)_4$ (2.0 mg, 0.0017 mmol) were added to a mixture of $CH_2Cl_2$:$NEt_3$ (1:1, 60 mL) and heated at reflux for 20 h. The solution was filtered through a short pad of alumina, eluting with $CH_2Cl_2$/acetone (1:1), and the solvent removed under reduced pressure. The residue was crystallized from $CH_2Cl_2$/petrol to give a yellow solid (94 mg, 62 %). Anal. Calcd for $C_{138}H_{113}NO_2P_8Ru_2$: C 73.10, H 5.02, N 0.62. Found: C 72.88, H 5.05, N 0.70 %. IR:

ν(RuC≡C) 2059, ν(C≡C) 2209 $cm^{-1}$. UV-vis: 277 [10.9], 330 [5.0]. $^{1}H$ NMR: δ 2.54-2.73 (m, 16H, $PCH_2CH_2P$), 6.71-7.96 (m, 97H, Ph). $^{31}P$ NMR: δ 54.4. ESI MS: 2267 ($[M]^+$, 20), 898 ($[Ru(dppe)_2]^+$, 100).

**Synthesis of 1,3-{*trans*-[(dppe)$_2$($O_2NC_6H_4$-4-C≡C)RuC≡C]}$_2$-5-(PhC≡C)$C_6H_3$ (41).** Iodobenzene (0.5 mL, 4.5 mmol), 1,3-{*trans*-[(dppe)$_2$($O_2NC_6H_4$-4-C≡C)RuC≡C]}$_2$-5-HC≡$CC_6H_3$ (**36**, 97 mg, 45 μmol) and $Pd(PPh_3)_4$ (10 mg, 8.7 μmol) were added to a mixture of $CH_2Cl_2$ and $NEt_3$ (1:1, 80 mL) and heated at reflux for 38 h. The solution was filtered through a short pad of alumina, eluting with $CH_2Cl_2$/acetone (1:1), and the solvent removed under reduced pressure. The residue was crystallized from $CH_2Cl_2$/petrol to give a red solid (45 mg, 43 %). Anal. Calcd for $C_{138}H_{112}N_2O_4P_8Ru_2$: C 71.68, H 4.88, N 1.21. Found: C 72.88, H 5.05, N 1.25 %. IR: ν(RuC≡C) 2046 $cm^{-1}$. UV-vis: 276 [19.6], 326 [6.0], 484 [4.7]. $^{1}H$ NMR: δ 2.56-2.78 (m, 16H, $PCH_2CH_2P$), 6.47-8.02 (m, 96H, Ph). $^{31}P$ NMR: δ 54.7. ESI MS: 2336 ($[M + Na]^+$, 30), 897 ($[Ru(dppe)_2 - H]^+$, 100).

**Synthesis of 1,3-{*trans*-[(dppe)$_2$($O_2NC_6H_4$-4-C≡C)RuC≡C]}$_2$-5-($O_2N$-4-$C_6H_4$C≡C) $C_6H_3$ (42).** 4-Iodonitrobenzene (46 mg, 0.179 mmol), 1,3-{*trans*-[(dppe)$_2$($O_2NC_6H_4$-4-C≡C)RuC≡C]}$_2$-5-HC≡$CC_6H_3$ (**36**, 160 mg, 0.072 mmol) and $Pd(PPh_3)_4$ (2.5 mg, 2.2 μmol) were added to a mixture of $CH_2Cl_2$:$NEt_3$ (1:1, 80 mL) and heated at reflux for 32 h. The solution was filtered through a short pad of alumina and the solvent removed under reduced pressure. The residue was crystallized from $CH_2Cl_2$/petrol to give a red solid (130 mg, 77 %). Anal. Calcd for $C_{138}H_{111}N_3O_6P_8Ru_2$: C 70.31, H 4.75, N 1.78. Found: C 69.82, H 5.02, N 1.76 %. IR: ν(RuC≡C) 2046, ν(C≡C) 2210 $cm^{-1}$. UV-vis: 336 [6.3], 484 [3.6]. $^{1}H$ NMR: δ 2.58-2.81 (m, 16H, $PCH_2CH_2P$), 6.50-8.17 (m, 95H, Ph). $^{31}P$ NMR: δ 54.7. ESI MS: 2380 ($[M + Na]^+$, 1), ($[M]^+$, 2), 897 ($[Ru(dppe)_2 - H]^+$, 10).

**Synthesis of 1,3-{*trans*-[(dppe)$_2$($Et_2NC_6H_4$-4-C≡C)RuC≡C]}$_2$-5-(PhC≡C)$C_6H_3$ (43).** Iodobenzene (1 mL, 9 mmol), 1,3-{*trans*-[(dppe)$_2$($Et_2NC_6H_4$-4-C≡C)RuC≡C]}$_2$-5-HC≡$CC_6H_3$ (**37**, 145 mg, 6.3 μmol) and $Pd(PPh_3)_4$ (2.1 mg, 1.8 μmol) were added to a mixture of $CH_2Cl_2$:$NEt_3$ (4:1, 100 mL) and heated at reflux for 20 h. The solution was filtered through a short pad of alumina and the solvent removed under reduced pressure.

The residue was crystallized from $CH_2Cl_2$/petrol to give a yellow solid (87 mg, 58 %). Anal. Calcd for $C_{146}H_{132}N_2P_8Ru_2{\cdot}2CH_2Cl_2$: C 70.14, H 5.60, N 1.11 %. Found: C 70.64, H 5.35, N 1.01 %. IR: ν(RuC≡C) 2059, ν(C≡C) 2209 $cm^{-1}$. UV-vis: 277 [17.2], 334 [5.9]. $^1$H NMR: δ 1.28 (t, $J_{HH}$ = 15 Hz, 12H, Me), 2.53-2.72 (m, 16H, $PCH_2CH_2P$), 3.34 (q, 8H, $NCH_2$), 5.30 (s, 4H, $CH_2Cl_2$), 6.13-7.89 (m, 96H, Ph). $^{31}$P NMR: δ 54.7. ESI MS: 1183 ($[M + H]^{2+}$, 10).

**Synthesis of 1,3-{*trans*-[(dppe)$_2$(Et$_2$NC$_6$H$_4$-4-C≡C)RuC≡C]}$_2$-5-(O$_2$N-4-C$_6$H$_4$C≡C)C$_6$H$_3$ (44).** 4-Iodonitrobenzene (65 mg, 0.26 mmol), 1,3-{*trans*-[(dppe)$_2$(Et$_2$NC$_6$H$_4$-4-C≡C)RuC≡C]}$_2$-5-HC≡CC$_6$H$_3$ (**37**, 205 mg, 90 μmol) and $Pd(PPh_3)_4$ (5.0 mg, 4.3 μmol) were added to a mixture of $CH_2Cl_2$:$NEt_3$ (1:1, 60 mL) and heated at reflux for 24 h. The solution was filtered through a short pad of alumina and the solvent was removed from the eluate under reduced pressure. The residue crystallized from $CH_2Cl_2$/petrol to give a yellow solid (165 mg, 76 %). Anal. Calcd for $C_{146}H_{131}N_3O_2P_8Ru_2{\cdot}2CH_2Cl_2$: C 68.91, H 5.28, N 1.74 %. Found: C 69.12, H 5.38, N 1.36 %. IR: ν(RuC≡C) 2054, ν(C≡C) 2209 $cm^{-1}$. UV-vis: 277 [15.1], 341 [7.5]. $^1$H NMR: δ 1.22 (t, $J_{HH}$ = 15 Hz, 12H, Me), 2.53-2.82 (m, 16H, $PCH_2CH_2P$), 3.39 (q, 8H, $NCH_2$), 5.30 (s, 4H, $CH_2Cl_2$), 6.41-7.88 (m, 95H, Ph). $^{31}$P NMR: δ 54.5. ESI MS: 2410 ($[M + H]^+$, 2), 897 ($[Ru(dppe)_2 - H]^+$, 100).

**Synthesis of [1,3-{*trans*-[(dppe)$_2$ClRuC≡C]}$_2$-5-C$_6$H$_3$C≡C]$_2$ (45).** 1,3-{*trans*-[(dppe)$_2$ClRuC≡C]}$_2$-5-(HC≡C)C$_6$H$_3$ (**34**, 39 mg, 19 μmol), $PdCl_2(PPh_3)_2$ (2.0 mg, 2.8 μmol), CuI (2.0 mg, 1.1 μmol) and $I_2$ (11 mg, 0.42 mmol) were added to a mixture of $CHCl_3$ and $Pr^i_2NH$ (2:1, 80 mL) and heated at reflux for 25 h. The resulting solution was filtered through a short pad of alumina and the solvent removed under reduced pressure. The residue was recrystallized from $CH_2Cl_2$/MeOH to give a yellow powder (36 mg, 92 %). Anal. Calcd for $C_{232}H_{198}P_{16}Ru_4$: C 69.18, H 4.95 %. Found: C 68.88, H 4.45 %. IR: ν(RuC≡C) 2059 $cm^{-1}$. UV-vis: 335 [13.9]. $^1$H NMR: δ 2.61-2.75 (m, 32H, $PCH_2CH_2P$), 6.45-7.75 (m, 166H, Ph). $^{31}$P NMR: δ 54.5. ESI MS: 897 ($[Ru(dppe)_2 - H]^+$, 100).

**Synthesis of [1,3-{*trans*-[(dppe)$_2$(PhC≡C)RuC≡C]}$_2$-5-C$_6$H$_3$C≡C]$_2$ (46).** 1,3-{*trans*-[(dppe)$_2$(PhC≡C)RuC≡C]}$_2$-5-C$_6$H$_3$C≡CH (**35**, 153 mg, 0.070mmol). $PdCl_2(PPh_3)_2$ (2.5 mg, 3.5 μmol), CuI (7.0 mg, 3.9 μmol) and $I_2$ (40 mg, 0.158 mmol) were added to a mixture of $CHCl_3$ and $Pr^i_2NH$ (2:1, 75 mL) and heated at reflux for 78 h. The solution was filtered through a short pad of alumina and the solvent removed under reduced pressure. The crude product was recrystallized from $CH_2Cl_2$/MeOH to give a yellow powder (82 mg, 54 %). Anal. Calcd for $C_{264}H_{218}P_{16}Ru_4$: C 73.91, H 5.12. Found: C 73.92, H 5.55 %. IR:ν(RuC≡C) 2056 cm$^{-1}$. UV-vis (thf): 335 [14.0]. $^1$H NMR: δ 2.63 (m, 32H, $PCH_2CH_2P$), 6.85-7.60 (m, 186H, Ph). $^{31}$P NMR: δ 54.4. ESI MS: 2245 ([1,3-{*trans*-[(dppe)$_2$(PhC≡C)RuC≡C]}$_2$-5-C$_6$H$_3$C≡C]$^+$, 30), 999 ([(dppe)$_2$(C≡CPh)Ru]$^+$, 20), 897 ([Ru(dppe)$_2$ - H]$^+$, 100).

**Synthesis of [1,3-{*trans*-[(dppe)$_2$(O$_2$NC$_6$H$_4$-4-C≡C)RuC≡C]}$_2$-5-(C≡C-4-C$_6$H$_4$C≡C) C$_6$H$_3$C≡C]$_2$ (47).** 1,3-{*trans*-[(dppe)$_2$(O$_2$NC$_6$H$_4$-4-C≡C)RuC≡C]}$_2$-5-(HC≡C)C$_6$H$_3$ (**36**, 80 mg, 36 μmol), $PdCl_2(PPh_3)_2$ (2.5 mg, 3.6 μmol), CuI (0.70 mg, 3.6 μmol) and $I_2$ (10 mg, 0.04 mmol) were added to a mixture of $CHCl_3$ and $Pr^i_2NH$ (2:1, 75 mL) and heated at reflux for 22 h. The solvent was removed under reduced pressure and the solute was redissolved in $CH_2Cl_2$. The solution was passed through a short pad of alumina, eluting with $CH_2Cl_2$:acetone (1:1) and the solvent removed under reduced pressure. The residue was crystallized from $CH_2Cl_2$/petrol to give a red solid (45 mg, 56 %). Anal. Calcd for $C_{264}H_{214}N_4O_8P_{16}Ru_4$: C 70.93, H 4.83, N 1.25. Found: C 70.16, H 4.65 %, N 1.03 %. IR: ν(RuC≡C) 2047 cm$^{-1}$. UV-vis: 342 [12.2], 481 [8.1]. $^1$H NMR: δ 2.54-2.78 (m, 32H, $PCH_2CH_2P$), 6.48-8.04 (m, 182H, Ph). $^{31}$P NMR: δ 53.4. ESI MS: 897 ([Ru(dppe)$_2$ - H]$^+$, 100).

**Synthesis of [1,3-{*trans*-[(dppe)$_2$(Et$_2$NC$_6$H$_4$-4-C≡C)RuC≡C]}$_2$-5-C$_6$H$_3$C≡C]$_2$ (48).** 1,3-{*trans*-[(dppe)$_2$(Et$_2$NC$_6$H$_4$-4-C≡C)RuC≡C]}$_2$-5-(HC≡C)C$_6$H$_3$ (**37**, 86 mg, 38 μmol), $PdCl_2(PPh_3)_2$ (4.0 mg, 5.7 μmol), CuI (1 mg, 6 μmol) and $I_2$ (11 mg, 0.42 mmol) were added to a mixture of $CHCl_3$ and $Pr^i_2NH$ (2:1, 90 mL) and heated at reflux for 25 h. The solvent was removed under reduced pressure and the solute was redissolved in $CH_2Cl_2$. The solution was filtered through a short pad of alumina and the solvent was removed under reduced pressure. The residue was crystallized from $CH_2Cl_2$/petrol to give a yellow solid (28 mg, 33 %). Anal. Calcd for $C_{280}H_{254}N_4P_{16}Ru_4$: C 73.51, H 5.60,

N 1.22. Found: C 73.11, H 5.73, N 1.34 %. IR: ν(RuC≡C) 2054 $cm^{-1}$. UV-vis: 342 [16.2]. $^{1}H$ NMR: δ 1.20 (t, 24H, Me, $J_{HH}$ = 15 Hz), 2.51-2.73 (m, 32H, $PCH_2CH_2P$), 3.29 (q, 16H, $NCH_2$, $J_{HH}$ = 15 Hz), 6.63-7.92 (m, 182H, Ph). $^{31}P$ NMR: δ 54.6. ESI MS: 4576 ($[M + H]^+$, 1), 898 ($[Ru(dppe)_2]^+$, 60).

# Changing the Substitution Level About the Aromatic Core

## 4.1 Introduction

Studies with organic molecules have demonstrated that increasing the number of substituents about the central core of a 'star-shaped'[xx] compound leads to increased optical effects.[143-147] Kondo, et. al., have determined that the magnitude of $\chi^{(3)}$ increases with the number of phenyleneethynylene moieties bound to a central benzene ring (Figure 4.1).[144]

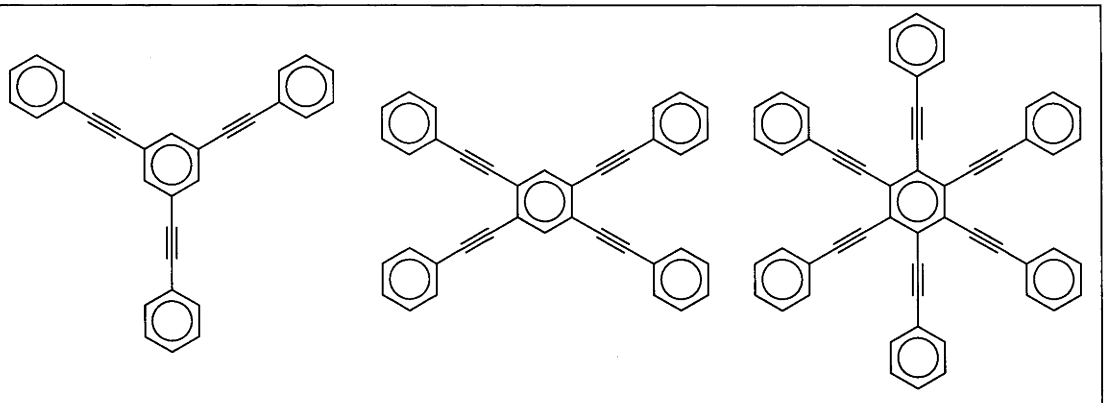

**Figure 4.1** A series of molecules that have increased cubic NLO response from left to right.[144]

While organometallic compounds (containing iron, palladium, gold and platinum) with hexaethynyl cores have been synthesized having 6-fold symmetry, nothing has (as yet) been published regarding their NLO characteristics.[148-150] Molecules in this chapter were designed to provide a series of ruthenium-alkynyl containing star-shaped structures in order to compare the cubic nonlinearities of the compounds and determine if the trends present in organic materials continue into organometallic materials.

[xx] A star is similar to a dendrimer, but without any branching in the arms. A 'zero-generation' dendrimer is a star-shaped compound, so stars may be viewed as the cores of dendrimers.

**Scheme 4.1**[151]

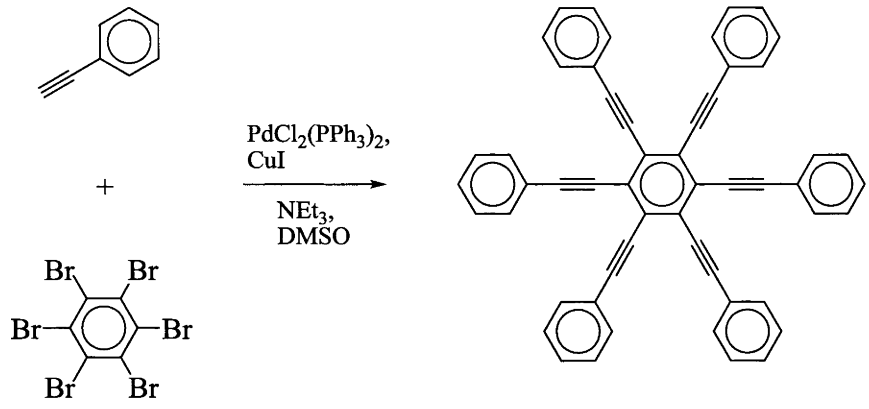


Hexaethynylbenzene was first prepared by Peter Vollhardt, using Sonogashira conditions, high pressure and heat for 10 days.[152] Using less severe coupling (also Sonogashira) methods, it is possible to prepare hexatolane from the reaction of hexabromobenzene and an excess of phenylacetylene (Scheme 4.1). Unfortunately, yields of these reactions are low, due to formation of the pentakis species (it is possible during the reaction for a bromide to be replaced by a proton).[150, 151] The pentatolane byproduct is very difficult to separate or distinguish and there is an argument that several hexaethynyl-substituted benzene compounds are actually a mix of hexa-substituted and penta-substituted benzenes.[151]

### 4.1.1 Synthesis of a Test Compound

While there is other literature supporting the synthesis of these compounds, all of them involve some variant of Sonogashira coupling.[153-156] Huang, et. al., use a method consisting of coupling a silyl-protected arm to hexabromobenzene under basic Sonogashira conditions (Scheme 4.2).[148] This method was used to prepare a TIPS-protected organic core (**51**) which has six-fold symmetry.

**Scheme 4.2**[148]

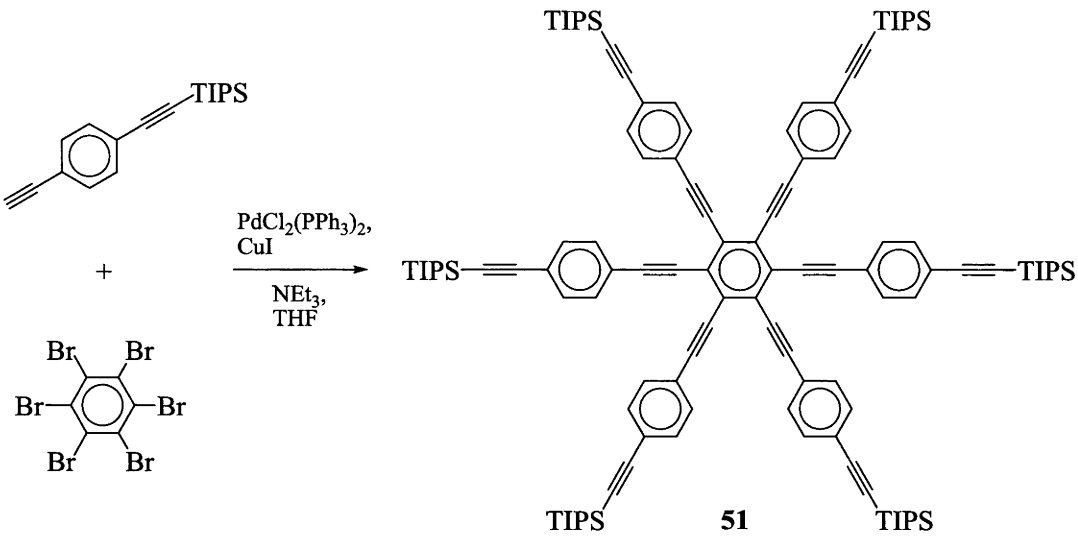


Compound **51** was then deprotected (tBAF) and coupled to six equivalents of tris(cyclohexylphosphine)gold chloride, forming compound **52**. When repeating this work, we found that compound **51**, when deprotected, is unstable. A dark, insoluble product forms from the pale yellow-orange precipitate as the volume of petrol used to precipitate the product decreases (on filtering). To circumvent this issue, trimethylsilylchloride was added to the deprotection reaction after one hour (Scheme 4.3) to neutralize any excess tBAF. Tris(cyclohexylphosphine)gold chloride and sodium hydroxide in ethanol were added to the reaction mixture and compound **52** was obtained.

**Scheme 4.3**[148]

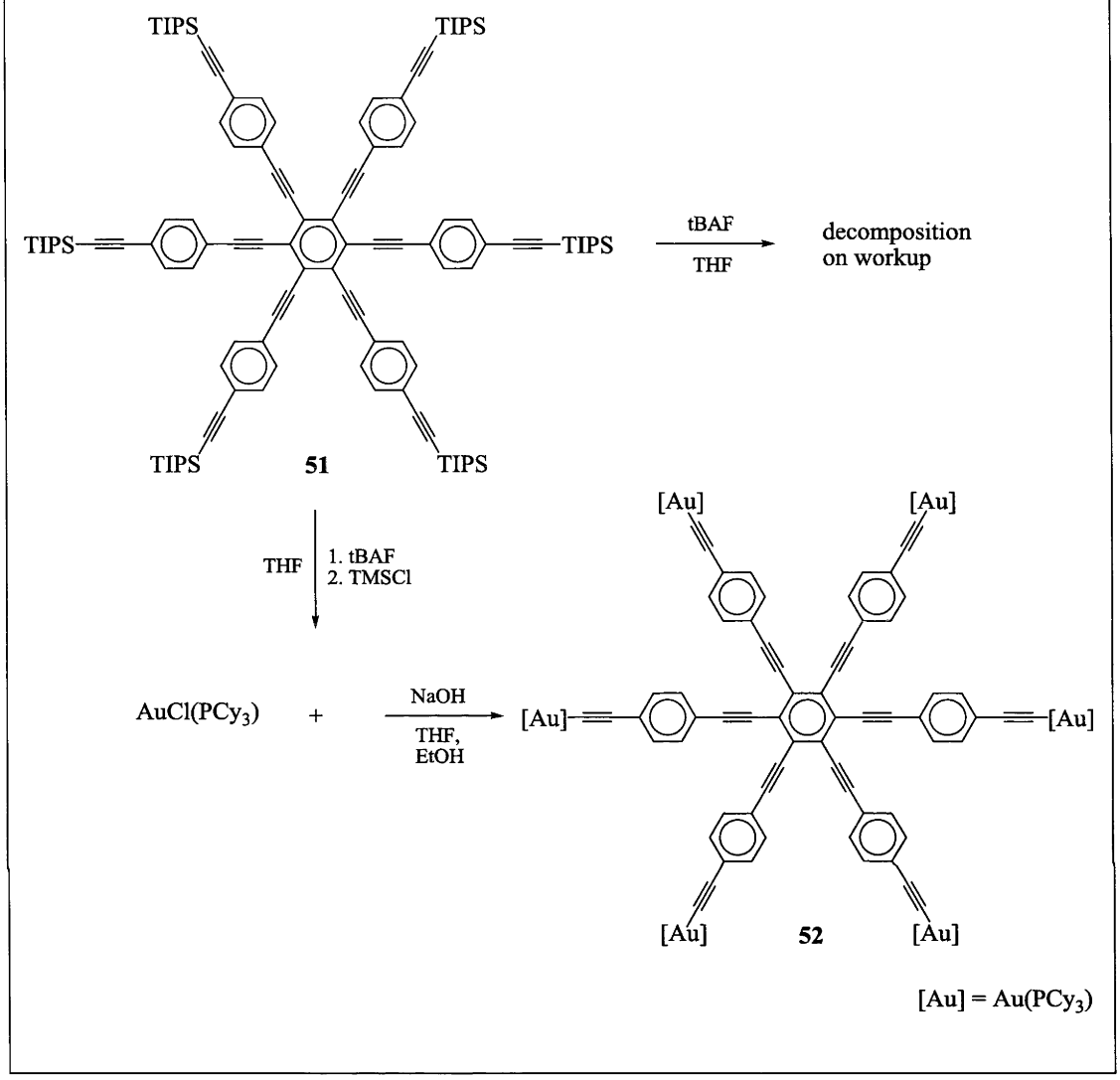


### 4.1.1.1 NLO Measurements

Compounds **52** and **53** (Figure 4.2) were then characterized by wavelength dependent femtosecond Z-scan.[xxi] The two compounds are not ideal for comparison: in order to only examine the effects of symmetry it would be preferable if there were three aromatic spacers between the two metal centres in compound **53**. The expectation was to see a higher NLO response from compound **52**, for several reasons. One is that there were simply more chromophores (3 times as many metal centres) in the molecule.

[xxi] Compound **53** was synthesized by Steph Hurst, while working in the research laboratory of Mark Humphrey at the Australian National University, Australia

Chain lengthening effects were probably also present and some portion of the remaining increase in magnitude may originate from the increased symmetry.

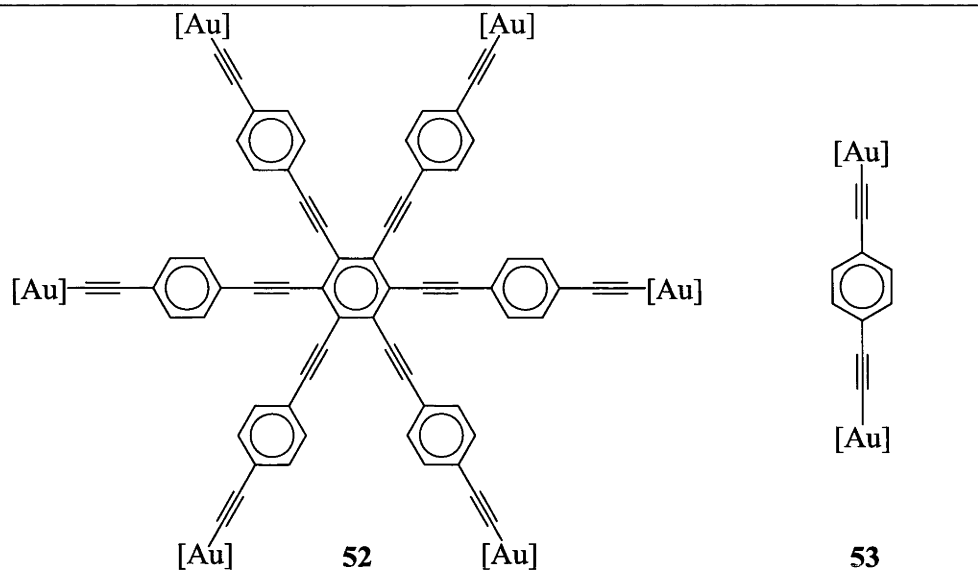


**Figure 4.2** Gold compounds used for preliminary examination of symmetry effects.

The results were inconclusive. Compound **52** had TPA responses more than three orders of magnitude greater than those of **53**. The real part of the hyperpolarizability was also much greater (50 times) but the shape of the dispersion curves (see appendix) was indicative of excited state absorption.

Despite the possible domination of excited state absorption, the results were heartening. The magnitude of the increase in the effective two-photon absorption cross section was sufficient to indicate that there was potential for higher symmetry organometallic molecules. Ruthenium was the metal centre of choice, both because of the ability to form robust bis-acetylides and because there is experience using it in the Humphrey research group.

### 4.1.2 Potential Concerns with Ruthenium

The first concern involving the use of ruthenium was a question of steric hindrance. Spartan™ space-filling models (Figure 4.3) indicated that there would not be room for six *trans*-RuCl(dppe)$_2$ moieties.

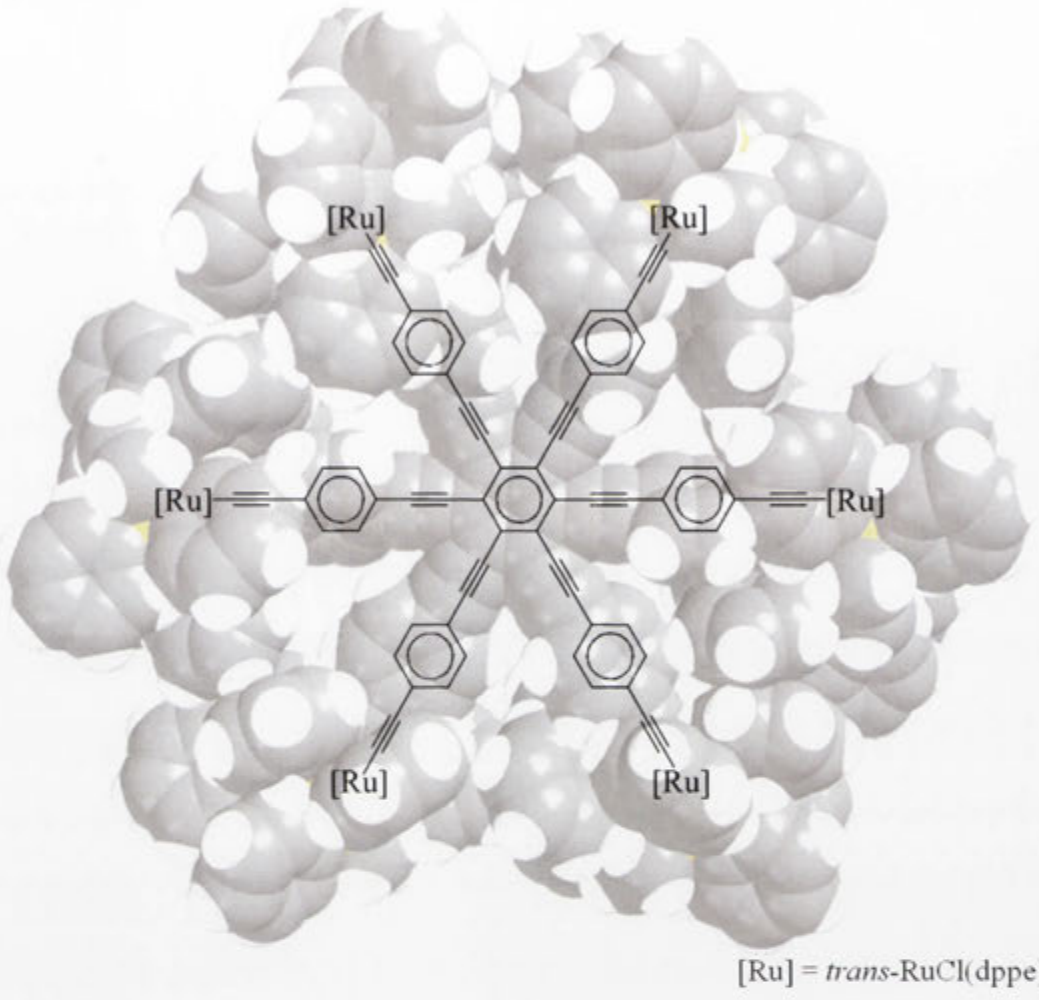


**Figure 4.3** Spartan™ model of the proposed 'singly-spaced' ruthenium molecule.

One solution to this problem was to use ruthenium centres with smaller cone angles (defined as the apex angle of a cylindrical cone, centred half the bonding distance behind the bonding atom, which just touches the van der Waals radii of the outermost atoms, and given by Θ).[157] $Ru(PPh_3)_2Cp$ and $Ru(PMe_3)_2Cp$ groups were chosen as they both have smaller cone angles than $RuCl(dppe)_2$. $RuCl(PPh_3)_2Cp$ was synthesized and a portion of it converted to $RuCl(PMe_3)_2Cp$, according to published procedures.[158, 159] Both compounds were reacted in situ, following the deprotection of compound **51**. Unfortunately, no product was obtained. This approach was abandoned in favour of a second phenylenethynylene 'spacer' in order to allow sufficient space for six $RuCl(dppe)_2$ moieties.

The incorporation of ethoxy groups as solubilizing moieties (as with Compounds **9** – **13**) was also planned, to help reduce the potential issue of reduced solubility (Figure 4.4).

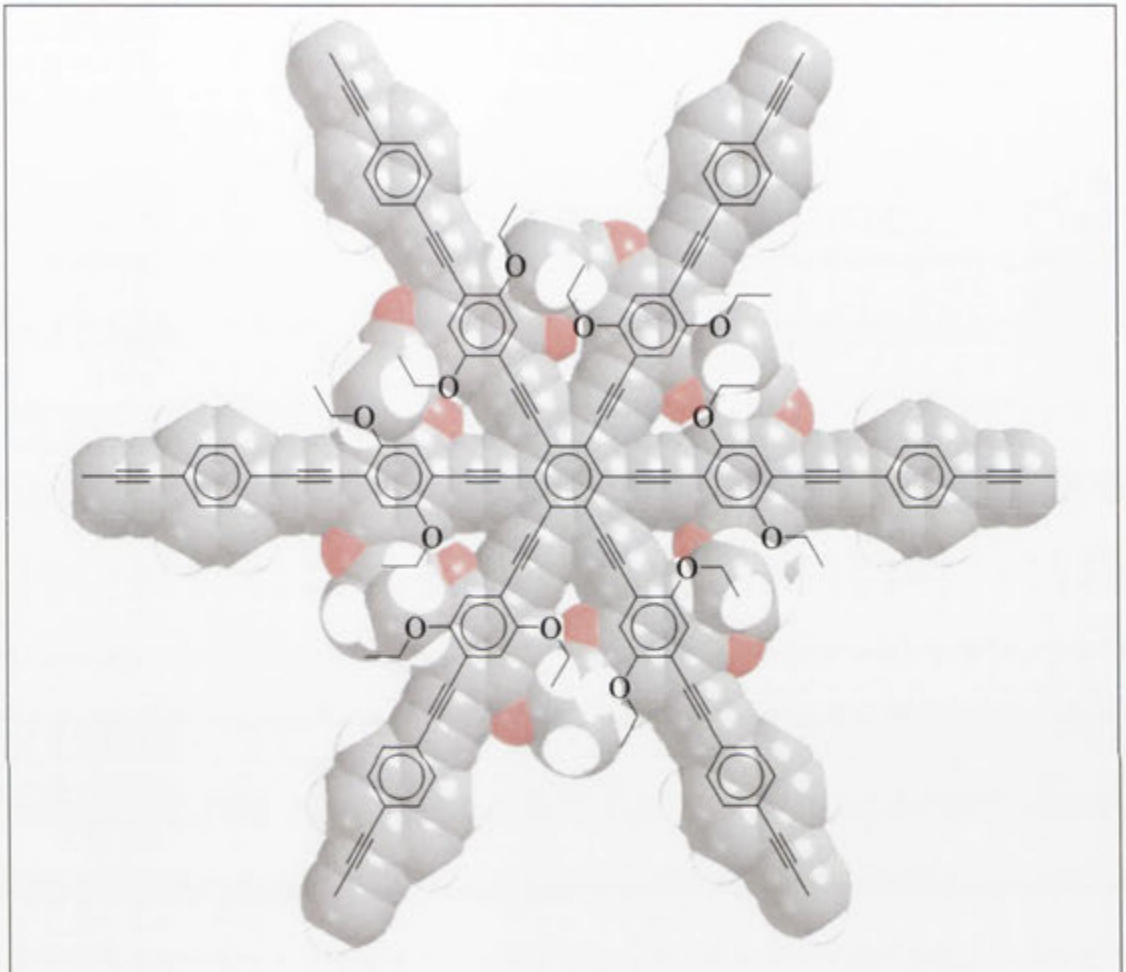

**Figure 4.4** Larger organic core, designed to allow space for *trans*-Ru(dppe)$_2$ moieties.

Options which have been used on aromatic rings to increase the solubility of larger molecules include hexyl[160] and vinylene[161] moieties, among many others, bound to the aromatic rings. Despite the possible damping effect (on $\chi^{(3)}$) of the ethoxy group, it was chosen due to the previous knowledge within the research group of its synthesis and effect upon NLO responses.[108] Additionally, if there is any reduction in the magnitude of NLO response due to the ethoxy groups, it will not interfere with the intended symmetry comparison, as the ethoxy groups will be present in equal proportion to the metal centres throughout all of the molecules. Final modeling of the intended product (Figure 4.5) showed that there is easily space for the *trans*-RuCl(dppe) centres.

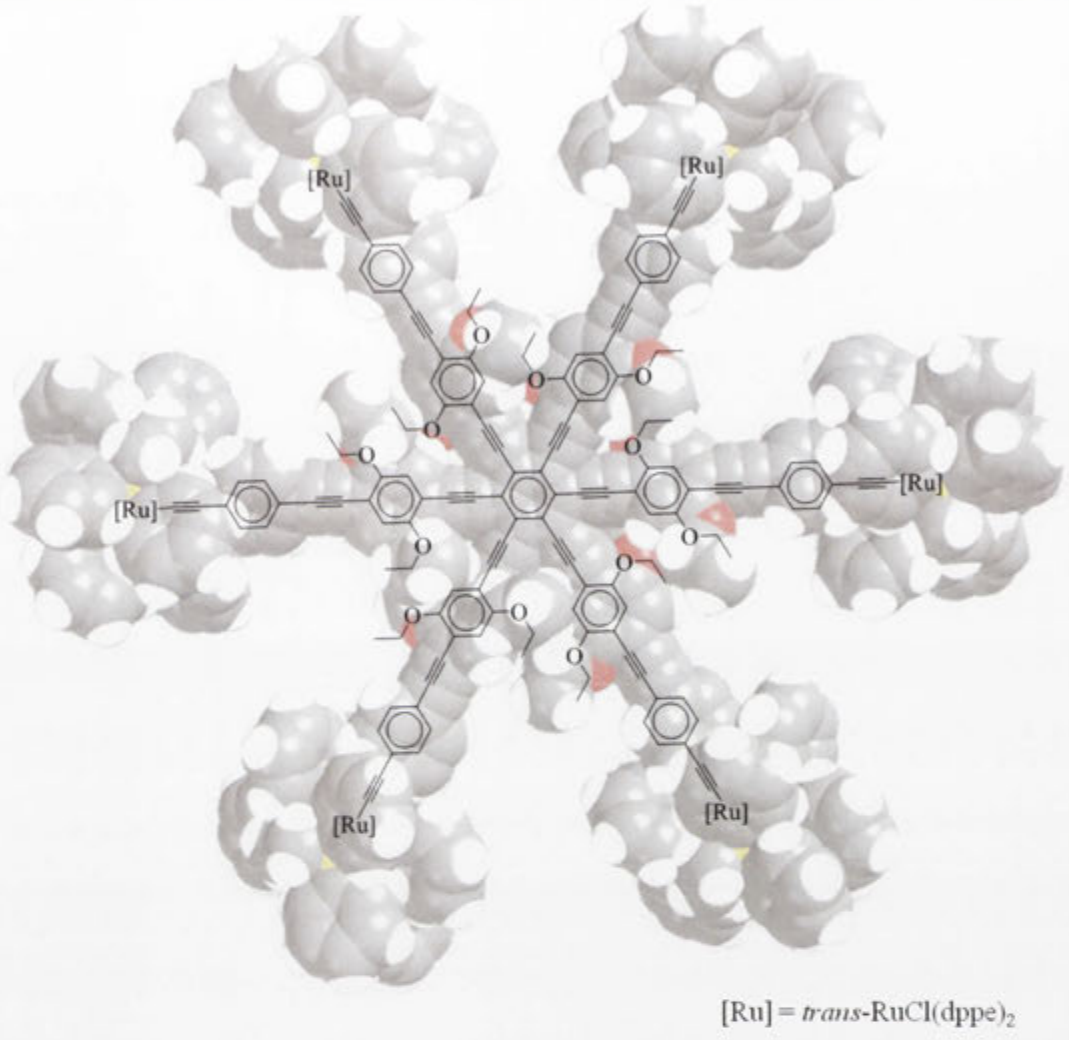


**Figure 4.5** Spartan™ model showing *trans*-RuCl(dppe)$_2$ about the larger organic core.

In order to undertake a full comparison, a series of compounds with six, four, three, two and one 'arm' attached to the central core were envisioned (some similar compounds have been synthesized previously, but never a full series for comparison). Additionally, the deliberate homocoupling of the arm to itself was planned. All together, this series would give a good indication as to the effects of increasing symmetry upon cubic NLO response.

## 4.2 Synthesis

The target compounds were synthesized in several stages. Several intermediate compounds were prepared as building blocks and then assembled into 4-$Pr^i_3SiC{\equiv}CC_6H_4C{\equiv}CC_6H_2$-2,5-$(OEt)_2$-4-Br (**54**), which is the 'arm' common to all compounds.[108] The first step was the synthesis of 1-bromo-2,5-diethoxy-4-iodobenzene, beginning with the formation of *p*-diethoxybenzene from quinol (Scheme 4.4).

**Scheme 4.4**[162, 163]

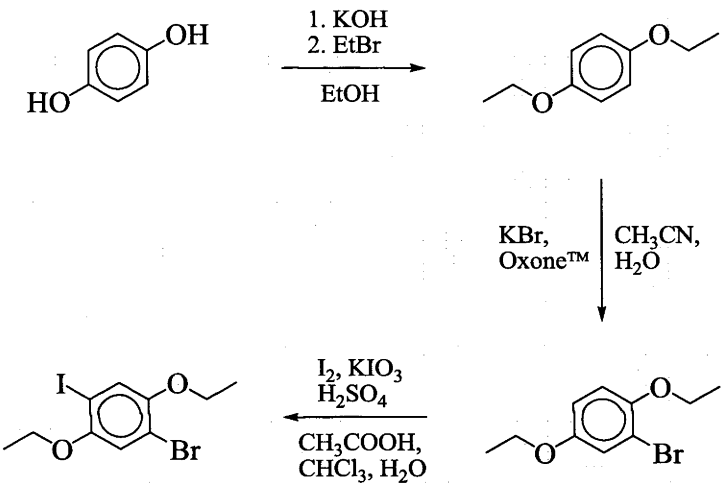


The only difficulty in repeating the literature procedures in Scheme 4.4 was the bromination of *p*-diethoxybenzene. All of the methods examined resulted in roughly equal portions of *p*-diethoxybenzene, 1-bromo-2,5-diethoxybenzene and 1,4-dibromo-2,5-diethoxybenzene (the doubly brominated byproduct) – it appears that there is little selectivity towards bromination. The method used was chosen for the ease of separation of the products: the byproduct is of low solubility in the reaction mixture and the unreacted starting material moves much more quickly down a non-polar silica column than the product.

4-(triisopropylsilyl)ethynylphenylacetylene was then prepared, utilizing the selectivity of Sonogashira reactions towards iodine. At room temperatures, most aryl bromides are unreactive towards Sonogashira conditions, while the iodide in an aryl iodide is readily replaced by a terminal alkyne. This methodology, coupled with selective deprotection

of the more easily removed trimethylsilyl protecting group, yields 4-(triisopropylsilyl)ethynylphenylacetylene (Scheme 4.5).

**Scheme 4.5**[135, 138]

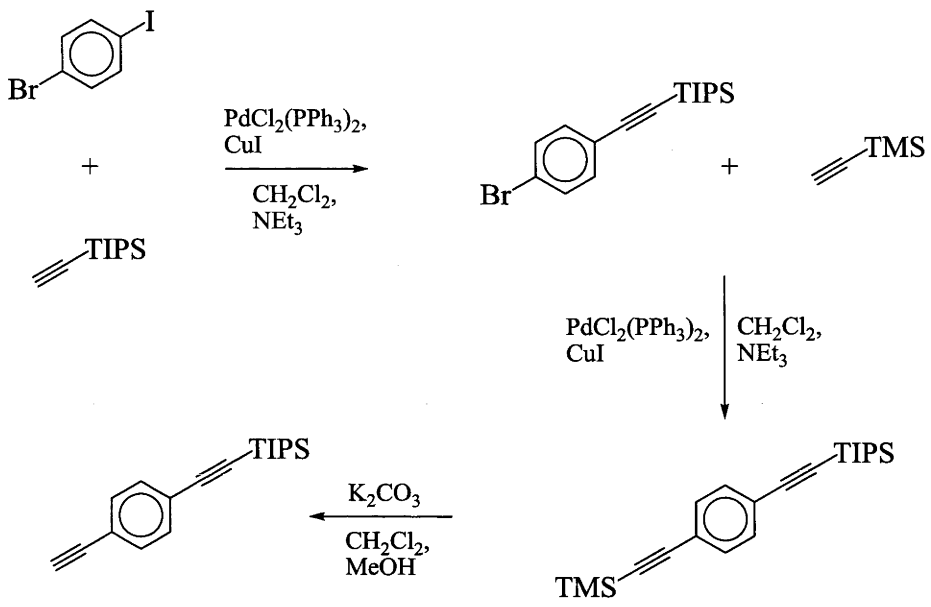


Combining (using Sonogashira selectivity again) 1-bromo-2,5-bisethoxy-4-iodobenzene and 4-(triisopropylsilylethynyl)phenylacetylene resulted in compound **54**, a 'double extender' consisting of two phenylenethynylene spacers, one of them with two ethoxy moieties to increase solubility (Scheme 4.6).

It had been found previously within the Humphrey group that *cis*-$RuCl_2(dppe)_2$ was unreactive towards terminal alkynes bound directly to aromatic rings with solubilizing moieties.[164] This meant that the diethoxybenzene rings would have to be closest to the central aromatic ring in the core. There was some concern about steric hindrance between the ethoxy groups, but the space filling model (Figure 4.4) showed that the steric interactions were not enough to cause the aromatic rings to strain out of the plane of the molecule.

**Scheme 4.6**[108]

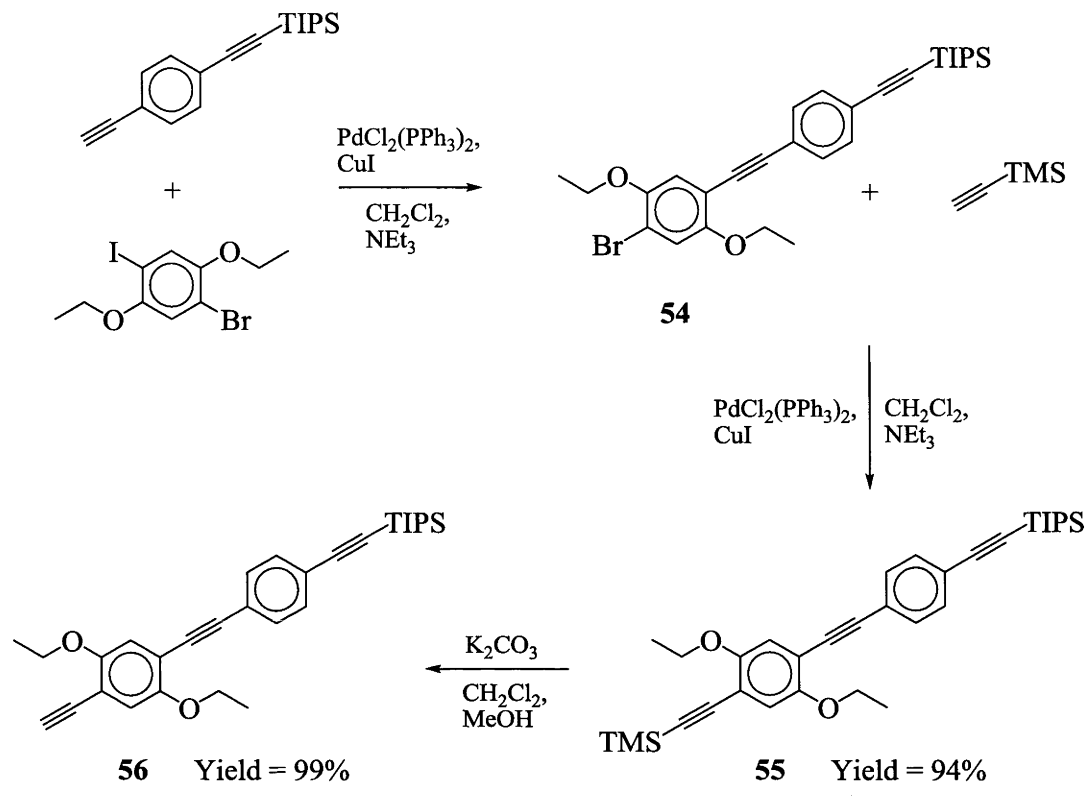


The bromide was replaced with a terminal alkyne (**55**) and the TMS selectively removed, in order to further react the product (**56**) with different aromatic halides. In the reaction of compound **54** with trimethylsilylacetylene, the electron-rich substituted aromatic ring acted as a deterrent to heterocoupling (as with the attempted reactions of *p*-N,N-diethylaminophenylacetylene in Chapter 3). The reaction proceeded, but with considerable homocoupling of the trimethylsilylacetylene. As compound **55** is an oil, purification was usually achieved[xxii] by further reaction (deprotection forming compound **56**) and evaporation of the 1,3-butadiyne under reduced pressure.

[xxii] To obtain a pure sample for characterization, normal phase column chromatography was used, with a petrol / EtOAc gradient elution.

**Scheme 4.7**

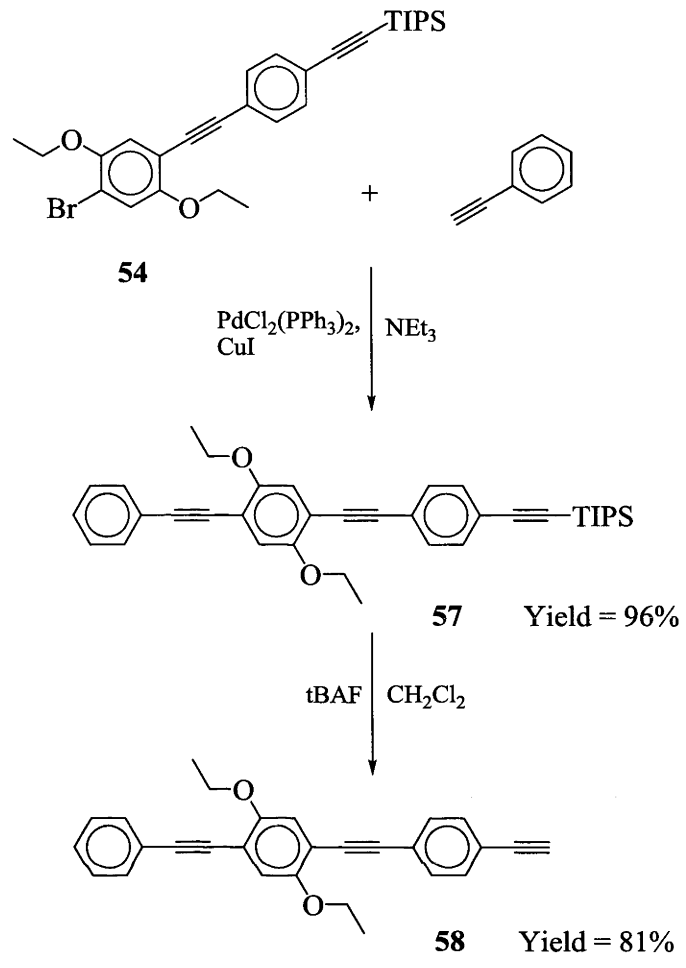


For the synthesis of the target compounds it was more economic to react compound **54** with phenylacetylene. Deprotection of this species (**57**) yielded **58**, which has a terminal alkyne that is available for metal-acetylide coupling (Scheme 4.7).

It was discovered that the homocoupling of **56** was remarkably facile compared to the homocoupling of compounds **35** – **37** in Chapter 3. TMS deprotection reactions can usually be easily purified by precipitation and stirring of the product in methanol. Unfortunately, because the previous reaction was not fully purified (the oily **55** had probably retained some Sonogashira catalysts and triethylamine), stirring in methanol resulted in the formation of **59** (Scheme 4.8). This was repeated in a more controlled environment and subsequent deprotection yielded **60**.

**Scheme 4.8**

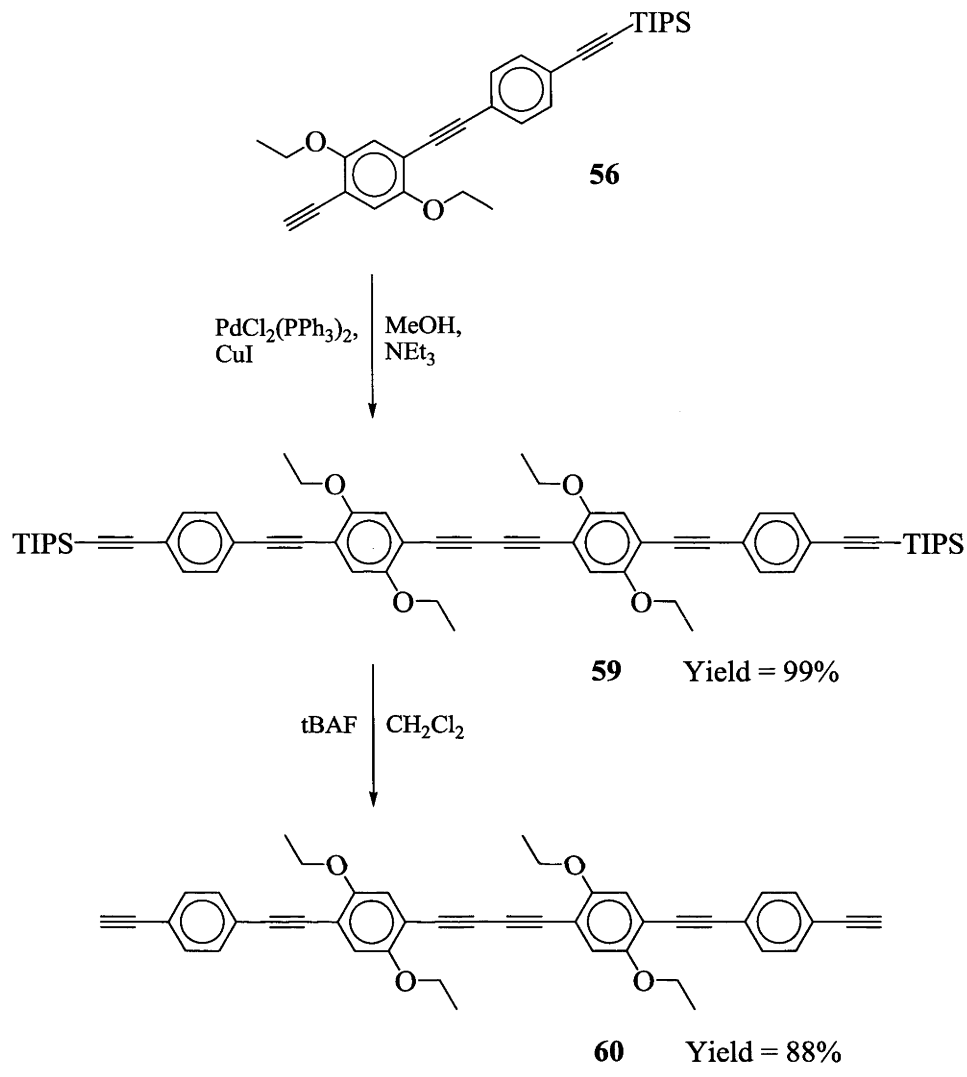


The remaining organic cores all required the reaction of **56** with aryl halides. These reactions were slow to proceed (despite the use of aryl iodides in the formation of **61** and **63**) and took progressively longer to react as the level of substitution increased (Scheme 4.9, Scheme 4.10 and Scheme 4.11). The reactions were monitored by $^{1}H$ NMR spectroscopy (see Section 4.3.1) and worked up when the protons on the central aromatic ring all resonated at the same frequency.

**Scheme 4.9**

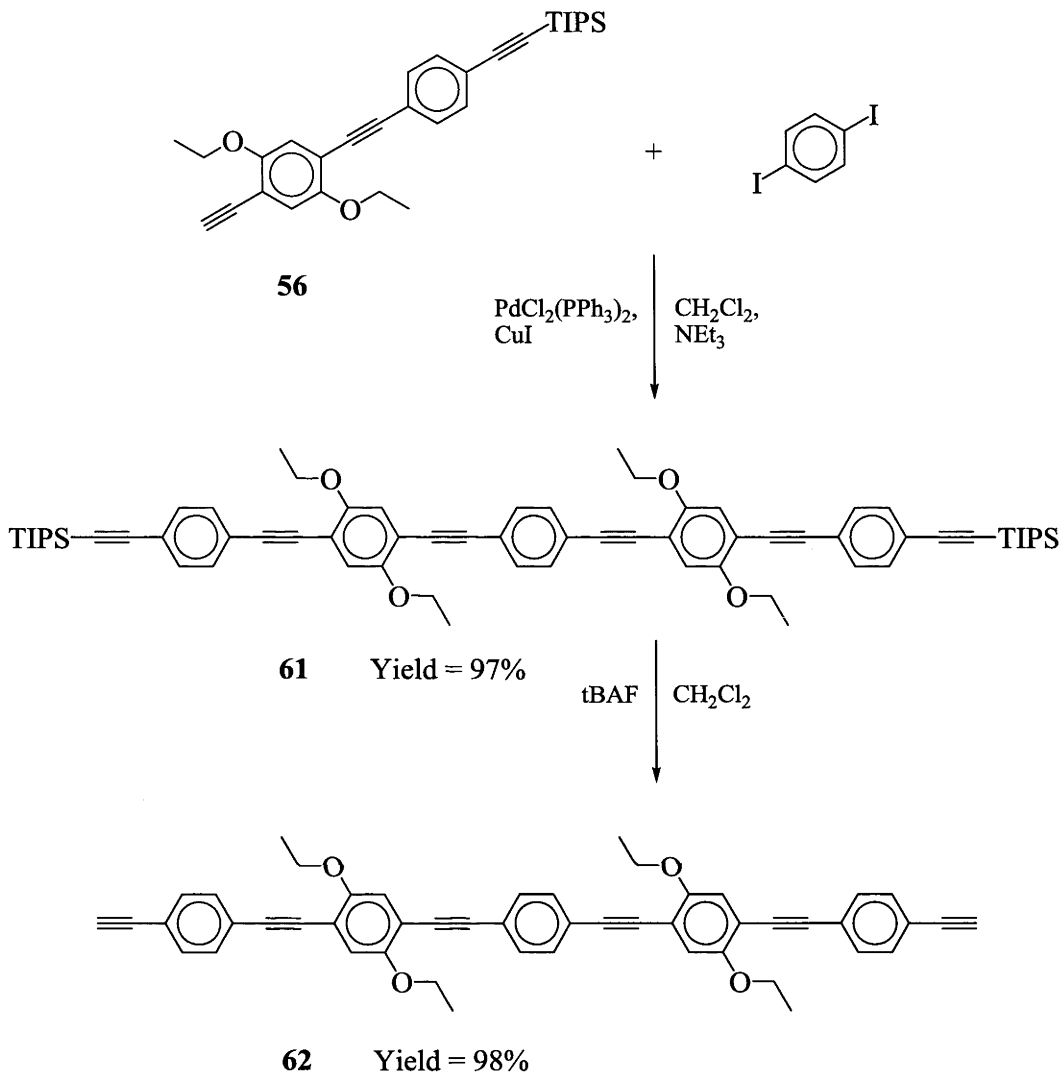
TIPS
O
O
+
I
I
56
PdCl2(PPh3)2,
CuI
CH2Cl2,
NEt3
O
O
TIPS
TIPS
O
O
61 Yield = 97%
tBAF
CH2Cl2
O
O
O
O
62 Yield = 98%

**Scheme 4.10**

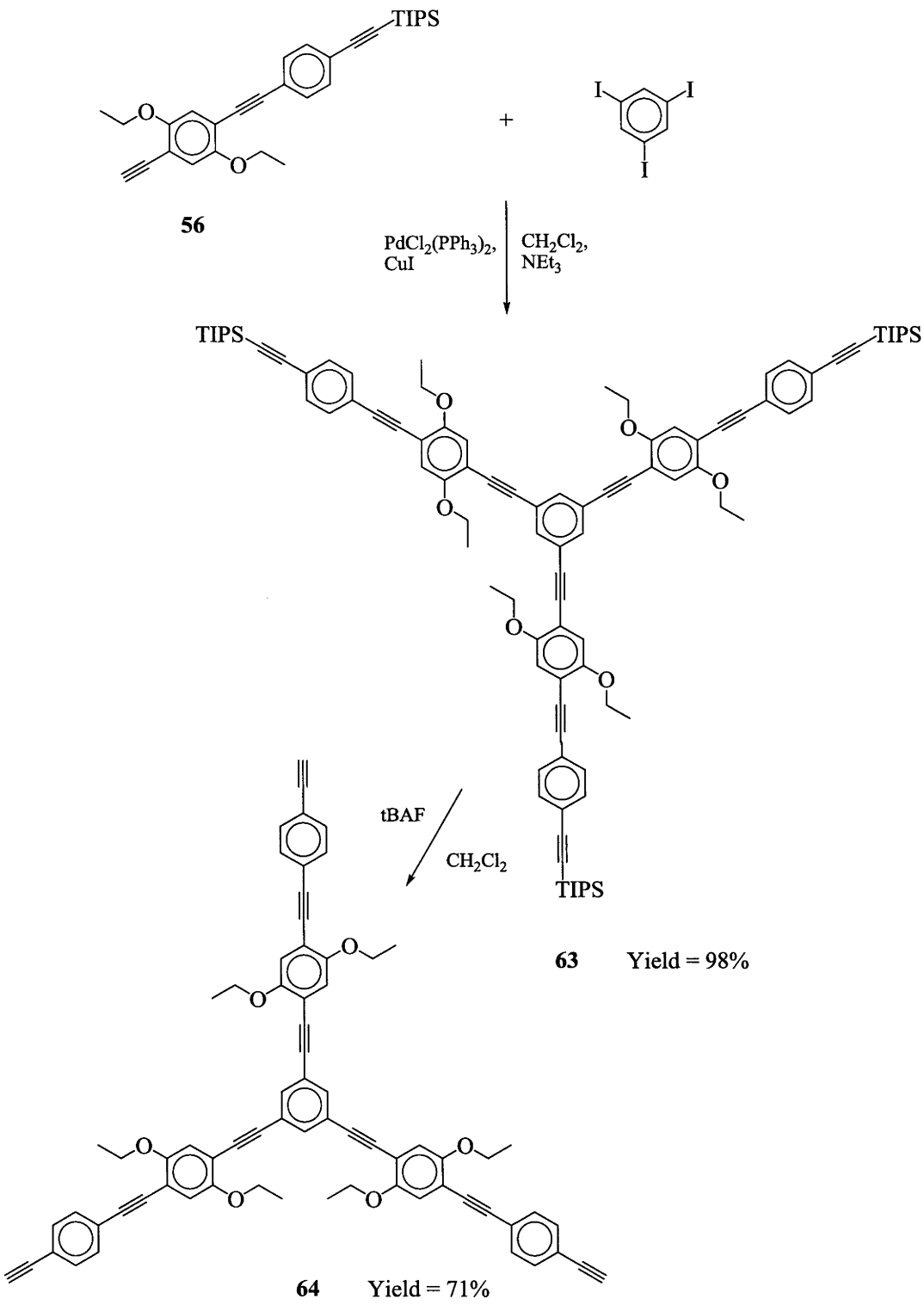
TIPS
O
O
56
+
I
I
I
PdCl2(PPh3)2,
CuI
CH2Cl2,
NEt3
TIPS
TIPS
O
O
O
O
O
O
TIPS
tBAF
CH2Cl2
63
Yield = 98%
O
O
O
O
O
O
64
Yield = 71%

**Scheme 4.11**

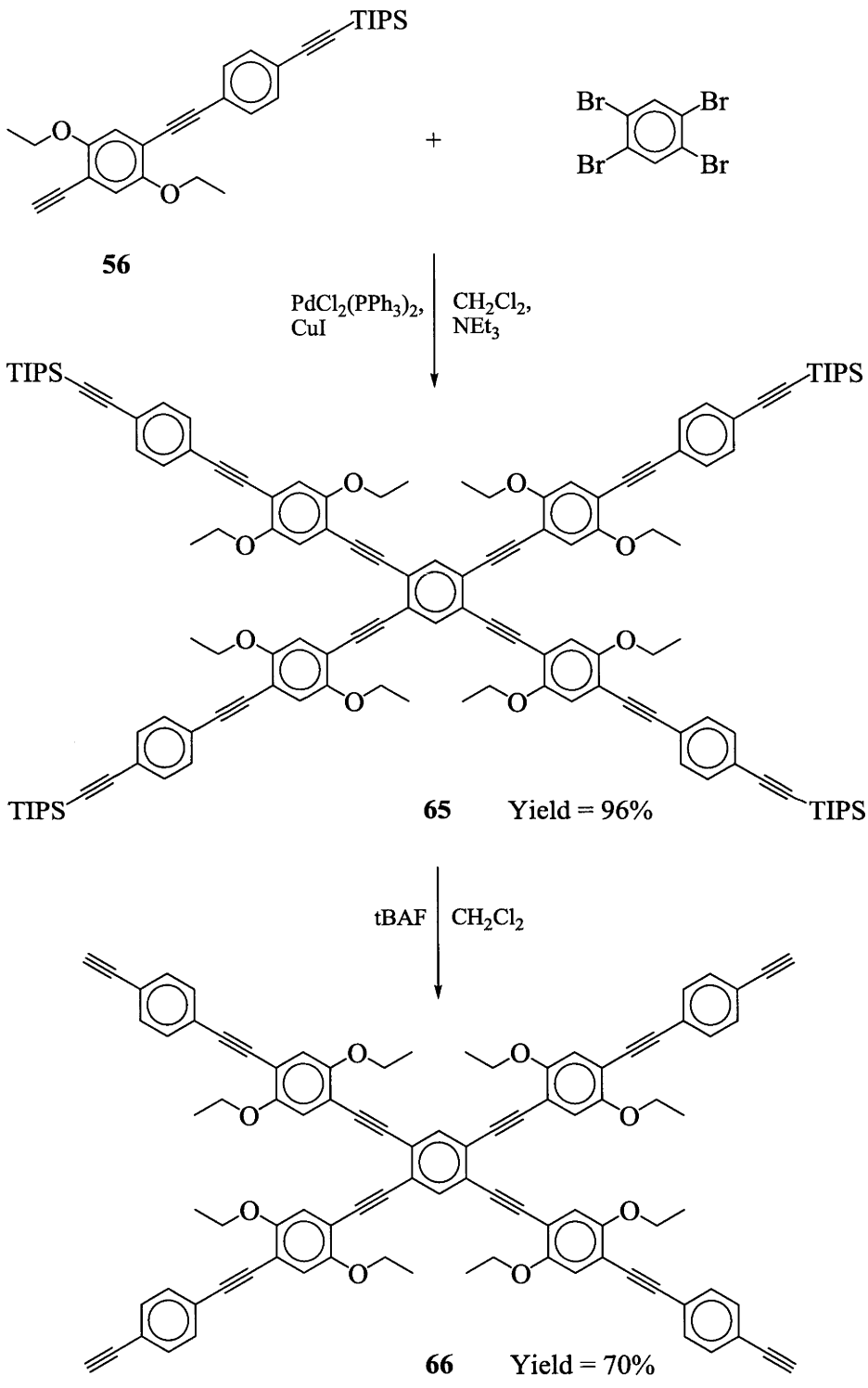
TIPS
Br
Br
Br
Br
56
$PdCl_2(PPh_3)_2$, CuI
$CH_2Cl_2$, $NEt_3$
TIPS
TIPS
TIPS
TIPS
65 Yield = 96%
tBAF
$CH_2Cl_2$
66 Yield = 70%

Homocoupling of **56** was an issue in all of the reactions forming compounds **61**, **63** and **65**. During reaction monitoring, when the acetylenic proton no longer resonated in the $^1$H spectrum (at 3.14 ppm), additional amounts of **56** were added. This was required in all three reactions. Compound **59** is slightly more soluble in a mix of petrol and ethanol than any of **61**, **63** or **65**, allowing for removal of homocoupled material through recrystallization. Although the stability of the products on deprotection (**62**, **64** and **66**) had been a matter of some trepidation, it was found that they were stable in air, possibly due to the presence of the ethoxy groups. The compounds were characterized immediately and not stored for longer than 24 hours.

**Scheme 4.12**

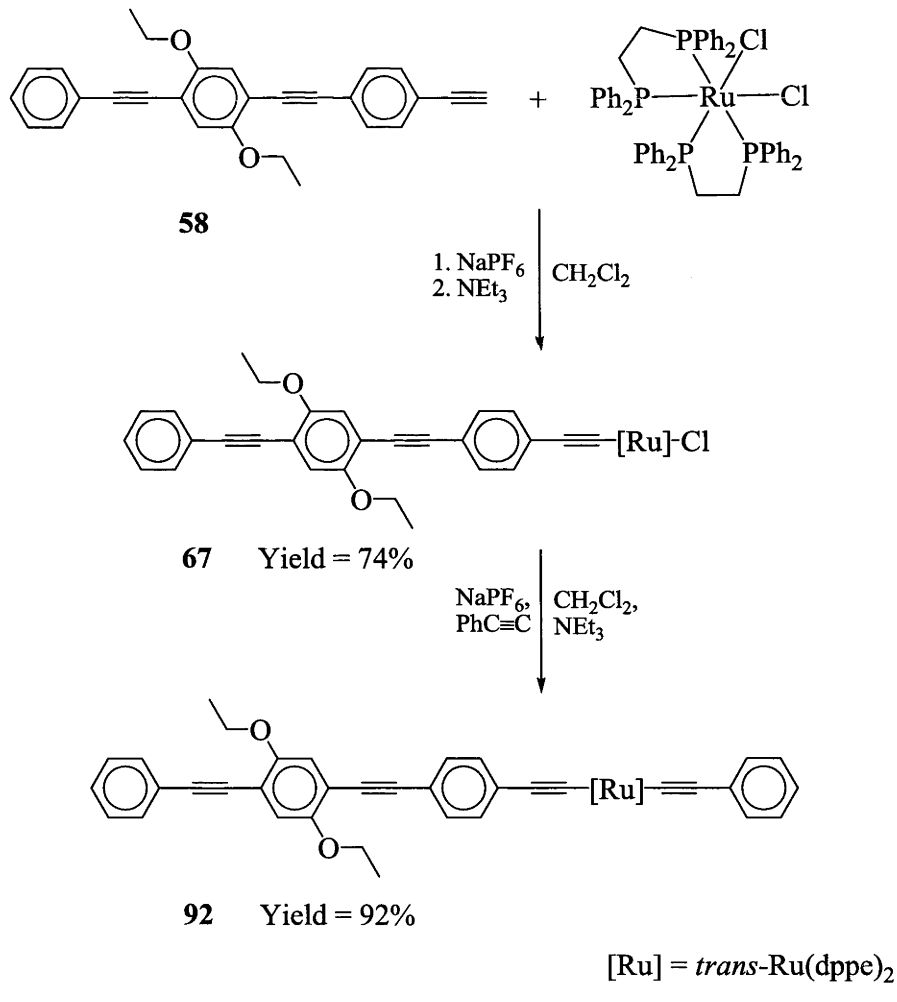

The set of organic compounds with terminal alkynes (**58**, **60**, **62**, **64**, **66**) were then coupled with *cis*-$RuCl_2(dppe)_2$ to form ruthenium complexes **67**, **69**, **71**, **73** and **75** (Scheme 4.12, Figure 4.6 and Figure 4.7). The five resulting ruthenium-acetylide molecules were reacted with phenylacetylene to replace the chloride ligand. This resulted in ten ruthenium-containing compounds with five different levels of substitution about the central aromatic ring (including the 'no-ring' structure).

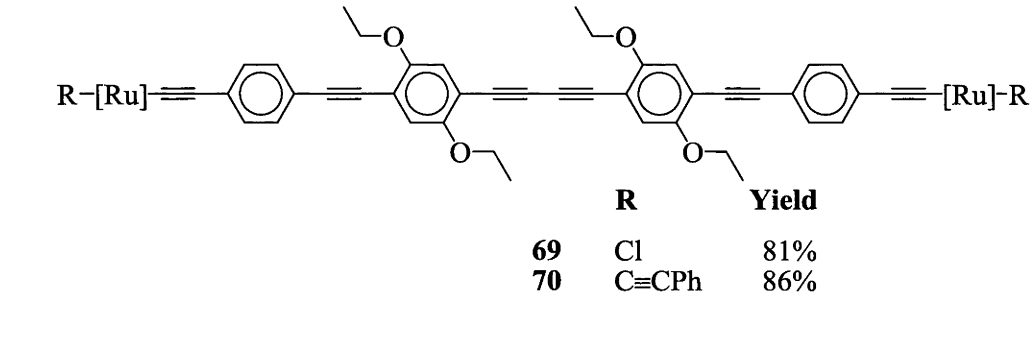


| | R | Yield |
|---|---|---|
| **69** | Cl | 81% |
| **70** | C≡CPh | 86% |

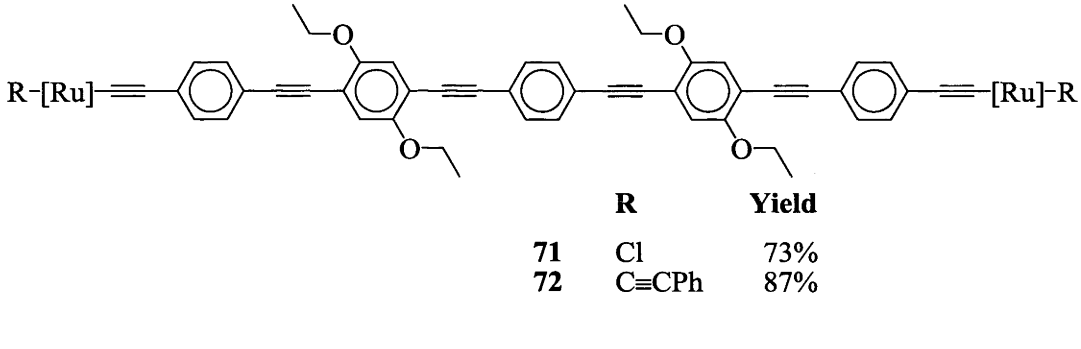


| | R | Yield |
|---|---|---|
| **71** | Cl | 73% |
| **72** | C≡CPh | 87% |

[Ru] = *trans*-$Ru(dppe)_2$

**Figure 4.6** Ruthenium compounds synthesized from compounds **60** and **62**.

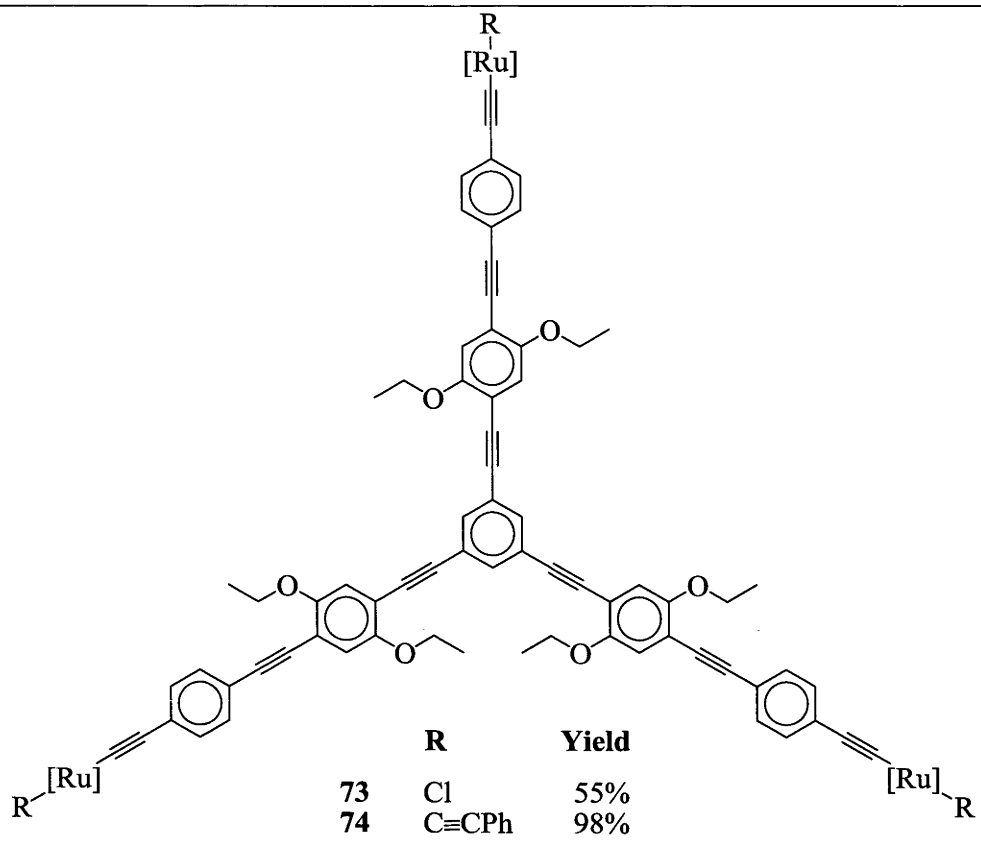


| | R | Yield |
|---|---|---|
| **73** | Cl | 55% |
| **74** | C≡CPh | 98% |

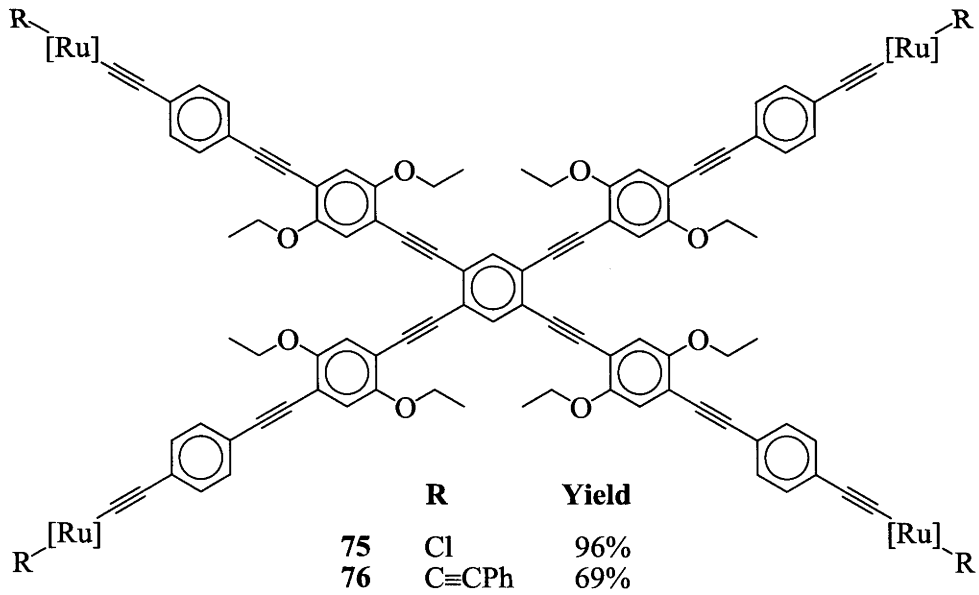


| | R | Yield |
|---|---|---|
| **75** | Cl | 96% |
| **76** | C≡CPh | 69% |

[Ru] = *trans*-Ru(dppe)$_2$

**Figure 4.7** Ruthenium compounds synthesized from compounds **64** and **66**.

### 4.2.1 Difficulty with Six-fold Symmetry Compound

It was not possible to react compound **56** with hexabromo- or hexaiodobenzene. With no protons in distinct new environments in the product (as compared to the starting material), it was not possible to monitor the progress of the reaction by $^{1}H$ NMR. $^{13}C$ NMR was used instead –the initial C-Br peak resonates at 127.3 ppm. The $^{13}C$ NMR spectrum of the four-fold substituted compound (**65**) has resonances of 134.6 ppm (for carbons in the central ring bonded to protons) and 125.5 ppm (carbons in the central ring bonded to acetylenic carbons).

The spectra of the attempts to synthesize the analogous six-fold compound all showed several peaks in this region (Figure 4.8). The resonances can probably be assigned to: successful coupling reactions (125.5 to 126.9 ppm), carbons still bound to a bromine atom (127.6-128.7 ppm) and carbons where the bromine has been removed and replaced by a proton (133.9 – 135.4 ppm). The multiple peaks in these regions (and not on other peaks in the spectrum) are indicative of a mix of structural isomers with varying levels of hydrogen-for-bromide replacement and successful heterocoupling.

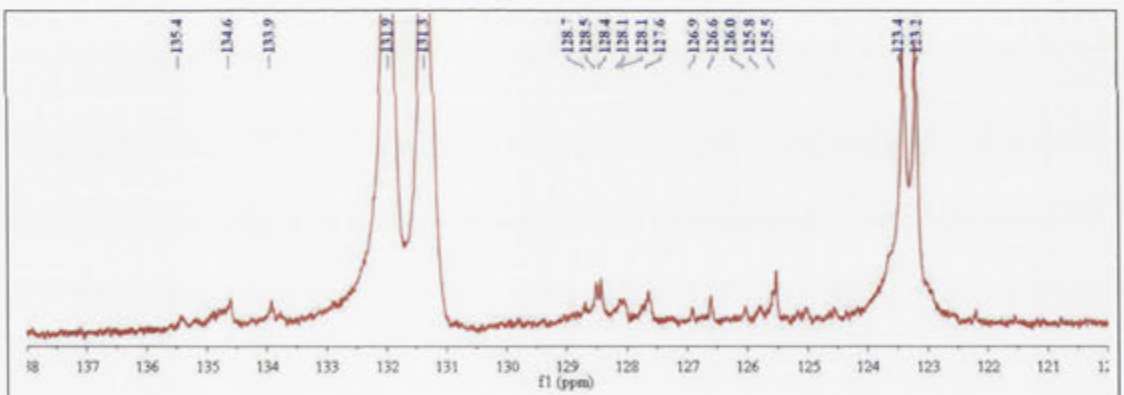


**Figure 4.8** The $^{13}C$ spectrum of the product of the reaction between compound **56** with hexabromobenzene.

Microanalyses of the products returned values that indicate that the level of substitution was between four- and five-fold. The presence of resonances at 135 ppm indicates that the halide (Br) has been stripped off in some cases and replaced with a proton. This is supported by similar results involving hexabromobenzene[xxiii] and phenylacetylenes.[150,

[xxiii] The reaction was also attempted with hexaiodobenzene, but it was found to be less successful. This is in accordance with literature reports for similar reactions.[155]

[151] It has been concluded that the reaction of these substituted phenylacetylenes with *per*-aryl halides is not possible. The hypothesis is that the additional steric hindrance of the ethoxy groups prevents the reaction from proceeding to completion.

These syntheses provided a series of organometallic molecules with increasing levels of substitution about the central core. By comparison of their characteristics, it should be possible to determine the effect of increasing the degree of symmetry upon the NLO properties of organometallic materials. This will also allow us to determine if the trends are similar to those of organic materials.

## 4.3 Characterization

All of the new complexes (**55** – **76**) were characterized by IR, UV-vis, $^{1}H$, $^{13}C$ and $^{31}P$ NMR spectroscopy, cyclic voltammetry and EI and HR ESI mass spectrometry. The organic analogs have absorbance maxima at 380 nm and 320 nm, while the lower energy band is red-shifted in the ruthenium-containing compounds, with maxima at 430 nm and 320 nm.

IR bands at 2055 $cm^{-1}$ correspond to the $\nu$(C≡C–Ru) energies. Organic acetylenic bands appear at 2210 $cm^{-1}$ for aromatically interdigitized alkynes ($\nu$(C≡C) 2210 $cm^{-1}$), 2150 $cm^{-1}$ for silyl-protected alkynes ($\nu$(SiC≡C) 2152 $cm^{-1}$), and 2105 for terminal alkynes ($\nu$(C≡C–H) 2105 $cm^{-1}$).

EI MS and ESI MS consistently returned values supporting the molecular ion. EI techniques were used for compounds with molecular weights below 700, while ESI was used for heavier molecules. High resolution measurements were done by electrospray ionization. The organic materials had masses corresponding to ($M + Na^{+}$), while the organometallic compounds had the chloride or phenylacetylide ligands replaced by acetonitrile ($M - Cl + MeCN^{+}$ or $M - C{\equiv}CPh + MeCN^{+}$). In cases where there were multiple metal centres, molecular ions with 2+, 3+ and 4+ charges were observed with masses corresponding to the replacement of 2, 3, or 4 ligands by acetonitrile, respectively.

Cubic NLO Z-scan measurements were taken using a setup with nanosecond-duration pulses. The data obtained under such conditions was dominated by excited-state absorption and thermal effects and is not useful for comparisons with the electronic

nonlinearity determined for other compounds in this thesis using the femtosecond setup. Femtosecond-duration measurements will be done when a setup again becomes available to the group.

### 4.3.1 Analyses of NMR Spectra

Figure 4.9 shows the numbering scheme used for proton and carbon atoms in the analysis of the NMR spectra. The numbers correspond to the carbon atom in the location of the number (for $^{13}C$ spectra), or the proton attached to that carbon (for $^{1}H$ spectra).[xxiv]

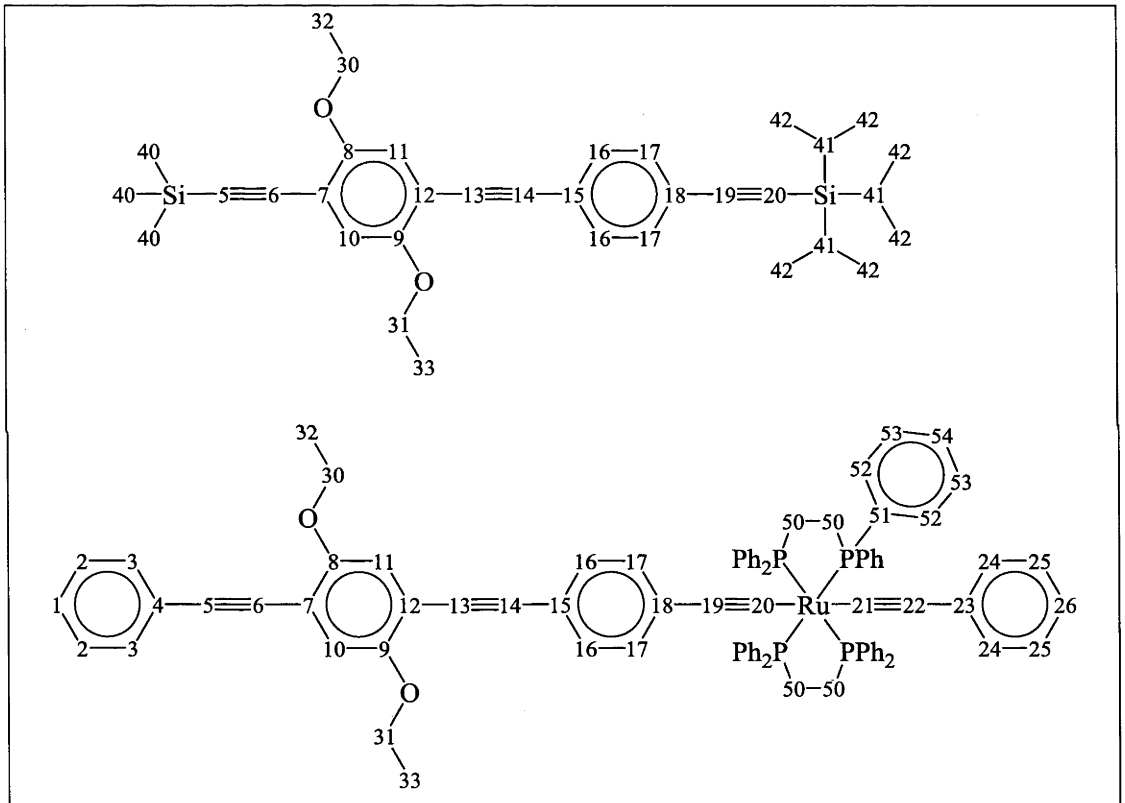


**Figure 4.9** Numbering scheme for NMR analysis of compounds **55** – **76**.

As mentioned previously, compounds **61**, **63** and **65** had to be separated from the homocoupled byproduct. It was possible to determine the purity of these compounds by $^{13}C$ NMR spectroscopy. For the TIPS-protected organic molecules, the acetylenic carbon atoms resonate downfield of 86 ppm, except for the homocoupled acetylenic

[xxiv] Fully annotated $^{1}H$ and $^{13}C$ NMR spectra are available in the appendices.

carbons, which resonate at 78 ppm (Figure 4.10). When the silyl protecting group is removed, the terminal alkynyl carbon (atoms 19 and 20) resonances shift upfield. Notice that compound **79** has less molecular symmetry and all six of the acetylenic carbon atoms resonate at different frequencies.

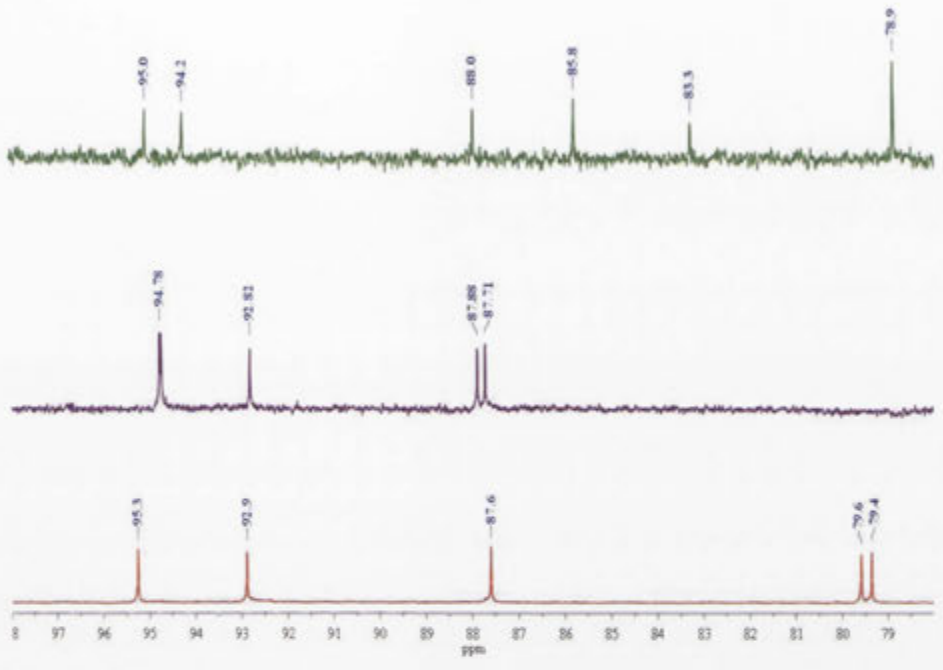


**Figure 4.10** $^{13}C$ NMR spectra of compounds **58** (green), **61** (magenta) and **59** (red).

The $^{1}H$ NMR spectral data also supports the theory that the incomplete reaction resulting from the hexa-substitution reaction of compound **56** with an aromatic ring is partly due to steric reasons. In compound **61** (twofold substitution), the ethoxy protons (bound to carbons 30 and 31) resonate at the same frequencies, forming sharp peaks (Figure 4.11). In compound **63** (threefold substitution), the peaks in the quartet are broadened. This is possibly because (as careful examination of the structures in Figure 4.7 will show) the ethoxy moiety may be in four different structural environments. In the fourfold substituted compound (**65**), the position 30 and 31 protons have split into two distinct quartets. This (and the sharpness of the peaks) indicates that there are less structural isomers for this compound. If this symmetry in compound **65** is due to the steric bulk of the ethoxy moieties, perhaps they prohibit complete reaction with hexabromobenzene.

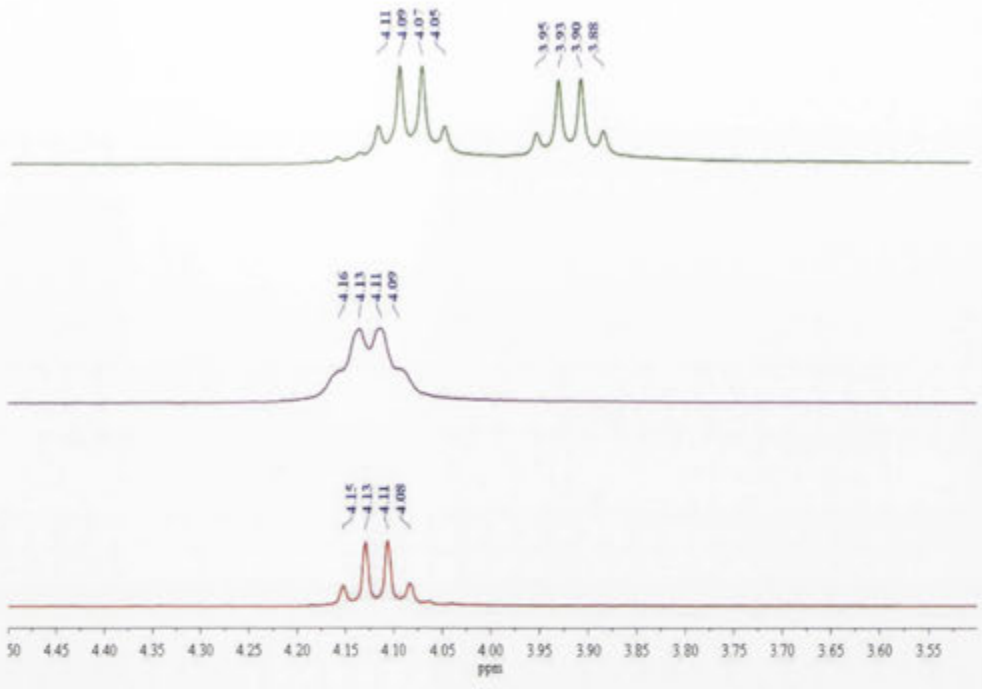


**Figure 4.11** $^{1}$H NMR spectra of compounds **65** (green), **63** (magenta) and **61** (red).

The compounds with twofold substitution (**61**, **62**, **71**, **72**) have (comparatively) the lowest solubility of the compounds in this chapter and the homocoupled compounds (**59**, **60**, **69**, **70**) are the most soluble. Based on these solubility characteristics and the NMR spectral data showing that there is interaction between close ethoxy groups, it is hypothesized that solvation is more readily achieved when the ethoxy groups are in close spatial proximity to each other.

### 4.3.2 Electrochemistry

UV-vis and IR spectra were taken of selected compounds in both the ground state ($Ru^{II}$) and oxidized ($Ru^{III}$) forms. The potential required for oxidation and the resulting changes in the IR spectral absorbances are summarized in Table 4.1.

**Table 4.1** Optical behaviour of selected compounds in the ground and excited states.[xxv]

| Compound | # of Metals / Ligand | $E_{1/2}$ (V) $Ru^{II/III}$ ($\Delta E$ (V), $i_{pc}/i_{pa}$) | ν(C≡C–Ru) $cm^{-1}$ $Ru^{II}$ | ν(C≡C–Ru) $cm^{-1}$ $Ru^{III}$ |
|---|---|---|---|---|
| **67** | 1 / Cl | 0.58 (0.08, 1) | 2065 | 1902 |
| **68** | 1 / C≡CPh | 0.47 (0.06, 1) | 2058 | 1900 |
| **73** | 3 / Cl | 0.58 (0.06, 1) | 2064 | 1907 |
| **74** | 3 / C≡CPh | 0.53 (0.06, 1) | 2056 | 1899 |
| **75** | 4 / Cl | 0.59 (0.07, 1) | 2064 | 1903 |
| **76** | 4 / C≡CPh | 0.56 (0.07, 1) | 2057 | 1898 |

Redox processes for all of the compounds were fully reversible. Upon oxidation, the absorption of the ν(C≡C–Ru) unit shifts from 2060 to 1900 $cm^{-1}$. This oxidized state absorbance is stronger than the ground state absorbance (Figure 4.12).

[xxv] Cyclic voltammetry experiments were carried out as outlined in Section 4.5.2.

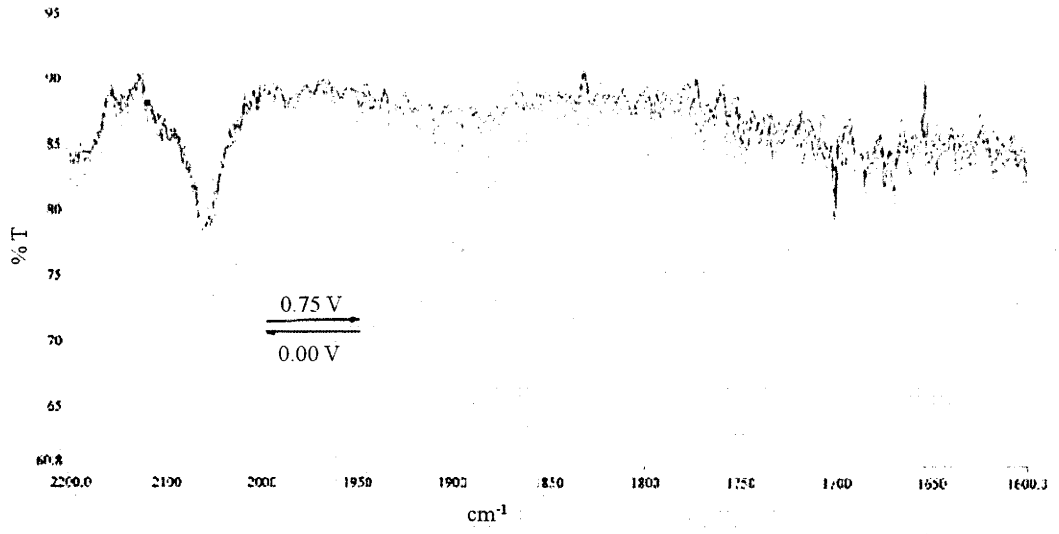


**Figure 4.12** Change in IR spectra upon oxidation / reduction of compound **76**.[165]

The compounds also absorb longer wavelength light differently when oxidized. UV-vis-NIR data of the ground state and excited state maxima are summarized in Table 4.2. For most local maxima, the absorption coefficients increase (in both the ground and excited states) as the number of metal centres increases. This is logical, as the number of chromophores per molecule is increasing, allowing for increased absorbance per molecule.

**Table 4.2** Effect of oxidation on the absorbance in the UV-vis-NIR ranges.[xxvi]

| Compound | # of Metals / Ligand | $Ru^{II}$ $cm^{-1}$ ($\varepsilon$ x $10^4$ $M^{-1}cm^{-1}$) | $Ru^{III}$ $cm^{-1}$ ($\varepsilon$ x $10^4$ $M^{-1}cm^{-1}$) |
|---|---|---|---|
| **67** | 1 / Cl | 24200 (4.1), 22500 (3.3) | 10400 (1.5), 20100 (1.3), 25101 (3.1), 26500 (3.1), 32300 (3.5), 36400 (4.6) |
| **68** | 1 / C≡CPh | 25400 (2.3), 32515 (1.6) | 8400 (0.4), 11600 (0.2), 18900 (0.5), 26500 (1.7), 32500 (1.7) |
| **73** | 3 / Cl | 24200 (13.8), 31685 (9.8) | 10100 (4.7), 20300 (5.0), 26500 (11.0), 31600 (9.8), 36500 (16.0) |
| **74** | 3 / C≡CPh | 252200 (9.3), 31765 (7.3) | 8200 (1.9), 20200 (0.7), 25900 (10.4), 31900 (6.6) |
| **75** | 4 / Cl | 24600 (11.5), 31155 (7.4) | 10400 (3.7), 24400 (10.0), 31800 (7.8), 36600 (12.6) |
| **76** | 4 / C≡CPh | 24600 (15.8), 31045 (12.3) | 8280 (4.1), 25300 (15.3), 30700 (15.3) |

Spectro electrochemical data (Figure 4.13) show that new absorption bands occur in the oxidized material with maxima at 2500 $cm^{-1}$, 4000 $cm^{-1}$ and 5800 $cm^{-1}$. This is accompanied by a blueshift of the band at 4500 $cm^{-1}$ in the starting material.

[xxvi] Cyclic voltammetry experiments were carried out as outlined in Section 4.5.2.

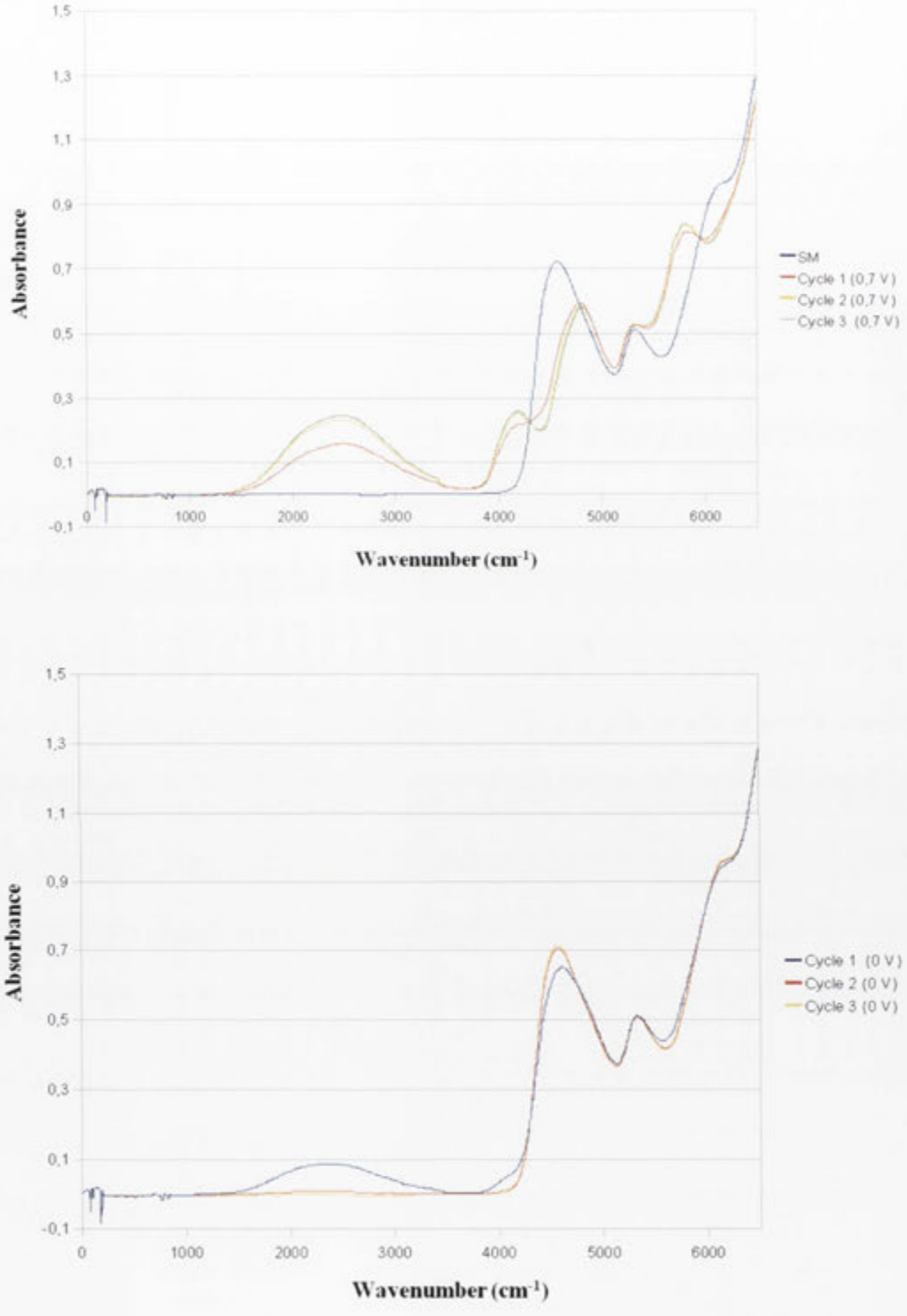


**Figure 4.13** Spectro-electrochemical data for compound **73**. The upper graph shows oxidation, while the lower graph shows the reduction process. Cycles are 6.2 minutes apart.

## 4.4 Conclusions

A series of organometallic compounds with increasing levels of substitution about the central aromatic core were synthesized. The bis-phenyleneethynylene segment was synthesized with ethoxy groups to increase the overall solubility of the molecules. These dendrimer subunits were than attached to differentially substituted phenyl halides using Sonogashira methods. The organic cores were metallated using *cis*-$RuCl_2(dppe)_2$ and finally the bis-acetylides were formed by ligand substitution of the chloride for phenylacetylide.

The compounds all have similar UV-vis absorption spectra, with the absorption coefficient increasing with the number of chromophores (metal centres) in the molecule. It is unknown if this increased linear absorption of electromagnetic radiation will translate to nonlinear absorption. The nonlinear measurements were taken with nanosecond length pulses of light and the spectra were dominated by excited state effects due to linear absorption.

## 4.5 Experimental Section

### 4.5.1 Materials

All reactions were performed under a nitrogen atmosphere with the use of Schlenk techniques. Dichloromethane was dried by distillation over calcium hydride; all other solvents were used as received. Petrol refers to the fraction of petroleum ether with a boiling range of 60-80°C. Chromatography was performed on silica gel (230-400 mesh ASTM) or ungraded basic alumina. The following were prepared by literature procedures: *cis*-$[RuCl_2(dppe)_2]$,[128] 4-$Pr^i_3SiC{\equiv}CC_6H_4C{\equiv}CC_6H_2$-2,5-$(OEt)_2$-4-Br (**54**).[108] All other reagents were obtained commercially and used as received.

### 4.5.2 Methods and Instrumentation

Microanalyses were carried out at the Australian National University. UV-vis-NIR spectra of solutions in $CH_2Cl_2$ in 1 cm quartz cells were recorded using a Cary 5 spectrophotometer and are reported as $\lambda_{max}$ (nm) [$\varepsilon$ $10^4$ $M^{-1}$ $cm^{-1}$)]. Infrared spectra were recorded as $CH_2Cl_2$ solutions using a Perkin-Elmer System 2000 FT-IR. $^1H$ (300 MHz) and $^{31}P$ NMR (121 MHz) spectra were recorded using a Varian Mercury-300 FT

NMR spectrometer and are referenced to residual chloroform (7.26 ppm) and external $H_3PO_4$ (0.0 ppm), respectively. $^{13}C$ NMR (75 MHz or 125 MHz) spectra were recorded using a Varian Mercury-300 FT NMR spectrometer or a Varian Gemini-500 FT NMR and are referenced to residual chloroform (77.00 ppm). Electron impact mass spectra (EI MS) were obtained using a VG Autospec instrument (70 eV electron energy, 8 kV accelerating potential). Electrospray ionization mass spectra (ESI MS) were recorded using a Bruker Apex3. Solutions in MeOH or acetonitrile were ionized with sodium or sodium and potassium ions; peaks are reported as *m/z* (assignment, relative intensity). Cyclic voltammetric measurements were recorded using a MacLab 400 interface and MacLab potentiostat from eDaq Pty Ltd. (using a Pt working, Pt auxiliary and Ag-AgCl reference minielectrodes from Cypress Systems). Scan rates were 100 mV $s^{-1}$. Electrochemical solutions contained 0.1 M $(Bu^n_4N)PF_6$ and ca. $10^{-3}$ M complex in freshly distilled DCM. Solutions were purged and maintained under an atmosphere of $N_2$. All values are referenced to an internal sample of ferrocene ($E^0$ 0.56 V, peak separation from 0.06 to 0.09V). UV-Vis-near IR and IR solution spectra of the oxidized species were obtained at 298K by electrogeneration in an optically-transparent thin-layer electrochemical (OTTLE) cell with potentials ca. 200 mV beyond $E_{1/2}$, to allow complete electrolysis; solutions were made up in 0.3 M $(Bu^n_4N)PF_6$ in DCM. Z-scan measurements were taken on an Opolette HE 355 II pumping a built in (βBB) optical parametric oscillator (OPO). The pulse length was 5 ns at a repetition rate of 20 Hz.

### 4.5.3 Experimental Data for Compounds 55 – 76

**Synthesis of 4-$Pr^i_3SiC{\equiv}CC_6H_4C{\equiv}CC_6H_2$-2,5-$(OEt)_2$-4-$SiMe_3$ (55).** 4-$Pr^i_3SiC{\equiv}CC_6H_4C{\equiv}CC_6H_2$-2,5-$(OEt)_2$-4-Br (**54**, 2.50 g, 4.76 mmol) and $(Me)_3SiC{\equiv}CH$ (0.50 mL, 7.43 mmol) were added to $NEt_3$ (200 mL) and deoxygenated. $PdCl_2(PPh_3)_2$ (0.100 g, 0.142 mmol) and CuI (0.014 g, 0.074 mmol) were then added and the mixture heated at 35 °C for 18 h. The solvents were removed under reduced pressure, the residue dissolved in petrol and ethyl acetate (15:1) and filtered through a short silica column. The solution was taken to dryness and the crude product recrystallized from $CH_2Cl_2$/MeOH to give a yellow solid (2.44 g, 94%). Anal. Calcd for $C_{34}H_{46}O_2Si_2$: C 75.22, H 8.19. Found: C 74.90, H 8.19%. IR: ν(C≡C) 2211 $cm^{-1}$, ν(SiC≡C) 2152 $cm^{-1}$. UV-vis: 365 [3.1], 319 [3.2]. $^1H$ NMR: δ 0.27 (s, 9H, $SiMe_3$), 1.13 (s, 21H, $SiPr^i_3$), 1.44 (t, $J_{HH}$ = 7 Hz, 3H, Me), 1.46 (t, $J_{HH}$ = 7 Hz, 3H, Me), 4.06 (q, $J_{HH}$ = 7 Hz, 2H, $OCH_2$), 4.07 (q, $J_{HH}$ = 7 Hz,

2H, $OCH_2$), 6.94, 6.96 (2 x s, 2H, 8, 9), 7.45 (s, 4H, 16, 17). $^{13}C$ NMR: δ 0.0 ($SiMe_3$), 11.3 (41), 14.9, 14.9 (32, 33), 18.7 (42), 65.2, 65.3 (30, 31), 87.7, 106.7 (19, 20), 92.9, 94.7 (13, 14), 100.5, 101.1 (5,6), 106.7 (20), 114.0, 114.1 (7, 12), 117.2, 117.4 (10, 11), 123.2, 123.4 (15, 18), 131.4, 132.0 (16, 17), 153.4, 154.0 (8, 9). HR EI MS Calcd for $C_{34}H_{46}O_2Si_2$: 542.3036 ($[M]^+$). Found: 542.3030 ($[M]^+$). EI MS: 542 ($[M]^+$, 100), 385 ($[M - SiPr^i_3]^+$, 30).

**Synthesis of 4-$Pr^i_3SiC{\equiv}CC_6H_4C{\equiv}CC_6H_2$-2,5-$(OEt)_2$-4-C≡CH (56).** 4-$Pr^i_3SiC{\equiv}CC_6H_4$ $C{\equiv}CC_6H_2$-2,5-$(OEt)_2$-4-$SiMe_3$ (**55**, 2.02 g, 3.72 mmol) and $K_2CO_3$ (1.5 g, 10.85 mmol) were added to a solution of $MeOH/CH_2Cl_2$ (100 mL, 1:1) and stirred at room temperature for 18 h. The solvents were removed under reduced pressure, the residue dissolved in $CH_2Cl_2$ (50 mL) and washed with water (50 mL x 3). The solution was dried over $MgSO_4$ and the solvent removed, giving yellow oil (1.74 g, 99%). IR: ν(C≡C) 2211 $cm^{-1}$, ν(SiC≡C) 2152 $cm^{-1}$, ν(C≡C–H) 2105 $cm^{-1}$. UV-vis: 359 [3.5], 316 [4.5]. $^1H$ NMR: δ 1.12 (s, 21H, $SiPr^i_3$), 1.45 (t, $J_{HH}$ = 7 Hz, 3H, Me), 1.46 (t, $J_{HH}$ = 7 Hz, 3H, Me), 3.14 (s, 1H, C≡C–H), 4.07 (q, $J_{HH}$ = 7 Hz, 2H, $OCH_2$), 4.09 (q, $J_{HH}$ = 7 Hz, 2H, $OCH_2$), 6.98, 6.98 (2 x s, 2H, 8, 9), 7.45 (s, 4H, 16, 17). $^{13}C$ NMR: δ 11.3 (41), 14.8, 14.8 (32, 33), 18.6 (42), 65.1, 65.2 (30, 31), 79.9 (5), 82.5 (6), 87.5, 106.7 (19, 20), 92.9, 94.7 (13, 14), 112.8, 114.4 (7, 12), 116.9, 117.9 (10, 11), 123.1, 123.4 (15, 18), 131.4, 131.9 (16, 17), 153.3, 154.0 (8, 9). HR ESI MS Calcd for $C_{31}H_{38}O_2Si$: 493.2539 ($[M + Na]^+$), 471.2719 ($[M + H]^+$). Found: 493.2557 ($[M + Na]^+$), 471.2726 ($[M + H]^+$). EI MS: 470 ($[M]^+$, 100), 427 ($[M - Pr^i]^+$, 60), 385 ($[M – (Pr^i)_2]^+$, 60).

**Synthesis of 4-$Pr^i_3SiC{\equiv}CC_6H_4C{\equiv}CC_6H_2$-2,5-$(OEt)_2$-4-C≡CPh (57).** 4-$Pr^i_3SiC{\equiv}CC_6H_4$ $C{\equiv}CC_6H_2$-2,5-$(OEt)_2$-4-Br (**54**, 3.312 g, 6.31 mmol), $PdCl_2(PPh_3)_2$ (0.100 g, 0.140 mmol) and CuI (0.027 g, 0.014 mmol) were added to $NEt_3$ (200 mL) and the solution deoxygenated. PhC≡CH (4.00 mL, 38.1 mmol) was then added under nitrogen, the solution deoxygenated again and stirred at 35 °C for 18 h. The solvent was removed under reduced pressure, the residue dissolved in petrol and ethyl acetate (15:1) and filtered through a short silica column. The solvent was removed and the resulting solid recrystallized from MeOH. Filtration gave a grey solid (3.304 g, 96%). Anal. Calcd for $C_{37}H_{42}O_2Si$: C 81.27, H 7.74. Found: C 80.72, H 7.83%. IR: ν(C≡C) 2211 $cm^{-1}$, ν(SiC≡C) 2153 $cm^{-1}$. UV-vis: 374 [4.3], 327 [4.4]. $^1H$ NMR: δ 1.14 (s, 21H, $SiPr^i_3$),

1.48 (t, $J_{HH}$ = 7 Hz, 6H, Me), 4.11 (q, $J_{HH}$ = 7 Hz, 4H, $OCH_2$), 7.02, 7.03 (2 x s, 2H, 8, 9), 7.34-7.36 (m, 3H, Ar-H), 7.46 (s, 4H, 16, 17), 7.53-7.57 (m, 2H, Ar-H). $^{13}$C NMR: δ 11.3 (41), 14.9 (32, 33), 18.7 (42), 65.2, 65.3 (30, 31), 85.9, 87.8, 94.6, 95.0 (5, 6, 13, 14), 92.8, 106.7 (19, 20), 113.7, 114.3 (7, 12), 117.1, 117.1 (10, 11), 123.3, 123.3, 123.4 (4, 15, 18), 128.3 (1, 2), 131.3, 131.6, 131.9 (3, 16, 17), 153.5, 153.5 (8, 9). HR EI MS Calcd for $C_{37}H_{42}O_2Si$: 546.2954 ($[M]^+$). Found: 546.2979 ($[M]^+$). EI MS: 546 ($[M]^+$, 100), 433 ($[M - C{\equiv}C\text{-}Ph + H]^+$, 50), 389 ($[M - SiPr^i_3]^+$, 20).

**Synthesis of 4-HC≡CC$_6$H$_4$C≡CC$_6$H$_2$-2,5-(OEt)$_2$-4-C≡CPh (58).** 4-$Pr^i_3$SiC≡CC$_6$H$_4$ C≡CC$_6$H$_2$-2,5-(OEt)$_2$-4-C≡CPh (**57**, 0.800 g, 1.46 mmol) was dissolved in $CH_2Cl_2$ (100 mL) and deoxygenated. Tetra-*n*-butylammonium fluoride (1 M in THF, 2.0 mL) was added and the mixture stirred at room temperature for 2.5 h. The solution was washed with water (50 mL x 3) and dried over $MgSO_4$. Reduction of the volume of solution and addition of MeOH gave a dark solid, which was filtered off, washing with petrol. The solution was taken to dryness and a fine, yellow solid remained (0.460 g, 81%). Anal. Calcd for $C_{28}H_{22}O_2$: C 86.13, H 5.68. Found: C 85.98, H 5.77%. IR: ν(C≡C) 2211 cm$^{-1}$, ν(C≡C–H) 2108 cm$^{-1}$. UV-vis: 372 [3.6], 320 [3.6]. $^1$H NMR: δ 1.48 (t, $J_{HH}$ = 7 Hz, 6H, Me), 3.18 (s, 1H, C≡C–H), 4.11 (q, $J_{HH}$ = 7 Hz, 4H, $OCH_2$), 7.02, 7.03 (2 x s, 2H, 8, 9), 7.34-7.36 (m, 3H, Ar-H), 7.48, 7.49 (2 x s, 4H, 16, 17), 7.54-7.57 (m, 2H, Ar-H). $^{13}$C NMR: δ 14.9 (32, 33), 65.2, 65.3 (30, 31), 78.9, 83.3 (19, 20), 85.8, 88.0, 94.3, 95.1 (5, 6, 13, 14), 113.6, 114.4 (7, 12), 117.1, 117.2 (10, 11), 121.8, 123.3, 123.9 (4, 15, 18), 128.3 (1, 2), 131.4, 131.6, 132.1 (3, 16, 17), 153.4, 153.5 (8, 9). HR EI MS Calcd for $C_{28}H_{22}O_2$: 390.1620 ($[M]^+$). Found: 390.1623 ($[M]^+$). EI MS: 390 ($[M]^+$, 100).

**Synthesis of {4-$Pr^i_3$SiC≡CC$_6$H$_4$C≡CC$_6$H$_2$-2,5-(OEt)$_2$-4-C≡C}$_2$ (59).** 4-$Pr^i_3$SiC≡CC$_6$H$_4$ C≡CC$_6$H$_2$-2,5-(OEt)$_2$-4-C≡CH (**56**, 0.96 g, 2.04 mmol), $PdCl_2(PPh_3)_2$ (0.010 g, 0.014 mmol) and CuI (0.001 g, 0.005 mmol) were added to a solution of MeOH / $NEt_3$ (19:1, 100 mL), deoxygenated and stirred at room temperature for 18 h. The solvent was removed under reduced pressure, the residue dissolved in petrol and EtOAc (15:1) and filtered through a short silica column. The solvent was removed and the resulting solid recrystallized from MeOH. Filtration gave a yellow solid (0.85 g, 89%). Anal. Calcd for $C_{62}H_{74}O_4Si_2$: C 79.27, H 7.94. Found: C 78.65, H 7.52%. IR: ν(C≡C) 2210 cm$^{-1}$,

ν(SiC≡C) 2153 $cm^{-1}$. UV-vis: 403 [4.4], 327 [4.0]. $^1$H NMR: δ 1.14 (s, 42H, $SiPr^i_3$), 1.47 (t, $J_{HH}$ = 7 Hz, 6H, Me), 1.48 (t, $J_{HH}$ = 7 Hz, 6H, Me), 4.08 (q, $J_{HH}$ = 7 Hz, 4H, $OCH_2$), 4.10 (q, $J_{HH}$ = 7 Hz, 4H, $OCH_2$), 6.99, 7.00 (2 x s, 4H, 8, 9), 7.47 (s, 8H, 16, 17). $^{13}$C NMR: δ 11.2 (41), 14.8 (32, 33), 18.6 (42), 65.1 (30, 31), 79.4, 79.6 (5, 6), 87.6, 106.6 (19, 20), 92.9, 95.3 (13, 14), 112.6, 114.8 (7, 12), 116.7, 117.7 (10, 11), 123.0, 123.4 (15, 18), 131.3, 131.9 (16, 17), 153.2, 154.7 (8, 9). HR ESI MS Calcd for $C_{62}H_{74}O_4Si_2$: 961.5023 ($[M + Na]^+$). Found: 961.5047 ($[M + Na]^+$). ESI MS: 961 ($[M + Na]^+$, 70), 671 ($[M - 4\text{-}Pr^i_3SiC{\equiv}CC_6H_4C{\equiv}C + Na]^+$, 15).

**Synthesis of {4-HC≡CC$_6$H$_4$C≡CC$_6$H$_2$-2,5-(OEt)$_2$-4-C≡C}$_2$ (60).** {4-$Pr^i_3$SiC≡CC$_6$H$_4$ C≡CC$_6$H$_2$-2,5-(OEt)$_2$-4-C≡C}$_2$ (**59**, 0.205 g, 0.218 mmol) was dissolved in $CH_2Cl_2$ (60 mL) and deoxygenated. Tetra-*n*-butylammonium fluoride (1 M in THF, 0.5 mL) was added and the mixture stirred at room temperature for 2 h. The solution was washed with water (50 mL x 3) and dried over $MgSO_4$. The volume of the solution was reduced and MeOH added to give a black solid, which was filtered off, washing with petrol. The solution was taken to dryness and a fine, yellow solid remained (0.117 g, 88%). Anal. Calcd for $C_{44}H_{34}O_4$: C 84.32, H 5.47. Found: C 85.20, H 5.58%. IR: ν(C≡C) 2208 $cm^{-1}$, ν(C≡C–C≡C) 2143 $cm^{-1}$, ν(C≡C–H) 2108 $cm^{-1}$. UV-vis: 402 [2.4], 324 [1.7]. $^1$H NMR: δ 1.47 (t, $J_{HH}$ = 7 Hz, 12H, Me), 3.18 (s, 2H, C≡C–H), 4.08 (q, $J_{HH}$ = 7 Hz, 4H, $OCH_2$), 4.10 (q, $J_{HH}$ = 7 Hz, 4H, $OCH_2$), 6.99, 7.00 (2 x s, 4H, 8, 9), 7.48 (s, 8H, 16, 17). $^{13}$C NMR: δ 14.8 (32, 33), 65.2 (30, 31), 79.0, 83.3 (19, 20), 79.4, 79.6 (5, 6), 87.8, 94.9 (13, 14), 112.8, 114.8 (7, 12), 116.9, 117.8 (10, 11), 122.0, 123.7 (15, 18), 131.5, 132.1 (16, 17), 153.3, 154.8 (8, 9). HR ESI MS Calcd for $C_{44}H_{34}O_4$: 649.2355 ($[M + Na]^+$). Found: 649.2355 ($[M + Na]^+$). ESI MS: 649 ($[M + Na]^+$, 80), 365 ($[4\text{-}HC{\equiv}CC_6H_4C{\equiv}CC_6H_2\text{-}2,5\text{-}(OEt)_2 + Na + MeCN]^+$, 90).

**Synthesis of 1,4-{4-$Pr^i_3$SiC≡CC$_6$H$_4$C≡CC$_6$H$_2$-2,5-(OEt)$_2$-4-C≡C}$_2$C$_6$H$_4$ (61).** 4-$Pr^i_3$SiC≡CC$_6$H$_4$ C≡CC$_6$H$_2$-2,5-(OEt)$_2$-4-C≡CH (**56**, 1.321 g, 2.810 mmol) and 1,4-diiodobenzene (0.456 g, 1.380 mmol) were added to $NEt_3/CH_2Cl_2$ (200 mL, 3:1) and the solution deoxygenated. $PdCl_2(PPh_3)_2$ (0.050 g, 0.070 mmol) and CuI (0.014 g, 0.007 mmol) were then added under nitrogen, the solution deoxygenated again and stirred at room temperature. The reaction was monitored by $^1$H NMR spectroscopy until aromatic resonances indicated complete reaction of the 1,2-diiodobenzene. The solvent

was then removed under reduced pressure and the residue was stirred for two days in MeOH. Filtering the solid and washing the filtrate with petrol gave a yellow solid (1.360 g, 97%). Anal. Calcd for $C_{68}H_{78}O_4Si_2$: C 80.42, H 7.72. Found: C 79.61, H 7.74 %. IR: ν(C≡C) 2212 $cm^{-1}$, ν(SiC≡C) 2153 $cm^{-1}$. UV-vis: 395 [9.6], 328 [5.9]. $^1H$ NMR: δ 1.14 (s, 42H, $SiPr^i_3$), 1.48 (t, $J_{HH}$ = 7 Hz, 6H, Me), 1.49 (t, $J_{HH}$ = 7 Hz, 6H, Me), 4.12 (q, $J_{HH}$ = 7 Hz, 8H, $OCH_2$), 7.02 (s, 4H, 8, 9), 7.46, 7.46 (2 x s, 8H, 16, 17), 7.52 (s, 4H, 3). $^{13}C$ NMR: δ 11.3 (41), 14.9 (32, 33), 18.6 (42), 65.2 (30, 31), 87.7, 87.9, 94.8, 94.8 (5, 6, 13, 14), 92.8, 106.7 (19, 20), 114.0 (7, 12), 117.0 (10, 11), 123.2, 123.4 (4, 15, 18), 131.4, 131.5, 131.9 (3, 16, 17), 153.5 (8, 9). HR ESI MS Calcd for $C_{68}H_{78}O_4Si_2$: 1038.5415 ($[M + H + Na]^+$), 1015.5517 ($[M + H]^+$). Found: 1038.5416 ($[M + H + Na]^+$), 1015.5514 ($[M + H]^+$). ESI MS: 1039 ($[M + H + Na]^+$, 1), 1015 ($[M]^+$, 4), 857 ($[M - 4\text{-}Pr^i_3SiC{\equiv}C + Na]^+$, 60), 757 ($[M - 4\text{-}Pr^i_3SiC{\equiv}CC_6H_4C{\equiv}C + Na]^+$, 100).

**Synthesis of 1,4-{4-HC≡CC$_6$H$_4$C≡CC$_6$H$_2$-2,5-(OEt)$_2$-4-C≡C}$_2$C$_6$H$_4$ (62).** 1,4-{4-$Pr^i_3$SiC≡CC$_6$H$_4$C≡CC$_6$H$_2$-2,5-(OEt)$_2$-4-C≡C}$_2$C$_6$H$_4$ (**61**, 0.500 g, 0.50 mmol) was dissolved in $CH_2Cl_2$ (80 mL) and deoxygenated. Tetra-*n*-butylammonium fluoride (1 M in THF, 0.5 mL) was added and the mixture stirred at room temperature for 2 h. The solution was washed with water (50 mL x 3) and dried over $MgSO_4$. Reduction in volume of the solution and addition of MeOH gave a pale solid, which was filtered. Washing with petrol left a very fine, yellow solid (0.344 g, 98%). Anal. Calcd for $C_{50}H_{38}O_4$: C 85.45, H 5.45. Found: C 84.55, H 5.50%. IR: ν(C≡C) 2209 $cm^{-1}$, ν(C≡C–H) 2105 $cm^{-1}$. UV-vis: 393 [5.6], 329 [3.1]. $^1H$ NMR: δ 1.49 (t, $J_{HH}$ = 7 Hz, 6H, Me), 1.49 (t, $J_{HH}$ = 7 Hz, 6H, Me), 3.18 (s, 2H, C≡C–H), 4.12 (q, $J_{HH}$ = 7 Hz, 8H, $OCH_2$), 7.02, 7.02 (2 x s, 4H, 8, 9), 7.48, 7.48 (2 x s, 8H, 16, 17), 7.52 (s, 4H, 3). $^{13}C$ NMR: δ 14.9 (32, 33), 65.2 (30, 31), 78.9, 83.3 (19, 20), 86.2, 87.9, 94.4, 94.8 (5, 6, 13, 14), 113.9, 114.1 (7, 12), 117.1, 117.1 (10, 11), 123.2, 123.2, 123.9 (4, 15, 18), 131.4, 131.5, 132.1 (3, 16, 17), 153.5, 153.5 (8, 9). HR EI MS Calcd for $C_{50}H_{38}O_4$: 766.2963 ($[M + Na + MeCN]^+$), 725.2668 ($[M + Na]^+$). Found: 766.2978 ($[M + Na + MeCN]^+$), 725.2668 ($[M + Na]^+$). EI MS: 766 ($[M + Na + MeCN]^+$, 15), 725.2668 ($[M + Na]^+$, 5), 500 ($M - C{\equiv}CC_6H_4C{\equiv}CH - C_6H_4C{\equiv}CH + Na]^+$, 100), 365 (4-HC≡CC$_6$H$_4$C≡CC$_6$H$_2$-2,5-(OEt)$_2$ + Na + MeCN]$^+$, 15).

**Synthesis of 1,3,5-{4-$Pr^i_3SiC{\equiv}CC_6H_4C{\equiv}CC_6H_2$-2,5-$(OEt)_2$-4-C≡C}$_3C_6H_3$ (63).** 4-$Pr^i_3SiC{\equiv}CC_6H_4C{\equiv}CC_6H_2$-2,5-$(OEt)_2$-4-C≡CH (**56**, 1.358 g, 2.89 mmol) and 1,3,5-triiodobenzene (0.420 g, 0.922 mmol) were added to $NEt_3/CH_2Cl_2$ (200 mL, 3:1) and the solution deoxygenated. $PdCl_2(PPh_3)_2$ (0.050 g, 0.070 mmol) and CuI (0.014 g, 0.007 mmol) were then added under nitrogen, the solution deoxygenated again and stirred at room temperature. The reaction was monitored by NMR until aromatic resonances indicated complete reaction of the 1,3,5-triiodobenzene. The solvent was the removed under reduced pressure and the residue was stirred for two days in MeOH. Filtering the solid and washing the filtrate with petrol gave a yellow solid (1.532 g, 98%). Anal. Calcd for $C_{99}H_{114}O_6Si_3$: C 80.11, H 7.74. Found: C 79.96, H 7.64%. IR: ν(C≡C) 2214 $cm^{-1}$, ν(SiC≡C) 2153 $cm^{-1}$. UV-vis: 384 [9.6], 323 [8.6]. $^1$H NMR: δ 1.14 (s, 63H, $SiPr^i_3$), 1.49 (t, $J_{HH}$ = 7 Hz, 9H, Me), 1.50 (t, $J_{HH}$ = 7 Hz, 9H, Me), 4.12 (q, $J_{HH}$ = 7 Hz, 6H, $OCH_2$), 4.13 (q, $J_{HH}$ = 7 Hz, 6H, $OCH_2$), 7.03 (s, 6H, 8, 9), 7.47, 7.47 (2 x s, 12H, 16, 17), 7.67 (s, 3H, 3). $^{13}$C NMR: δ 11.3 (41), 14.9 (32, 33), 18.7 (42), 65.2 (30, 31), 87.1, 87.7, 93.4, 94.8 (5, 6, 13, 14), 92.9, 106.7 (19, 20), 113.7, 114.2 (7, 12), 117.1, 117.2 (10, 11), 123.2, 123.4, 124.1 (4, 15, 18), 131.4, 132.0 (16, 17), 134.0, (3), 153.5, 153.6 (8, 9). HR ESI MS Calcd for $C_{99}H_{114}O_6Si_3$: 1546.8086 ([M + Na + MeCN]$^+$), 1505.7821 ([M + Na]$^+$). Found: 1546.8112 ([M + Na + MeCN]$^+$), 1505.7776 ([M + Na]$^+$). ESI MS: 1548 ([M + Na + MeCN]$^+$, 20), 1507 ([M + Na]$^+$, 5).

**Synthesis of 1,3,5-{4-HC≡$CC_6H_4C{\equiv}CC_6H_2$-2,5-$(OEt)_2$-4-C≡C}$_3C_6H_3$ (64).** 1,3,5-{4-$Pr^i_3SiC{\equiv}CC_6H_4C{\equiv}CC_6H_2$-2,5-$(OEt)_2$-4-C≡C}$_3C_6H_3$ (**63**, 0.387 g, 0.26 mmol) was dissolved in $CH_2Cl_2$ (200 mL) and deoxygenated. Tetra-*n*-butylammonium fluoride (1 M in THF, 1.2 mL) was added and the mixture stirred at room temperature for 2 h. The solution was washed with water (50 mL x 3) and dried over $MgSO_4$. Reduction in volume of the solution and addition of MeOH gave a brown solid, which was filtered. Washing with petrol left a light brown solid (0.186 g, 71%). Anal. Calcd for $C_{72}H_{54}O_6$: C 85.18, H 5.36. Found: C 84.35, H 5.16%. IR: ν(C≡C) 2213 $cm^{-1}$, ν(C≡C–H) 2108 $cm^{-1}$. UV-vis: 383 [11.9], 319 [10.0]. $^1$H NMR: δ 1.49 (t, $J_{HH}$ = 7 Hz, 9H, Me), 1.50 (t, $J_{HH}$ = 7 Hz, 9H, Me), 3.18 (s, 3H, C≡C–H), 4.12 (q, $J_{HH}$ = 7 Hz, 6H, $OCH_2$), 4.13 (q, $J_{HH}$ = 7 Hz, 6H, $OCH_2$), 7.03 (s, 6H, 8, 9), 7.48, 7.49 (2 x s, 12H, 16, 17), 7.67 (s, 3H, 3). $^{13}$C NMR: δ 14.9 (32, 33), 65.2 (30, 31), 79.0, 83.3 (19, 20), 87.0, 87.9, 93.4, 94.5 (5, 6, 13, 14), 113.8, 114.1 (7, 12), 117.1, 117.2 (10, 11), 121.9, 123.8,

124.1 (4, 15, 18), 131.4, 132.0, 134.1 (3, 16, 17), 153.5, 153.6 (8, 9). HR EI MS Calcd for $C_{72}H_{54}O_6$: 1015.3920 ($[M + H]^+$). Found: 1015.3937 ($[M + H]^+$). EI MS: 1015 ($[M + H]^+$, 15), 763 ($[M - (C{\equiv}CC_6H_4C{\equiv}CH)_2 - C{\equiv}CH + Na]^+$, 30), 671 ($M - (C{\equiv}CC_6H_4C{\equiv}CH)_3 + MeCN]^+$, 100).

**Synthesis of 1,2,4,5-{4-Pr$^i_3$SiC≡CC$_6$H$_4$C≡CC$_6$H$_2$-2,5-(OEt)$_2$-4-C≡C}$_4$C$_6$H$_2$ (65).** 4-Pr$^i_3$SiC≡CC$_6$H$_4$C≡CC$_6$H$_2$-2,5-(OEt)$_2$-4-C≡CH (**56**, 2.050 g, 4.36 mmol) and 1,2,4,5-tetrabromobenzene (0.429 g, 1.090 mmol) were added to $NEt_3/CH_2Cl_2$ (200 mL, 1:1) and the solution deoxygenated. $Pd(PPh_3)_4$ (0.050 g, 0.004 mmol) was then added under nitrogen, the solution deoxygenated again and stirred at room temperature for 2 days. The reaction was monitored by $^1$H NMR spectroscopy until aromatic resonances indicated complete reaction of the 1,2,4,5-tetrabromobenzene. The temperature was then increased to reflux and the reaction continued for 2 further days. After 4 days, Pr$^i_3$SiC≡CC$_6$H$_4$C≡CC$_6$H$_2$-2,5-(OEt)$_2$-4-C≡CH (**56**, 1.01 g, 2.14 mmol) and $Pd(PPh_3)_4$ (0.025 g, 0.002 mmol) were added. The reaction was complete (by $^1$H NMR) after a total of 7 days. The solvent was then removed under reduced pressure and the residue was stirred overnight in MeOH. Filtering the solid and washing the filtrate with petrol gave a yellow solid which was recrystallized from $CH_2Cl_2$ into MeOH (2.04 g, 96%). Anal. Calcd for $C_{130}H_{150}O_8Si_4$: C 79.95, H 7.74. Found: C 79.71, H 8.12%. IR: ν(C≡C) 2208 cm$^{-1}$, ν(SiC≡C) 2153 cm$^{-1}$. UV-vis: 385 [12.2], 323 [11.4]. $^1$H NMR: δ 1.14 (s, 84H, SiPr$^i_3$), 1.39 (t, $J_{HH}$ = 8 Hz, 12H, Me), 1.42 (t, $J_{HH}$ = 8 Hz, 12H, Me), 3.92 (q, $J_{HH}$ = 7 Hz, 8H, $OCH_2$), 4.08 (q, $J_{HH}$ = 7 Hz, 8H, $OCH_2$), 7.02, 7.03 (2 x s, 8H, 8, 9), 7.46 (s, 16H, 16, 17), 7.77 (s, 2H, 3). $^{13}$C NMR: δ 11.3 (41), 14.8, 14.9 (32, 33), 18.7 (42), 65.2, 65.5 (30, 31), 87.7, 92.2, 93.1, 95.0 (5, 6, 13, 14), 92.9, 106.7 (19, 20), 114.1, 114.3 (7, 12), 117.4, 117.5 (10, 11), 123.2, 123.4, 125.5 (4, 15, 18), 131.4, 132.0 (16, 17), 134.6, (3), 153.5, 153.6 (8, 9). HR ESI MS Calcd for $C_{130}H_{150}O_8Si_4$: 1991.0078 ($[M + K]^+$), 1974.0306 ($[M + Na]^+$). Found: 1991.0087 ($[M + K]^+$), 1974.0275 ($[M + Na]^+$). ESI MS: 1991 ($[M + K]^+$, 8), 1975 ($[M + Na]^+$, 10).

**Synthesis of 1,2,4,5-{4-HC≡CC$_6$H$_4$C≡CC$_6$H$_2$-2,5-(OEt)$_2$-4-C≡C}$_4$C$_6$H$_2$ (66).** 1,2,4,5-{4-Pr$^i_3$SiC≡CC$_6$H$_4$C≡CC$_6$H$_2$-2,5-(OEt)$_2$-4-C≡C}$_4$C$_6$H$_2$ (**65**, 0.513 g, 0.263 mmol) was dissolved in $CH_2Cl_2$ (200 mL) and deoxygenated. Tetra-*n*-butylammonium fluoride (1 M in THF, 1.2 mL) was added and the mixture stirred at room temperature for 2 h. The solution was washed with water (100 mL x 4) and dried over $MgSO_4$. The

solution was taken to dryness and then stirred in MeOH gave a light brown solid, which was filtered. Washing with petrol left a fine, light brown solid (0.243 g, 70%). Anal. Calcd for $C_{94}H_{70}O_8$: C 85.05, H 5.31. Found: C 84.46, H 5.44%. IR: ν(C≡C) 2212 $cm^{-1}$, ν(C≡C–H) 2108 $cm^{-1}$. UV-vis: 386 [12.4], 320 [10.7]. $^1$H NMR: δ 1.39 (t, $J_{HH}$ = 7 Hz, 12H, Me), 1.42 (t, $J_{HH}$ = 7 Hz, 12H, Me), 3.18 (s, 4H, C≡C–H), 3.91 (q, $J_{HH}$ = 7 Hz, 8H, $OCH_2$), 4.08 (q, $J_{HH}$ = 7 Hz, 8H, $OCH_2$), 7.01, 7.03 (2 x s, 8H, 8, 9), 7.48 (s, 16H, 16, 17), 7.77 (s, 2H, 3). $^{13}$C NMR: δ 14.8, 14.9 (32, 33), 65.1, 65.5 (30, 31), 79.0, 83.3 (19, 20), 87.9, 92.2, 93.1, 94.6 (5, 6, 13, 14), 114.2 (7, 12), 117.5 (10, 11), 121.9, 123.8, 125.5 (4, 15, 18), 131.4, 132.1, 134.6 (3, 16, 17), 153.5, 153.6 (8, 9). HR EI MS Calcd for $C_{94}H_{70}O_8$: 1349.4968 ($[M + Na]^+$). Found: 1349.4988 ($[M + Na]^+$). EI MS: 1367 ($[M + Na + MeCN]^+$, 3), 1349 ($[M + Na]^+$, 6), 365 (4-HC≡C$C_6H_4$C≡C$C_6H_2$-2,5-$(OEt)_2$ + Na + $MeCN]^+$, 80), 261 (C≡C$C_6H_2$-2,5-$(OEt)_2$ + Na + $MeCN]^+$, 100).

**Synthesis of Cl-*trans*-[Ru(dppe)$_2$]-4-C≡C$C_6H_4$C≡C$C_6H_2$-2,5-$(OEt)_2$-4-C≡CPh (67).** 4-HC≡C$C_6H_4$C≡C$C_6H_2$-2,5-$(OEt)_2$-4-C≡CPh (**58**, 0.169 g, 0.433 mmol), $RuCl_2(dppe)_2$ (0.484 g, 0.500 mmol) and $NaPF_6$ (0.168 g, 1.00 mmol) were dissolved in $CH_2Cl_2$ (100 mL). The solution was deoxygenated and stirred at room temperature for 18 h. $NEt_3$ (1 mL) was added, the volume reduced (10 mL) and the mixture added to MeOH (100 mL). The precipitate was filtered and washed with petrol (30 mL x 3) to give a yellow solid (0.426 g, 74%). Anal. Calcd for $C_{80}H_{69}ClO_2P_4Ru$: C 72.64, H 5.26. Found: C 72.86, H 5.32%. IR: ν(C≡C) 2200 $cm^{-1}$, ν(C≡C–Ru) 2064 $cm^{-1}$. UV-vis: 423 [2.4], 308 [1.8]. $^1$H NMR: δ 1.50 (t, $J_{HH}$ = 7 Hz, 3H, Me), 1.52 (t, $J_{HH}$ = 7 Hz, 3H, Me), 2.70 (bs, 8H, 50), 4.13 (q, $J_{HH}$ = 7 Hz, 2H, $OCH_2$), 4.14 (q, $J_{HH}$ = 7 Hz, 2H, $OCH_2$), 6.55-7.55 (m, 57H, Ar-H). $^{13}$C NMR: δ 15.0, 15.0 (32, 33), 30.5-30.8 (m, 50), 65.2, 65.3 (30, 31), 86.1, 94.7, 96.4, 96.4 (5, 6, 13, 14), 113.4, 114.6 (7, 12), 114.8, 116.7 (15, 18), 117.1, 117.3 (10, 11), 123.5 (19), 127.0, 127.2 (2 x s, 53), 128.2 (4), 128.3 (1, 2), 128.9 (54), 129.9, 131.6 (16, 17), 130.5 (m, 20), 130.9 (3), 134.2, 134.4 (2 x s, 52), 135.4-136.4 (m, 51), 153.2, 153.5 (8, 9). $^{31}$P NMR: δ 49.9. HR ESI MS Calcd for $C_{80}H_{69}ClO_2P_4Ru$: 1328.3557 ($[M – Cl + MeCN]^+$), 1287.3292 ($[M - Cl]^+$). Found: 1328.3560 ($[M – Cl + MeCN]^+$), 1287.3304 ($[M - Cl]^+$). ESI MS: 1328 ($[M – Cl + MeCN]^+$, 100), 1287 ($[M - Cl]^+$, 5).

**Synthesis of PhC≡C-*trans*-[Ru(dppe)$_2$]-4-C≡CC$_6$H$_4$C≡CC$_6$H$_2$-2,5-(OEt)$_2$-4-C≡CPh (68).** Cl-*trans*-[Ru(dppe)$_2$]-4-C≡CC$_6$H$_4$C≡CC$_6$H$_2$-2,5-(OEt)$_2$-4-C≡CPh (**67**, 0.130 g, 0.098 mmol), PhC≡CH (0.50 mL, 5.0 mmol) and $NaPF_6$ (0.050 g, 0.298 mmol) were dissolved in $CH_2Cl_2$/$NEt_3$ (120 mL, 2:1) and deoxygenated. The solution was stirred at reflux for 16 hours and the solvent was removed. The residue was dissolved in a minimum of $CH_2Cl_2$ (5 mL) and added to MeOH (100 mL). A yellow solid precipitated and was filtered. Washing with petrol (30 mL x 2) gave a yellow solid (0.125 g, 92%). Anal. Calcd for $C_{88}H_{74}O_2P_4Ru$: C 76.12, H 5.37. Found: C 76.21, H 5.49%. IR: ν(C≡C) 2198 cm$^{-1}$, ν(C≡C–Ru) 2057 cm$^{-1}$. UV-vis: 423 [5.6], 308 [4.7]. $^1$H NMR: δ 1.50 (t, $J_{HH}$ = 7 Hz, 3H, Me), 1.52 (t, $J_{HH}$ = 7 Hz, 3H, Me), 2.63 (bs, 8H, 50), 4.13 (q, $J_{HH}$ = 7 Hz, 2H, $OCH_2$), 4.14 (q, $J_{HH}$ = 7 Hz, 2H, $OCH_2$), 6.63-7.61 (m, 56H, Ar-H). $^{13}$C NMR: δ 15.0, 15.0 (32, 33), 31.4-31.6 (m, 50), 65.3, 65.4 (30, 31), 86.0, 94.7, 96.8, 96.8 (5, 6, 13, 14), 110.0, 114.7 (7, 12), 114.9, 116.6 (15, 18), 117.1, 117.4 (10, 11), 122.9, 123.5 (2 x m, 19, 22), 127.0 (53), 127.4 (25), 128.2 (4), 128.3 (1, 2), 128.6, 128.7 (26, 54), 129.9, 129.9, 131.6 (16, 17, 24), 130.5 (m, 20, 21), 130.9 (3), 134.1, 134.3 (2 x s, 52), 137.4-137.3 (m, 51), 153.2, 153.5 (8, 9). $^{31}$P NMR: δ 54.3. HR ESI MS Calcd for $C_{88}H_{74}O_2P_4Ru$: 1388.3683 ([M]$^+$). Found: 1388.3733 ([M]$^+$). ESI MS: 1388 ([M]$^+$, 5), 898 ([Ru(dppe)$_2$]$^+$, 10).

**Synthesis of {Cl-*trans*-[Ru(dppe)$_2$]-4-C≡CC$_6$H$_4$C≡CC$_6$H$_2$-2,5-(OEt)$_2$-4-C≡C}$_2$ (69).** {4-HC≡CC$_6$H$_4$C≡CC$_6$H$_2$-2,5-(OEt)$_2$-4-C≡C}$_2$ (**60**, 0.105 g, 0.187 mmol), $RuCl_2$(dppe)$_2$ (0.363 g, 0.375 mmol) and $NaPF_6$ (0.126 g, 0.750 mmol) were dissolved in DCM (80 mL). The solution was deoxygenated and stirred at room temperature for 18 h. $NEt_3$ (1 mL) was added, the volume reduced (10 mL) and the mixture added to MeOH (100 mL). An orange solid precipitated and was filtered. Washing with petrol (30 mL x 2) gave an orange solid (0.368 g, 81%). Anal. Calcd for $C_{148}H_{128}Cl_2O_4P_8Ru_2$: C 71.35, H 5.18. Found: C 71.10, H 5.21%. IR: ν(C≡C) 2197 cm$^{-1}$, ν(C≡C–Ru) 2063 cm$^{-1}$. UV-vis: 452 [9.4], 327 [4.7]. $^1$H NMR: δ 1.49 (t, $J_{HH}$ = 7 Hz, 6H, Me), 1.51 (t, $J_{HH}$ = 7 Hz, 6H, Me), 2.70 (bs, 16H, 50), 4.11 (q, $J_{HH}$ = 7 Hz, 4H, $OCH_2$), 4.12 (q, $J_{HH}$ = 7 Hz, 4H, $OCH_2$), 6.55-7.44 (m, 92H, Ar-H). $^{13}$C NMR: δ 14.8, 14.9 (32, 33), 30.5-30.7 (m, 50), 65.1, 65.2 (30, 31), 79.1, 79.7 (5, 6), 86.0, 97.1 (13, 14), 111.7, 115.9 (7, 12), 114.6, 116.4 (15, 18), 116.6, 117.9 (10, 11), 123.8 (m, 19), 126.9, 127.2 (2 x s, 53), 128.8 (54), 129.9, 130.9 (16, 17), 130.5, (m, 20), 134.1, 134.3 (2 x s, 52), 135.5-136.2 (m, 51),

152.9, 154.8 (8, 9). $^{31}$P NMR: δ 49.9. HR ESI MS Calcd for $C_{148}H_{128}Cl_2O_4P_8Ru_2$: 1230.8033 ([M – $Cl_2$ + MeCN]$^{2+}$), 1210.2894 ([M – $Cl_2$]$^{2+}$). Found: 1230.8011 ([M – $Cl_2$ + MeCN]$^{2+}$), 1210.2900 ([M – $Cl_2$]$^{2+}$). ESI MS: 1251 ([M – $Cl_2$ + $(MeCN)_2$]$^{2+}$, 100), 1230 ([M – $Cl_2$ + (MeCN)]$^{2+}$, 5), 957 ([C≡C–RuCl(dppe)$_2$]$^+$, 20).

**Synthesis of {PhC≡C-*trans*-[Ru(dppe)$_2$]-4-C≡CC$_6$H$_4$C≡CC$_6$H$_2$-2,5-(OEt)$_2$-4-C≡C}$_2$ (70).** {Cl-*trans*-[Ru(dppe)$_2$]-4-C≡CC$_6$H$_4$C≡CC$_6$H$_2$-2,5-(OEt)$_2$-4-C≡C}$_2$ (**69**, 0.060 g, 0.025 mmol), PhC≡CH (0.40 mL, 4.0 mmol) and $NaPF_6$ (0.050 g, 0.298 mmol) were dissolved in $CH_2Cl_2$/$NEt_3$ (120 mL, 2:1) and deoxygenated. The solution was stirred at reflux for 16 hours and the solvent was removed under reduced pressure. The residue was dissolved in a minimum of $CH_2Cl_2$ (5 mL) and added to MeOH (100 mL). An orange solid precipitated and was filtered. Washing with petrol (30 mL x 2) gave an orange solid (0.054 g, 86%). Anal. Calcd for $C_{164}H_{138}O_4P_8Ru_2$: C 75.10, H 5.30. Found: C 75.37, H 5.23%. IR: ν(C≡C) 2197 cm$^{-1}$, ν(C≡C–Ru) 2057 cm$^{-1}$. UV-vis: 450 [3.9], 327 [2.9]. $^1$H NMR: δ 1.49 (t, $J_{HH}$ = 7 Hz, 6H, Me), 1.51 (t, $J_{HH}$ = 7 Hz, 6H, Me), 2.63 (bs, 16H, 50), 4.11 (q, $J_{HH}$ = 7 Hz, 4H, $OCH_2$), 4.13 (q, $J_{HH}$ = 7 Hz, 4H, $OCH_2$), 6.63-7.59 (m, 102H, Ar-H). $^{13}$C NMR: δ 14.9, 15.0 (32, 33), 31.3-31.6 (m, 50), 65.2, 65.3 (30, 31), 79.2, 79.3 (5, 6), 85.9, 97.2 (13, 14), 111.8, 116.1 (7, 12), 116.6, 117.2, 117.3 (15, 18, 23), 116.7, 118.1 (10, 11), 123.9 (m, 19, 22), 130.5 (m, 20, 21), 127.1 (53), 127.5 (25), 128.6, 128.7 (26, 54), 129.9, 129.9, 130.9 (16, 17, 24), 134.1, 134.3 (2 x s, 52), 135.5-137.0 (m, 51), 153.0, 154.9 (8, 9). $^{31}$P NMR: δ 54.3. HR ESI MS Calcd for $C_{164}H_{138}O_4P_8Ru_2$: 2623.6661 ([M + H]$^+$), 1311.3292 ([M]$^{2+}$). Found: 2623.6677 ([M + H]$^+$), 1311.3289 ([M]$^{2+}$). ESI MS: 2563 ([M - PhC≡C + MeCN]$^+$, 1), 2545 ([M - PhC≡C + Na]$^+$, 5), 1027 ([C≡C–Ru(dppe)$_2$–C≡C + $(MeCN)_2$]$^+$, 100).

**Synthesis of 1,4-{Cl-*trans*-[Ru(dppe)$_2$]-HC≡CC$_6$H$_4$C≡CC$_6$H$_2$-2,5-(OEt)$_2$-4-C≡C}$_2$C$_6$H$_4$ (71).** 1,4-{4-HC≡CC$_6$H$_4$C≡CC$_6$H$_2$-2,5-(OEt)$_2$-4-C≡C}$_2$C$_6$H$_4$ (**62**, 0.155 g, 0.22 mmol), $RuCl_2(dppe)_2$ (0.436 g, 0.45 mmol) and $NaPF_6$ (0.168 g, 1.00 mmol) were dissolved in $CH_2Cl_2$ (200 mL). The solution was deoxygenated and stirred at room temperature for 18 h. $NEt_3$ (1 mL) was added, the solvent removed under reduced pressure and the residue dissolved in $CH_2Cl_2$ (15 mL). This solution was then added to MeOH (100 mL), filtered and washed with petrol (30 mL x 3) to give a yellow solid. Crystallization from petrol/$CH_2Cl_2$ (2 : 1) and filtration removed any bis-acetylides that

had formed. The solution was again precipitated by addition to MeOH and produced an orange solid (0.413 g, 73%). Anal. Calcd for $C_{154}H_{132}Cl_2O_4P_8Ru_2$: C 72.04, H 5.18. Found: C 72.20, H 5.29%. IR: ν(C≡C) 2201 $cm^{-1}$, ν(C≡C–Ru) 2062 $cm^{-1}$. UV-vis: 442 [12.6], 326 [6.3]. $^1$H NMR: δ 1.51 (t, $J_{HH}$ = 7 Hz, 6H, Me), 1.52 (t, $J_{HH}$ = 7 Hz, 6H, Me), 2.69 (bs, 16H, 50), 4.14 (q, $J_{HH}$ = 7 Hz, 4H, $OCH_2$), 4.15 (q, $J_{HH}$ = 7 Hz, 4H, $OCH_2$), 6.55-7.54 (m, 96H, Ar-H). $^{13}$C NMR: δ 14.9, 15.0 (32, 33), 30.5-30.8 (m, 50), 65.2, 65.3 (30, 31), 86.1, 86.1, 94.5, 96.6 (5, 6, 13, 14), 113.1, 114.6 (7, 12), 115.1, 116.6 (15, 18), 117.0, 117.3 (10, 11), 119.4 (4), 123.3 (19), 127.0, 127.2 (2 x s, 53), 128.8 (54), 129.9, 131.5 (16, 17), 130.5 (m, 20), 130.9 (3), 134.1, 134.4 (2 x s, 52), 135.4-136.4 (m, 51), 153.2, 153.6 (8, 9). $^{31}$P NMR: δ 49.9. HR ESI MS Calcd for $C_{154}H_{132}Cl_2O_4P_8Ru_2$: 2614.6397 ($[M - Cl + 2MeCN]^+$), 2573.6131 ($[M - Cl + MeCN]^+$). Found: 2614.6379 ($[M - Cl + 2MeCN]^+$), 2573.6128 ($[M - Cl + MeCN]^+$). ESI MS: 2615 ($[M - Cl + (MeCN)_2]^+$, 3), 2574 ($[M - Cl + MeCN]^+$, 1), 1289 ($[M - Cl + 2Na]^{2+}$, 100).

**Synthesis of 1,4-{PhC≡C-*trans*-[Ru(dppe)$_2$]-HC≡CC$_6$H$_4$C≡CC$_6$H$_2$-2,5-(OEt)$_2$-4-C≡C}$_2$C$_6$H$_4$ (72).** 1,4-{Cl-*trans*-[Ru(dppe)$_2$]-HC≡CC$_6$H$_4$C≡CC$_6$H$_2$-2,5-(OEt)$_2$-4-C≡C}$_2$ C$_6$H$_4$ (**71**, 0.065 g, 0.026 mmol) ), PhC≡CH (0.50 mL, 5.0 mmol) and $NaPF_6$ (0.168 g, 1.00 mmol) were dissolved in $CH_2Cl_2$/$NEt_3$ (100 mL, 4:1) and deoxygenated. The solution was stirred at reflux for 16 hours and the solvent volume was reduced (10 mL) under reduced pressure. MeOH (100 mL) was added, an orange solid precipitated and the mixture stirred for 1 h. The solid was filtered and washed with MeOH (30 mL x 2, petrol (30 mL x 2) and MeOH (30 mL x 2) again (0.061 g, 87%). Anal. Calcd for $C_{170}H_{142}O_4P_8Ru_2$: C 75.66, H 5.30. Found: C 75.88, H 5.39%. IR: ν(C≡C) 2198 $cm^{-1}$, ν(C≡C–Ru) 2057 $cm^{-1}$. UV-vis: 441 [7.0], 326 [4.5]. $^1$H NMR: δ 1.51 (t, $J_{HH}$ = 7 Hz, 6H, Me), 1.53 (t, $J_{HH}$ = 7 Hz, 6H, Me), 2.63 (bs, 16H, 50), 4.14 (q, $J_{HH}$ = 7 Hz, 4H, $OCH_2$), 4.15 (q, $J_{HH}$ = 7 Hz, 4H, $OCH_2$), 6.63-7.61 (m, 106H, Ar-H). $^{13}$C NMR: δ 15.0 (32, 33), 31.4-31.5 (m, 50), 65.2, 65.3 (30, 31), 86.0, 94.5, 96.6 (5, 6, 13, 14), 113.0, 114.1 (7, 12), 115.1, 116.7, 116.8, 117.2 (4, 15, 18, 23), 117.0, 117.3 (10, 11), 122.9, 123.3 (2 x m, 19, 22), 127.0 (53), 127.4 (25), 128.2 (4), 128.6, 128.7 (54), 128.8 (26), 129.9, 129.9 (16, 17), 130.6 (m, 20, 21), 130.9 (3), 131.5 (24), 134.1, 134.3 (2 x s, 52), 136.8-137.1 (m, 51), 153.2, 153.6 (8, 9). $^{31}$P NMR: δ 54.3. HR ESI MS Calcd for $C_{170}H_{142}O_4P_8Ru_2$: 2638.6770 ($[M - C≡CPh + MeCN]^+$), 2625.6566 ($[M - C≡CPh + N_2]^+$),

1282.8252 ([M – $(C{\equiv}CPh)_2$ + MeCN + $N_2]^+$). Found: 2638.6821 ([M - C≡CPh + MeCN]$^+$), 2625.6541 ([M - C≡CPh + $N_2]^+$), 1282.8210 ([M – $(C{\equiv}CPh)_2$ + MeCN + $N_2]^+$). ESI MS: 2639 ([M - C≡CPh + MeCN]$^+$, 2), 2626 ([M - C≡CPh + $N_2]^+$, 4), 1282 ([M – $(C{\equiv}CPh)_2$ + MeCN + $N_2]^+$, 5) , 1027 ([PhC≡C-Ru$(dppe)_2$ + $N_2]^+$, 100).

**Synthesis of 1,3,5-{Cl-*trans*-[Ru$(dppe)_2$]-HC≡C$C_6H_4$C≡C$C_6H_2$-2,5-$(OEt)_2$-4-C≡C}$_3$ $C_6H_3$ (73).** 1,3,5-{4-HC≡C$C_6H_4$C≡C$C_6H_2$-2,5-$(OEt)_2$-4-C≡C}$_3C_6H_3$ (**64**, 0.102 g, 0.10 mmol), $RuCl_2(dppe)_2$ (0.387 g, 0.40 mmol) and $NaPF_6$ (0.168 g, 1.00 mmol) were dissolved in $CH_2Cl_2/NEt_2$ (202 mL, 100:1). The solution was deoxygenated and stirred at room temperature for 18 h. The solvent was removed under reduced pressure and the residue dissolved in $CH_2Cl_2$ (15 mL). This solution was added to MeOH (150 mL), filtered and washed with petrol (50 mL x 3) to give a yellow solid. The product was dissolved in $CH_2Cl_2$ (15 mL) a second time and again precipitated by addition to petrol producing a yellow-orange solid (0.210 g, 55%). Anal. Calcd for $C_{228}H_{195}Cl_3O_6P_{12}Ru_3$: C 71.83, H 5.16. Found: C 72.00, H 4.94%. IR: ν(C≡C) 2201 cm$^{-1}$, ν(C≡C–Ru) 2065 cm$^{-1}$. UV-vis: 423 [9.5], 316 [6.3]. $^1$H NMR: δ 1.25 (bs, 18H, Me), 2.69 (bs, 24H, 50), 4.02-4.22 (m, 12H, $OCH_2$), 6.55-7.68 (m, 141H, Ar-H). $^{13}$C NMR: δ 15.0 (32, 33), 30.5-30.8 (m, 50), 65.2 (30, 31), 117.4 (10, 11), 127.0, 127.2 (2 x s, 53), 128.8 (54), 129.9, 130.9, 131.7 (3, 16, 17), 134.2, 134.4 (2 x s, 52), 136.1-136.5 (m, 51). $^{31}$P NMR: δ 49.9. HR ESI MS Calcd for $C_{228}H_{195}Cl_3O_6P_{12}Ru_3$: 1445.8958 ([M – RuCl$(dppe)_2$ – 2Cl + 2(MeCN)]$^{2+}$), 1277.9972 ([M – 3Cl + 3MeCN]$^{3+}$). Found: 1445.8931 ([M – RuCl$(dppe)_2$ – 2Cl + 2(MeCN)]$^{2+}$), 1277.9977 ([M – 3Cl + 3MeCN]$^{3+}$). ESI MS: 1446 ([M – RuCl$(dppe)_2$ – 2Cl + 2(MeCN)]$^{2+}$, 15), 1278 ([M – 3Cl + 3MeCN]$^{3+}$, 10), 961 ([Ru$(dppe)_2$ + Na + MeCN]$^+$, 100).

**Synthesis of 1,3,5-{PhC≡C-*trans*-[Ru$(dppe)_2$]-HC≡C$C_6H_4$C≡C$C_6H_2$-2,5-$(OEt)_2$-4-C≡C}$_3C_6H_3$ (74).** 1,3,5-{Cl-*trans*-[Ru$(dppe)_2$]-HC≡C$C_6H_4$C≡C$C_6H_2$-2,5-$(OEt)_2$-4-C≡C}$_3$ $C_6H_3$ (**73**, 0.098 g, 0.026 mmol) ), PhC≡CH (2.0 mL, 20.0 mmol) and $NaPF_6$ (0.150 g, 0.89 mmol) were dissolved in $CH_2Cl_2/NEt_3$ (152 mL, 75:1) and deoxygenated. The solution was stirred at reflux for 16 hours and the solvent was removed under reduced pressure. The resulting solid was dissolved in $CH_2Cl_2$ (10 mL) and added to MeOH (80 mL). An orange solid precipitated and was filtered, washed with MeOH (30 mL x 2, petrol (30 mL x 2) and MeOH (30 mL x 2) again, yielding a dark orange solid

(0.103 g, 98%). Anal. Calcd for $C_{252}H_{210}O_6P_{12}Ru_3$: C 75.49, H 5.28. Found: C 75.58, H 5.48%. IR: ν(C≡C) 2201 $cm^{-1}$, ν(C≡C–Ru) 2057 $cm^{-1}$. UV-vis: 420 [10.1], 319 [8.9]. $^1$H NMR: δ 1.29 (bs, 18H, Me), 2.64 (bs, 24H, 50), 3.94-4.25 (m, 12H, $OCH_2$), 6.64-7.78 (m, 156H, Ar-H). $^{13}$C NMR: δ 15.0 (32, 33), 31.3-31.8 (m, 50), 65.2 (30, 31), 117.2, 117.3 (10, 11), 127.0 (53), 127.4 (25), 128.6 (26, 54), 129.9 (16, 17), 130.9 (3), 133.4 (24), 134.1, 134.3 (2 x s, 52), 136.8-137.2 (m, 51). $^{31}$P NMR: δ 54.3. ESI MS: 1040 ([Ph-C≡C-Ru(dppe) + MeCN]$^+$, 70), 1027 ([Ph-C≡C-Ru(dppe) + $N_2$]$^+$, 100), 961 ([Ru(dppe)$_2$ + Na + MeCN]$^+$, 30).

**Synthesis of 1,2,4,5-{Cl-*trans*-[Ru(dppe)$_2$]-HC≡CC$_6$H$_4$C≡CC$_6$H$_2$-2,5-(OEt)$_2$-4-C≡C}$_4$C$_6$H$_2$ (75).** 1,2,4,5-{4-HC≡CC$_6$H$_4$C≡CC$_6$H$_2$-2,5-(OEt)$_2$-4-C≡C}$_4$C$_6$H$_2$ (**66**, 0.106 g, 0.080 mmol), $RuCl_2(dppe)_2$ (0.317 g, 0.33 mmol) and $NaPF_6$ (0.168 g, 1.00 mmol) were dissolved in $CH_2Cl_2$/$NEt_2$ (201 mL, 200:1). The solution was deoxygenated and stirred at room temperature for 18 h. The solvent was removed under reduced pressure and the residue dissolved in $CH_2Cl_2$ (15 mL). This solution was added to MeOH (150 mL), filtered and washed with petrol (50 mL x 3) to give an orange solid (0.385 g, 96%). Anal. Calcd for $C_{302}H_{258}Cl_4O_8P_{16}Ru_4$: C 71.83, H 5.16. Found: C 71.92, H 5.22%. IR: ν(C≡C) 2199 $cm^{-1}$, ν(C≡C–Ru) 2064 $cm^{-1}$. UV-vis: 405 [13.0], 321 [7.7]. $^1$H NMR: δ 1.43 (t, $J_{HH}$ = 7 Hz, 12H, Me), 1.48 (t, $J_{HH}$ = 7 Hz, 12H, Me), 2.67 (bs, 32H, 50), 3.97 (q, $J_{HH}$ = 7 Hz, 8H, $OCH_2$), 4.12 (q, $J_{HH}$ = 7 Hz, 8H, $OCH_2$), 6.56-7.59 (m, 184H, Ar-H), 7.80 (s, 2H, 3). $^{13}$C NMR: δ 14.9 (32, 33), 30.4-30.6 (m, 50), 65.2, 65.5 (30, 31), 117.0 (10, 11), 127.0, 127.2 (2 x s, 53), 128.9 (54), 129.9, 130.9, 131.0 (3, 16, 17), 134.2, 134.4 (2 x s, 52), 135.4-136.4 (m, 51). $^{31}$P NMR: δ 49.9. HR ESI MS Calcd for $C_{302}H_{258}Cl_4O_8P_{16}Ru_4$: 1270.0741 ([M – 4Cl + 4MeCN)]$^{4+}$). Found: 1270.0714 ([M – 4Cl + 4MeCN)]$^{4+}$). ESI MS: 1741 ([M – 2Cl + 3Na + 4MeCN)]$^{3+}$, 10), 1705 ([M – 2Cl + 2Na + 2MeCN)]$^{3+}$, 8), 1380 ([M – RuCl(dppe)$_2$ – 3Cl + 3MeCN]$^{3+}$, 30), 1270 ([M – 4Cl + 4MeCN)]$^{4+}$, 40), 974 ([RuCl(dppe)$_2$ + MeCN]$^+$, 100).

**Synthesis of 1,2,4,5-{PhC≡C-*trans*-[Ru(dppe)$_2$]-HC≡CC$_6$H$_4$C≡CC$_6$H$_2$-2,5-(OEt)$_2$-4-C≡C}$_4$C$_6$H$_2$ (76).** 1,2,4,5-{Cl-*trans*-[Ru(dppe)$_2$]-HC≡CC$_6$H$_4$C≡CC$_6$H$_2$-2,5-(OEt)$_2$-4-C≡C }$_4$C$_6$H$_2$ (**75**, 0.210 g, 0.042 mmol) ), PhC≡CH (2.0 mL, 20.0 mmol) and $NaPF_6$ (0.150 g, 0.89 mmol) were dissolved in $CH_2Cl_2$/$NEt_3$ (152 mL, 75:1) and deoxygenated. The solution was stirred at reflux for 16 hours and the solvent volume was reduced (10

mL) under reduced pressure. The resulting solution was added to MeOH (100 mL). An orange solid precipitated and was filtered, washed with MeOH (40 mL x 2, petrol (40 mL x 2) and MeOH (40 mL x 2) again, yielding a dark orange solid (0.155 g, 69%). Anal. Calcd for $C_{334}H_{278}O_8P_{16}Ru_4$: C 75.41, H 5.27. Found: C 75.64, H 5.29%. IR: ν(C≡C) 2199 $cm^{-1}$, ν(C≡C–Ru) 2057 $cm^{-1}$. UV-vis: 405 [19.4], 321 [15.6]. $^1$H NMR: δ 1.44 (t, $J_{HH}$ = 7 Hz, 12H, Me), 1.49 (t, $J_{HH}$ = 7 Hz, 12H, Me), 2.62 (bs, 32H, 50), 3.97 (q, $J_{HH}$ = 7 Hz, 8H, $OCH_2$), 4.13 (q, $J_{HH}$ = 7 Hz, 8H, $OCH_2$), 6.64-7.64 (m, 204H, Ar-H), 7.80 (s, 2H, 3). $^{13}$C NMR: δ 14.9, 15.0 (32, 33), 31.2-31.6 (m, 50), 65.2, 65.8 (30, 31), 117.3, 117.6 (10, 11), 127.0 (53), 127.4 (25), 128.6, 128.7 (26, 54), 129.9 (16, 17), 130.9 (3), 134.1, 134.3 (24, 52), 136.6-137.1 (m, 51). $^{31}$P NMR: δ 54.3. ESI MS: 1040 ([Ph-C≡C-Ru(dppe) + MeCN]$^+$, 35), 1027 ([Ph-C≡C-Ru(dppe) + $N_2$]$^+$, 100), 961 ([$Ru(dppe)_2$ + Na + MeCN]$^+$, 55).

# Appendices

## NLO Data for Section 2.4

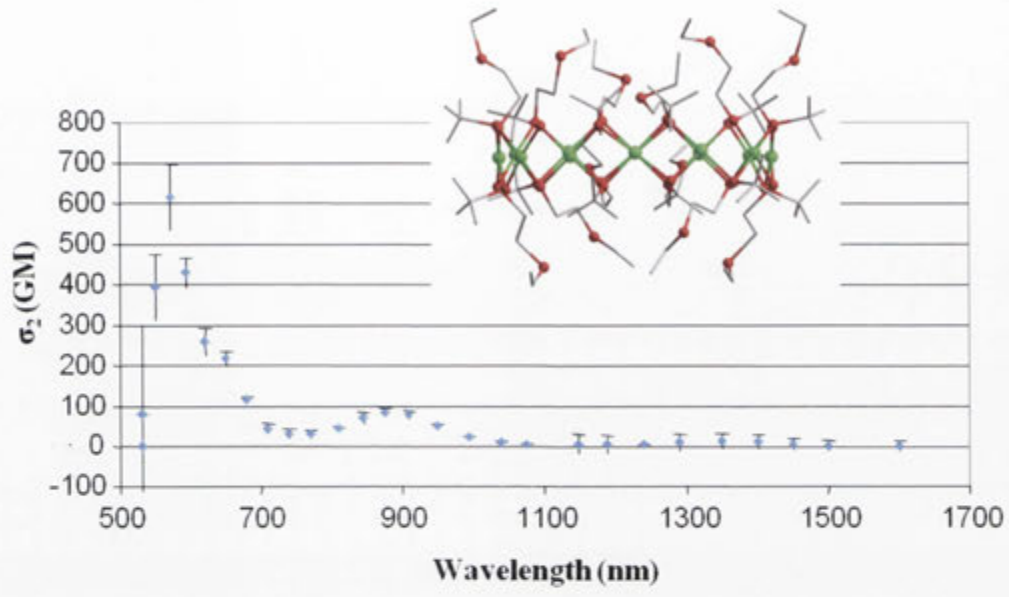


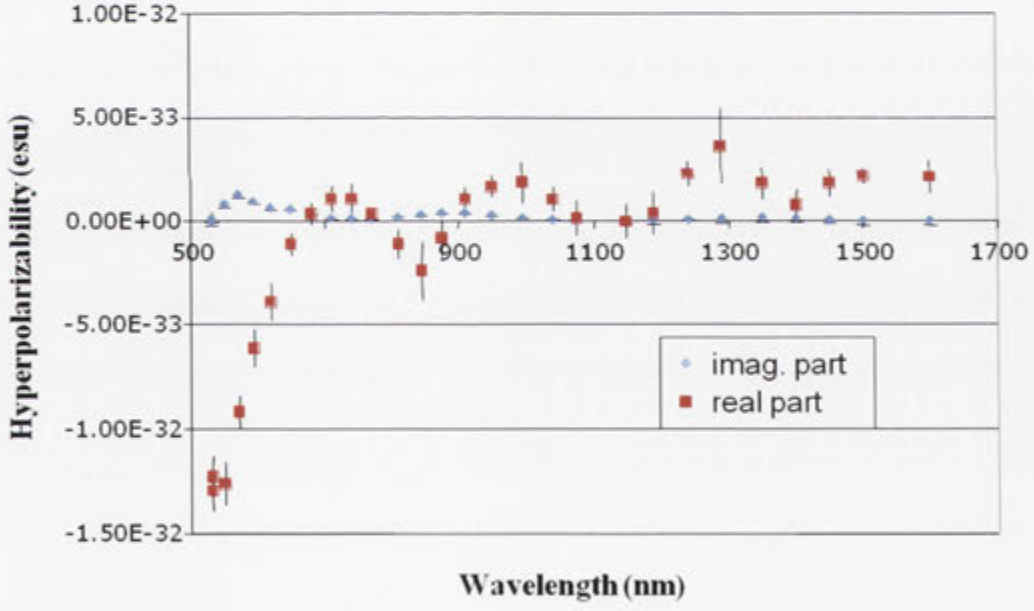


Cubic NLO spectra for compound **8**.

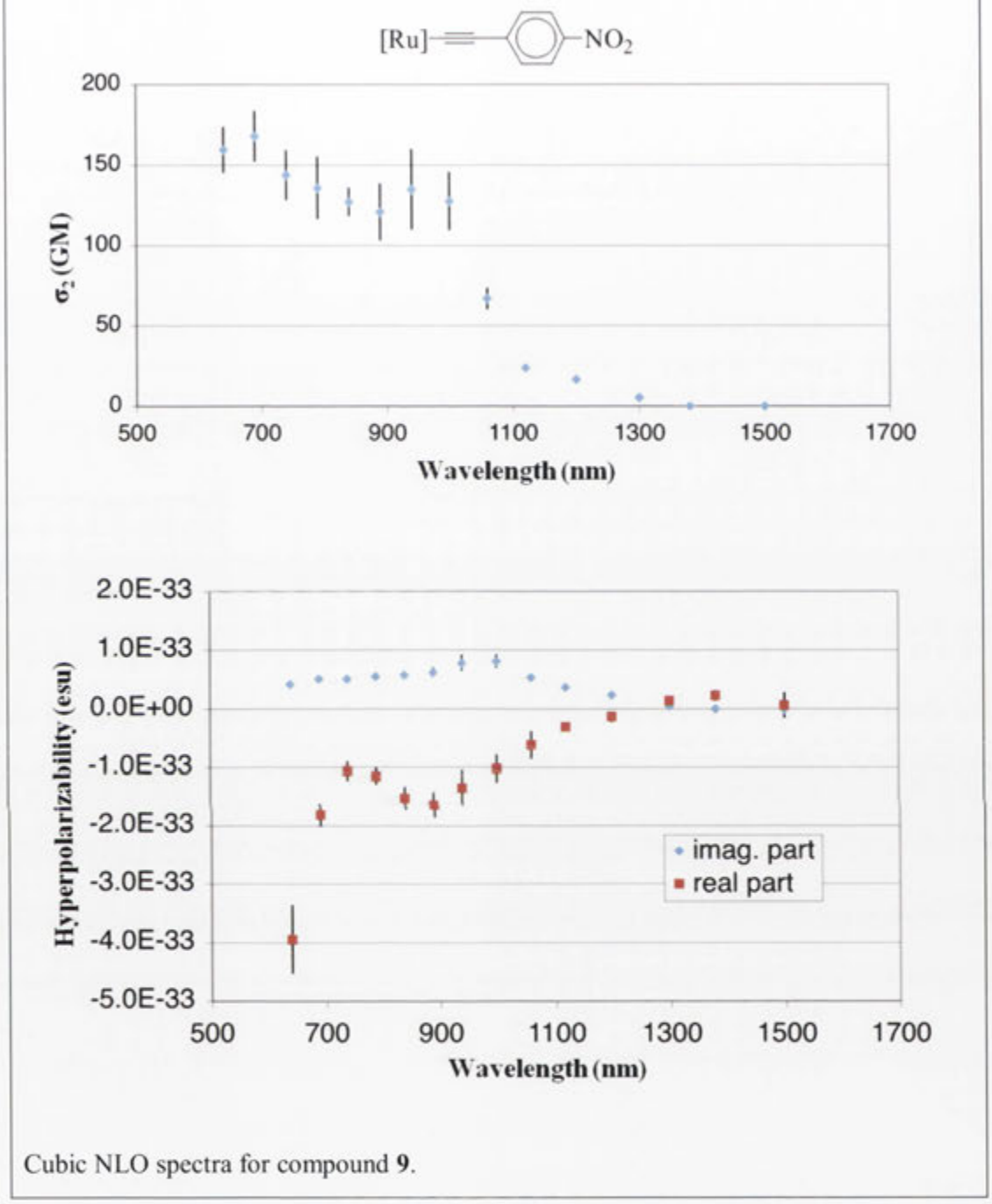


Cubic NLO spectra for compound **9**.

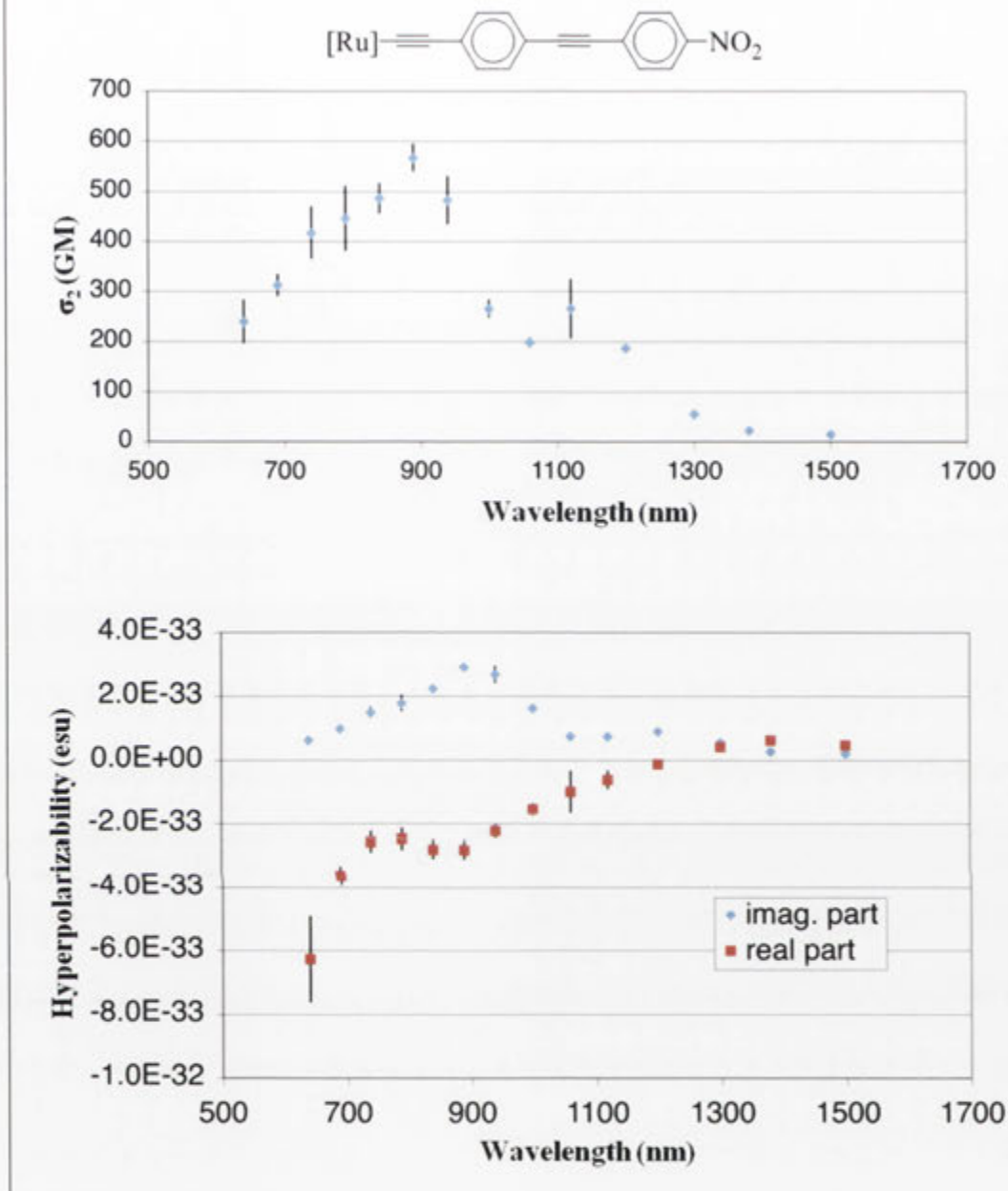


Cubic NLO spectra for compound **10**.

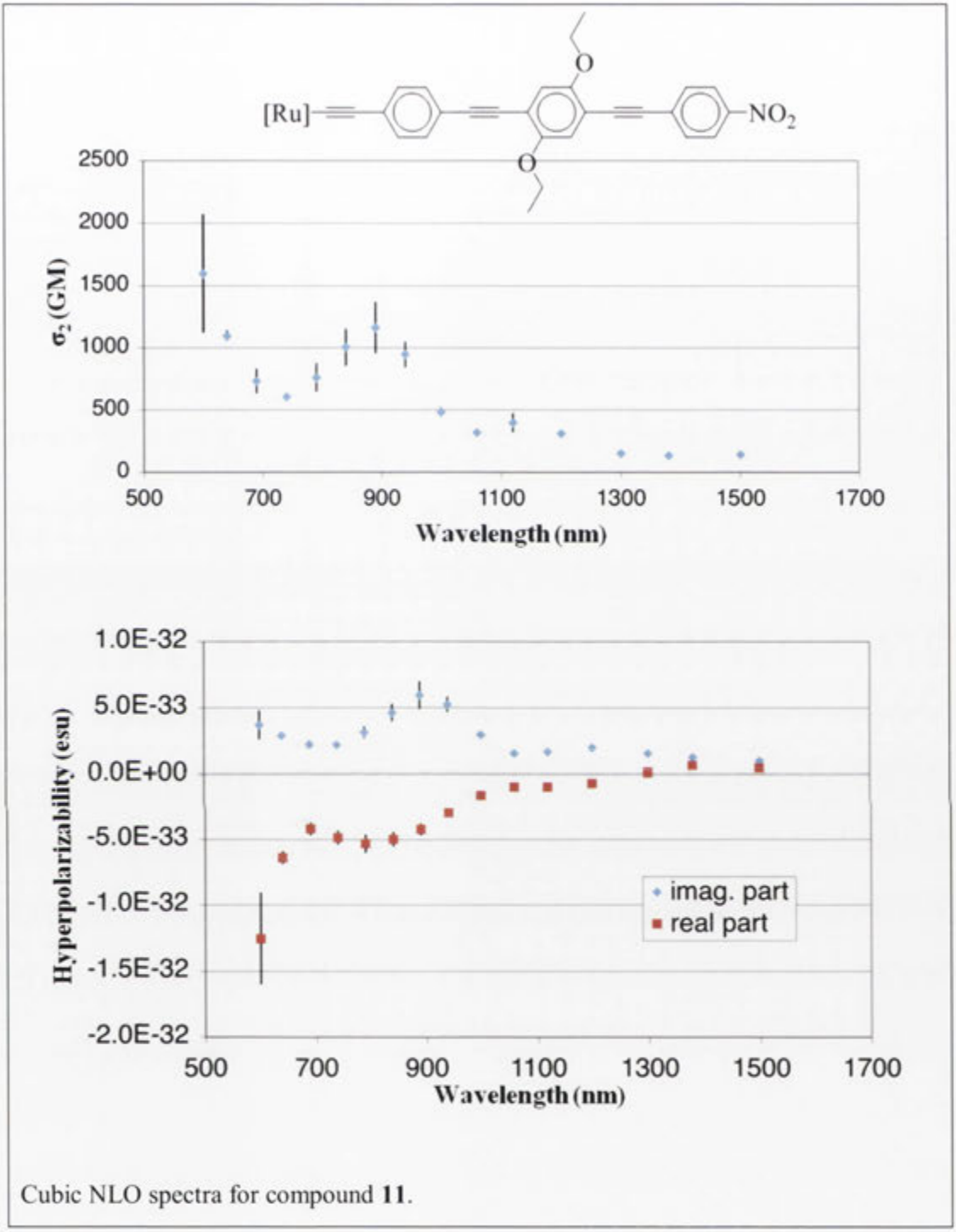


Cubic NLO spectra for compound **11**.

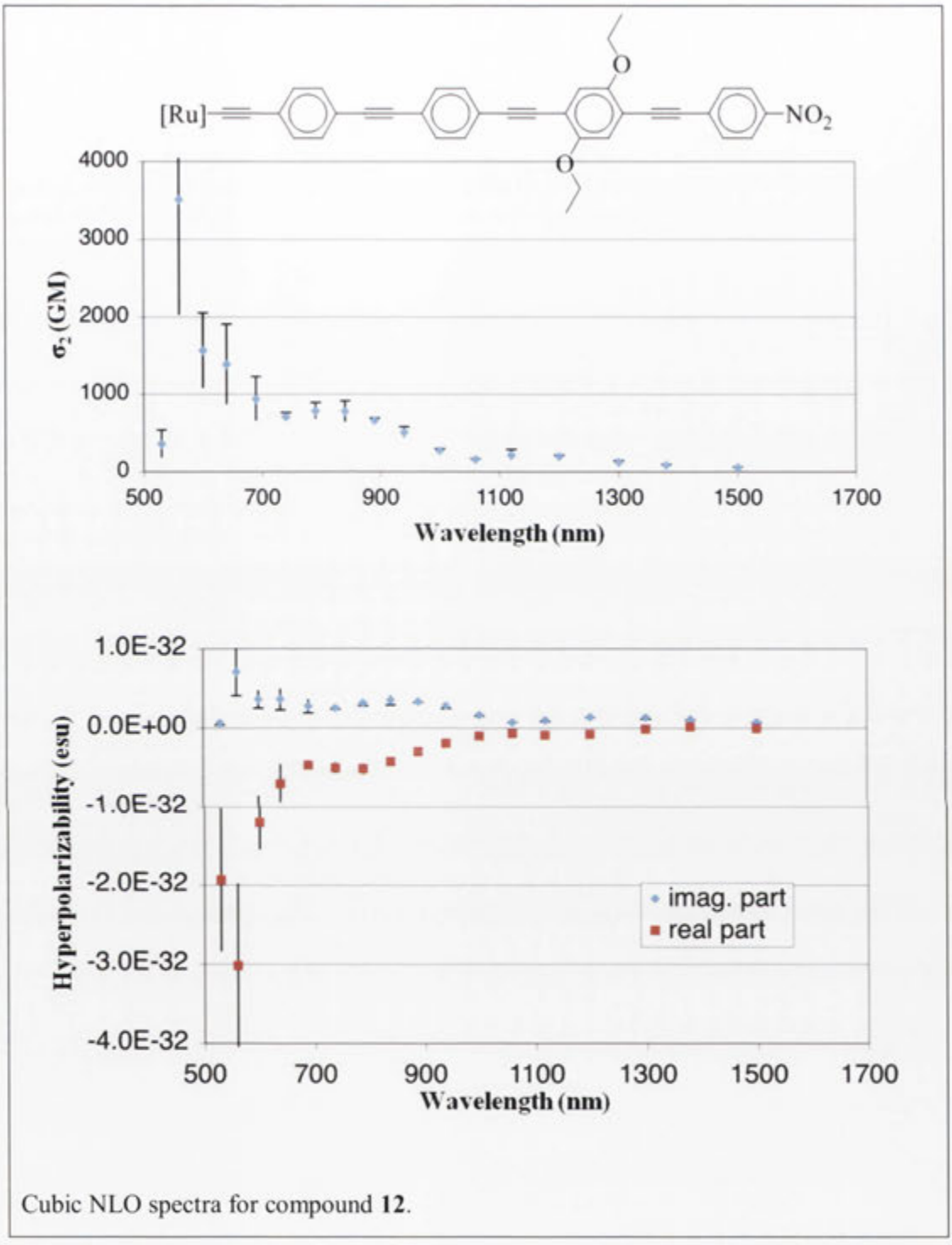


Cubic NLO spectra for compound **12**.

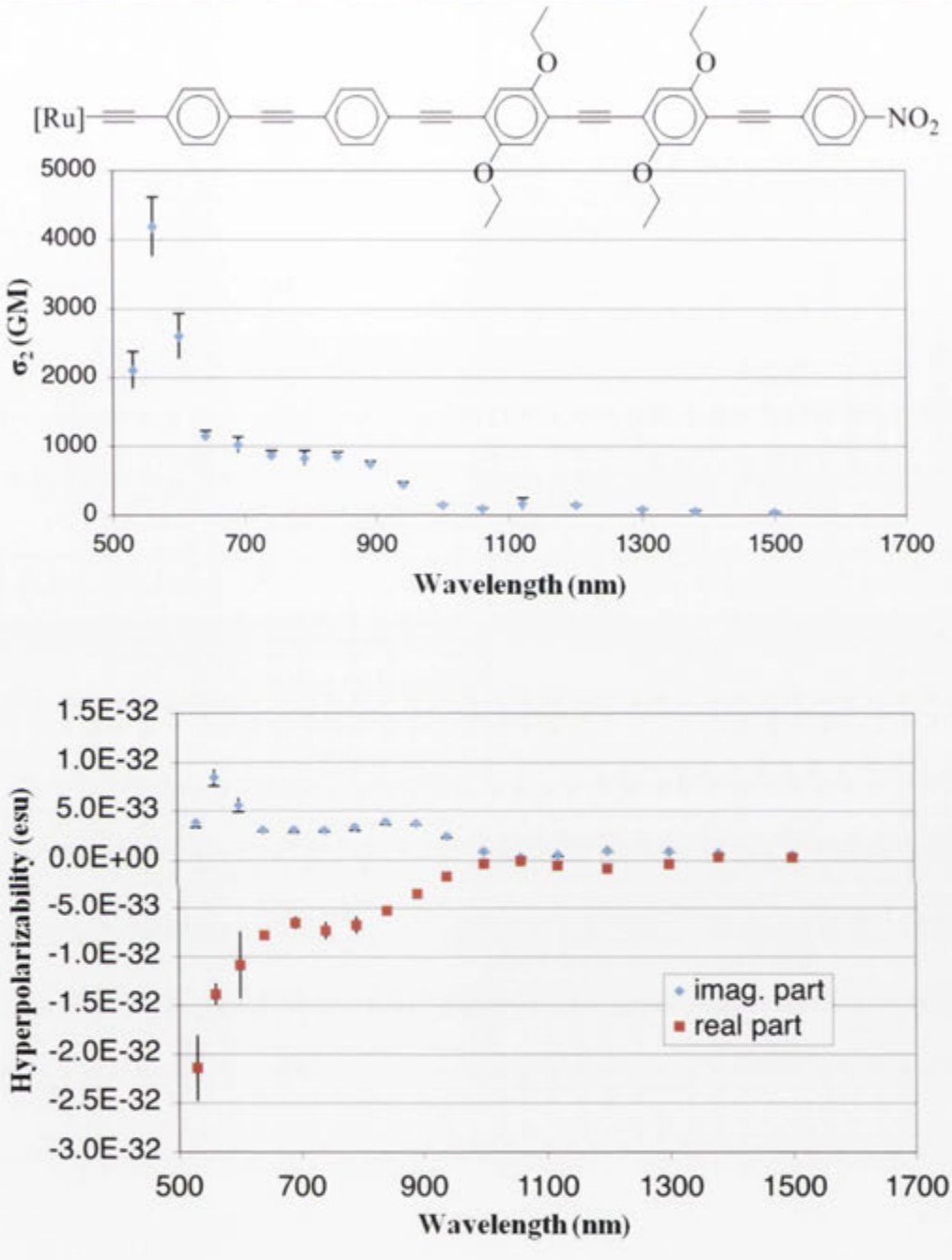


Cubic NLO spectra for compound **13**.

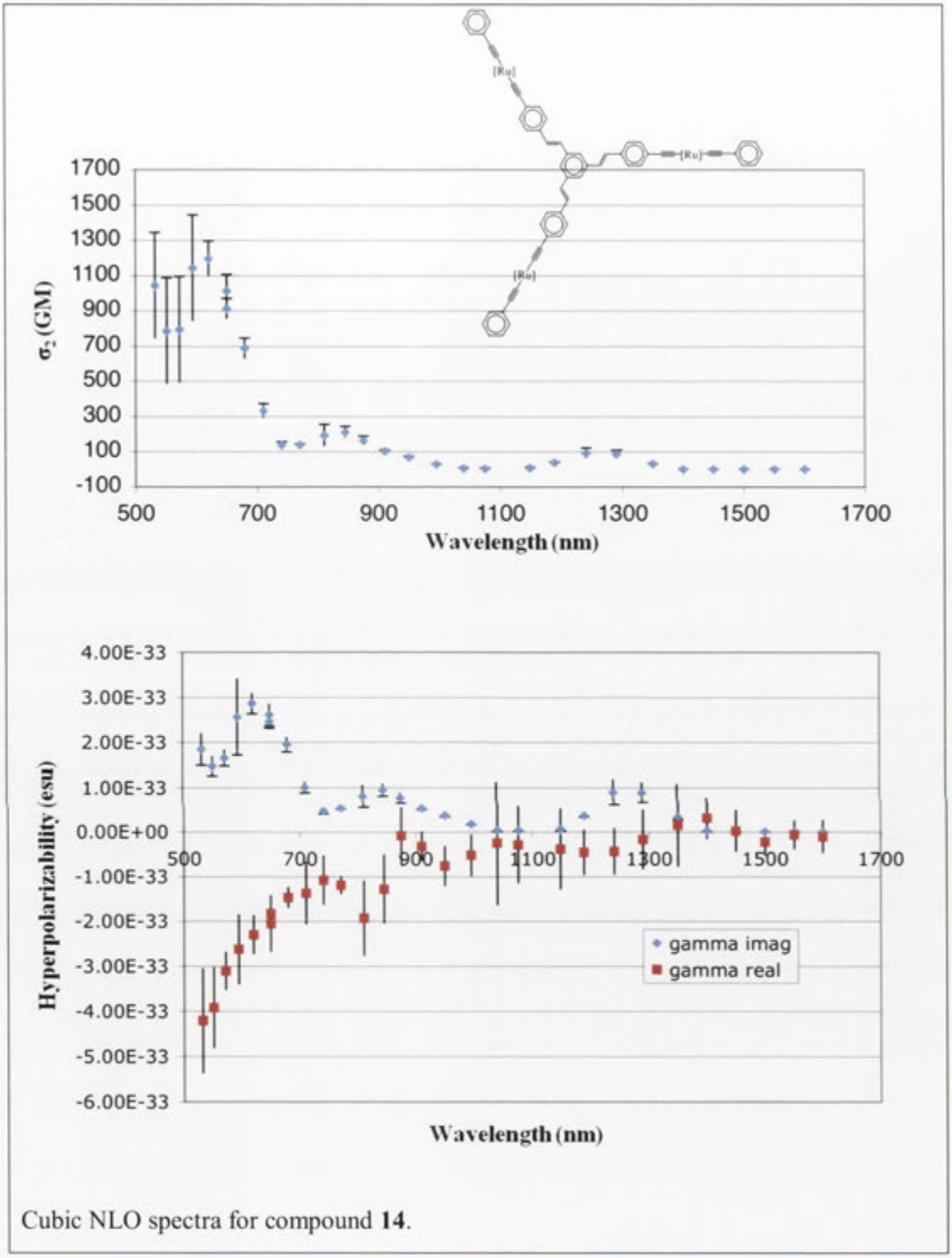


Cubic NLO spectra for compound **14**.

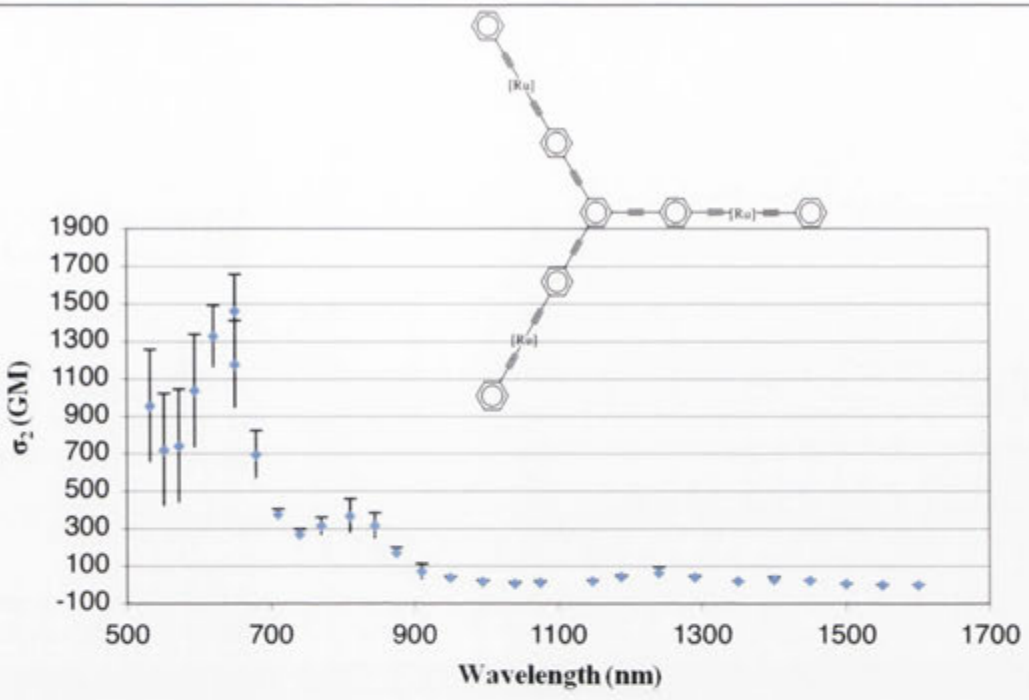


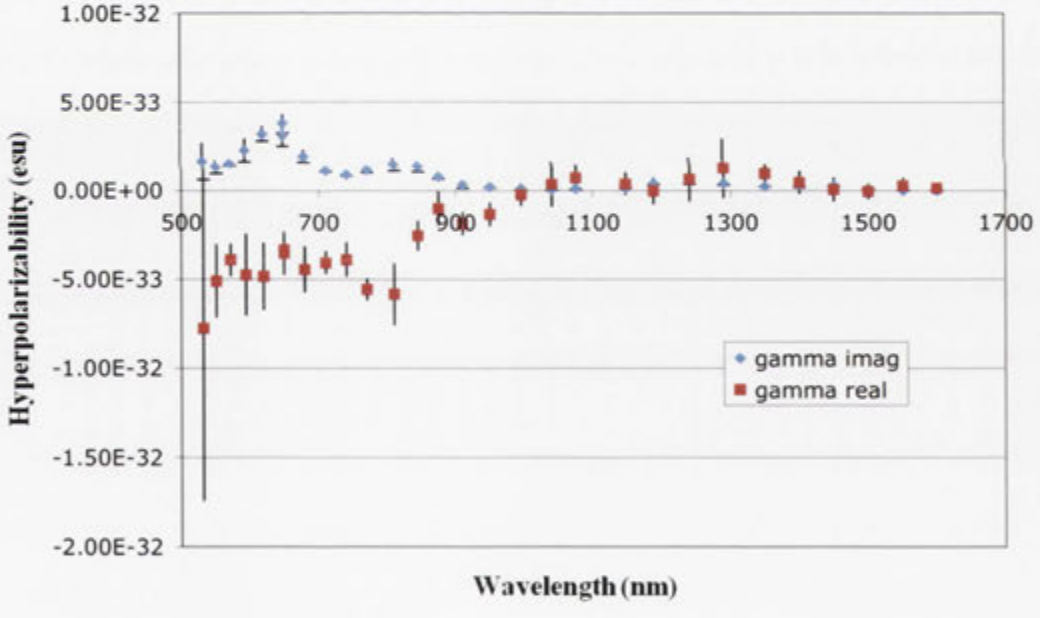


Cubic NLO spectra for compound **15**.

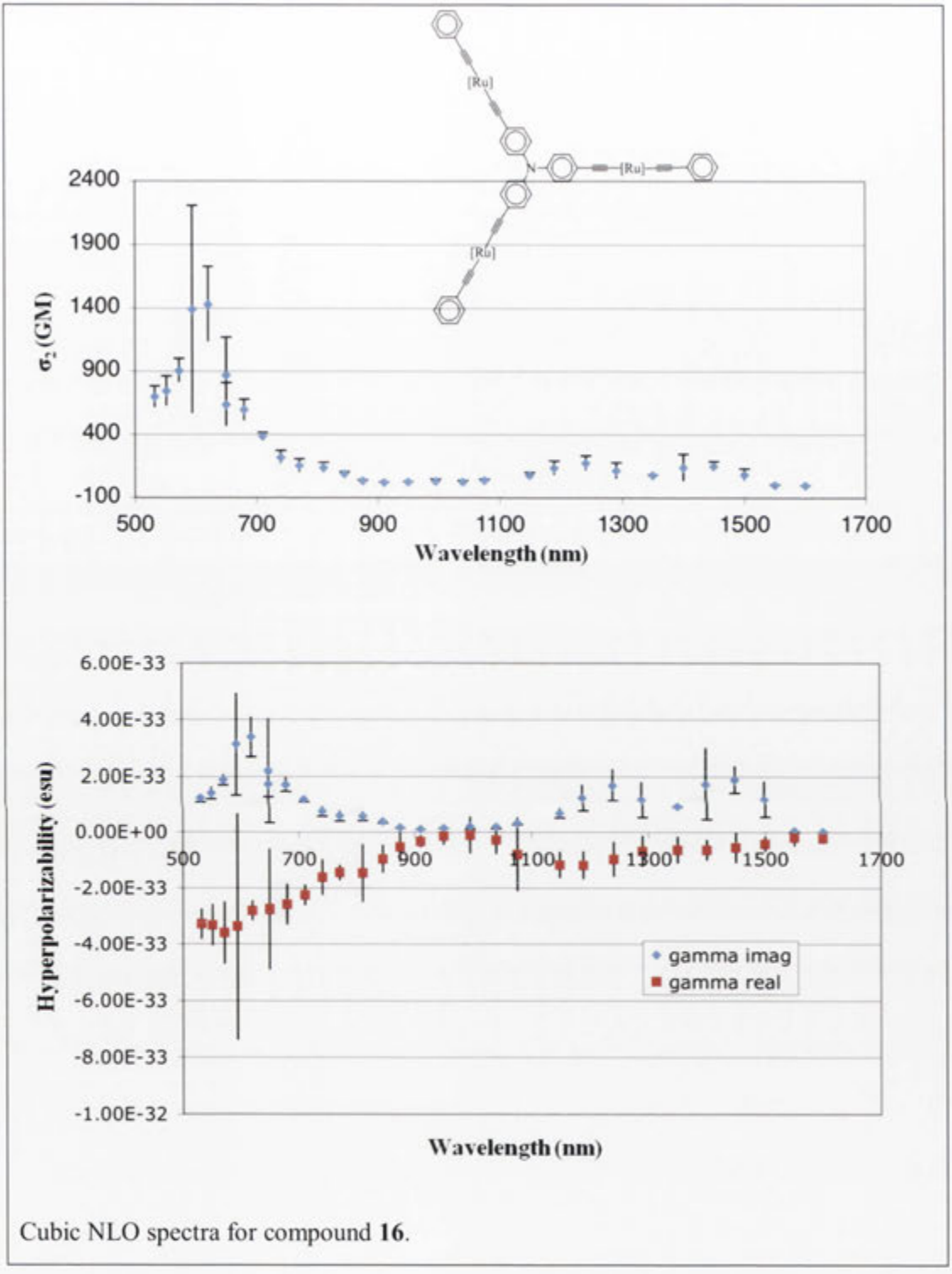


Cubic NLO spectra for compound **16**.

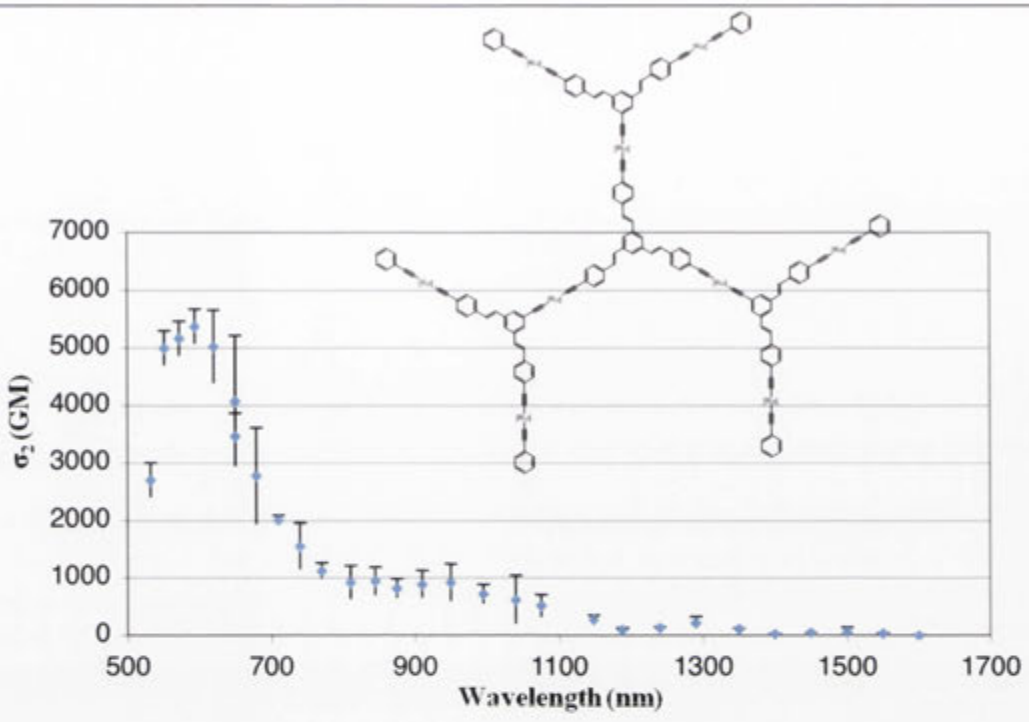


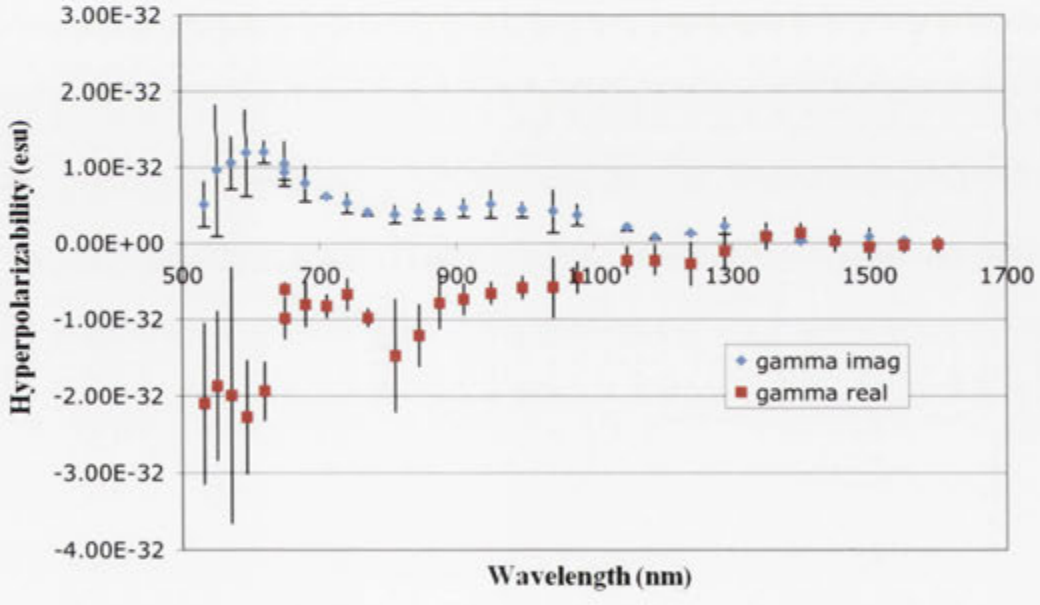


Cubic NLO spectra for compound **17**.

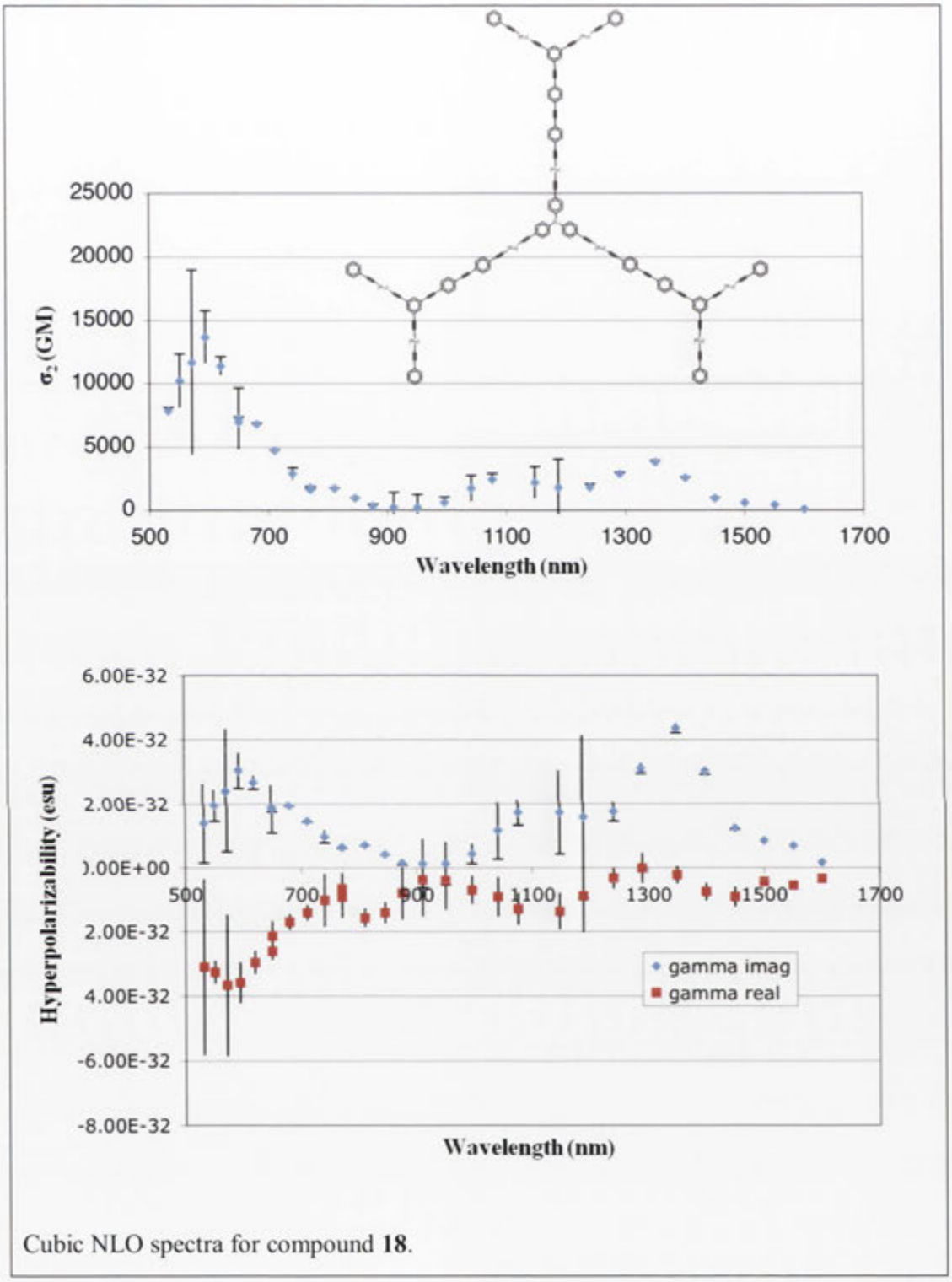


Cubic NLO spectra for compound **18**.

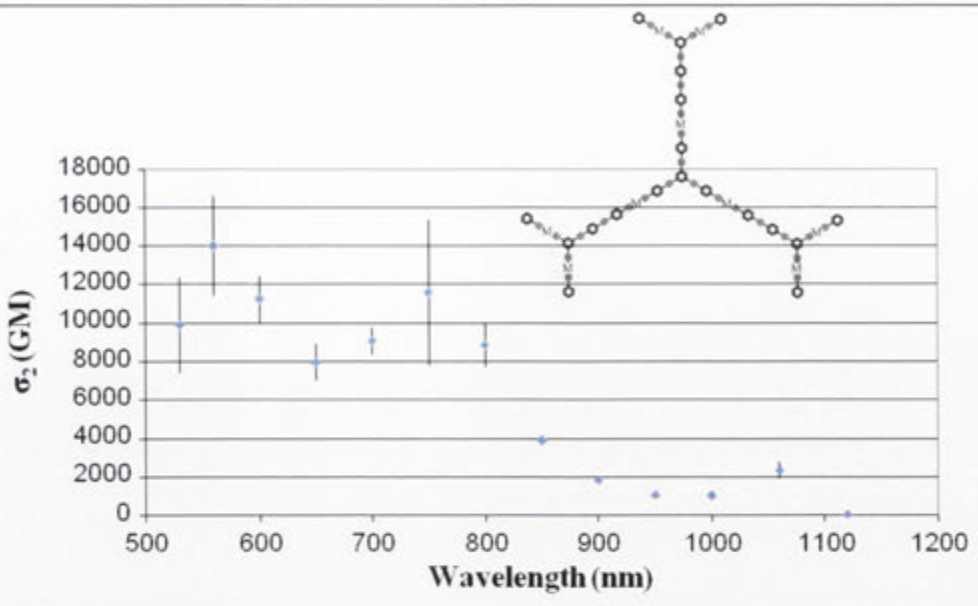


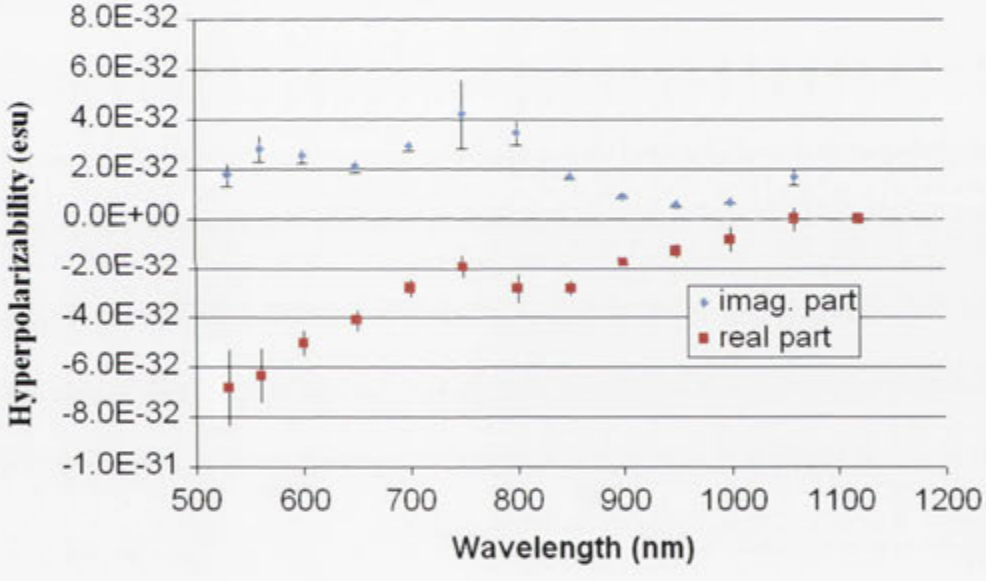


Cubic NLO spectra for compound **19**.

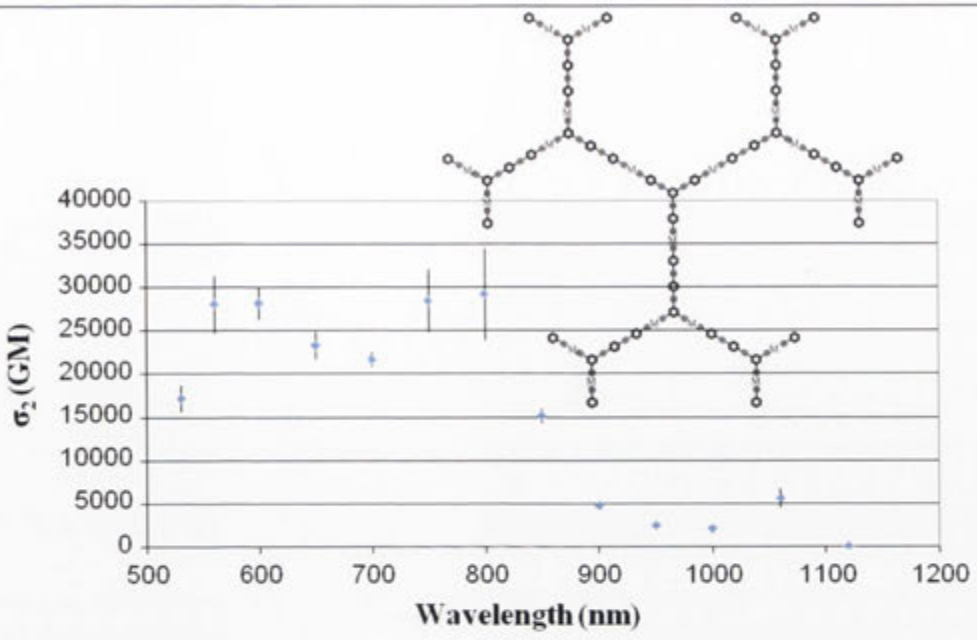


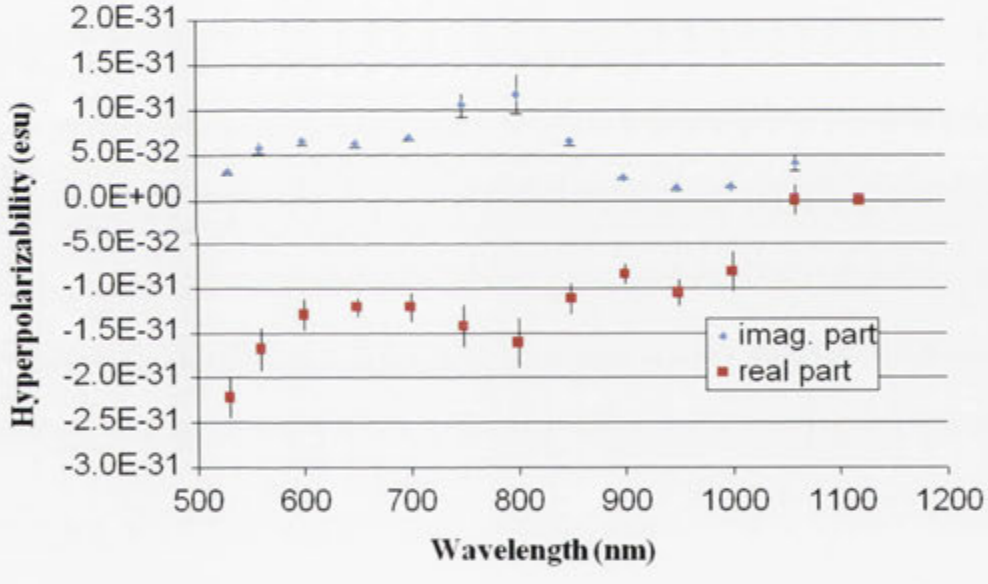


Cubic NLO spectra for compound **20**.

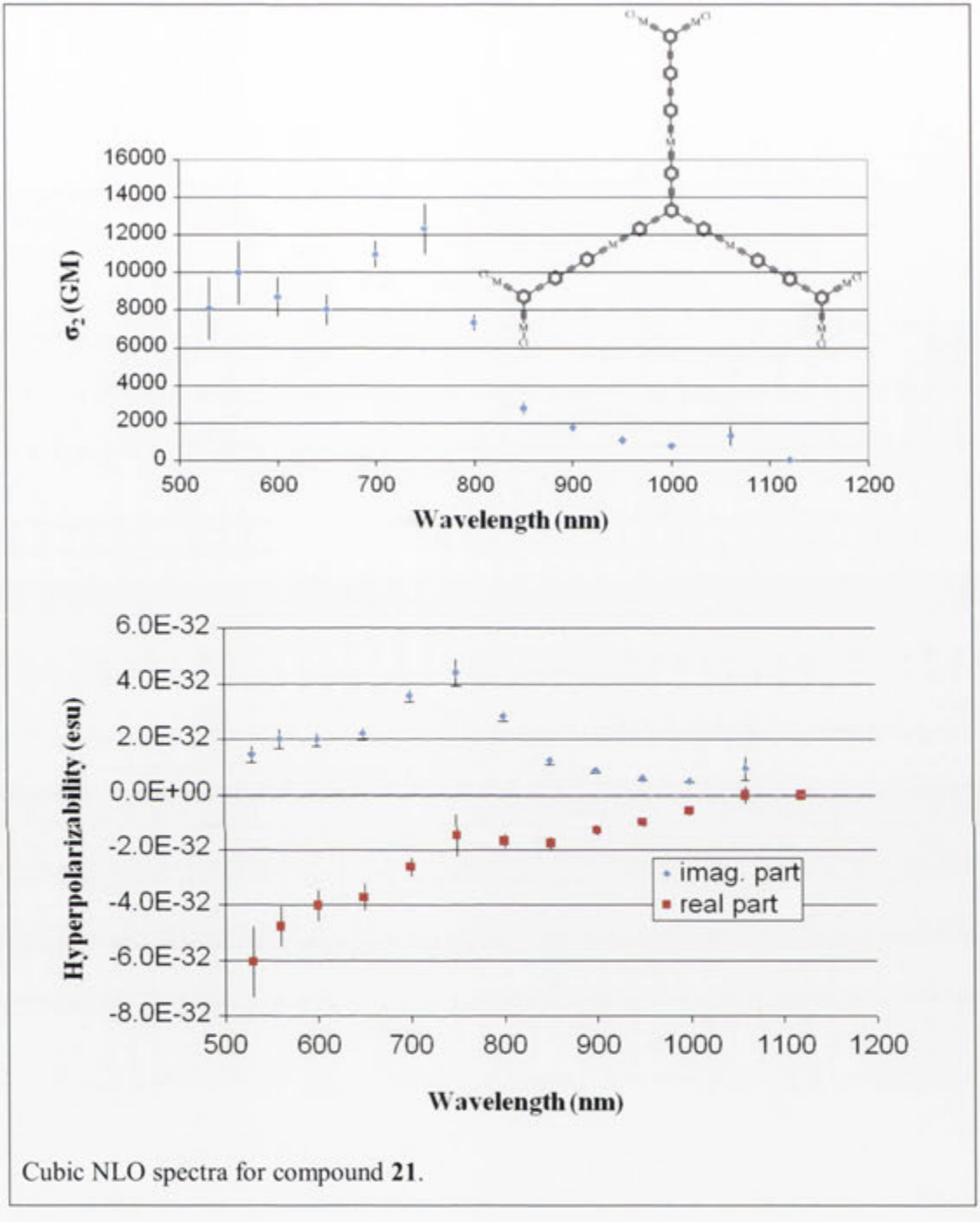


Cubic NLO spectra for compound **21**.

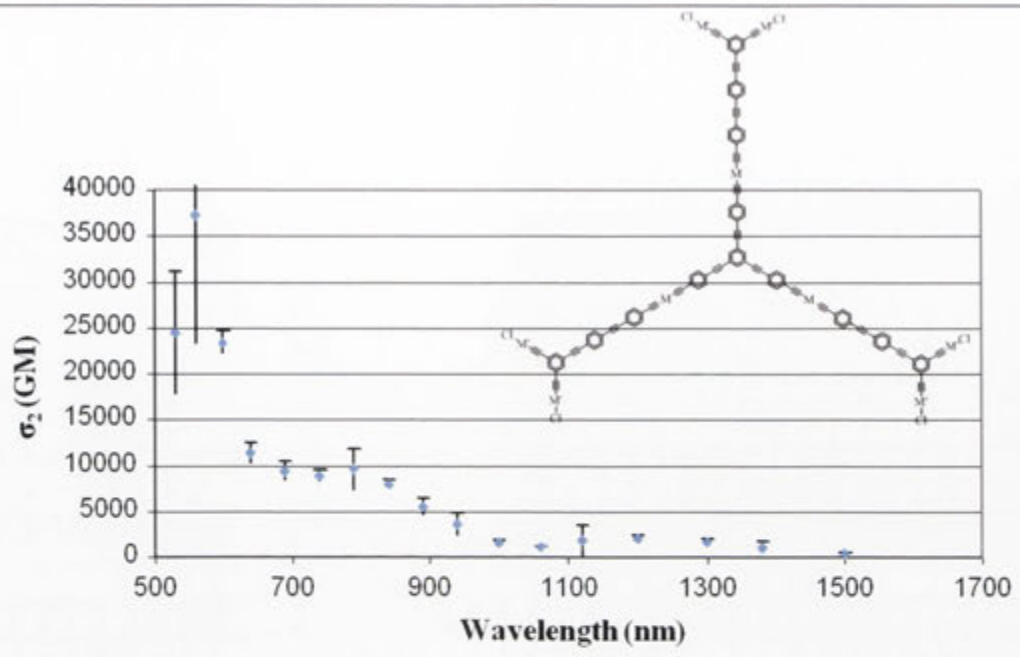


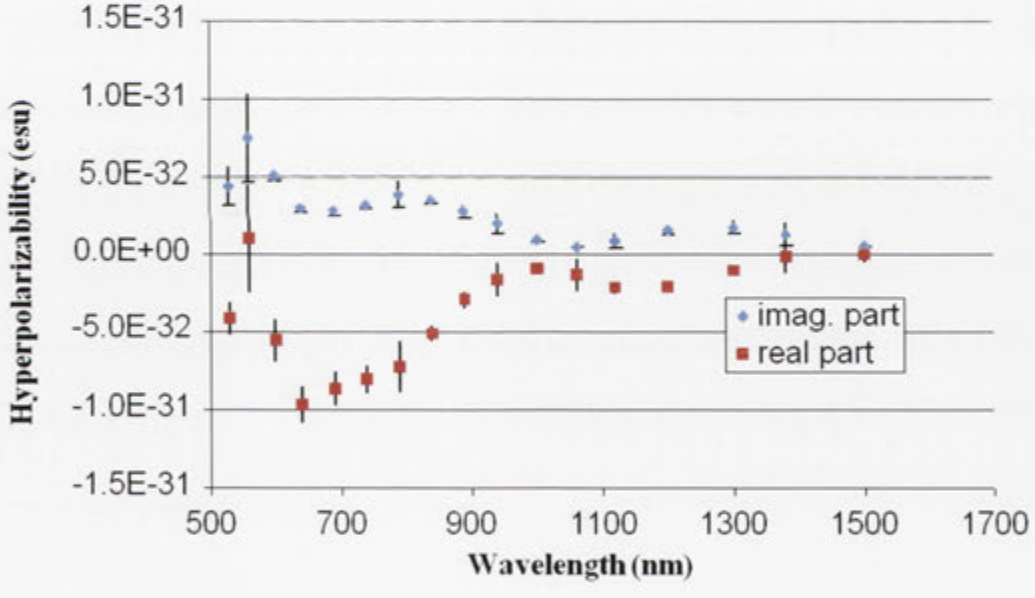


Cubic NLO spectra for compound **22**.

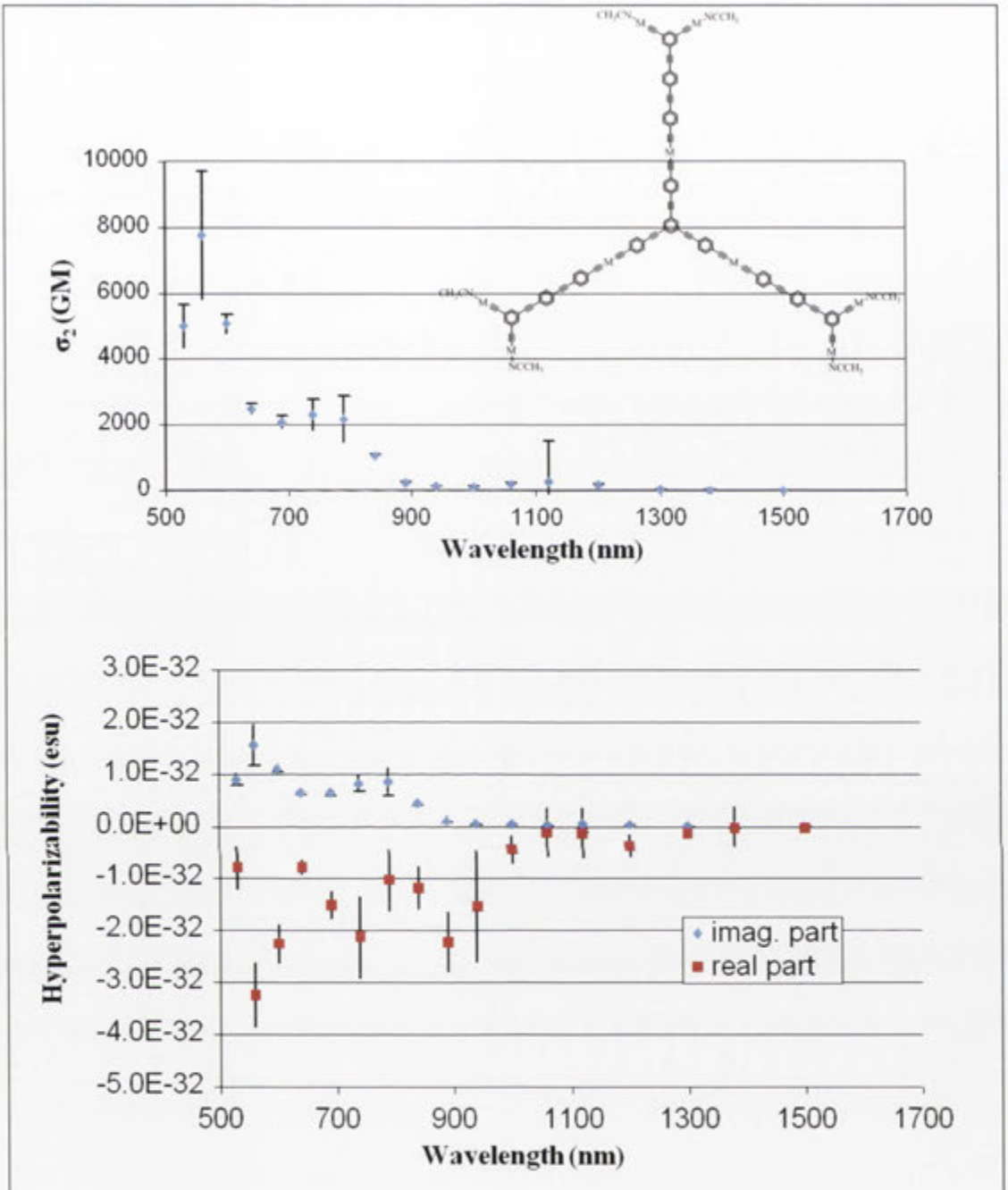


Cubic NLO spectra for compound **23**.

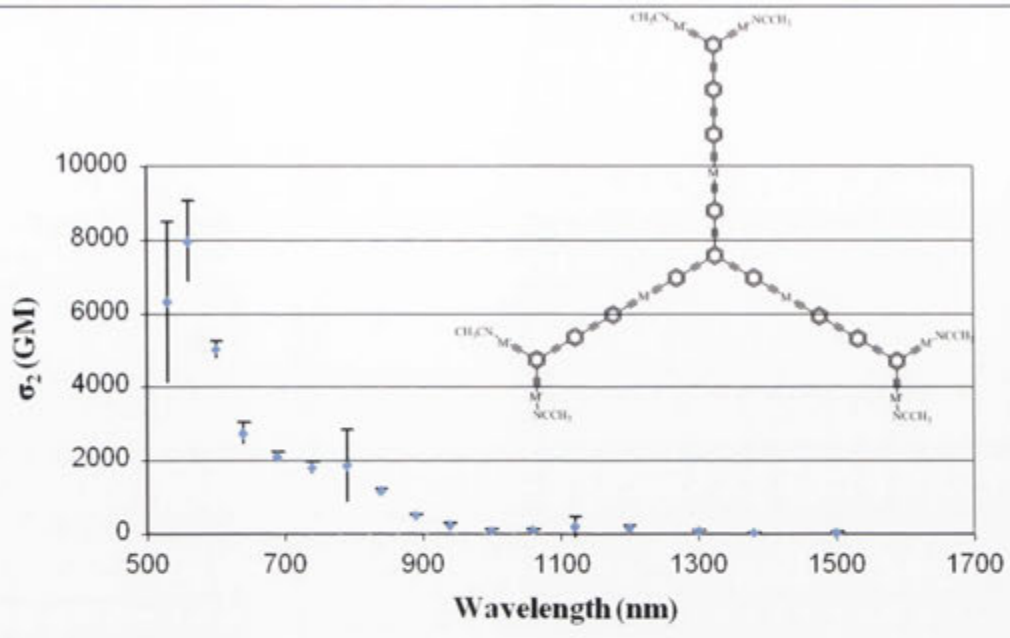


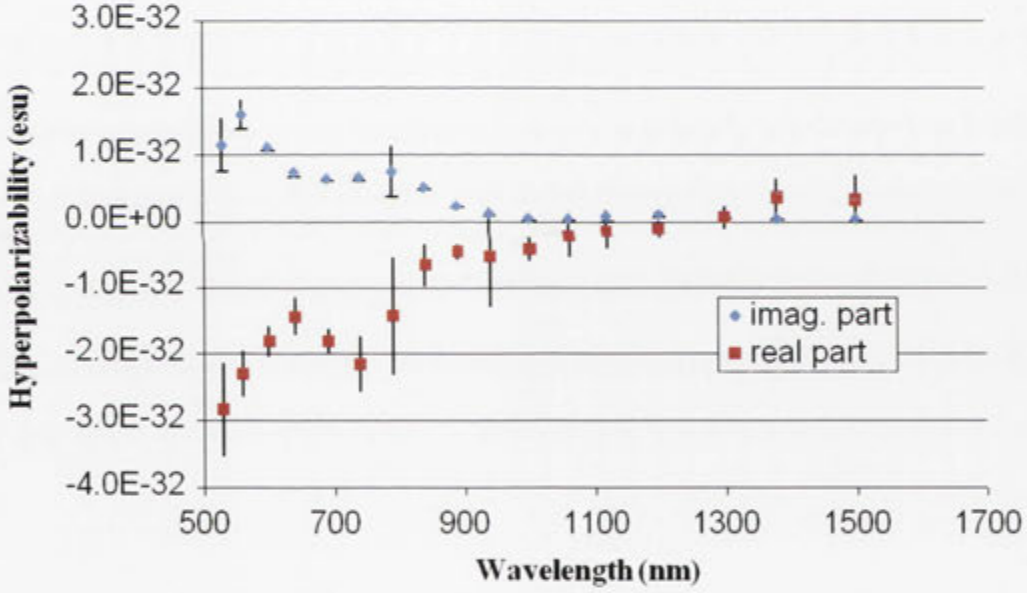


Cubic NLO spectra for compound **24**.

## NLO Data for Section 2.5

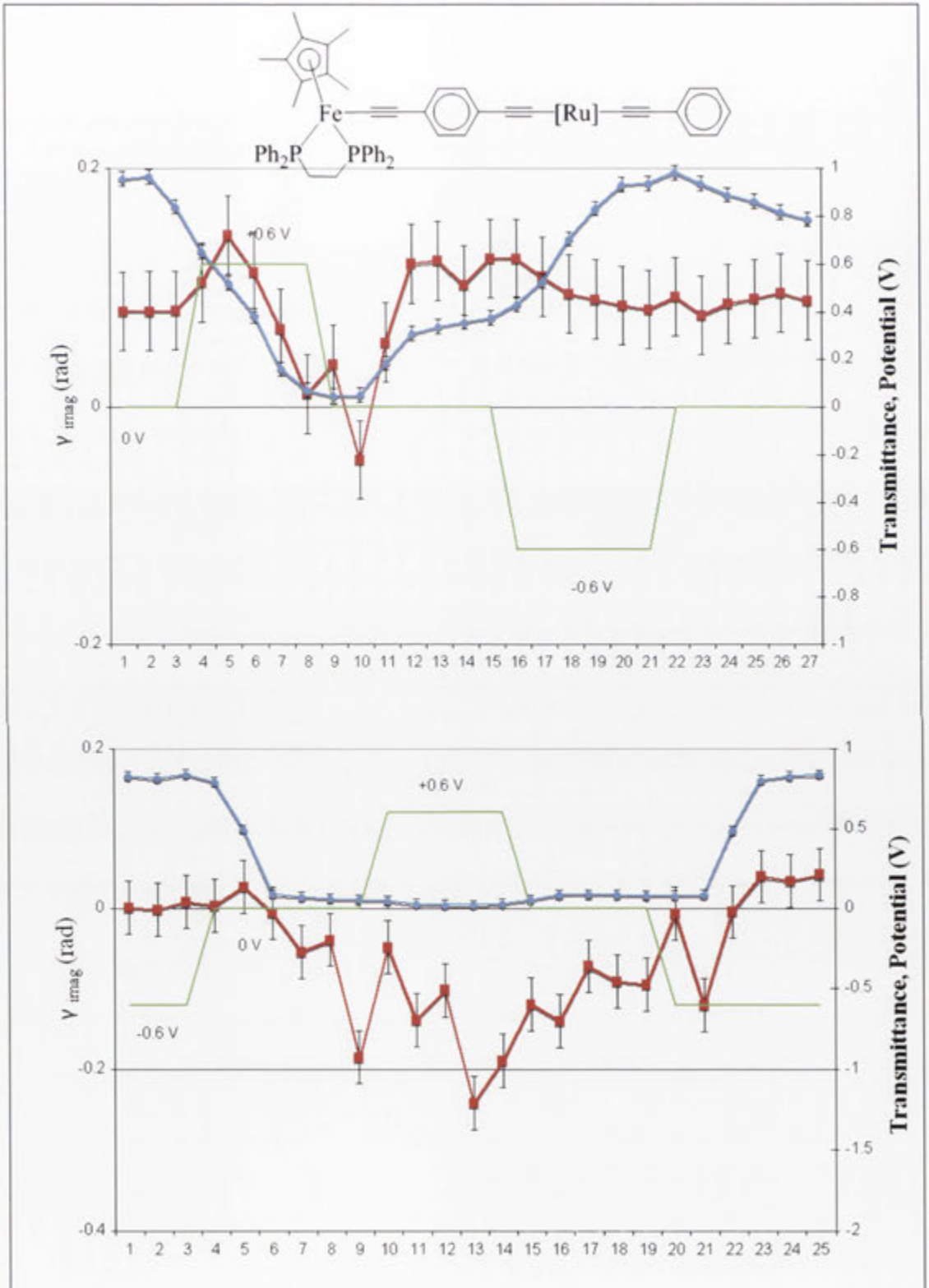


Potential dependent traces showing the transmittance (blue) and imaginary part of the nonlinear phase shift (red) of compound **25**, at 750 nm (top) and 1250 nm (bottom).

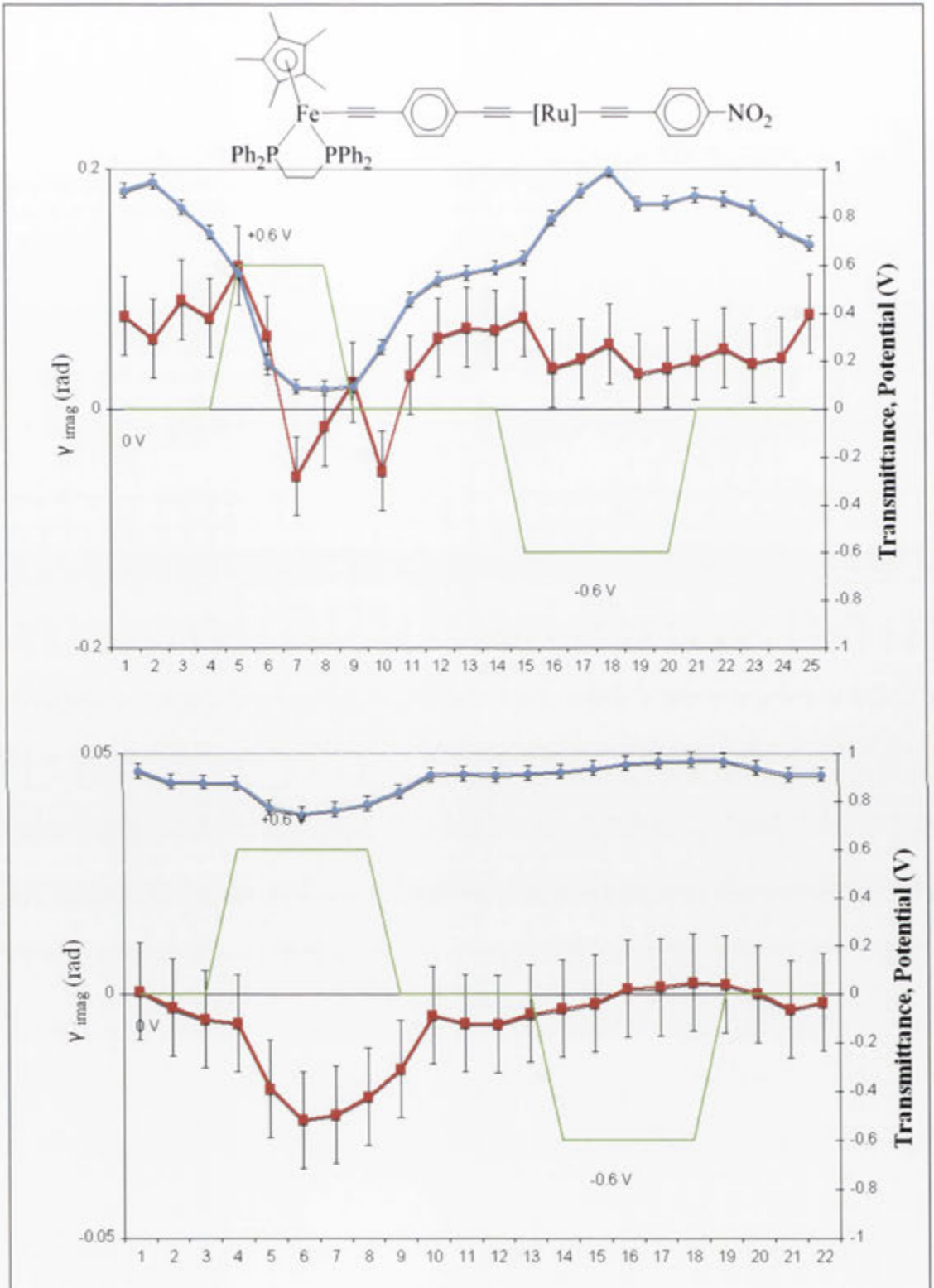


Potential dependent traces showing the transmittance (blue) and imaginary part of the nonlinear phase shift (red) of compound **26**, at 750 nm (top) and 1250 nm (bottom).

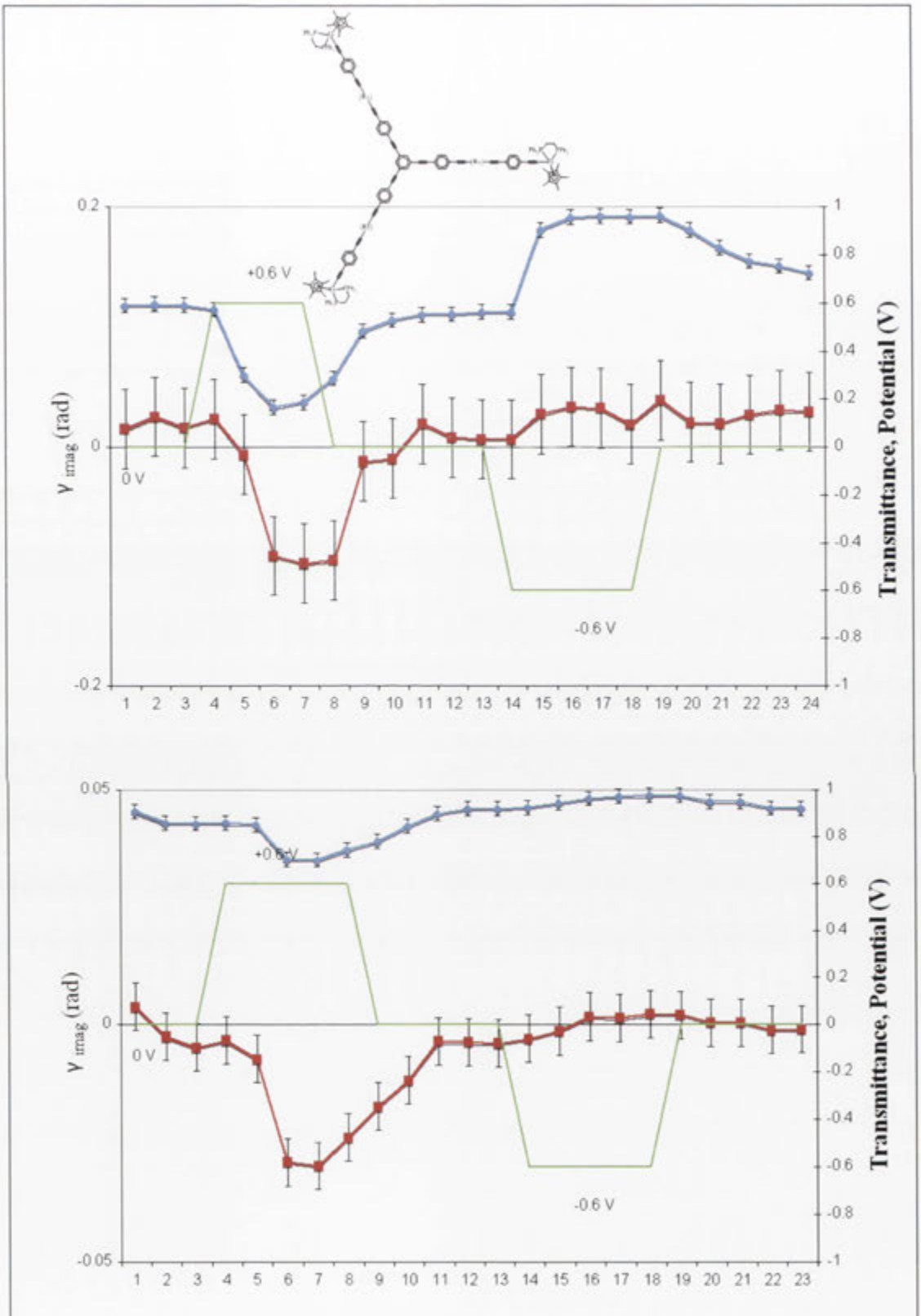


Potential dependent traces showing the transmittance (blue) and imaginary part of the nonlinear phase shift (red) of compound **27**, at 750 nm (top) and 1250 nm (bottom).

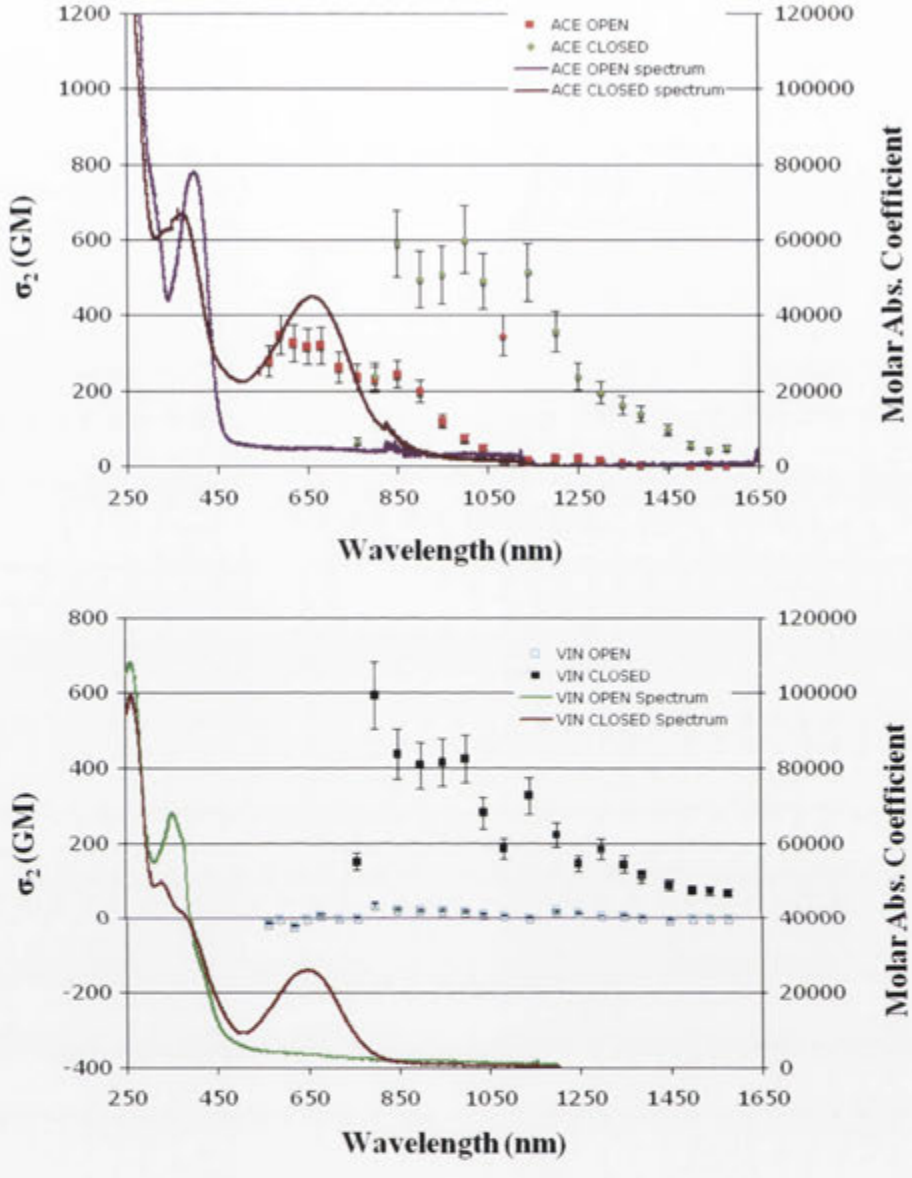


Switching comparisons of the cubic NLO spectra of **29** and **28** (top) and **31** and **30** (bottom). Linear spectra are included for comparison, plotted normally.

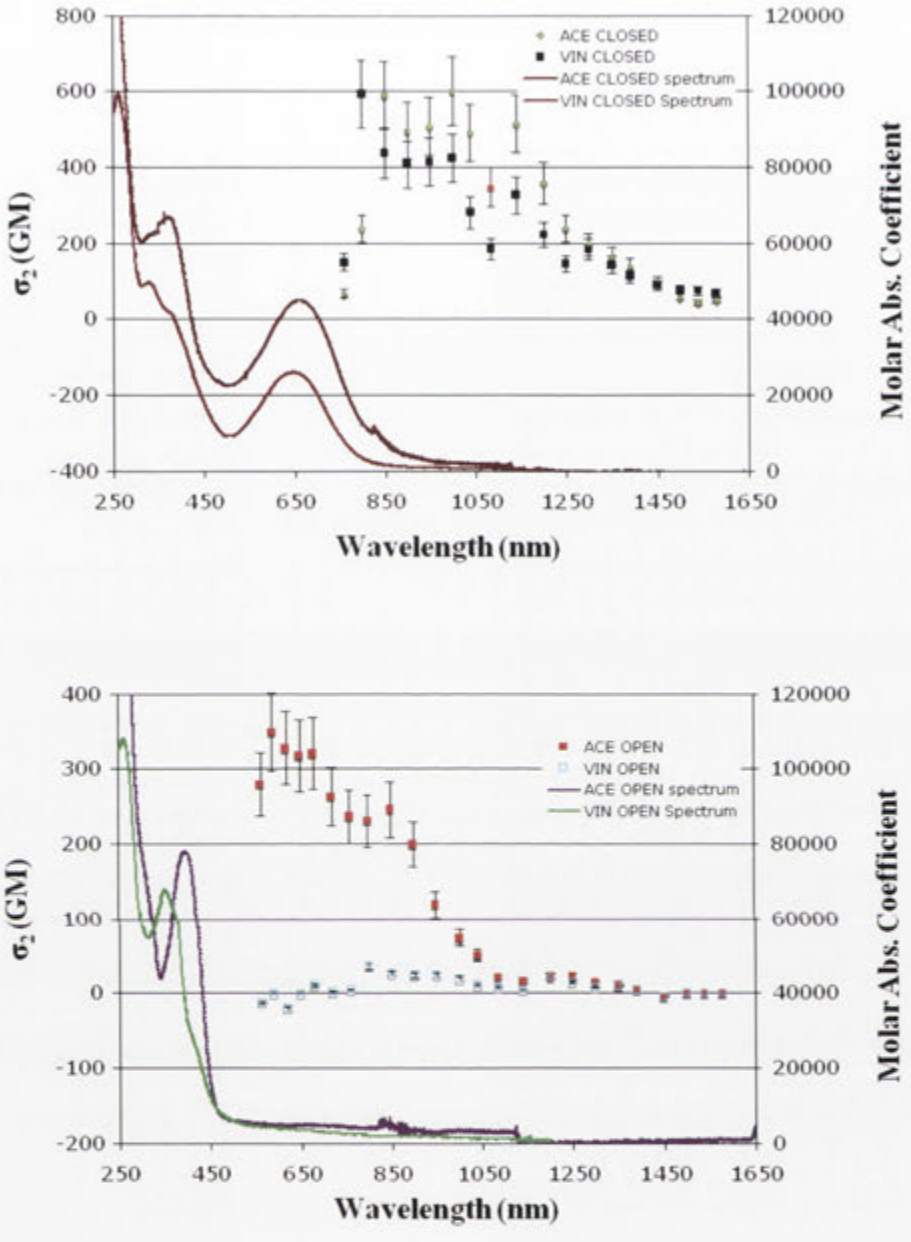


Switching comparisons of the cubic NLO spectra of **28** and **30** (top) and **29** and **31** (bottom). Linear spectra are included for comparison, plotted normally.

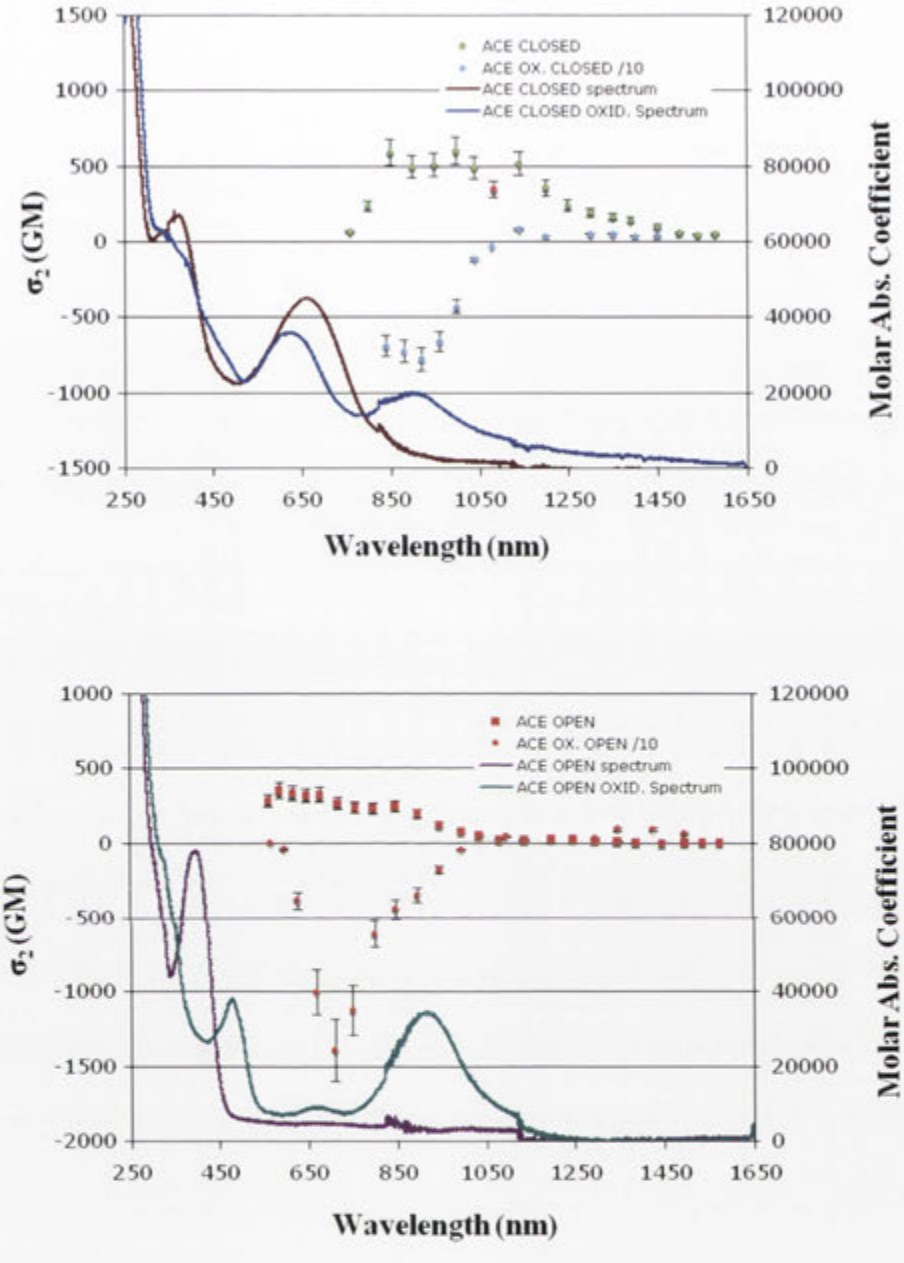


Switching comparisons of the cubic NLO spectra of **28** and **32** (top) and **29** and **33** (bottom). Linear spectra are included for comparison, plotted normally.

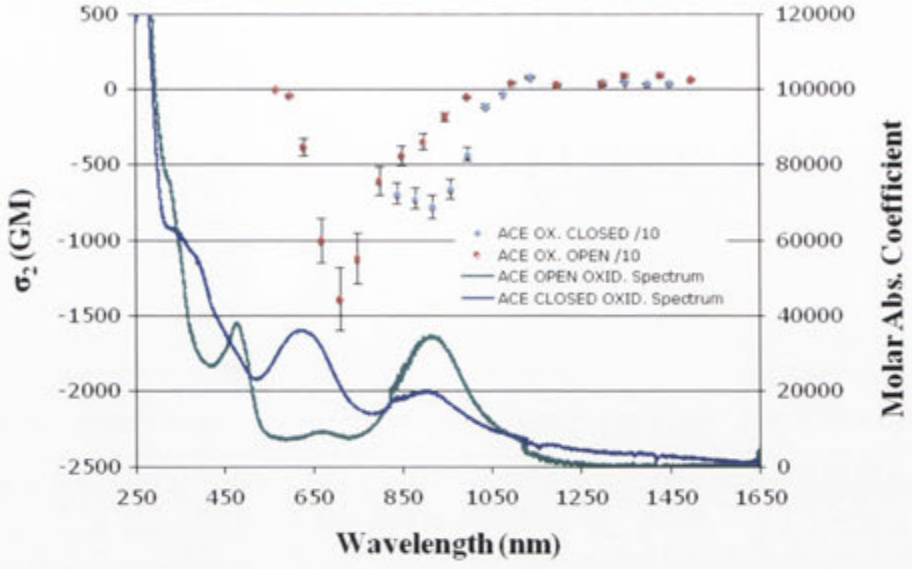


Switching comparisons of the cubic NLO spectra of **32** and **33**. Linear spectra are included for comparison, plotted normally.

## NLO Data for Section 3.4

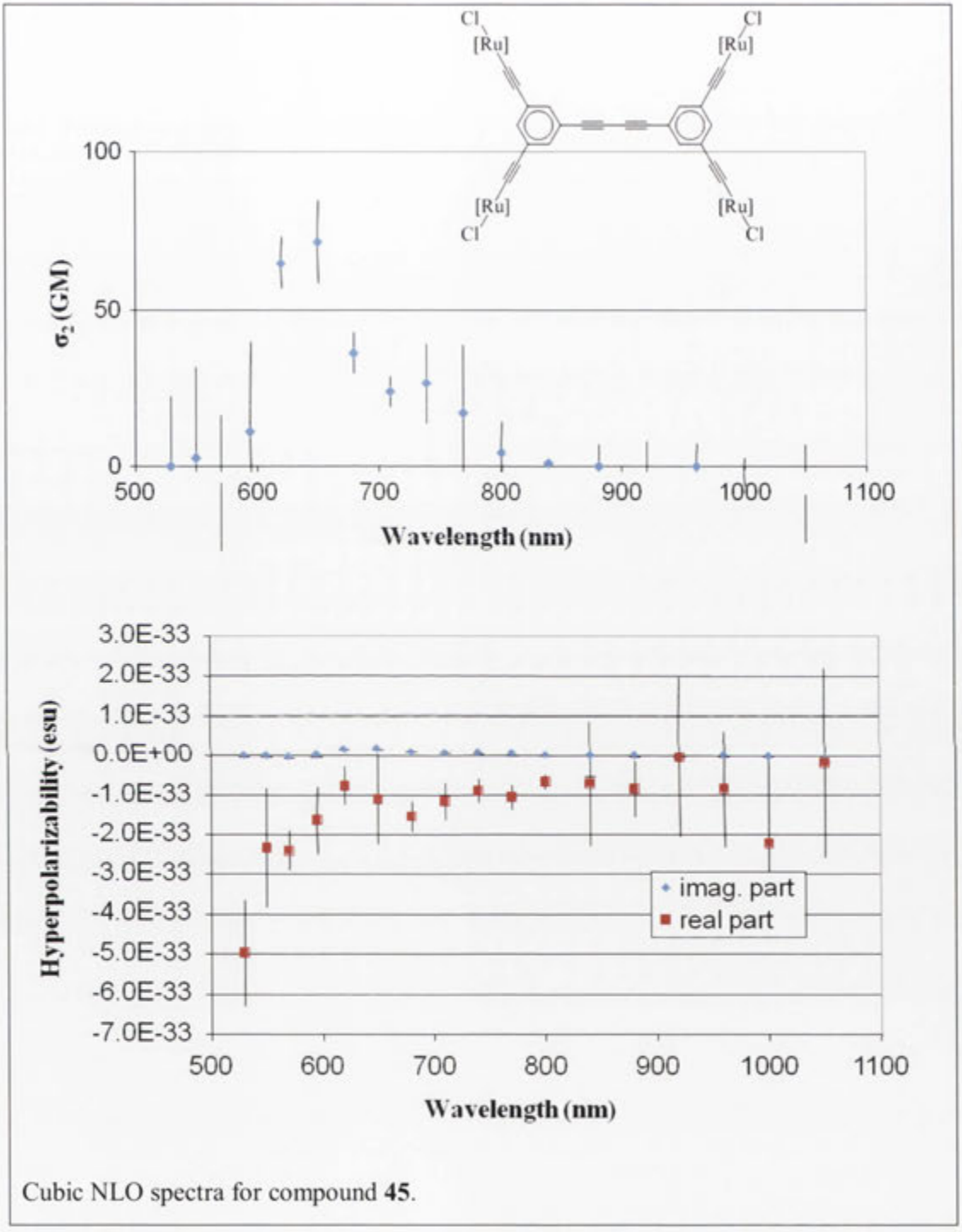


Cubic NLO spectra for compound **45**.

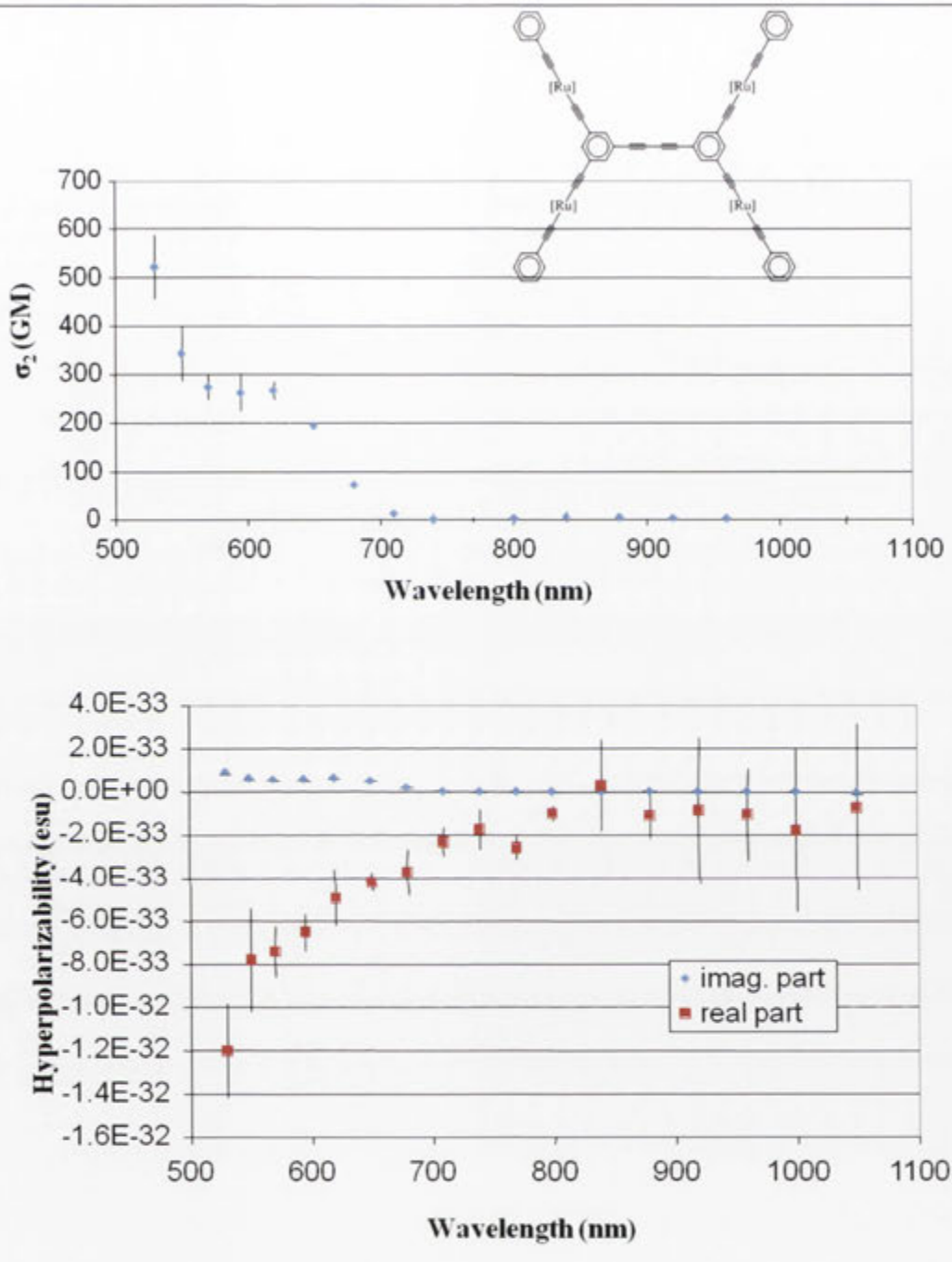


Cubic NLO spectra for compound **46**.

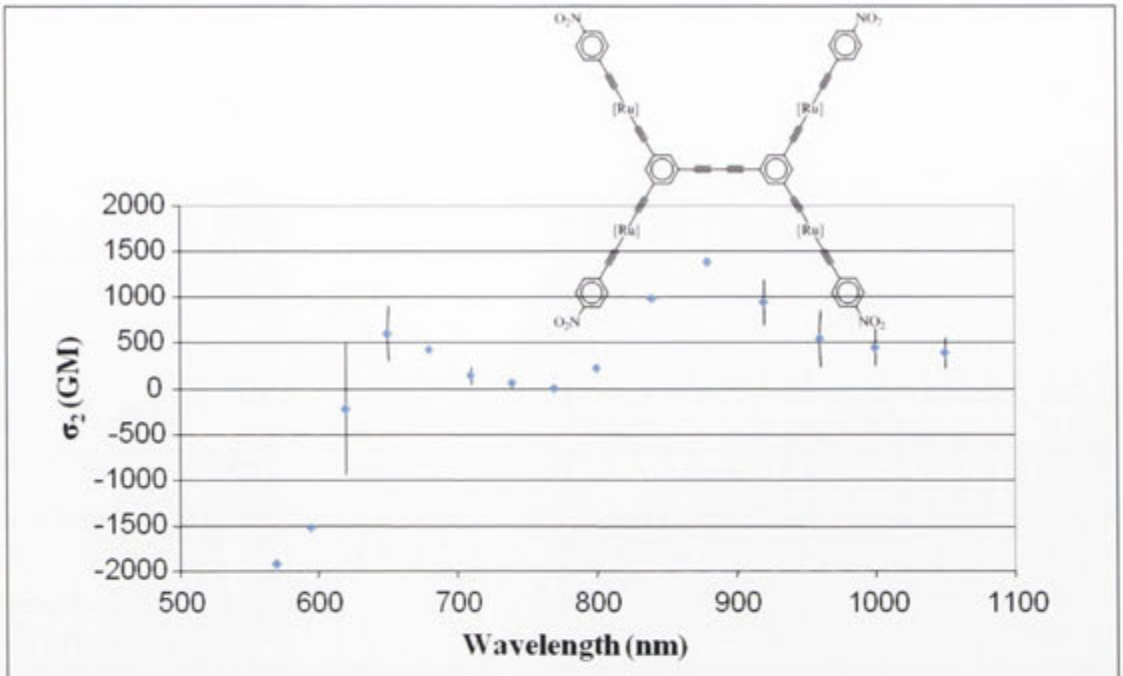


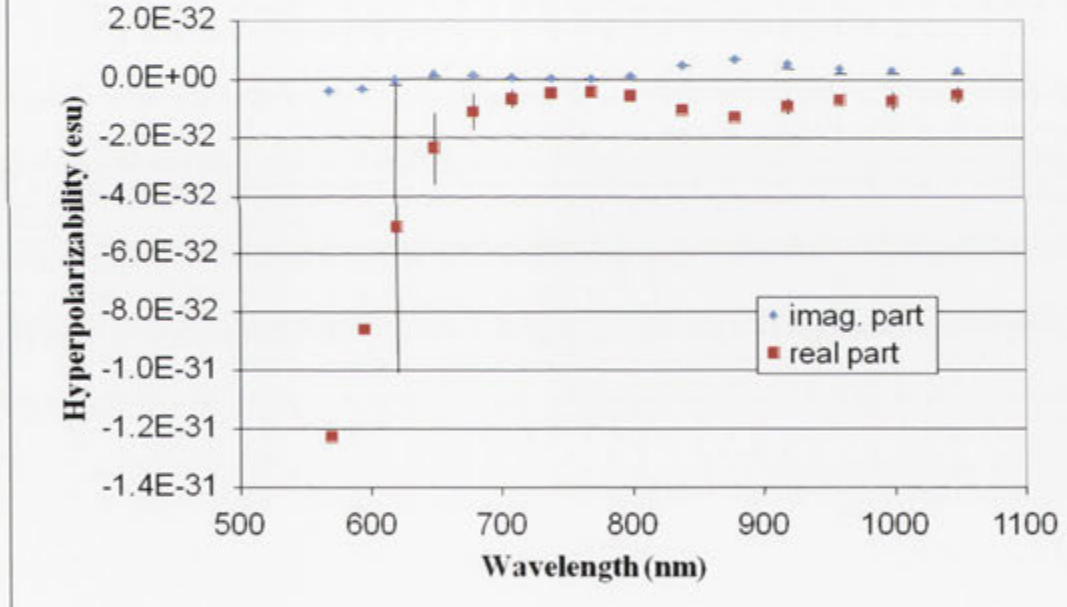


Cubic NLO spectra for compound **47**.

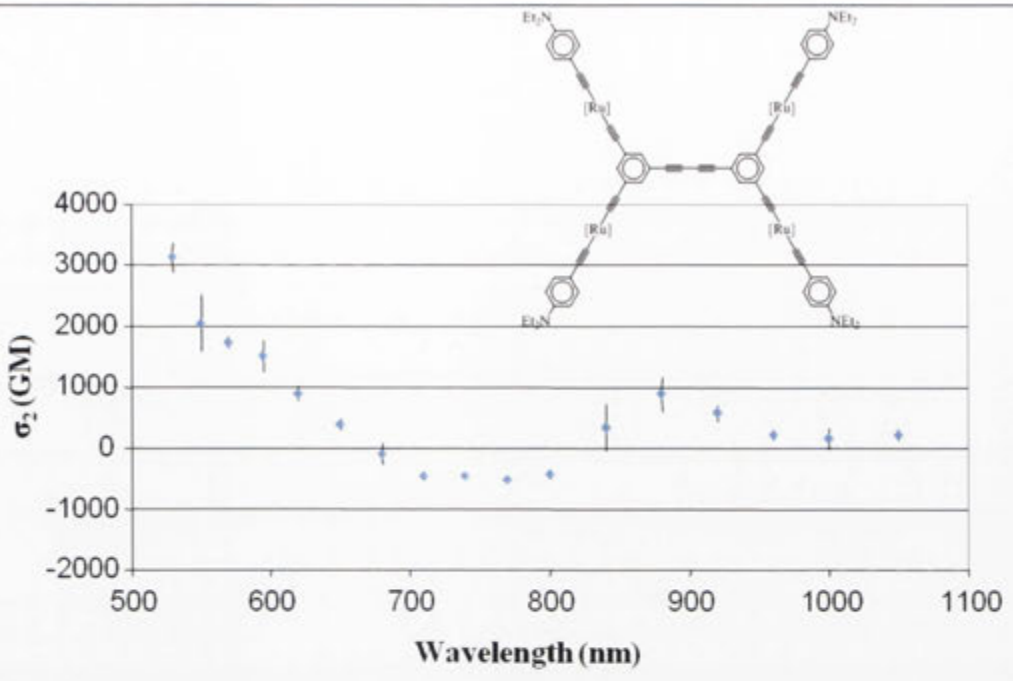


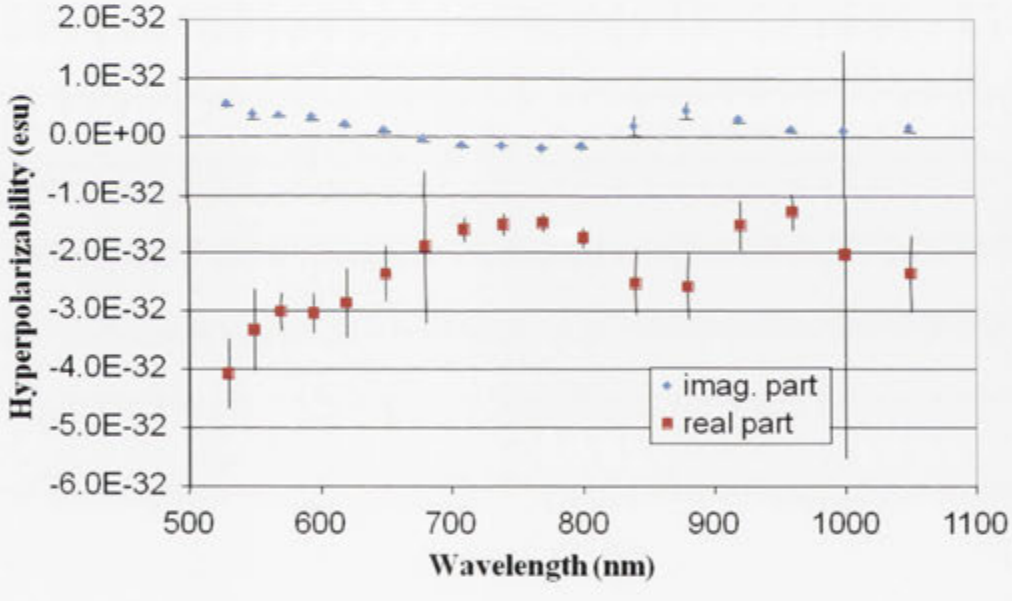


Cubic NLO spectra for compound **48**.

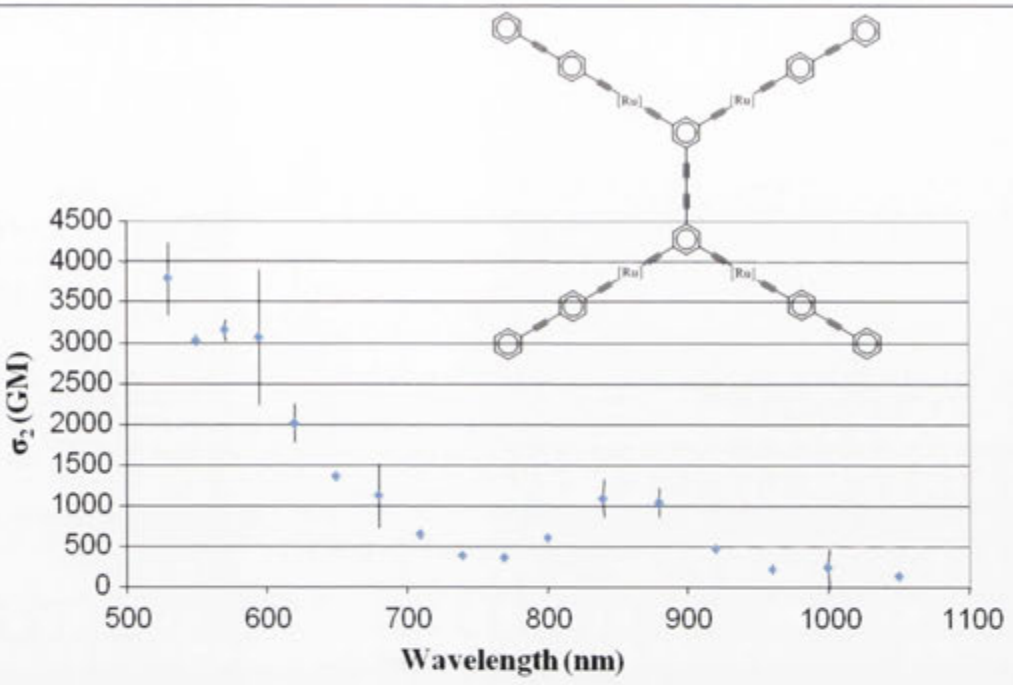


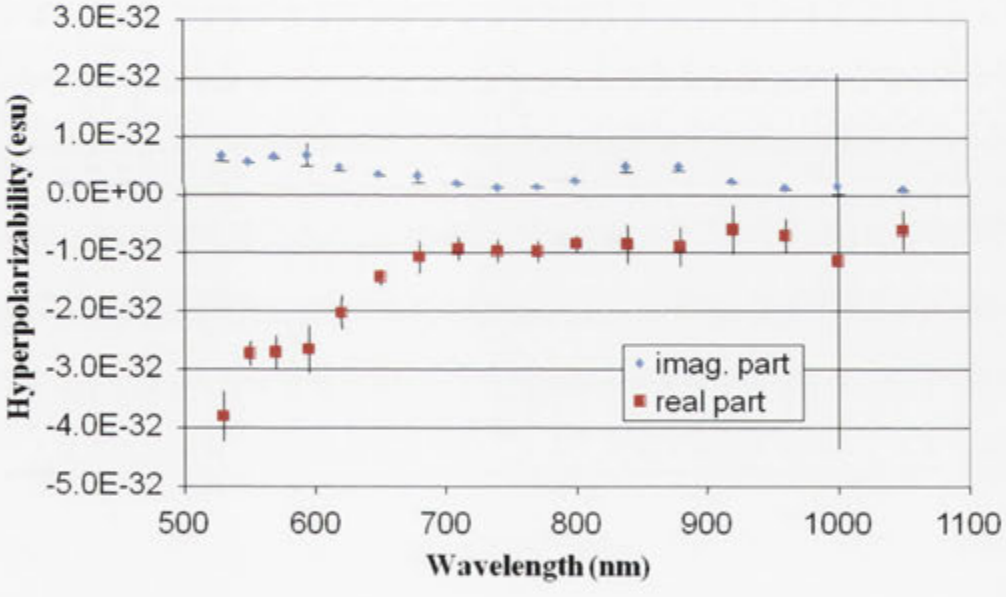


Cubic NLO spectra for compound **49**.

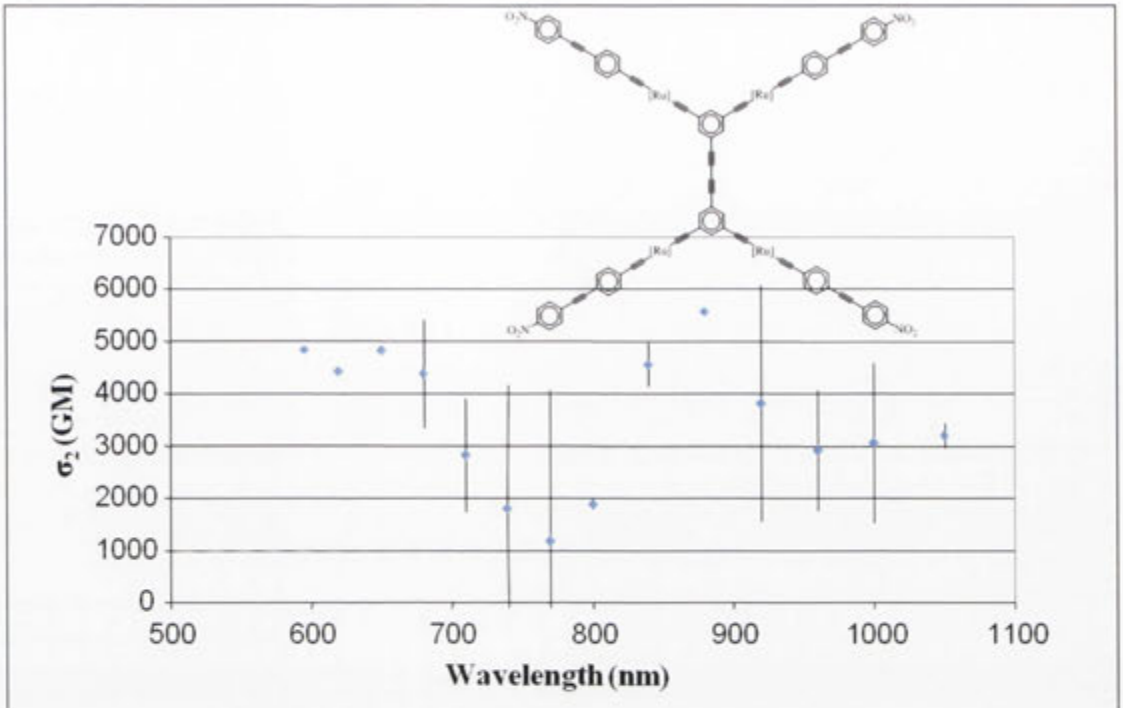


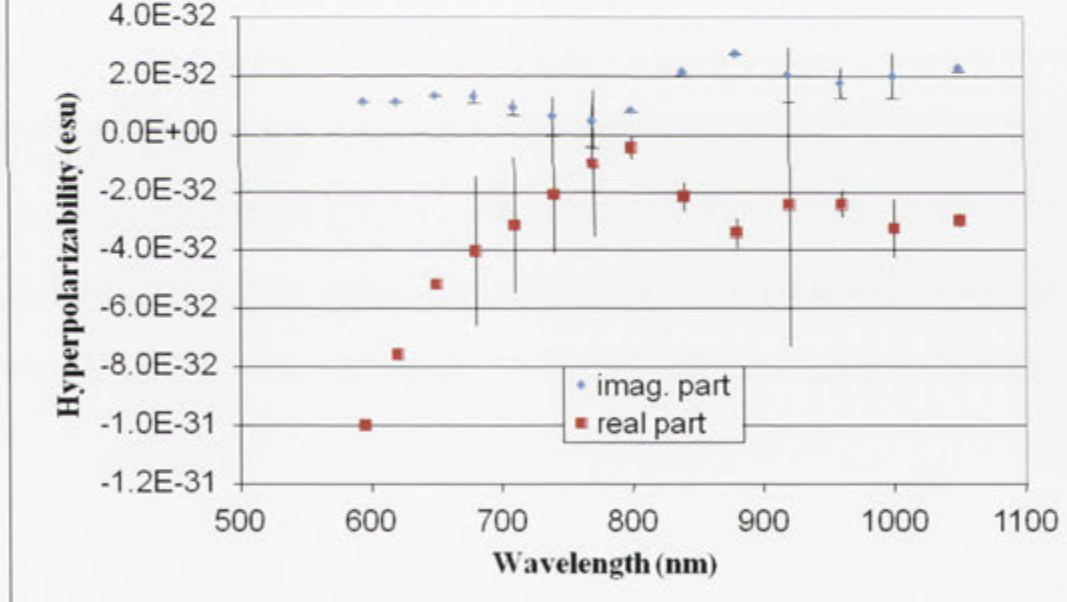


Cubic NLO spectra for compound **50**.

## NLO Data for Section 4.1

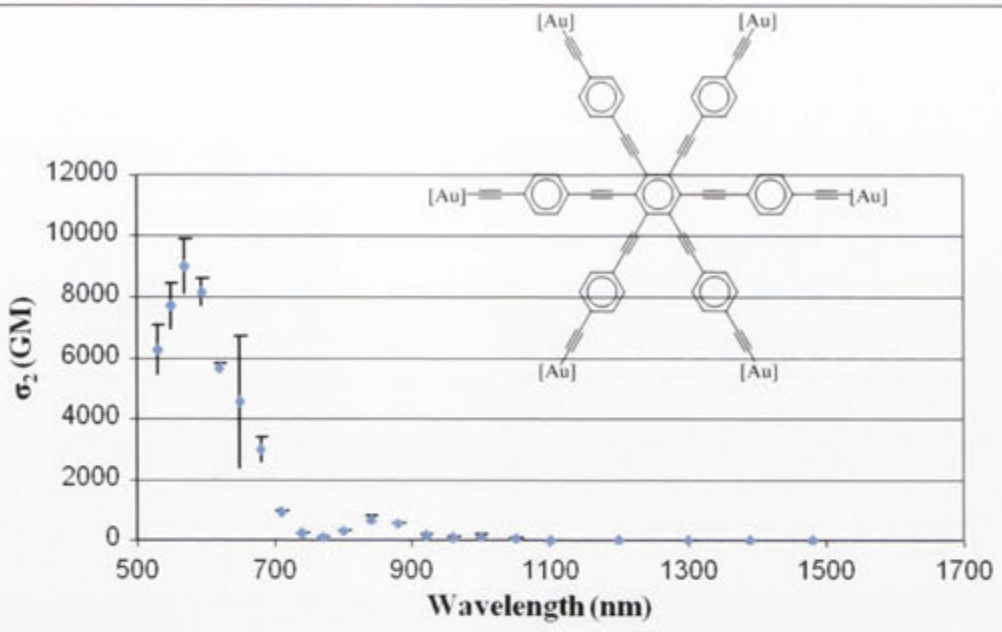


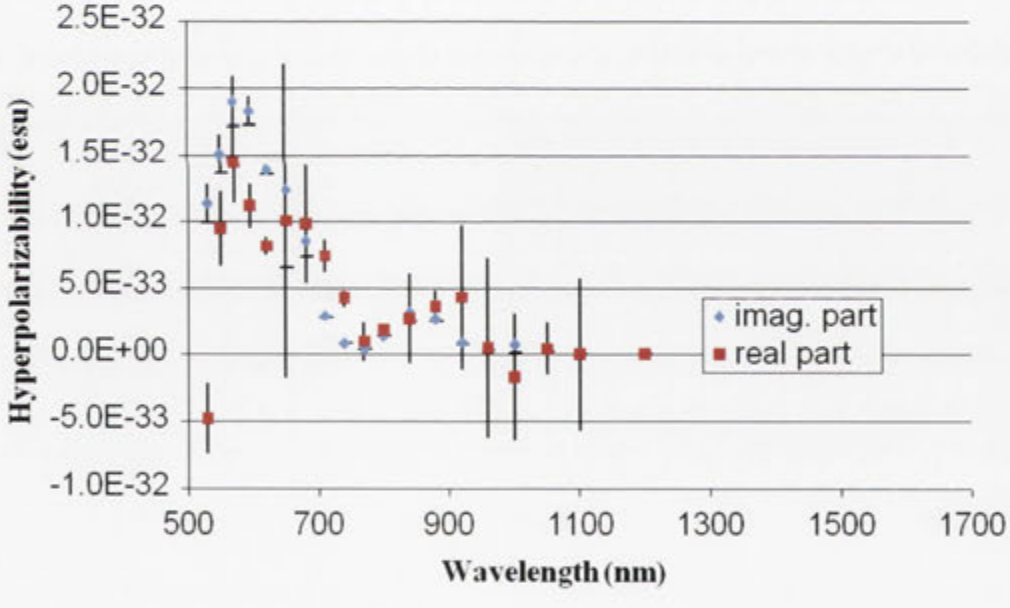


Cubic NLO spectra for compound **52**.

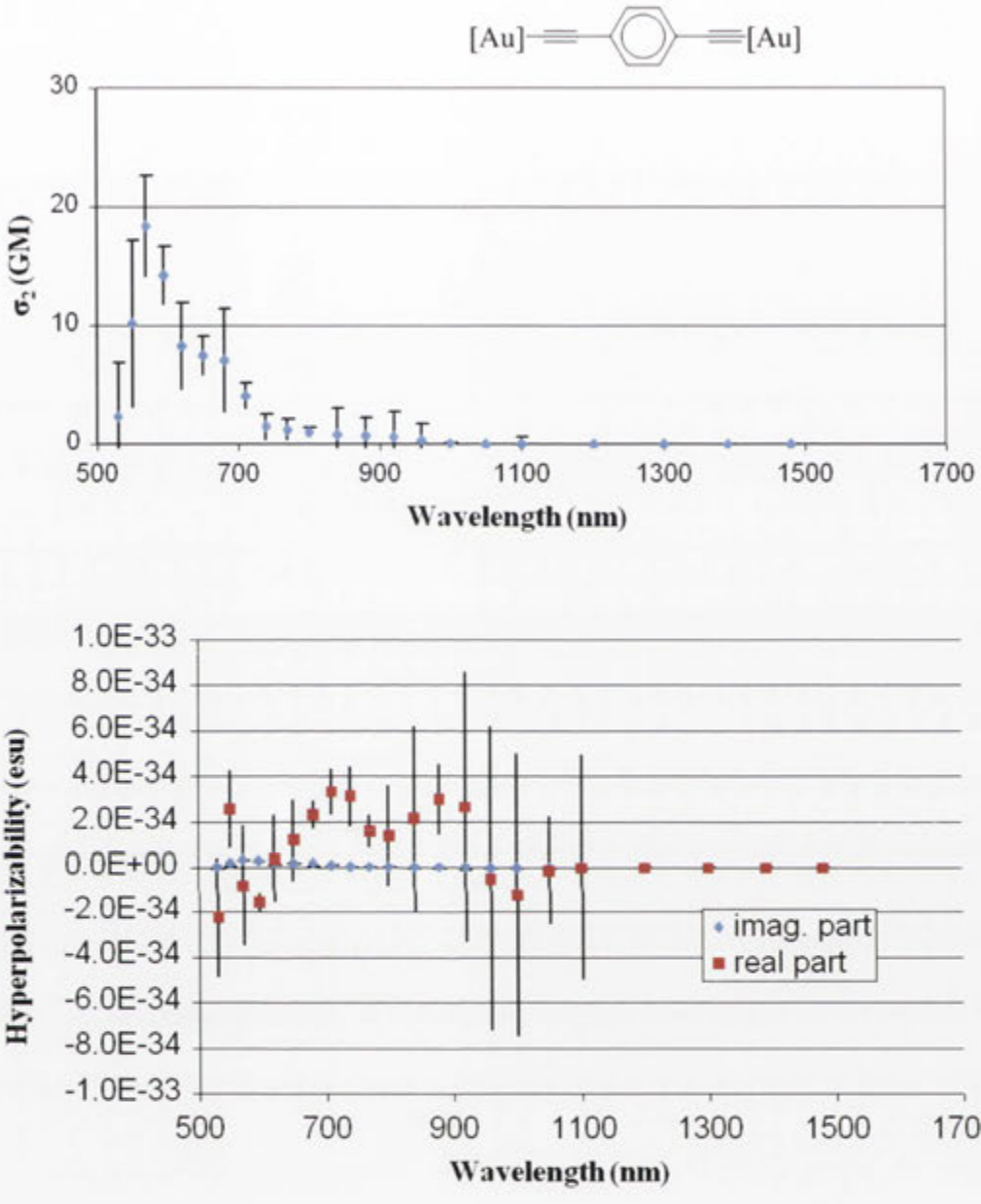


Cubic NLO spectra for compound **53**.

## NMR Spectra for Section 4.3

Spectra are presented following synthetic lines (e.g. all four compounds with fourfold substitution are presented together). The ordering of the spectra for individual compounds is: $^{1}H$, $^{13}C$ then $^{31}P$ (where applicable). The $^{1}H$ spectrum has the structure of the compound included, for ease of reference. Despite 64-72 hour acquisition times, quaternary carbons failed to resolve on some compounds. These compounds do not have the quaternary peaks annotated.

All compounds are annotated using the same numbering scheme (Figure 4.9 is reproduced below for convenience). In every case, where a carbon atom has multiple protons bound to it, all of those protons are equivalent, therefore they are annotated using the number of the carbon atom they are bound to. Phosphorous atoms within each molecule are all equivalent and not annotated.

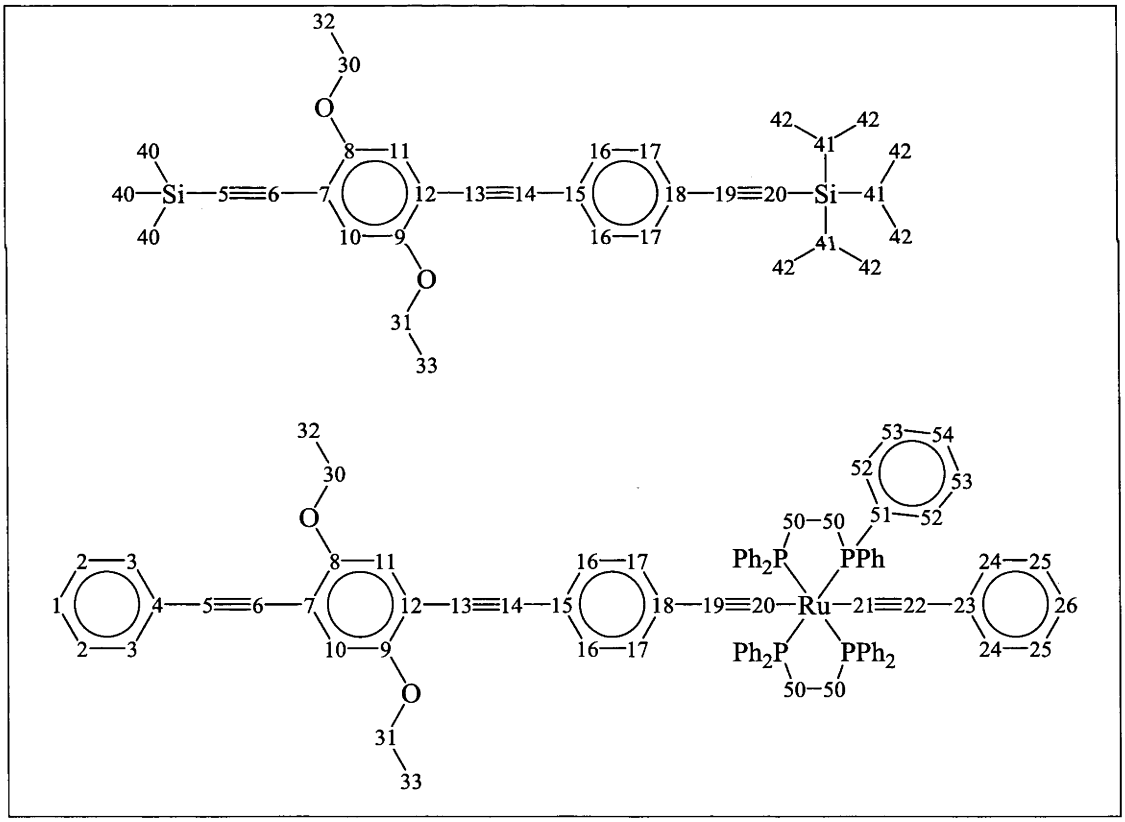

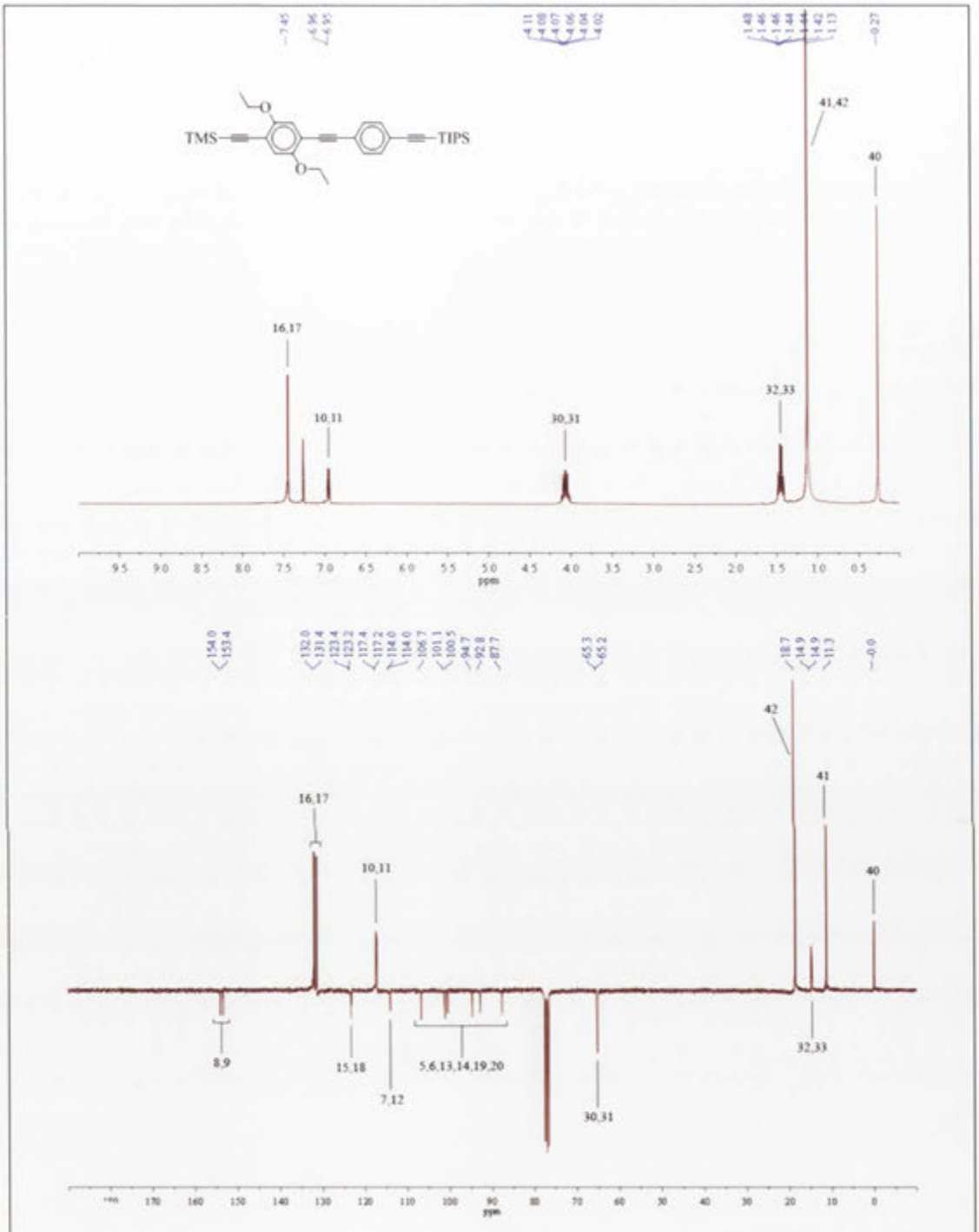


$^{1}H$ (top) and $^{13}C$ (bottom) spectra for compound **55**.

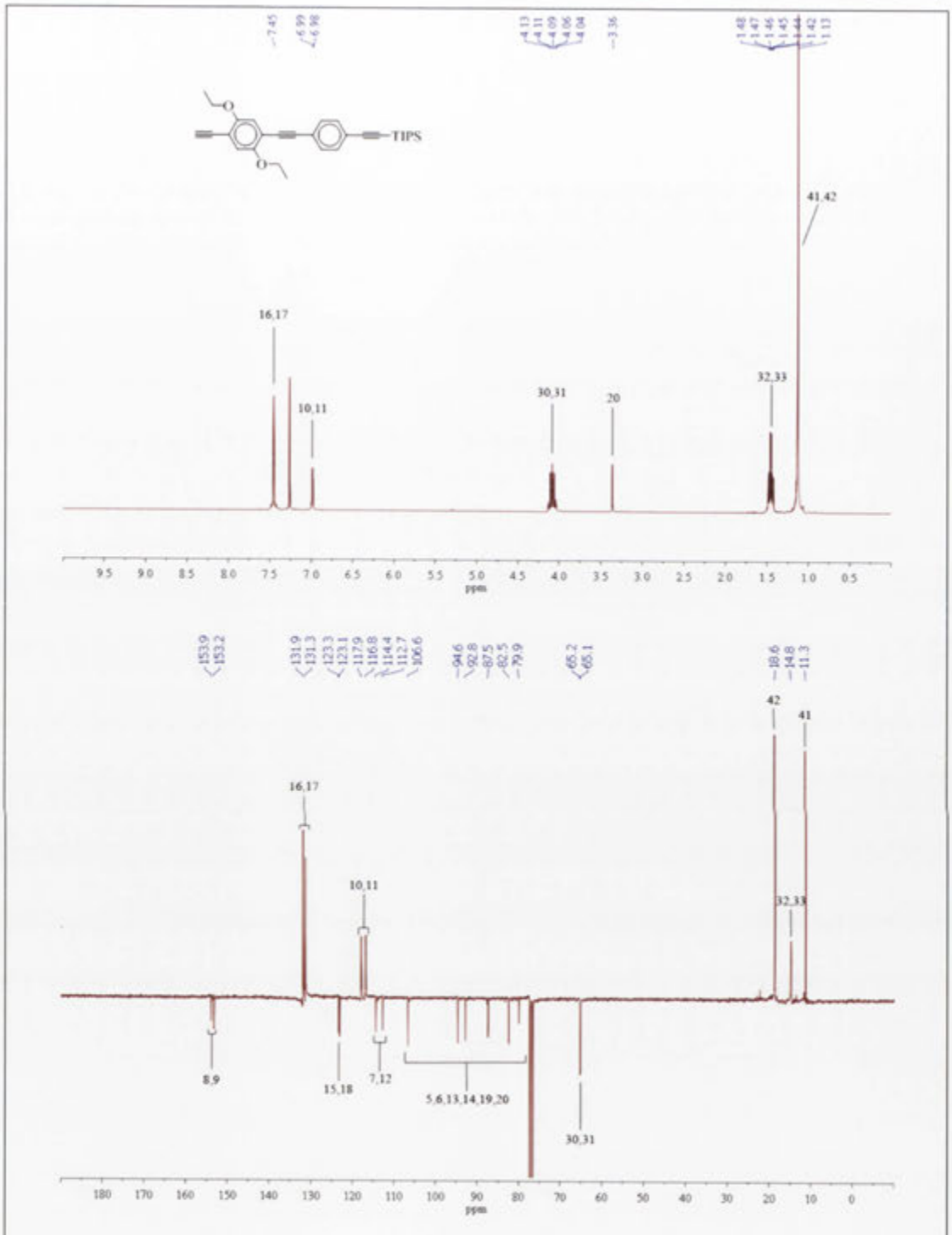


$^{1}H$ (top) and $^{13}C$ (bottom) spectra for compound **56**.

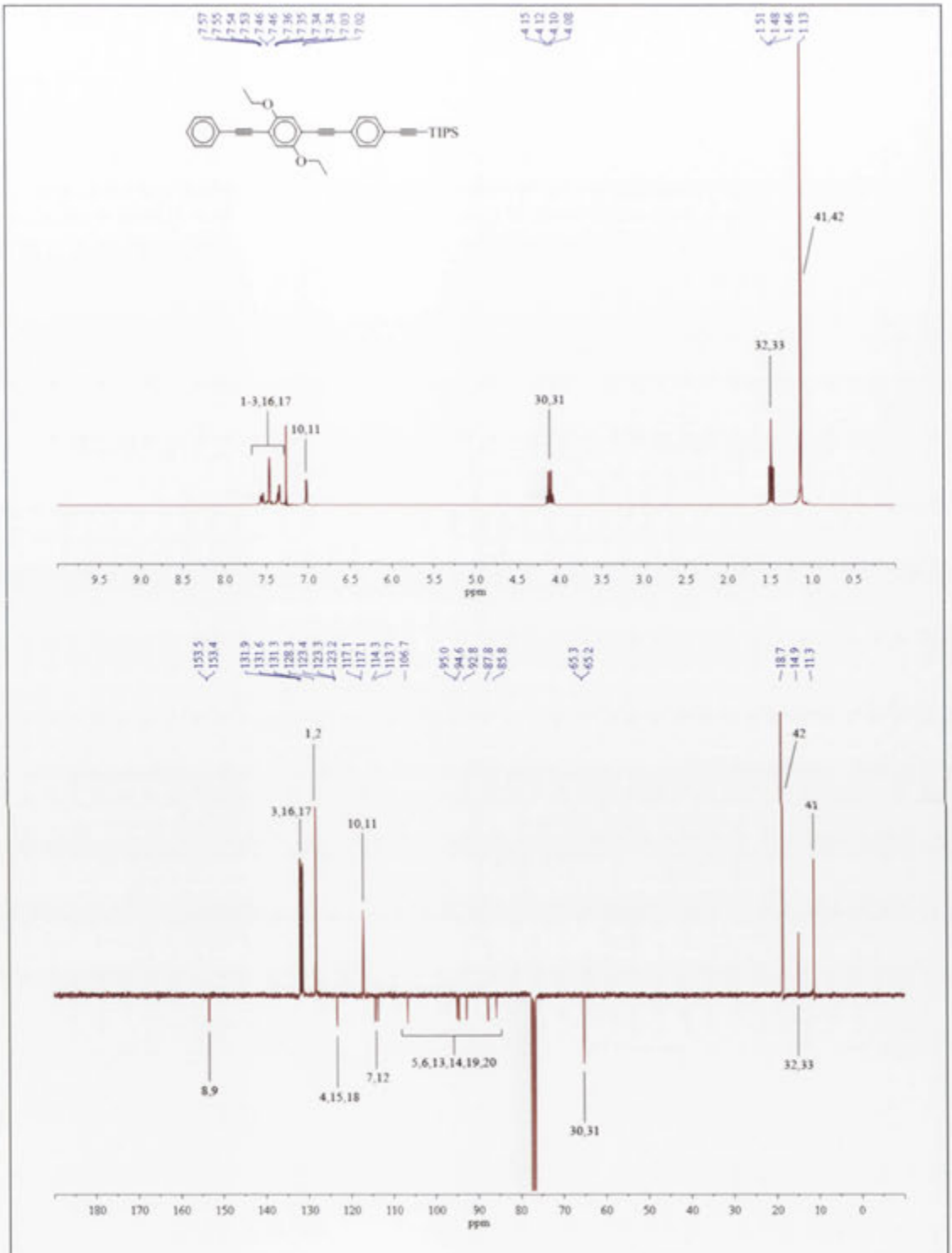


$^{1}H$ (top) and $^{13}C$ (bottom) spectra for compound **57**.

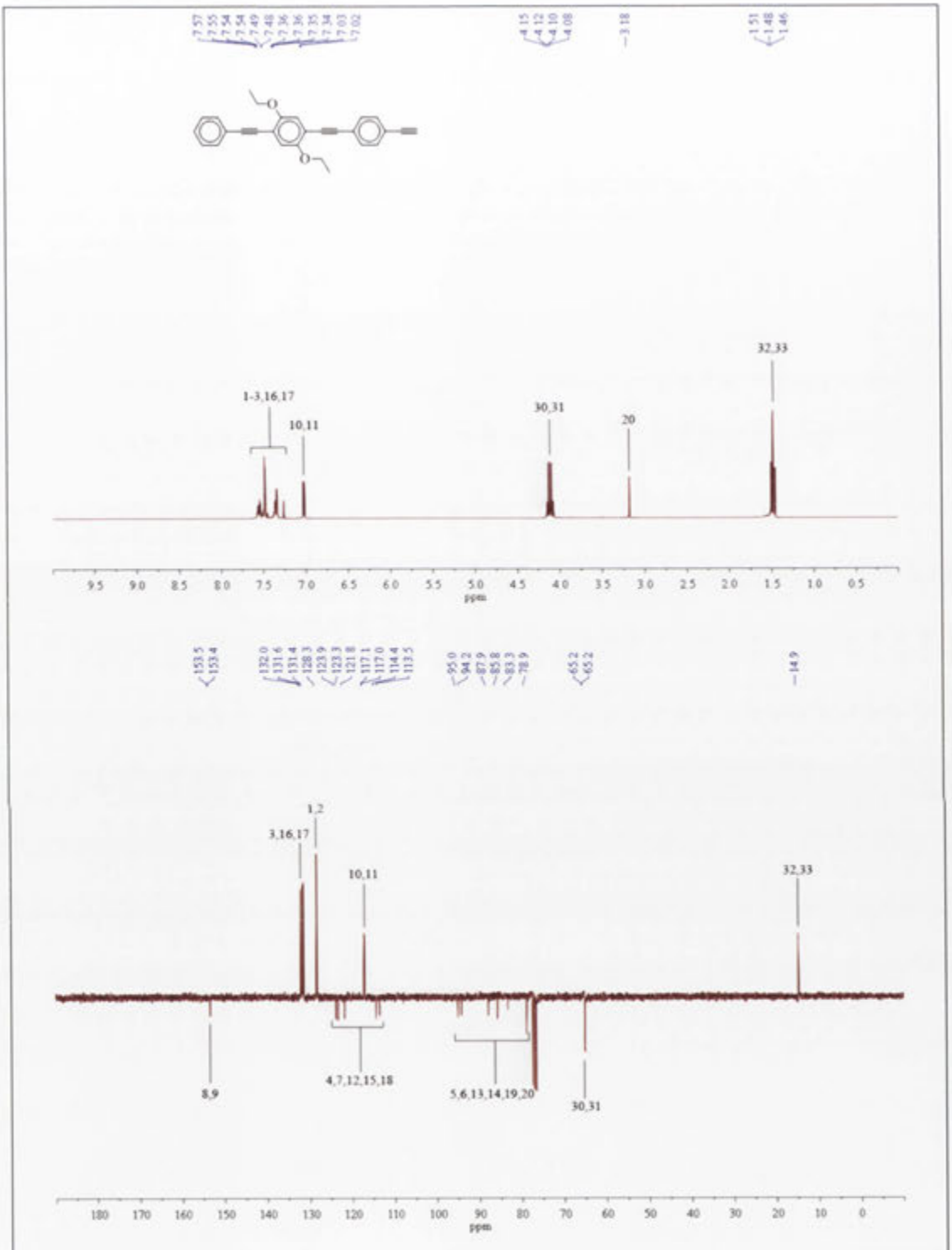


$^{1}H$ (top) and $^{13}C$ (bottom) spectra for compound **58**.

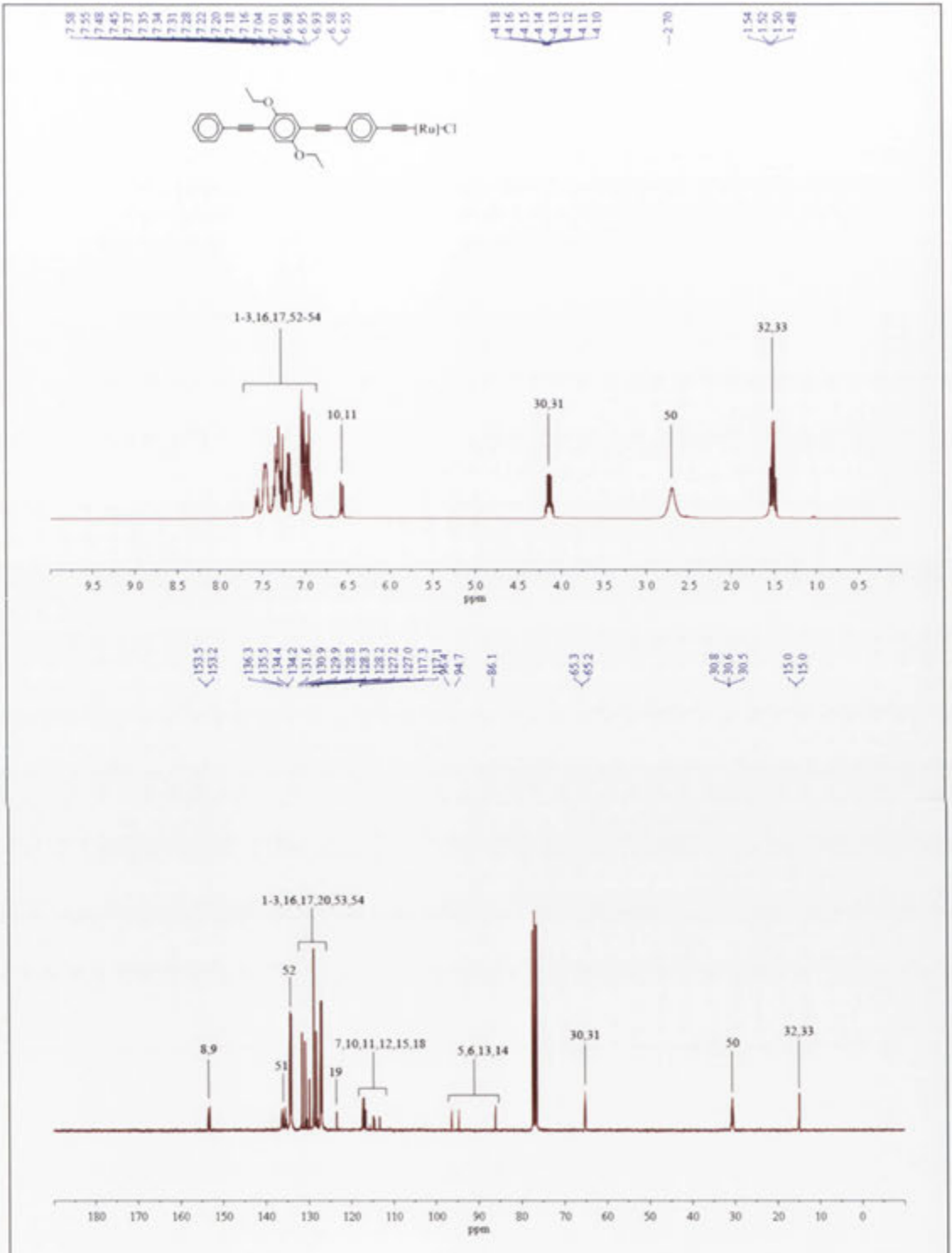


$^{1}H$ (top) and $^{13}C$ (bottom) spectra for compound **67**.

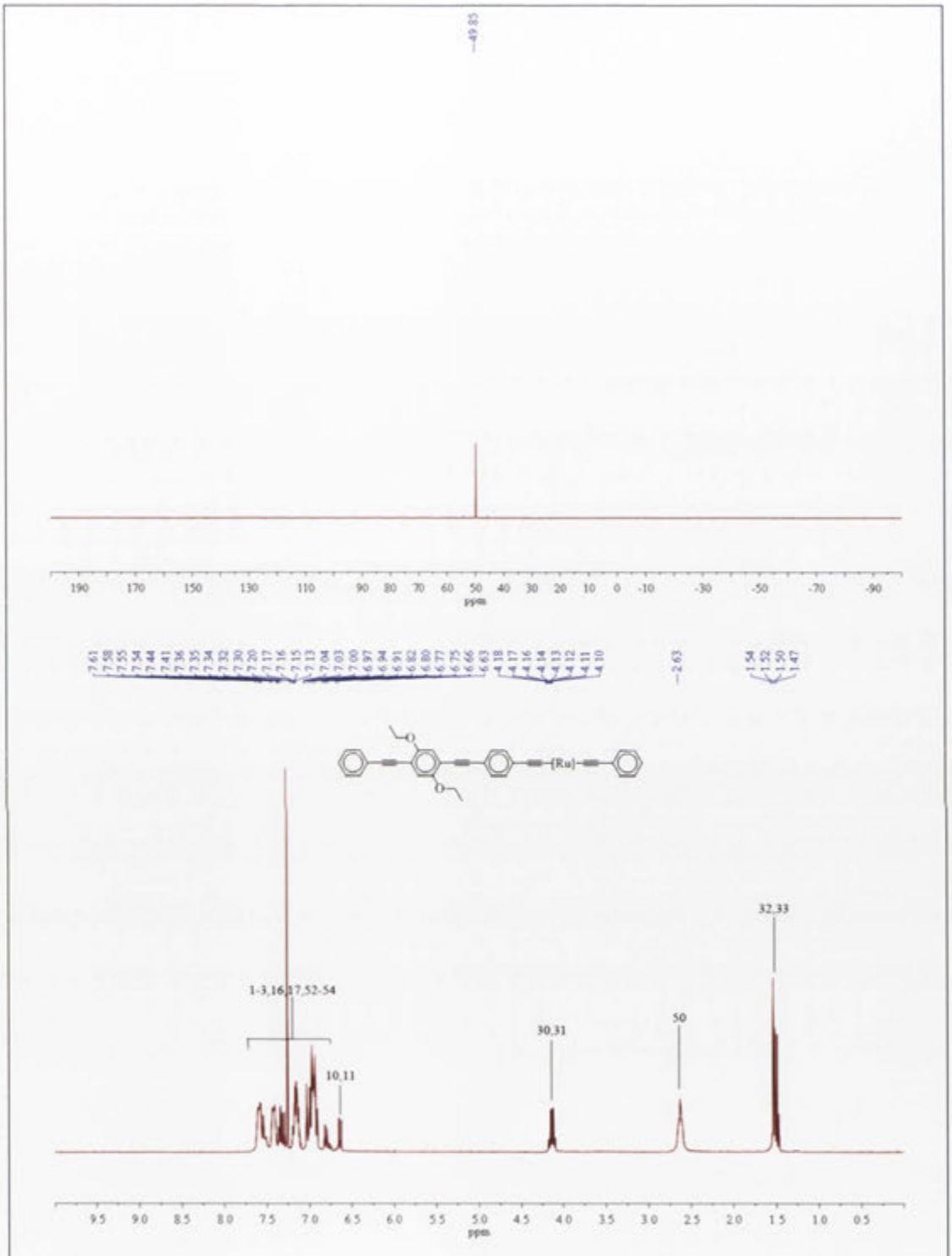


$^{31}P$ spectrum for compound **67** (top) and $^{1}H$ spectrum for compound **68** (bottom).

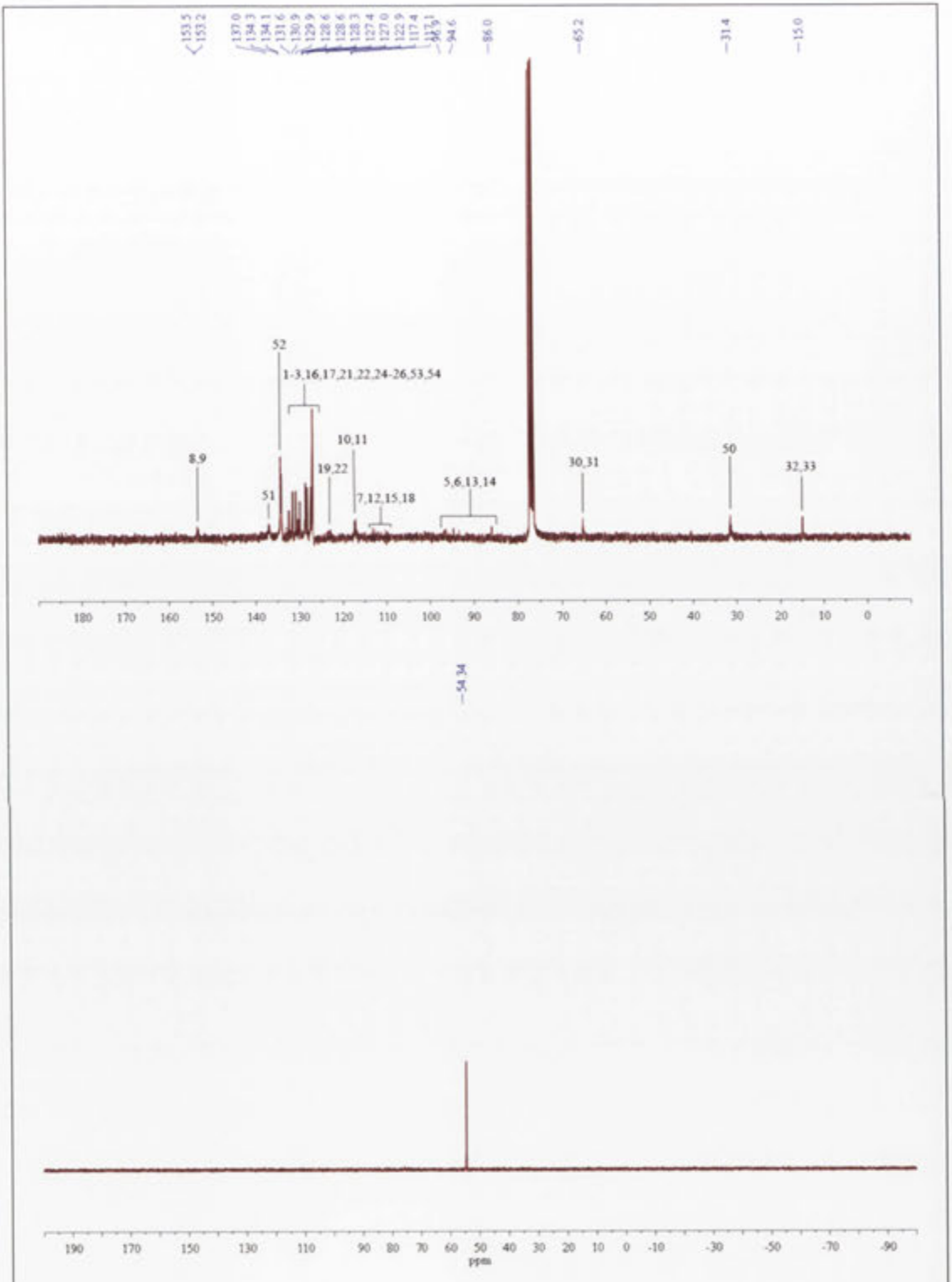


$^{13}C$ (top) and $^{31}P$ (bottom) spectra for compound **68**.

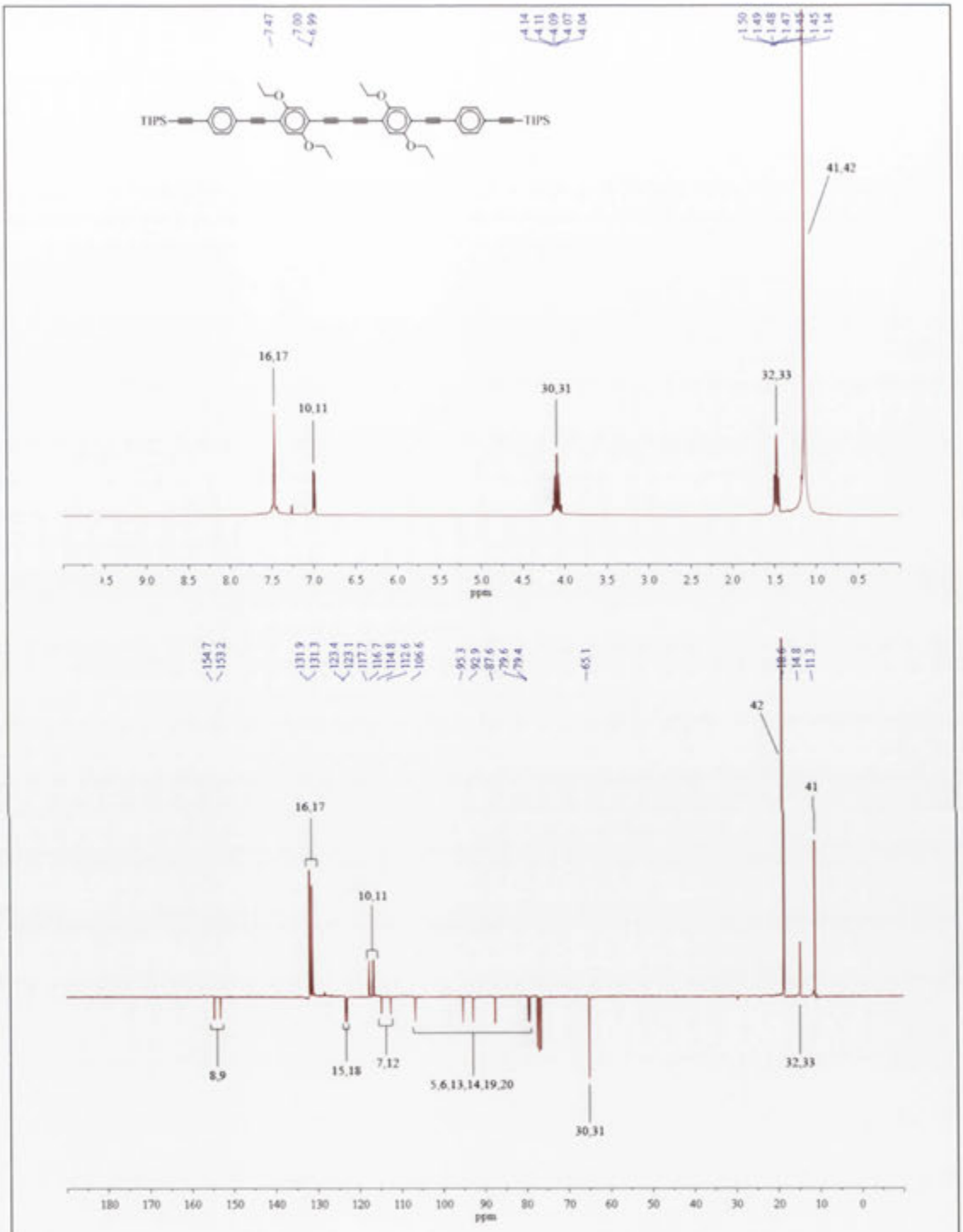


$^{1}H$ (top) and $^{13}C$ (bottom) spectra for compound **59**.

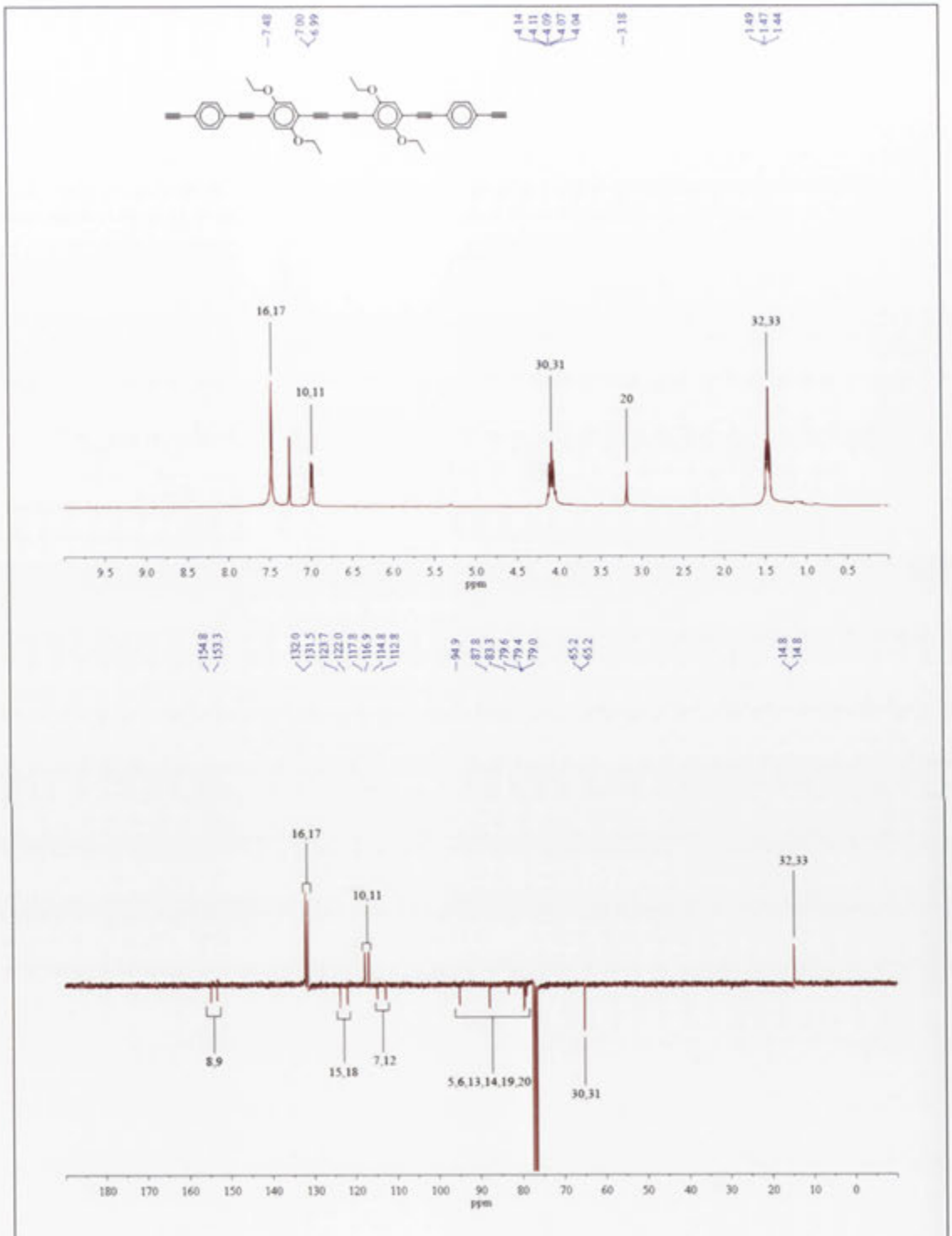


$^{1}H$ (top) and $^{13}C$ (bottom) spectra for compound **60**.

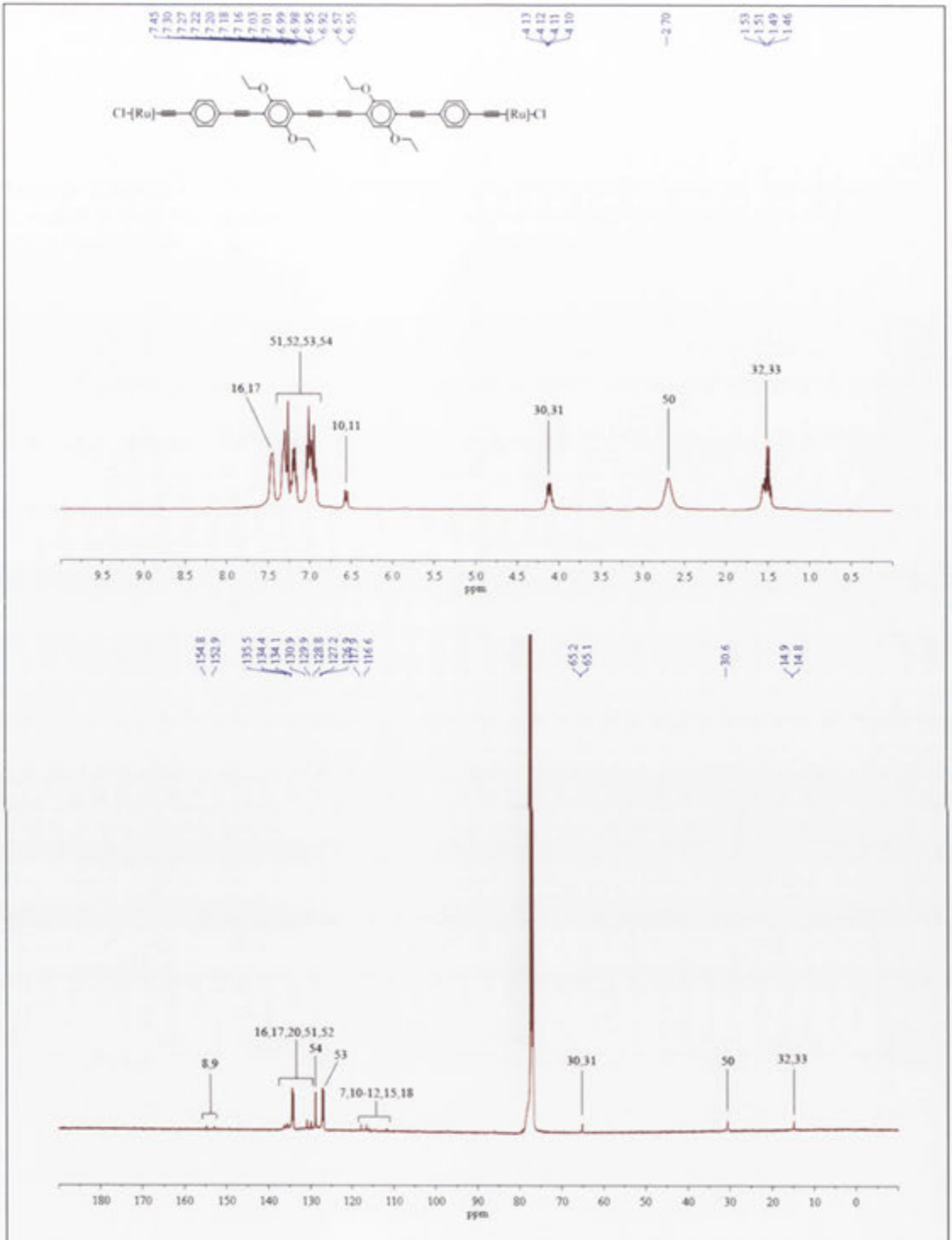


$^{1}H$ (top) and $^{13}C$ (bottom) spectra for compound **69**.

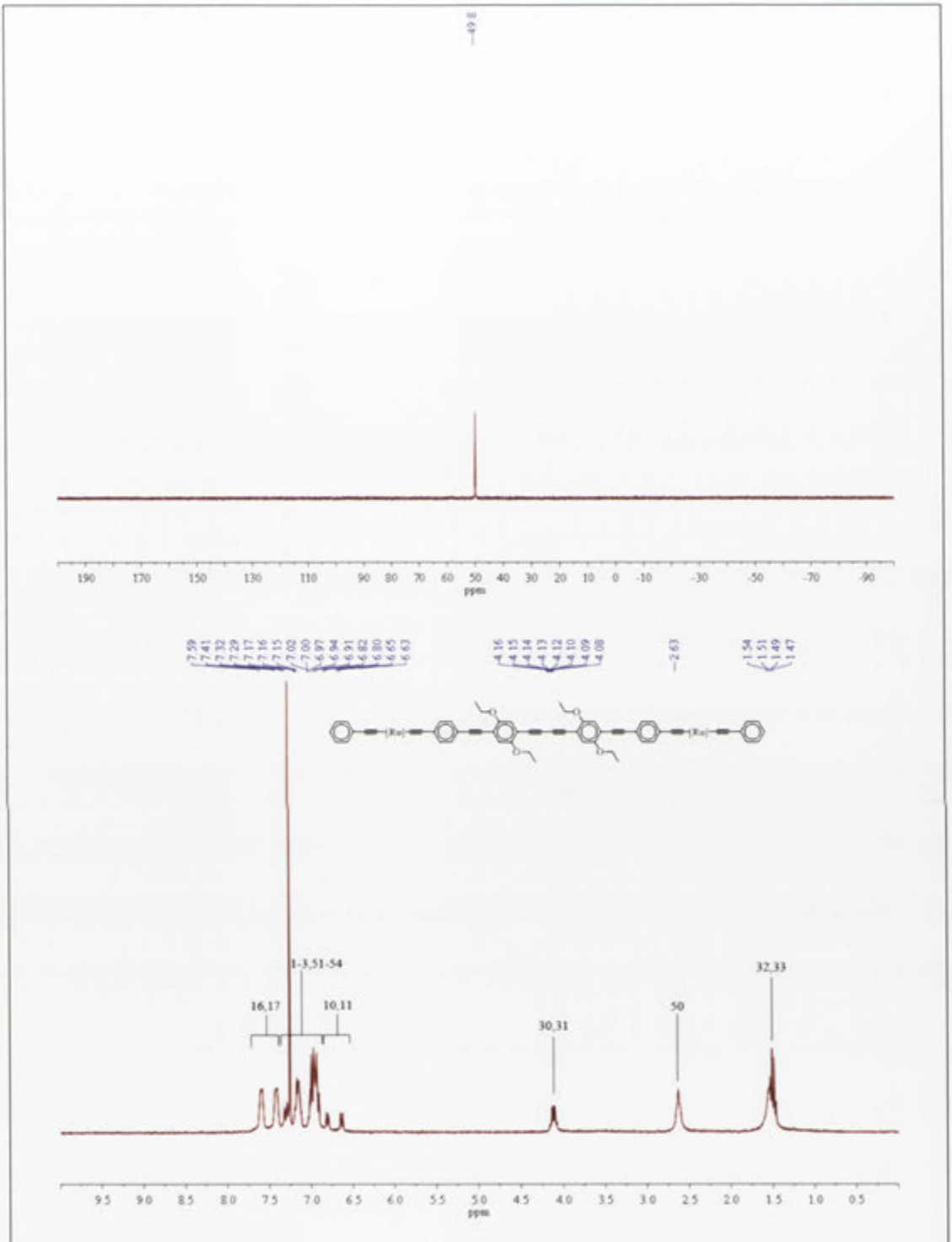


$^{31}P$ spectrum for compound **69** (top) and $^{1}H$ spectrum for compound **70** (bottom).

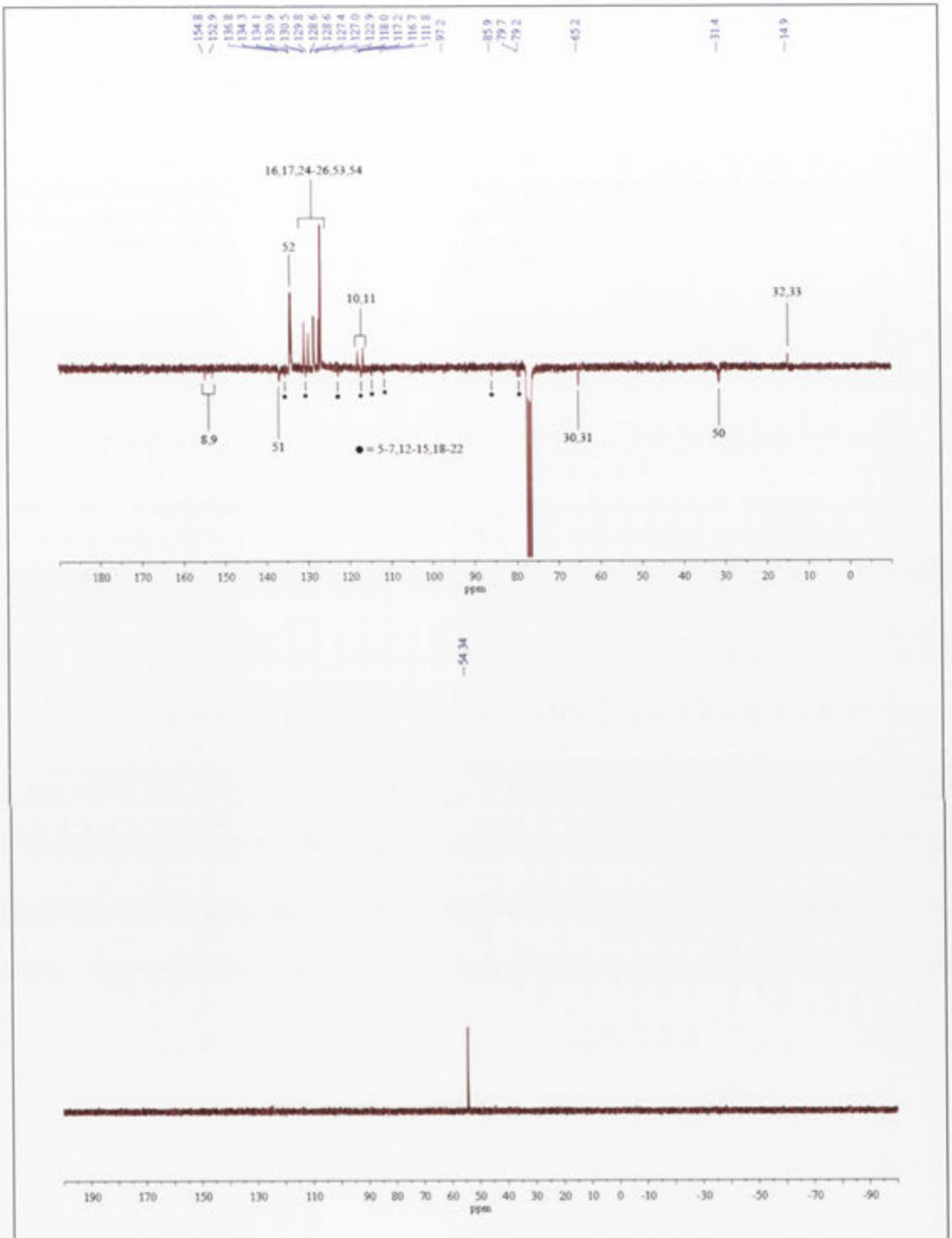


$^{13}C$ (top) and $^{31}P$ (bottom) spectra for compound **70**.

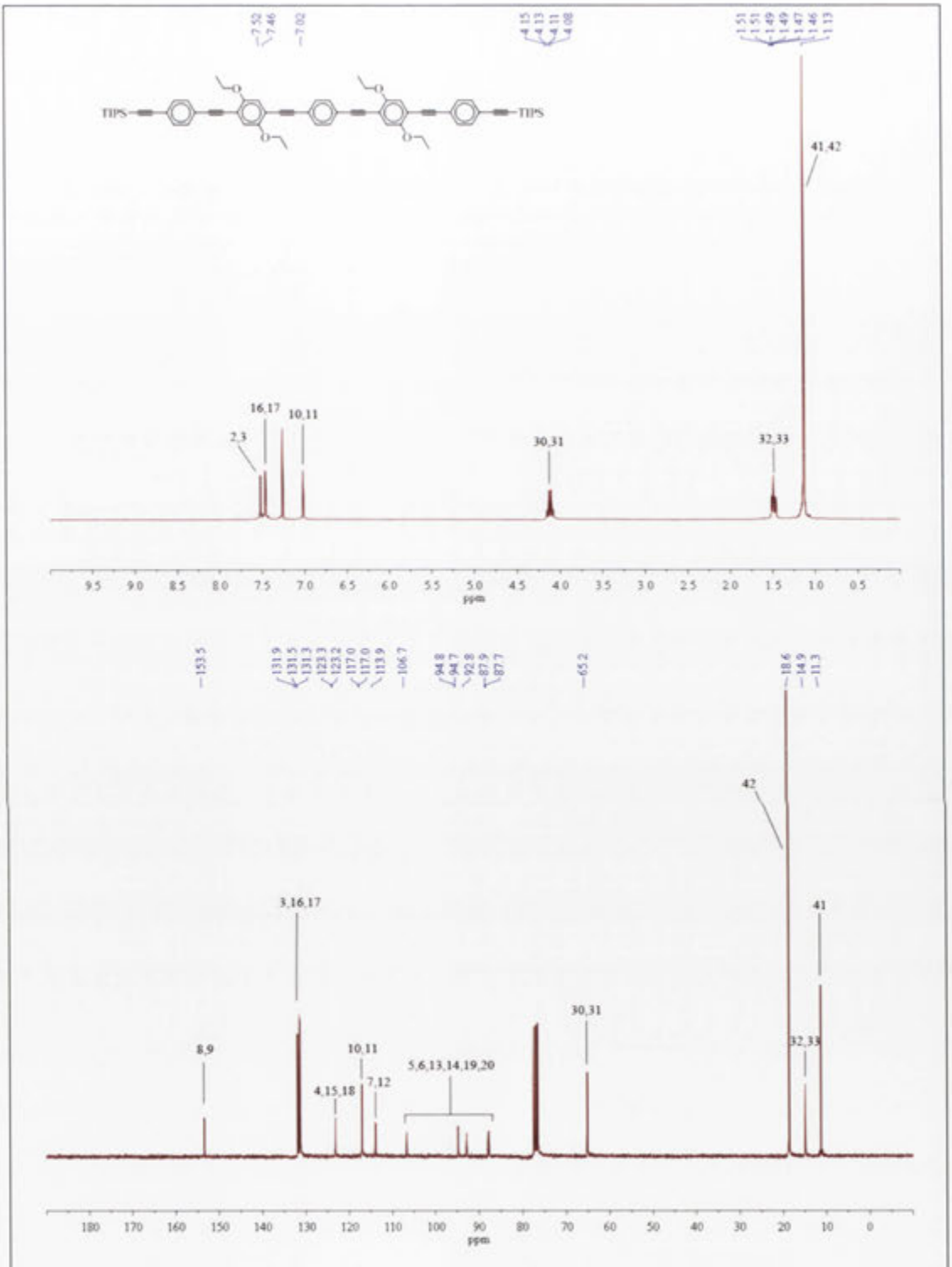


$^{1}H$ (top) and $^{13}C$ (bottom) spectra for compound **61**.

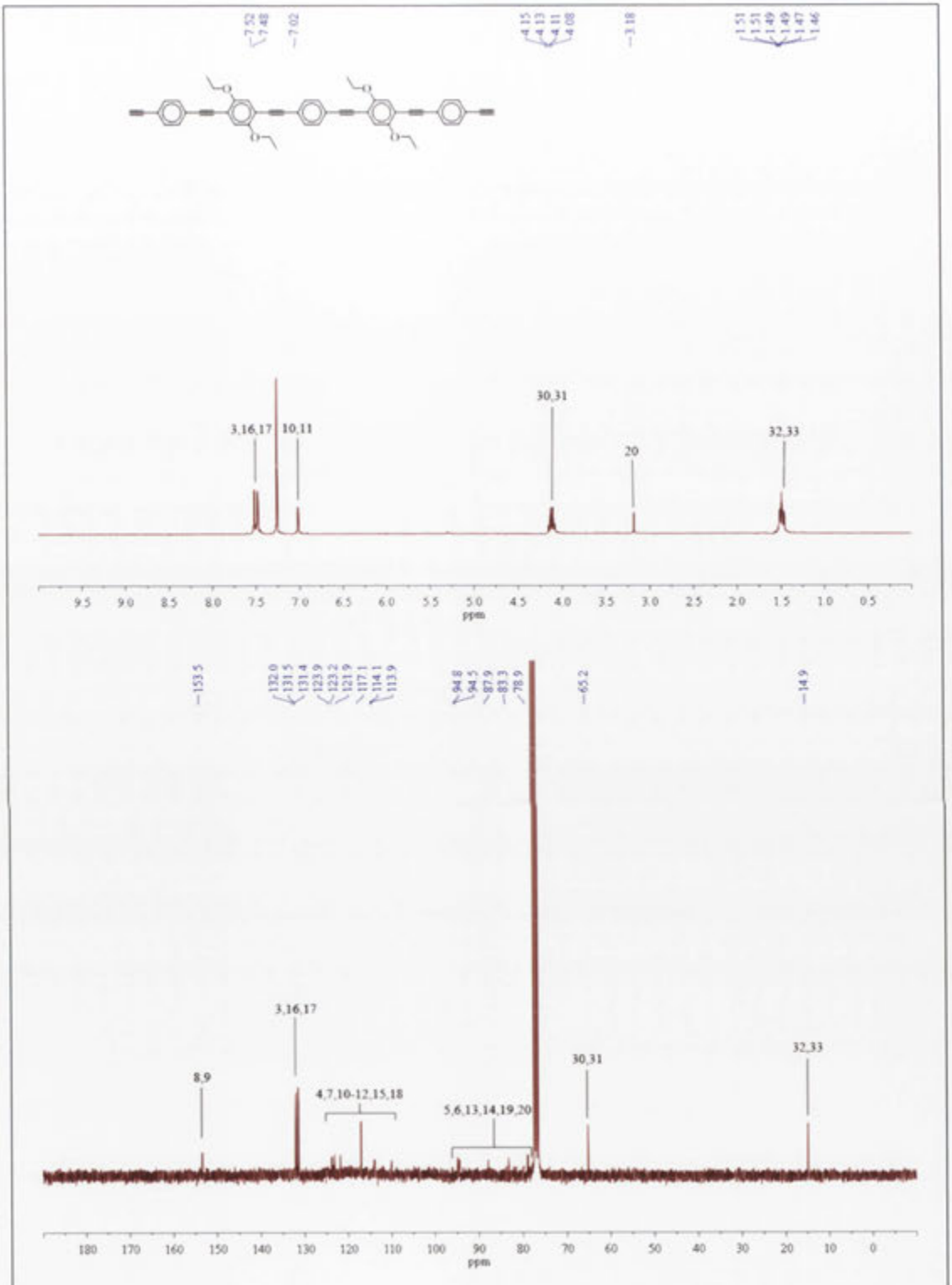


$^{1}H$ (top) and $^{13}C$ (bottom) spectra for compound **62**.

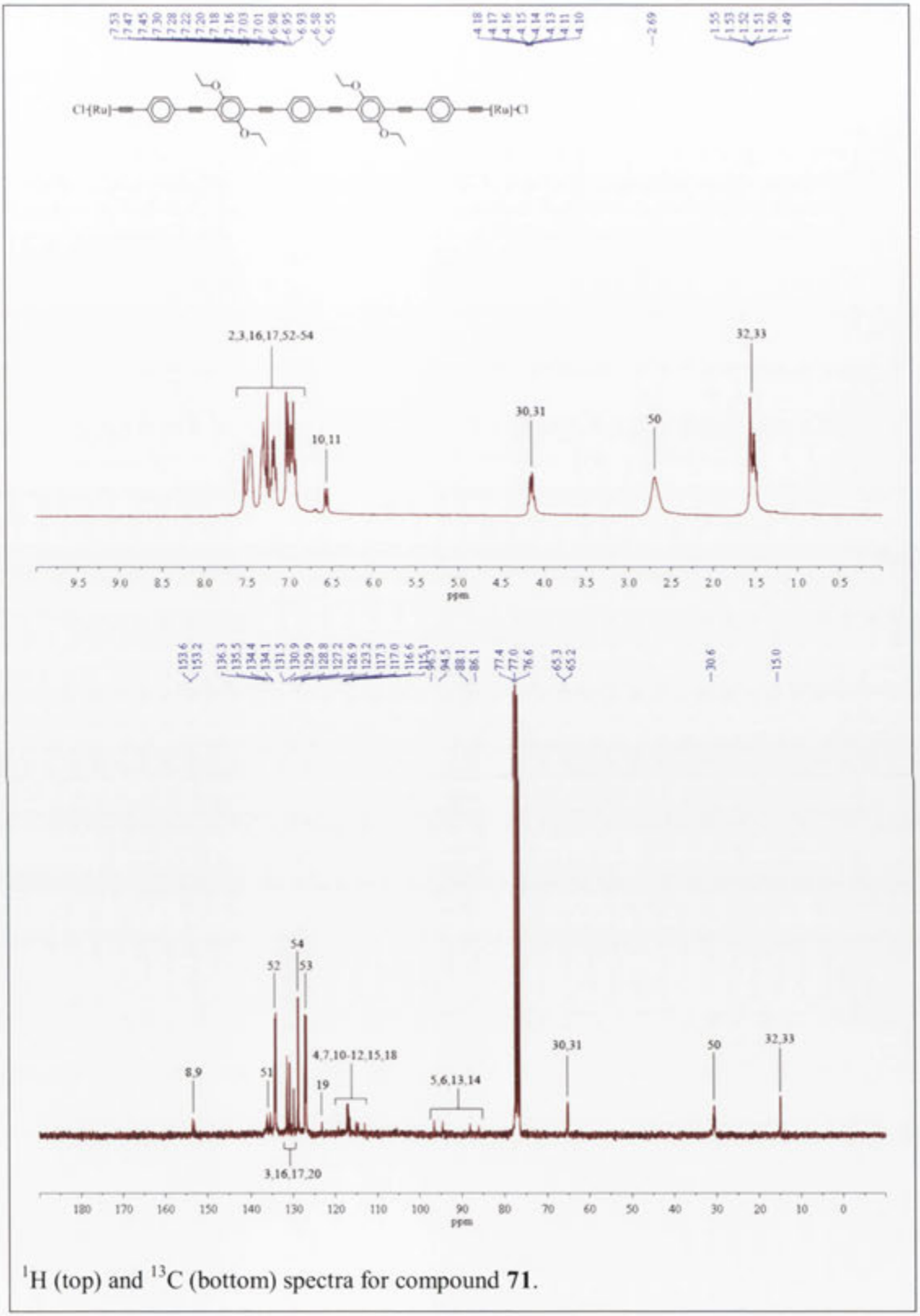


$^{1}H$ (top) and $^{13}C$ (bottom) spectra for compound **71**.

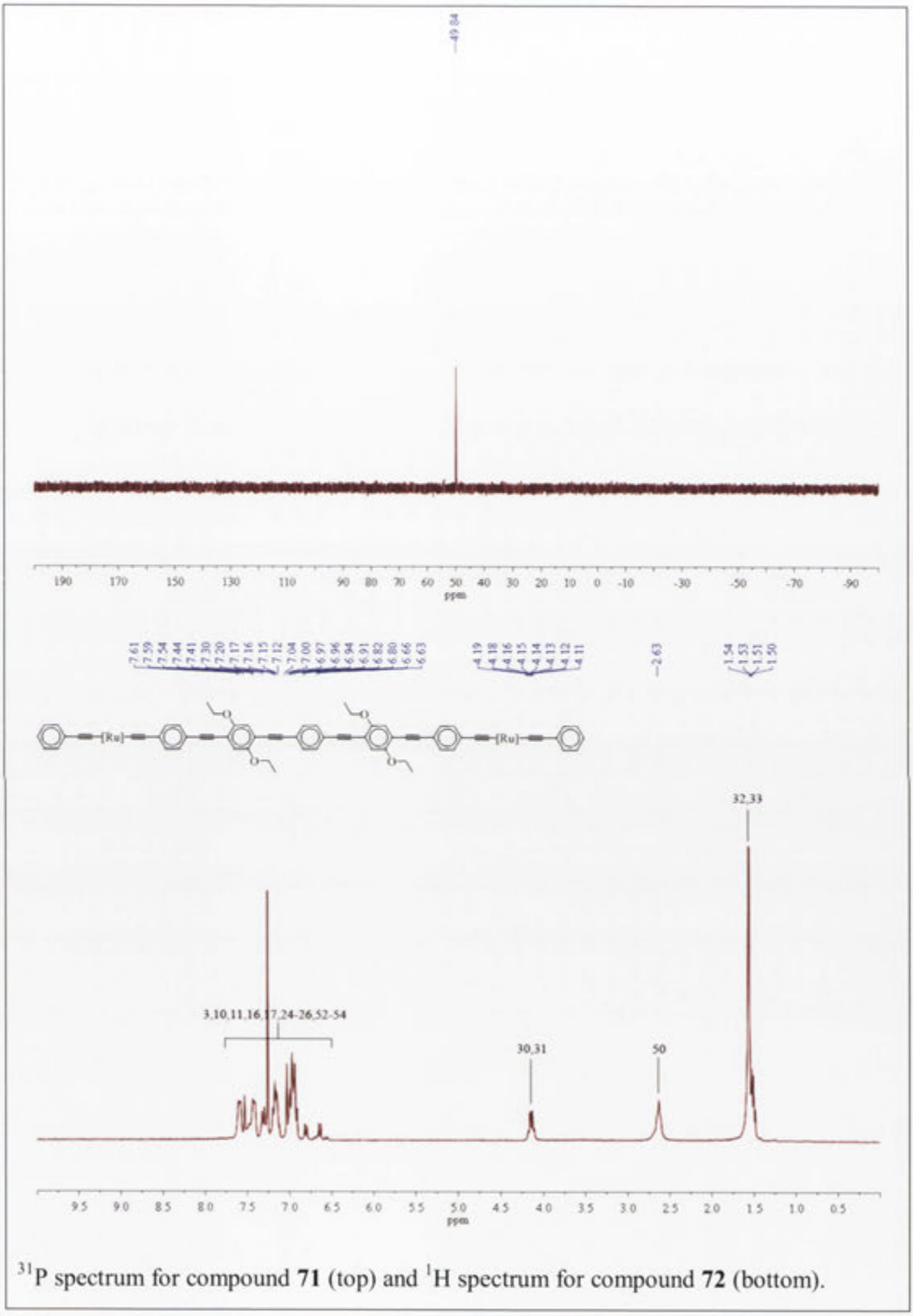


$^{31}$P spectrum for compound **71** (top) and $^{1}$H spectrum for compound **72** (bottom).

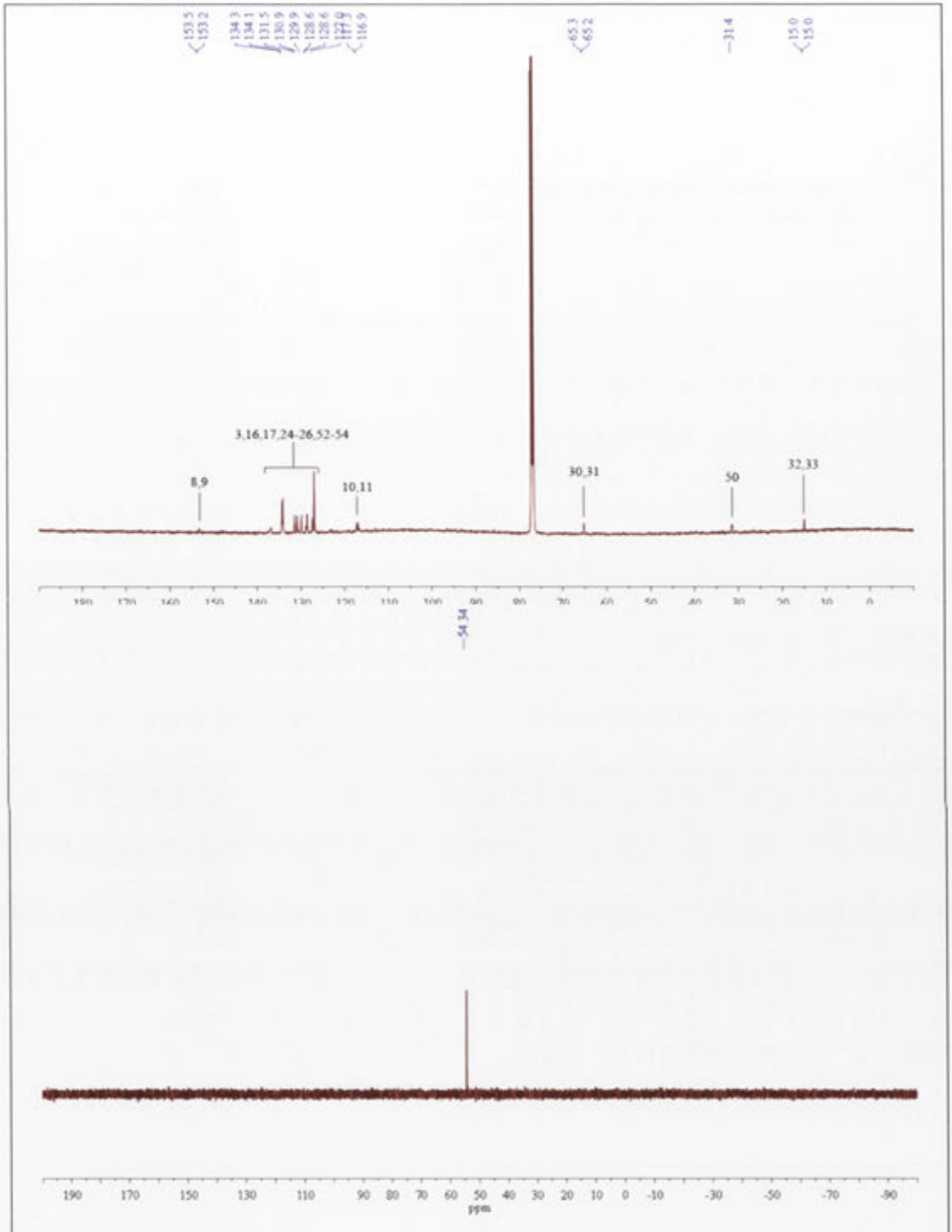


$^{13}C$ (top) and $^{31}P$ (bottom) spectra for compound **72**.

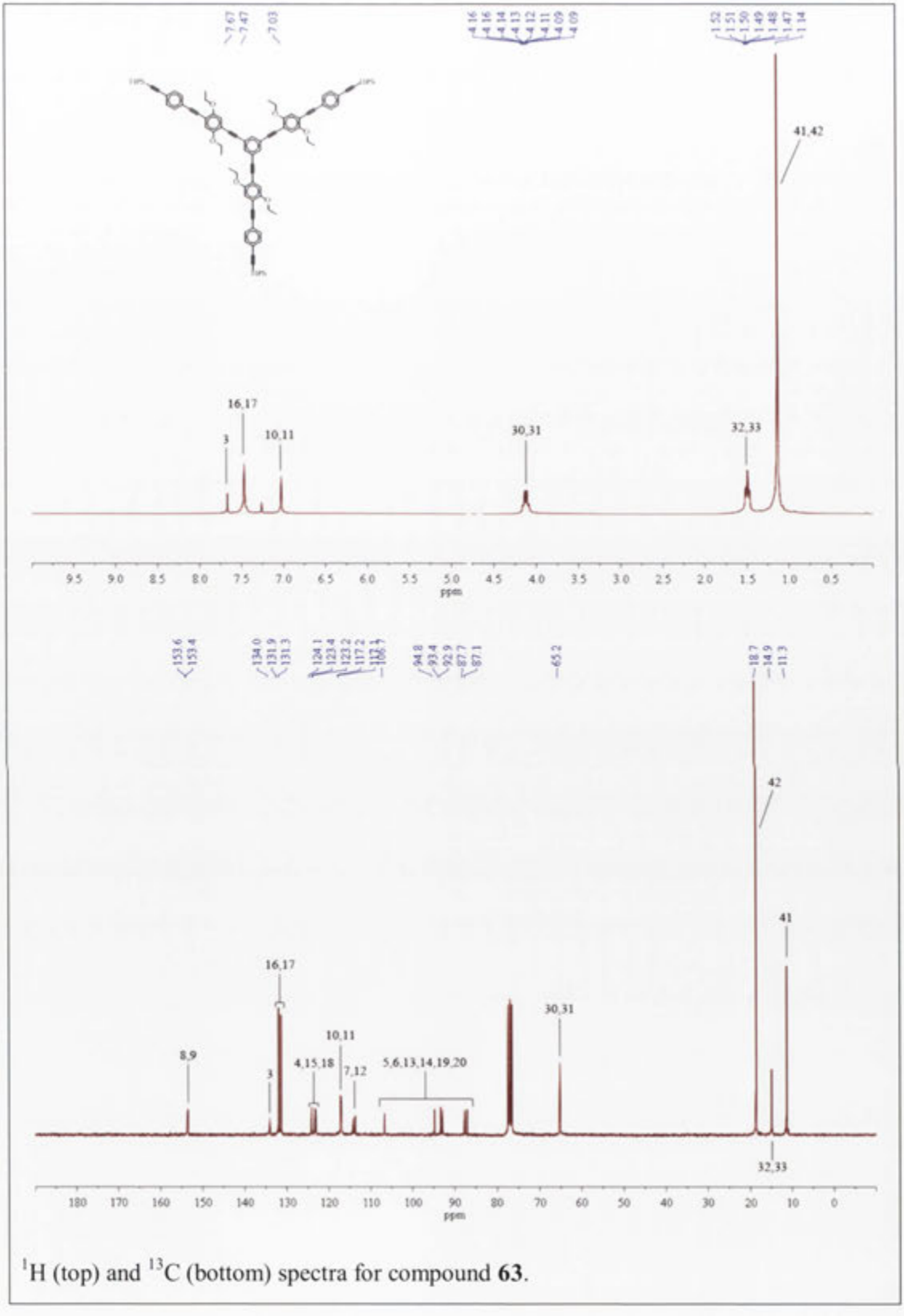


$^{1}H$ (top) and $^{13}C$ (bottom) spectra for compound **63**.

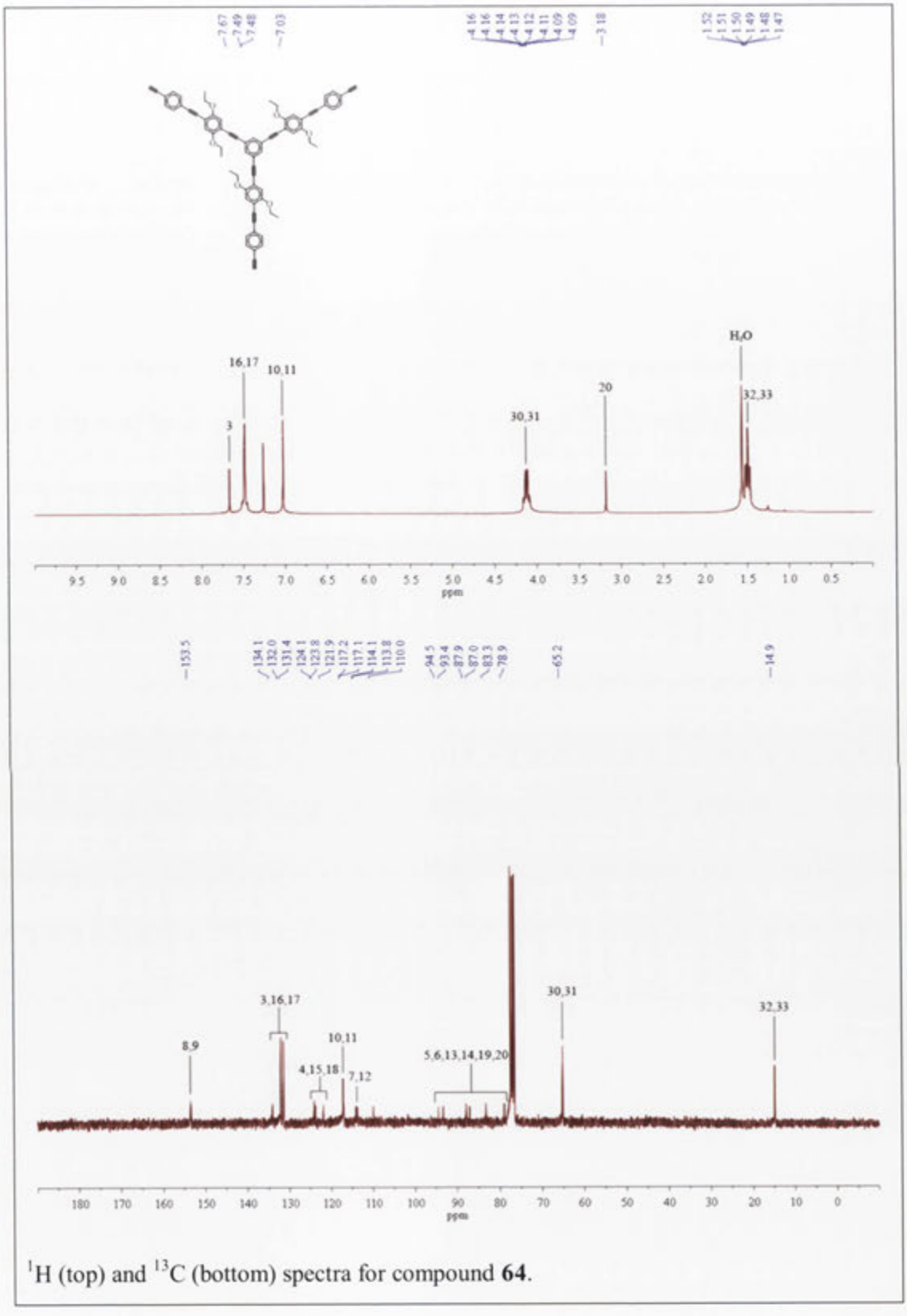


$^{1}H$ (top) and $^{13}C$ (bottom) spectra for compound **64**.

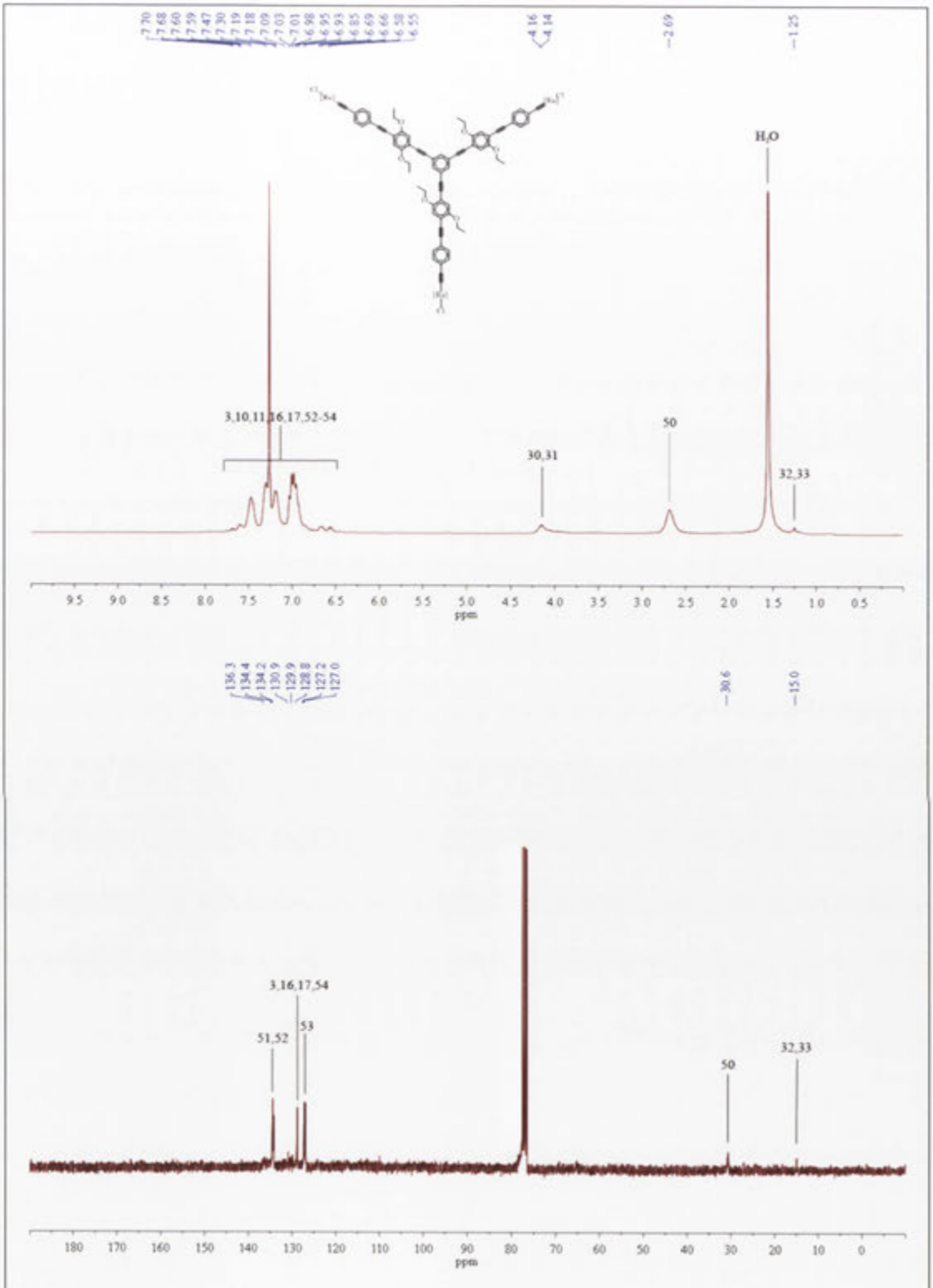


$^{1}H$ (top) and $^{13}C$ (bottom) spectra for compound **73**.

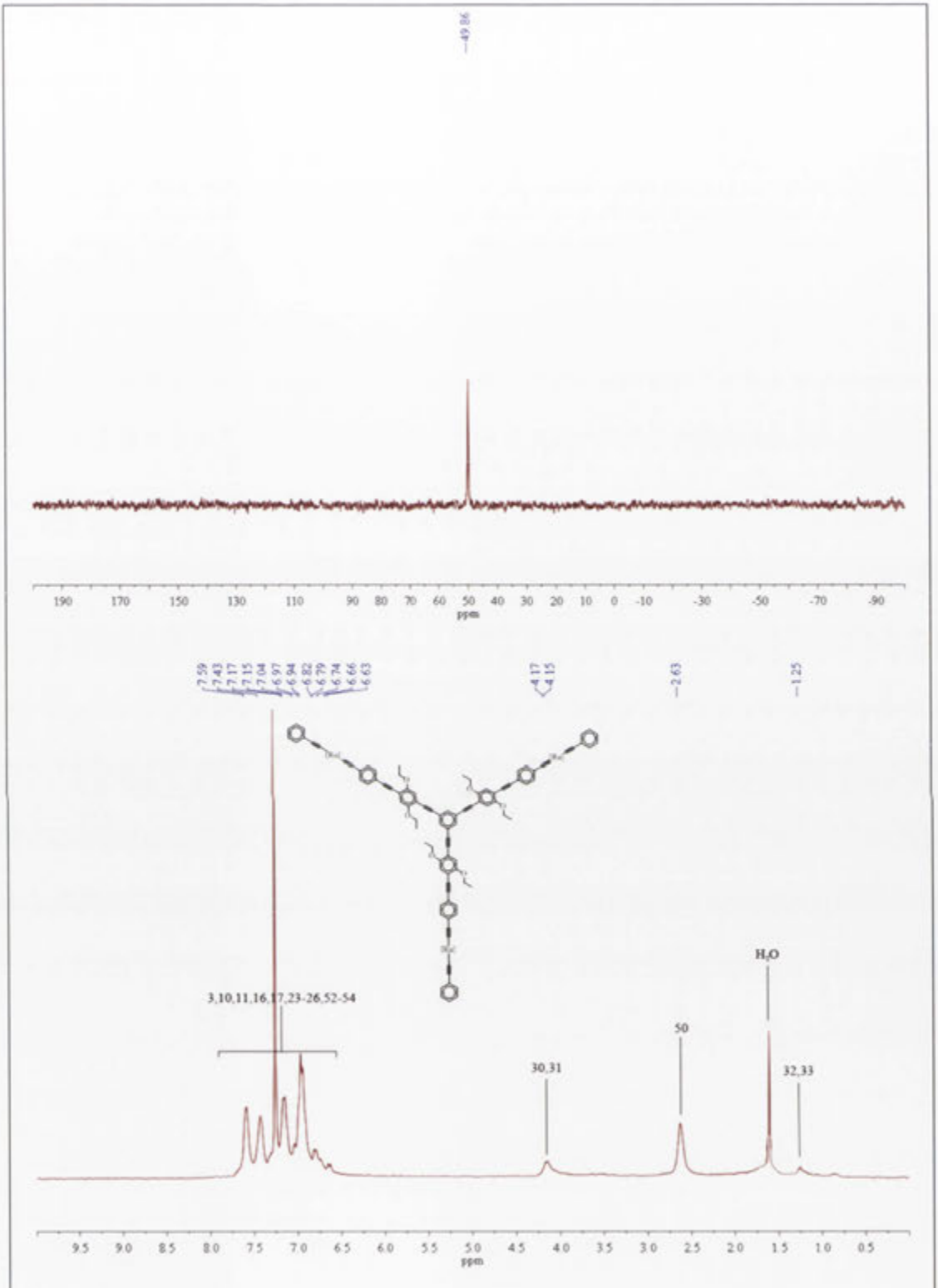


$^{31}P$ spectrum for compound **73** (top) and $^{1}H$ spectrum for compound **74** (bottom).

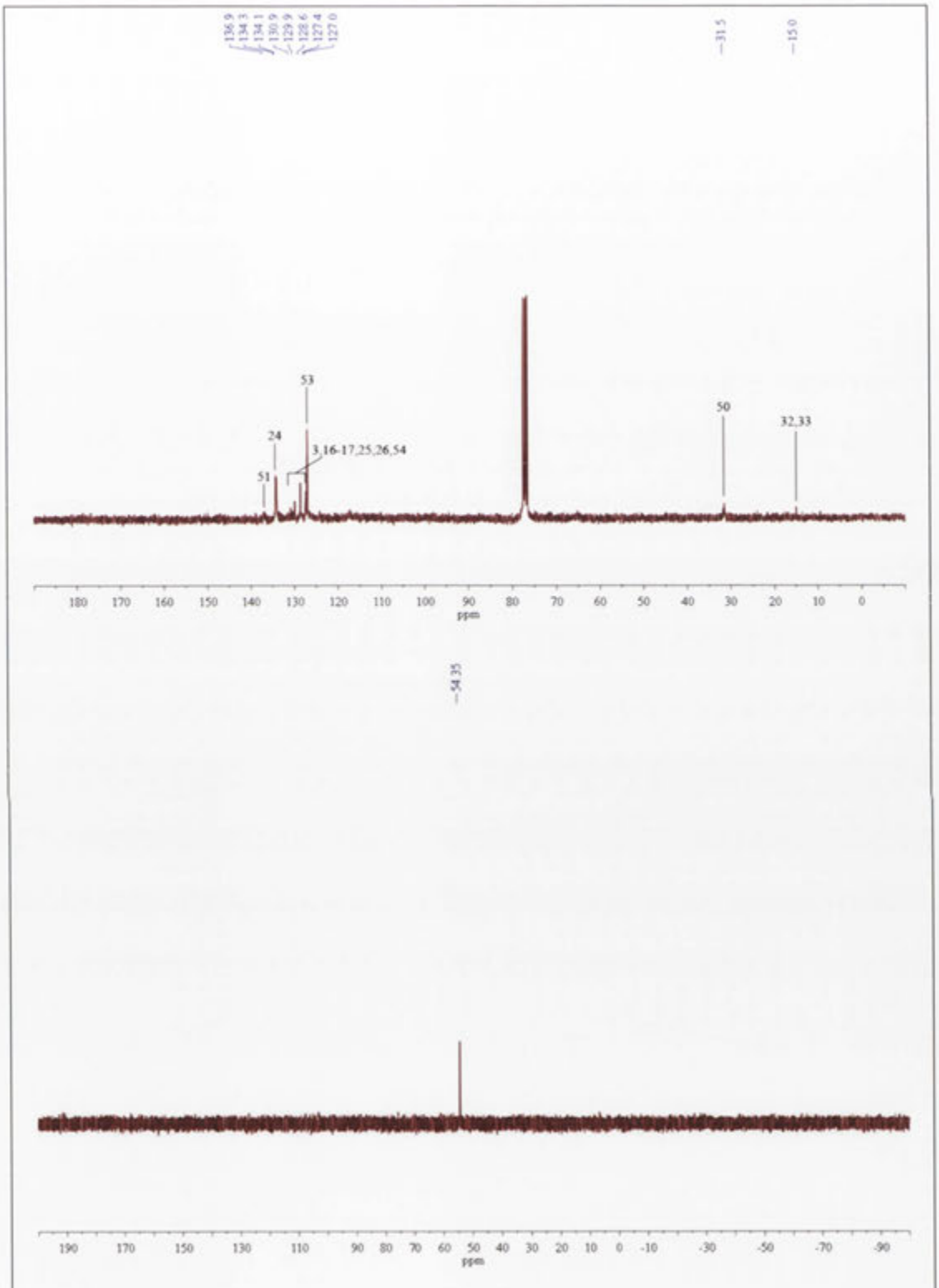


$^{13}C$ (top) and $^{31}P$ (bottom) spectra for compound **74**.

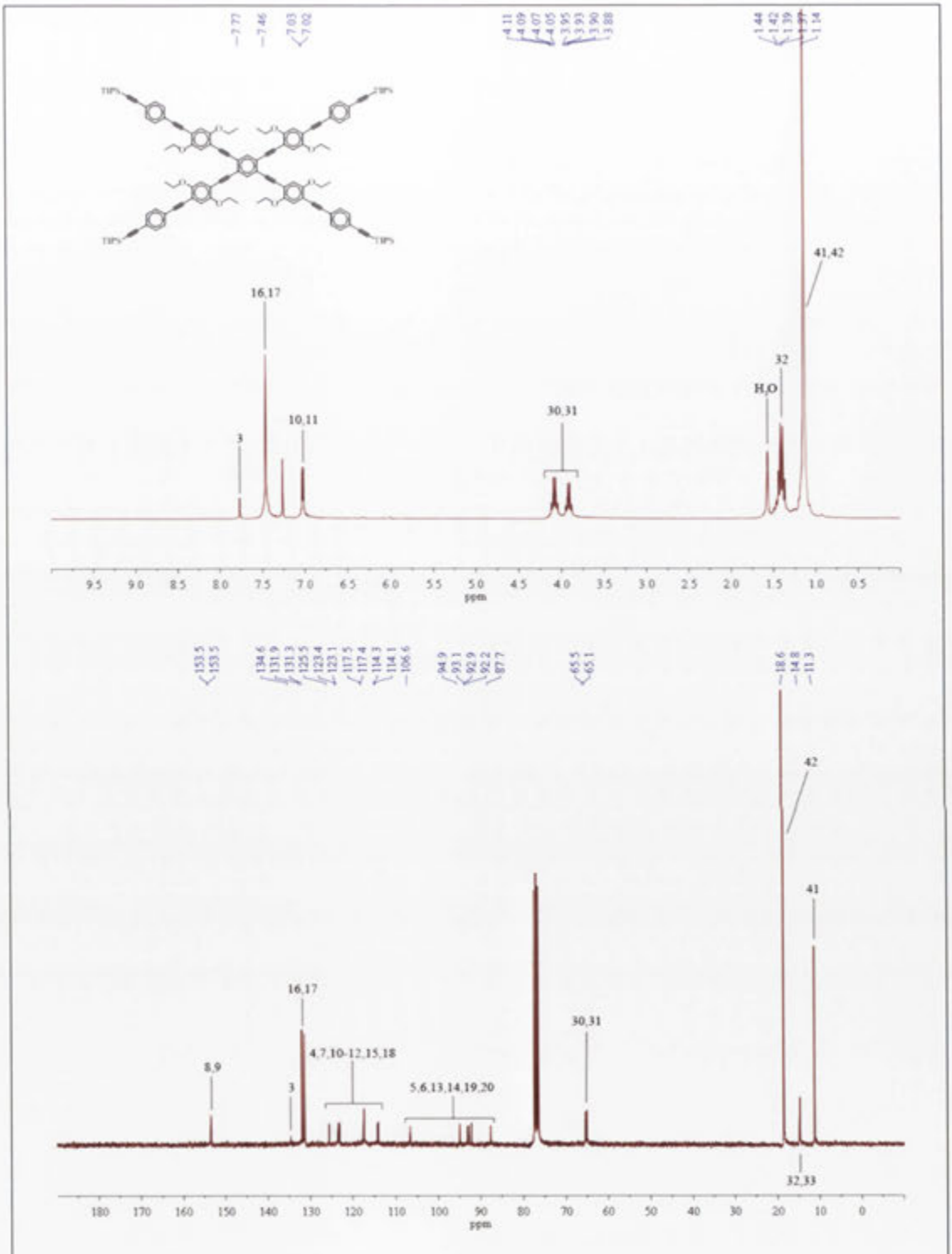


$^{1}H$ (top) and $^{13}C$ (bottom) spectra for compound **65**.

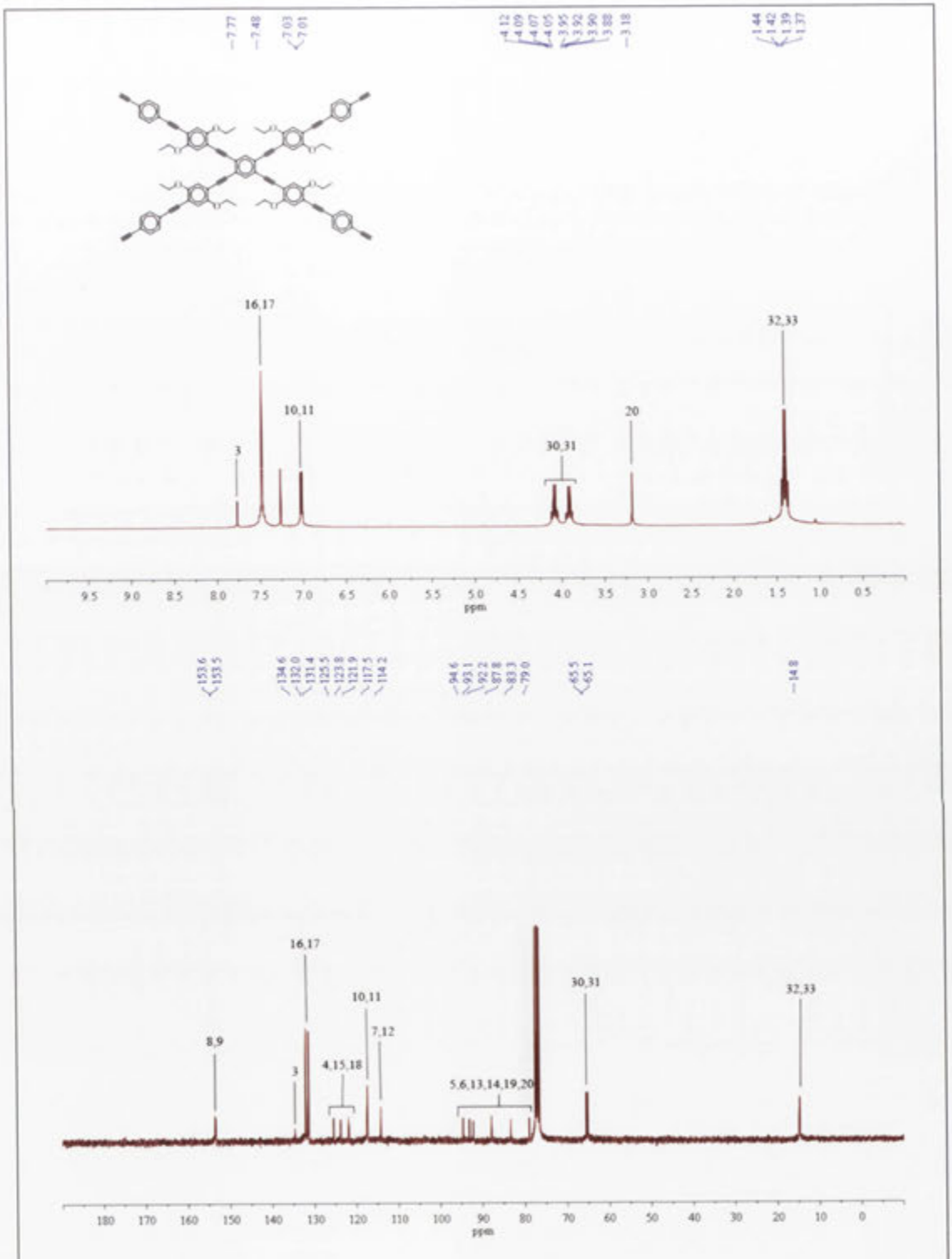


$^{1}H$ (top) and $^{13}C$ (bottom) spectra for compound **66**.

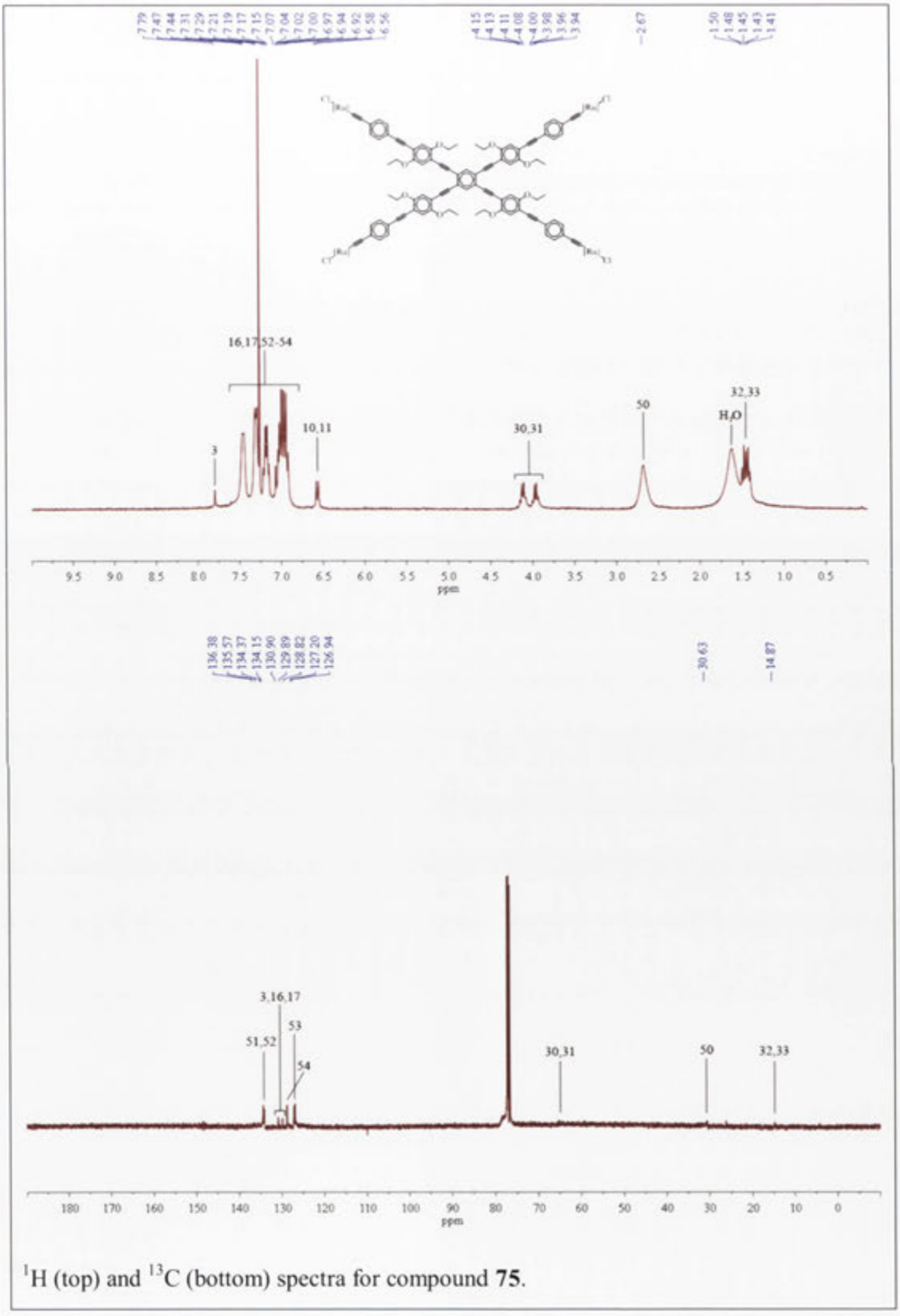


$^{1}H$ (top) and $^{13}C$ (bottom) spectra for compound **75**.

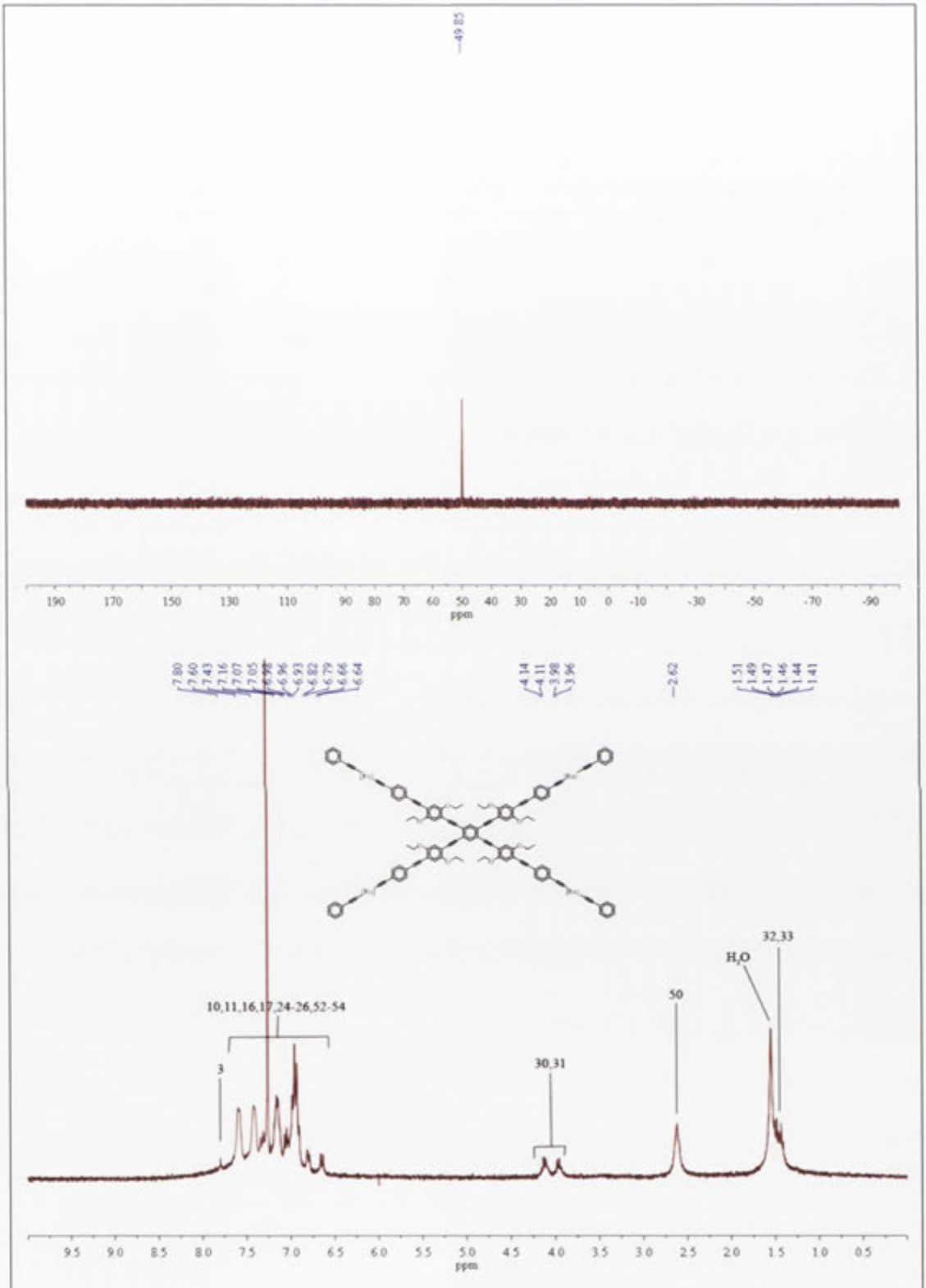


$^{31}$P spectrum for compound **75** (top) and $^{1}$H spectrum for compound **76** (bottom).

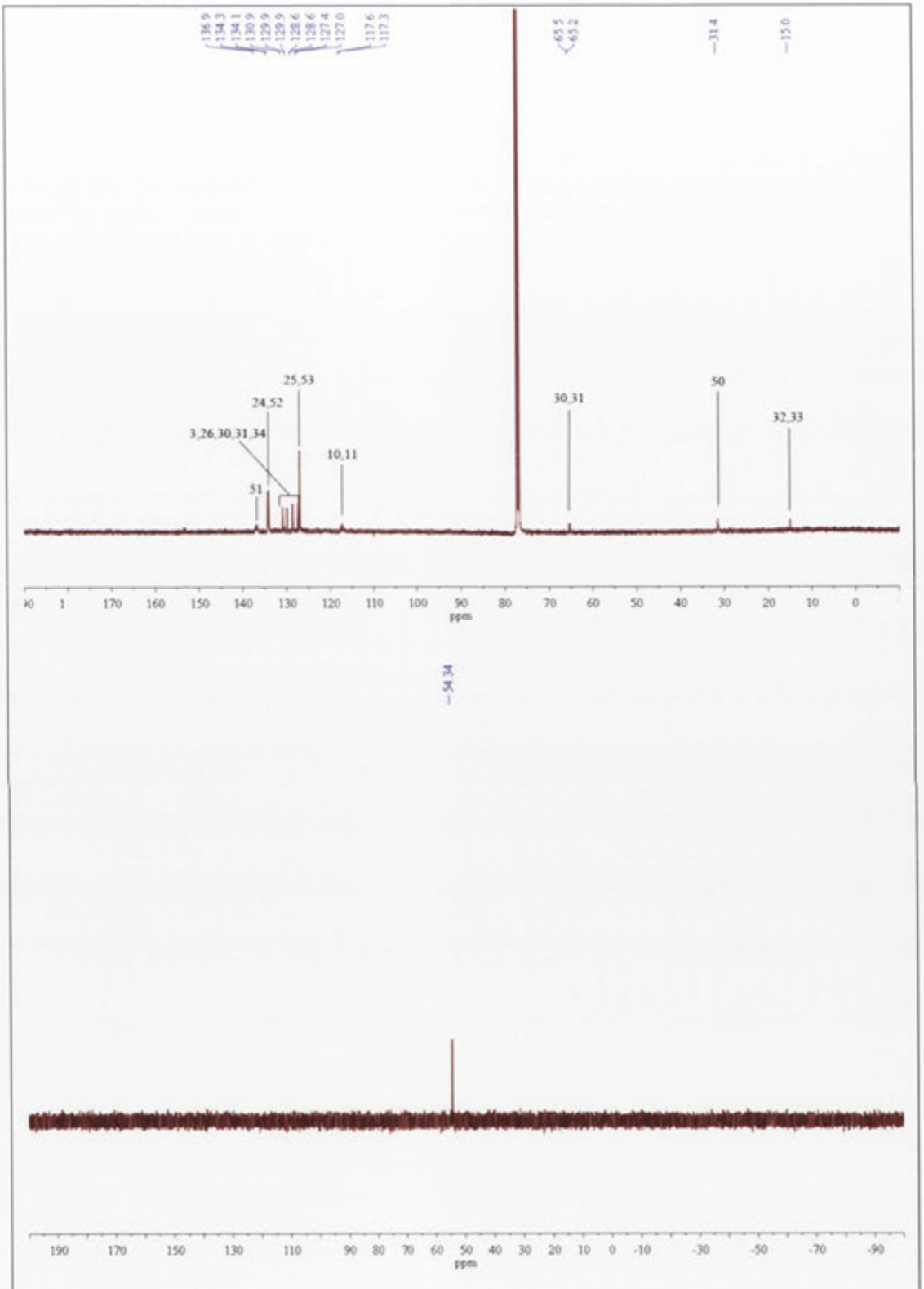


$^{13}C$ (top) and $^{31}P$ (bottom) spectra for compound **76**.

## Published Results

Gauthier, N., Argouarch, G., Paul, F., Ladjarafi, A. K., Costuas, K., Halet, J.-F., Samoc, M., Cifuentes, M. P., Corkery, T. C., Humphrey, M. G., "Electron-rich Iron-Ruthenium Arylalkynyl Complexes for Third-Order Nonlinear Optics. Redox-switching Between Three States", *In Preparation*

Corkery, T. C., Chavan, S. S., Hurst, S. K., Cifuentes, M. P., Samoc, M., van Cleuvenbergen, S., Asselberghs, I., Clays, K., Humphrey, M. G., "Electrochemical, Linear Optical and Quadratic and Cubic Nonlinear Optical Properties of Arylalkynylruthenium-containing Organometallic Wedges and C-C Coupling Derivatives", *In Preparation*

Chi, Z.; Tsuyoshi, M.; Samoc, M.; Suci, M.; Corkery, T. C.; Petrie, S.; Stranger, R.; Jiafang, Z.; Humphrey, M. G.Kazuyuki, T. "Dodecanuclear Ellipse and Decanuclear Wheel Nickel(II) Thiolato Clusters with Efficient fs Nonlinear Absorption" *Angewandte Chemie International Edition*, **2010**, 42, 4209-4212

Jeffery, C. J.; Cifuentes, M. P.; Dalton, G. T.; Corkery, T. C.; Randles, M. D.; Willis, A. C.; Samoc, M.; Humphrey, M. G. "Synthesis and Cubic Optical Nonlinearity of a Stilbenylethynylruthenium Dendrimer" *Macromolecular Rapid Communications*, **2010**, 31, 846-849

Green, K.; Corkery, T. C.; Cifuentes, M. P.; Humphrey, M. G.; Samoc, M. "Various Mechanisms of Controlling Optical Nonlinearity in Organometallics: Wide Wavelength Range Studies" *Nonlinear Optics and Quantum Optics*, **2010**, 40, 235-240

Green, K. A.; Cifuentes, M. P.; Corkery, T. C.; Samoc, M.; Humphrey, M. G. "Switching the Cubic Nonlinear Optical Properties of an Electro-, Halo-, and Photochromic Ruthenium Alkynyl Complex Across Six States" *Angewandte Chemie*, **2009**, 48, 7867-7870

Humphrey, M. G.; Green, K. A.; Cifuentes, M. P.; Corkery, T. C.; Samoc, M. "Metal Alkynyl-Based Nonlinear Optical Switches" *Polymer Preprints*, **2009**

Babgi, B.; Rigamonti, L.; Cifuientes, M. P.; Corkery, T. C.; Randles, M. D.; Schwich, T.; Petrie, S.; Stranger, R.; Teshome, A.; Asselberghs, I.; Clays, K.; Samoc, M.; Humphrey, M. G. "Length-Dependent Convergence and Saturation Behavior of

Electrochemical, Linear Optical, Quadratic Nonlinear Optical and Cubic Nonlinear Optical Properties of Dipolar Alkynylruthenium Complexes with Oligo(phenyleneethynylene) Bridges" *Journal of the American Chemical Society*, **2009**, 131, 10293-10307

Ge, Q.; Corkery, T. C.; Humphrey, M. G.; Samoc, M.; Hor, T. S. A. "Organobimetallic $Ru^{II}$-$Re^{I}$ 4-ethynylpyridyl complexes: structures and non-linear optical properties" *Dalton Transactions*, **2009**, 6192-6200

Roberts, R. L.; Schwich, T.; Corkery, T. C.; Cifuentes, M. P.; Green, K. A.; Farmer, J. D.; Low, P. J.; Marder, T. B.; Samoc, M.; Humphrey, M. G. "Organometallic Complexes for Nonlinear Optics. 45. Dispersion of the Third-Order Nonlinear Optical Properties of Triphenylamine-Cored Alkynylruthenium Dendrimers" *Advanced Materials*, **2009**, 21, 2318-2322

# References

(1) Feynman, R. P. *Engineering and Science* **1960**, 22.

(2) Morrall, J. P., Dalton, G. T., Humphrey, M. G., Samoc, M. *Adv. Organomet. Chem.* **2008**, *55*, 61.

(3) Lehn, J.-M. *Supramolecular Chemistry - Concepts and Perspectives*; V. C. H.: Weinheim, **1995**.

(4) Whittall, I. R., McDonagh, A. M., Humphrey, M. G., Samoc, M. *Adv. Organomet. Chem.* **1998**, *42*, 291.

(5) Allen, S. D. *New Scientist* **1989**, *July 1*.

(6) Ashwell, G. J., Bloor, D., Eds. *Organic Materials for Nonlinear Optics III*; Royal Society of Chemistry: Cambridge, **1993**.

(7) Chemla, D. S., Zyss, J. Eds. *Nonlinear Optical Properties of Organic Molecules and Crystals I*; Academic Press: Orlando, **1987**.

(8) Chemla, D. S., Zyss, J. Eds. *Nonlinear Optical Properties of Organic Molecules and Crystals II*; Academic Press: Orlando, **1987**.

(9) Cheng, L.-T. *Organic Molecules for Nonlinear Optics and Photonics*; Springer: Berlin, **1991**.

(10) Di Bella, S. *Chem. Soc. Rev.* **2001**, *30*, 355.

(11) Hann, R. A., Bloor, D., Eds. *Organic Materials for Nonlinear Optics*; Royal Society of Chemistry: London, **1989**.

(12) Hann, R. A., Bloor, D., Eds. *Organic Materials for Nonlinear Optics II*; Royal Society of Chemistry: London, **1991**.

(13) Heeger, A. J., Orenstein, J., Ulrich, D., Eds. *Nonlinear Optical Properties of Polymers*; Materials Research Society: Pittsburgh, **1988**.

(14) Kobayashi, T., Ed. *Nonlinear Optics of Organics and Semiconductors*; Springer-Verlag: Berlin, **1989**.

(15) Long, N. J. *Angew. Chem., Int. Ed. Engl.* **1995**, *34*, 21.

(16) Lyons, M., Ed. *Materials for Nonlinear and Electro-optics*; Institute of Physics: Bristol, **1989**.

(17) Marder, S. R., Sohn, J. E., Stucky, G. D., Eds. *Materials for Nonlinear Optics: Chemical Perspectives*; American Chemical Society: Washington, **1991**.

(18) Marder, S. R., Beratan, D. N., Tiemann, B. G., Cheng, L.-T., Tam, W. *Organic Materials for Nonlinear Optics II*; Royal Society of Chemistry: London, **1991**.

(19) Marder, S. R. (Bruce, D. W., O'Hare, D., Eds.), *Inorganic Materials*; John Wiley: Chichester, **1992**.

(20) Messier, J., Kajzar, F., Prasad, P., Ulrich, D., Eds. *Nonlinear Optical Effects in Organic Polymers*; Kluwer Academic Publishers: Dordrecht, **1989**.

(21) Messier, J., Kajzar, F., Prasad, P., Eds. *Organic Molecules for Nonlinear Optics and Photonics*; Springer-Verlag: Berlin, **1991**.

(22) Nie, W. *Adv. Mater.* **1993**, *5*, 520.

(23) Prasad, P. N., Williams, D. J. *Introduction to Non-linear Optical Effects in Molecules and Polymers*; Wiley-Interscience: New York, **1991**.

(24) Sheik-Bahae, M.; Said, A. A.; Wei, T. H.; Hagan, D. J.; Van Stryland, E. W. *IEEE J. Quantum Electron.* **1990**, *26*, 760.

(25) Sutherland, R. L. *Handbook of Nonlinear Optics*; Marcel Dekker: New York, **1996**.

(26) Verbiest, T., Houbrechts, S., Kauranen, M., Clays, K. Persoons, A. J. *Journal of Materials Chemistry* **1997**, *7*, 2175.

(27) Williams, D. J., Ed. *Nonlinear Optical Properties of Organic and Polymeric Materials*; American Chemical Society: Washington, DC, **1983**.

(28) Zyss, J., Chemla, D. S. *Nonlinear Optical Properties of Organic Molecules and Crystals I*; Academic Press: Orlando, **1987**.

(29) Whittall, I. R., McDonagh, A. M., Humphrey, M. G., Samoc, M. *Adv. Organomet. Chem.* **1999**, *43*, 349.

(30) Coe, B. J. *Chem. Eur. J.l* **1999**, *5*, 2464.

(31) Humphrey M. G., C., M. P., Samoc, M. *Top. Organomet. Chem.* **2010**, *28*, 57.

(32) Eaton, D. F. *Science* **1991**, *253*, 281.

(33) Kuzyk, M. G. *J. Mater. Chem.* **2009**, *19*, 7444.

(34) McDonagh, A. M., Cifuentes, M. P., Whittall, I. R., Humphrey, M. G., Samoc, M.; Luther-Davies, B., Hockless, D. C. R. *J. Organomet. Chem.* **1996**, *526*, 99.

(35) Cyvin, S. J,; Rauch, J. E., Decius, J. C. *J. Chem. Phys.* **1965**, *43*, 4083.

(36) Cifuentes, M. P., Humphrey, M. G. *J. Organomet. Chem.* **2004**, *689*, 3968.

(37) Franken, P. A., Hill, A. E., Peters, C. W., Weinreich, G. *Phys. Rev. Lett.* **1961**, 7, 118.

(38) Goeppert-Mayer, M. *Ann. Phys.* **1931**, *9*, 273.

(39) Coulson, C. A., Maccoll, A., Sutton, L. E. *Trans. Faraday Soc.* **1952**, *48*.

(40) Clays, K., Persoons, A. *Rev. Sci. Instrum.* **1992**, *63*.

(41) Kaatz, P., Shelton, D. P. *J. Chem. Phys.* **1996**, *105*, 3918.

(42) Houbrechts, S., Clays, K., Persoons, A., Pikramenou, Z., Lehn, J.-M. *Chem. Phys. Lett.* **1996**, *258*, 485.

(43) Morrison, I. D., Denning, R. G., Laidlaw, W. M., Stammers, M. A. *Rev. Sci. Instrum.* **1995**, *64*, 1445.

(44) Vance, F. W.; Hupp, J. T. *J. Am. Chem. Soc.* **1999**, *121*, 4047.

(45) Verbiest, T., Clays, K., Persoons, A., Meyers, F., Brédas, J. L. *Opt. Lett.* **1993**, *18*, 525.

(46) Verbiest, T., Clays, K., Samyn, C., Wolff, J., Reinhoudt, D., Persoons, A. *J. Am. Chem. Soc.* **1994**, *116*, 9320.

(47) Heesink, G. J. T.; Ruiter, A. G. T.; van Hulst, N. F.; Bolger, B. *Phys. Rev. Lett.* **1993**, *71*, 999.

(48) Oudar, J. L., Chemla, D. S. *J. Chem. Phys.* **1977**, *66*, 2664.

(49) Dirk, C. W., Kuzyk, M. G. *Phys. Rev. B* **1990**, *41*, 1636.

(50) Dirk, C. W., Kuzyk, M. G. *Phys. Rev. A* **1989**, *39*, 1219.

(51) Isborn, C. M., Leclercq, A., Vila, F. D., Dalton, L. R., Bredas, J. L., Eichinger, B. E., Robinson, B. H. *J. Phys. Chem. A* **2007**, *111*, 1319.

(52) Kuzyk, M. G. *IEEE J. Quantum Electron.* **2001**, *7*, 774.

(53) Christodoulides, D. N., Khoo, I. C., Salamo, G. J., Stegeman, G. I., Van Stryland, E. W. *Adv. Opt. Photon.* **2010**, *2*, 60.

(54) Bruce, M. I., Hall, B. C., Kelly, B. D., Low, P. J., Skelton, B. W., White, A. H. *Dalton Trans.* **1999**, 3719.

(55) Calabrese, J. C., Cheng, L.-T., Green, J. C., Marder, S. R., Tam, W. *J. Am. Chem. Soc.* **1991**, *113*, 7227.

(56) Khairul, W. M., Porres, L., Albesa-Jove, D., Senn, M. S., Jones, M., Lydon, D. P., Howard, J. A. K., Beeby, A., Marder, T. B., Low, P. J. *J. Cluster Sci.* **2006**, *17*, 65-85.

(57) Naulty, R. H., Cifuentes, M. P., Humphrey, M. G., Houbrechts, S., Boutton, C., Persoons, A., Heath, G. A., Hockless, D. C. R., Luther-Davies, B., Samoc, M. *Dalton Trans.* **1997**, 4167.

(58) Whittall, I. R., Cifuentes, M. P., Humphrey, M. G., Luther-Davies, B., Samoc, M., Houbrechts, S., Persoons, A., Heath, G. A., Hockless, D. C. R. *J. Organomet. Chem.* **1997**, *549*, 127.

(59) Whittall, I. R., Humphrey, M. G., Houbrechts, S., Persoons, A., Hockless, D. C. R. *Organometallics* **1996**, *15*, 5738.

(60) Bruce, M. I., Ellis, B. G., Gaudio, M., Lapinte, C., Melino, G., Paul, F., Skelton, B. W., Smith, M. E., Toupet, L., White, A. H. *Dalton Trans.* **2004**, 1601.

(61) Marder, S. R., Beratan, D. N., Cheng, L.-T. *Science* **1991**, *252*, 103.

(62) Marder, S. R., Perry, J. W., Tiemann, B. G., Gorman, C. B., Gilmour, S., Biddle, S. L., Bourhill, G. *J. Am. Chem. Soc.* **1993**, *115*, 2524.

(63) Hurst, S. K., Australian National University, Canberra, **2001**.

(64) Cifuentes, M. P., Powell, C. E., Morrall, J. P., McDonagh, A. M., Lucas, N. T., Humphrey, M. G., Samoc, M., Houbrechts, S., Asselberghs, I., Clays, K., Persoons, A., Isoshima, T. *J. Am. Chem. Soc.* **2006**, *128*, 10819.

(65) Powell, C. E., Hurst, S. K., Morrall, J. P., Cifuentes, M. P., Roberts, R. L., Samoc, M., Humphrey, M. G. *Organometallics* **2007**, *26*, 4456.

(66) Tamm, M., Grzegorzewski, A., Steiner, T., Jentzsch, T., Werncke, W. *Organometallics* **1996**, *15*, 4984.

(67) Cheng, L. T., Tam, W., Meredith, G. R., Marder, S. R. *Mol. Cryst. Liq. Cryst.* **1990**, *189*, 137.

(68) Muller, T. J. J., Netz, A., Ansorge, M., Schmalzlin, E., Brauchle, C., Meerholz, K. *Organometallics* **1999**, *18*, 5066.

(69) Behrens, U., Brussaard, H., Haganau, U., Heck, J., Hendrickx, E., Kornich, J., van der Linden, J. G. M., Persoons, A., Spek, A. L., Veldman, N., Voss, B., Wong, H. *Chem. Eur. J.* **1996**, *2*, 98.

(70) Marder, S. R., Perry, J. W., Bourhill, G., Gorman, C. B., Tiemann, B. G., Mansour, K. *Science* **1993**, *261*, 186.

(71) Laidlaw, W. M., Denning, R. G., Verbiest, T., Cauchard, R., Persoons, A. *Proc. SPIE-Int. Soc. Opt. Eng.* **1994**, *14*, 2143.

(72) Dalton, G. T., Australian National University, Canberra, **2007**.

(73) Whittall, I. R., Australian National University, Canberra, **1997**.

(74) Powell, C. E., Australian National University, Canberra, **2004**.

(75) Dirk, C. W., Cheng, L.-T., Kuzyk, M. G. *Int. J. Quant. Chem.* **1992**, *43*, 27.

(76) Dirk, C. W., Caballerro, N., Kuzyk, M. G. *Chem. Mater.* **1993**, *5*, 733.

(77) Orr, B. J., Ward, J. F. *Mol. Phys.* **1971**, *20*, 513.

(78) Zyss, J., Ledoux, I. *Chem. Rev.* **1994**, *94*.

(79) Albota, M., Beljonne, D., Bredas, J.-L., Ehrlich, J. E., Fu, J.-Y., Heikal, A. A., Hess, S. E., Kogej, T., Levin, M. D., Marder, S. R., McCord-Maughon, D., Perry, J. W., Rockel, H., Rumi, M., Subramaniam, G., Webb, W. W., Wu, X.-L., Xu. C. *Science* **1998**, *281*, 1653.

(80) Myers, L. K., Langhoff, C., Thompson, M. E. *J. Am. Chem. Soc.* **1992**, *114*, 7560.

(81) Myers, L. K., Ho, D. M., Thompson, M. E., Langhoff, C. *Polyhedron* **1995**, *14*, 57.

(82) Powell, C. E., Cifuentes, M. P., McDonagh, A. M., Hurst, S. K., Lucas, N. T., Delfs, C. D., Stranger, R., Humphrey, M. G., Houbrechts, S., Asselberghs, I., Persoons, A., Hockless, D. C. R. *Inorg. Chim. Acta* **2003**, *352*, 9.

(83) Hurst, S. K., Humphrey, M. G., Morrall, J. P., Cifuentes, M. P., Samoc, M., Luther-Davies, B., Heath, G. A., Willis, A. C. *J. Organomet. Chem.* **2003**, *670*, 56.

(84) Touchard, D., Haquette, P., Guesmi, S., Le Pichon, L., Daridor, A., Toupet, L., Dixneuf, P. H. *Organometallics* **1997**, *16*, 3640.

(85) Cifuentes, M. P., Powell, C. E., Humphrey, M. G., Heath, G. A., Samoc, M., Luther-Davies, B. *J. Phys. Chem. A* **2001**, *105*, 9625.

(86) Hurst, S. K., Lucas, N. T., Humphrey, M. G., Isoshima, T., Wostyn, K., Asselberghs, I., Clays, K., Persoons, A., Samoc, M., Luther-Davies, B. *Inorg. Chim. Acta* **2003**, *350*, 62.

(87) Wortmann, R.; Glania, C., Kramer, P., Matschiner, R., Wolff, J. J., Kraft, S., Treptow, B., Barbu, E., Langle, D., Gorlitz, G. *Chem. Eur. J.* **1997**, *3*, 1765.

(88) McDonagh, A. M., Humphrey, M. G., Samoc, M., Luther-Davies, B. *Organometallics* **1999**, *18*, 5195.

(89) Hurst, S. K., Humphrey, M. G., Isoshima, T., Wostyn, K., Asselberghs, I., Clays, K., Persoons, A., Samoc, M., Luther-Davies, B. *Organometallics* **2002**, *21*, 2024.

(90) Chung, S.-J., Kim, K.-S., Lin, T.-C., He, G. S., Swiatkiewicz, J., Prasad, P. N. *J. Phys. Chem. B* **1999**, *103*, 10741.

(91) Kim, O. K., Lee, K. S., Woo, H. Y., Kim, K.-S., He, G. S., Swiatkiewicz, J., Prasad, P. N. *Chem. Mater.* **2000**, *12*, 284.

(92) Adronov, A., Freched, J. M., He, G. S., Kim, K.-S., Chung, S.-J., Swiatkiewicz, J., Prasad, P. N. *Chem. Mater.* **2000**, *12*, 2838.

(93) Prasad, P. N. *Nanophotonics*; John Wiley & Sons: Hoboken, **2004**.

(94) Ohshiro, N.; Takei, F.; Onitsuka, K.; Takahashi, S. *J. Organomet. Chem.* **1998**, *569*, 195.

(95) Onitsuka, K., Fujimoto, M., Kitajima, H., Ohshiro, N., Takei, F., Takahashi, S. *Chem. Eur. J.* **2004**, *10*, 6433.

(96) Whittall, I. R., Humphrey, M. G., Persoons, A., Houbrechts, S. *Organometallics* **1996**, *15*, 1935.

(97) Powell, C. E., Morrall, J. P., Ward, S. A., Cifuentes, M. P., Notaras, E. G. A., Samoc, M., Humphrey, M. G. *J. Am. Chem. Soc.* **2004**, *126*, 12234.

(98) Samoc, M., Australian National University, Canberra, **2006**.

(99) Blau, W., Byrne, W. M. D., Kelly, J. M. *Opt. Commun.* **1986**, *56*, 25.

(100) Samoc, M., Samoc, A., Luther-Davies, B., Humphrey, M. G. H., Wong, M. S. *Opt. Mater.* **2002**, *21*, 485.

(101) Choi, M. Y., Chan, C. W., Peng, S. M., Cheung, K. K., Che, C. M. *Chem. Commun.* **2000**, *14*, 1259.

(102) Kuhn, F. E., Zuo, J. L., de Biani, F. F., Santos, A. M., Zhang, Y., Zhao, J., Sandulache, A., Herdtweck, E. *New J. Chem.* **2004**, *28*, 43.

(103) Zuo, J. L., Herdtweck, E., Kuhn, F. E. *Dalton Trans.* **2002**, 1244.

(104) Ge, Q., Dalton, G. T., Humphrey, M. G., Samoc, M., Hor, T. S. A. *Chem. Asian J.* **2009**, *4*, 998.

(105) Powell, C. E., Humphrey, M. G., Cifuentes, M. P., Morrall, J. P., Samoc, M., Luther-Davies, B. *J Phys. Chem. A* **2003**, *107*, 11264.

(106) Samoc, M., Gauthier, N., Cifuentes, M. P., Paul, F., Lapinte, C., Humphrey, M. G. *Angew. Chem. Int. Ed.* **2006**, *45*, 7376.

(107) Zhang, C., Matsumoto, T., Samoc, M., Petrie, S., Meng, S., Corkery, T. C., Stranger, R., Zhang, J., Humphrey, M. G., Tatsumi, K. *Angew. Chem. Int. Ed.* **2010**, *49*, 4209.

(108) Babgi, B., Rigamonti, L., Cifuentes, M. P., Corkery, T. C., Randles, M. D., Schwich, T., Petrie, S., Stranger, R., Teshome, A., Asselberghs, I., Clays, K., Samoc. M., Humphrey, M. G. *J. Am. Chem. Soc.* **2009**, *131*, 10293.

(109) Jeffery, C. J., Cifuentes, M. P., Dalton, G. T., Corkery, T. C., Randles, M. D., Willis, A. C., Samoc, M., Humphrey, M. G. *Macromol. Rapid Commun.* **2010**, *31*, 846.

(110) McDonagh, A. M., Powell, C. E., Morrall, J. P., Cifuentes, M. P., Humphrey, M. G. *Organometallics* **2003**, *22*, 1402.

(111) Long, J. N., Martin, A. J., de Biani, F. F., Zanello, P. *Dalton Trans.* **1998**, 2017.

(112) Long, J. N., Martin, A. J., White, A. J. P., Williams, D. J., Fontani, M., Laschi, F., Zanello, P. *Dalton Trans.* **2000**, 3387.

(113) Onitsuka, K., Ohara, N., Takei, F., Takahashi, S. *Dalton Trans.* **2006**, 3693.

(114) Uno, M.; Dixneuf, P. H. *Angew. Chem. Int. Ed.* **1998**, *37*, 1714.

(115) Roberts, R. L., Schwich, T., Corkery, T. C., Cifuentes, M. P., Green, K. A., Farmer, J. D., Low, P. J., Marder, T. B., Samoc, M., Humphrey, M. G. *Adv. Mater.* **2009**, *21*, 2318.

(116) Green, K. A., Australian National University, Canberra, 2010.

(117) Ghazala, S., Paul, F., Toupet, L., Roisnel, T., Hapiot, P., Lapinte, C. *J. Am. Chem. Soc.* **2006**, *128*, 2463.

(118) Bruce, M. I., Humphrey, P. A., Jevric, M., Perkins, G. J., Skelton, B. W., White, A. H. *J. Organomet. Chem.* **2006**, *692*, 1748.

(119) Dalton, G. T., Cifuentes, M. P., Petrie, S., Stranger, R., Humphrey, M. G., Samoc, M. *J. Am. Chem. Soc.* **2007**, *129*, 11882.

(120) Gauthier, N., Argouarch, G., Paul, F., Ladjarafi, A. K., Costuas, K., Halet, J.-F., Samoc, M., Cifuentes, M. P., Corkery, T. C., Humphrey, M. G. *In Preparation* **2010**.

(121) Green, K. A., Cifuentes, M. P., Corkery, T. C., Samoc, M., Humphrey, M. G *Angew. Chem. Int. Ed.* **2009**, *48*, 7867.

(122) Gilat, S. L.; Kawai, S. H.; Lehn, J.-M. *Chem. Eur. J.* **1995**, *1*, 275.

(123) Balu, M., Hales, J., Hagan, D. J., van Stryland, E. W. *Opt. Express* **2004**, *12*, 3820.

(124) Balu, M., Hales, J., Hagan, D. J., van Stryland, E. W. *Opt. Express* **2005**, *13*, 3594.

(125) De Boni, L., Andrade, A., Misoguti, L, Mendonca, C., Zilio, S. *Opt. Express* **2004**, *12*, 3921.

(126) Milam, D. *Appl. Opt.* **1998**, *37*, 546.

(127) Naulty, R. H., McDonagh, A. M., Whittall, I. R., Cifuentes, M. P., Humphrey, M. G., Houbrechts, S., Maes, J., Persoons, A., Heath, G. A., Hockless, D. C. R. *J. Organomet. Chem.* **1998**, *563*, 137.

(128) Morrall, J. P. L., Cifuentes, M. P., Humphrey, M. G., Kellens, R., Robijns, E., Asselberghs, I., Clays, K., Persoons, A., Samoc, M., Willis, A. C. *Inorg. Chim. Acta* **2006**, *359*, 998.

(129) Chaudret, B., Commenges, G., Poilblanc, R. *Dalton Trans.* **1984**, 1635.

(130) Sonogashira, K., Tohda, Y., Hagihara, N. *Tetrahedron Lett.* **1975**, *16*, 4467.

(131) Siemsen, P., Livingston, R. C., Deiderich, F. *Angew. Chem. Int. Ed.* **2000**, *39*, 2632.

(132) Watson, L. A., Australian National University, Canberra, **2006**.

(133) Elangovan, A., Wang, Y.-H., Ho, T.-I. *Org. Lett.* **2003**, *5*, 1841.

(134) Liu, Q., Burton, D. J. *Tetrahedron Lett.* **1997**, *38*, 4371.

(135) Touchard, D., Haquette, P., Pirio, N., Toupet, L., Dixneuf, P. H. *Organometallics* **1993**, *12*, 3132.

(136) Hawker, C. J., Fréchet, J. M. J. *J. Am. Chem. Soc.* **1990**, *112*, 7638.

(137) Newkome, G. R., Yao, Z. Q., Baker, G. R., Gupta, V. K. *J. Org. Chem.* **1985**, *50*, 2003.

(138) Newkome, G. R., Moorefield, C. N., Vogtle, F. *Dendrimers and Dendrons: Concepts, Synthesis, Applications*; Wiley-VCH: New York, **2001**.

(139) Takahashi, S., Kuroyama, Y., Sonogashira, K., Hagihara, N. *Synthesis* **1980**, 627.

(140) Bardamova, M. I., Trotsenko, Z. P., Kotlyarevskii, I. L. *Izv. Akad. Nauk SSSR* **1982**, *5*, 1184.

(141) Dimroth, K., Neubauer, G. *Chem. Ber.* **1959**, *92*, 2042.

(142) Lavastre, O., Olivier, L., Dixneuf, P. H., Sibhandit, S. *Tetrahedron* **1996**, *52*, 5495.

(143) Gibtner, T., Hampel, F., Gisselbrecht, J.-P., Hirsch, A. *Chem. Eur. J.* **2002**, *68*, 408.

(144) Rodriguez, J. G., Tejedor, J. L., La Parra, T., Diaz, C. *Tetrahedron* **2006**, *62*, 3355.

(145) Chavan, S. S., Australian National University, Canberra, **2008**.

(146) MacBride, J. A. H., Wade, K. *Synth. Commun.* **1996**, *26*, 2309.

(147) Kamada, K., Antonov, L., Yamada, S., Ohta, K., Yoshimura, T., Tahara, K., Inaba, A., Sonoda, M., Tobe, Y. *Chem. Phys. Lett.* **2007**, *8*, 2671.

(148) Kondo, K., Yasuda, S., Sakaguchi, T., Miya, M. *Chem. Commun.* **1995**, 55.

(149) Piao, M. J., Chajara, K., Yoon, S. J., Kim, H. M., Jeon, S.-J., Kim, T.-H., Song, K., Asselberghs, I., Persoons, A., Clays, K., Cho, B. R. *J. Mater. Chem.* **2006**, *16*, 2273.

(150) Yamaguchi, Y., Matsubara, Y., Ochi, T., Wakamiya, T., Yoshida, Z.-I. *J. Am. Chem. Soc.* **2008**, *130*, 13867.

(151) Wan, W. B., Haley, M. M. *J. Org. Chem.* **2001**, *66*, 3893.

(152) Huang, C.-C., Lin, Y.-C., Lin, P.-Y., Chen, Y.-J. *Eur. J. Org. Chem* **2006**, 4510.

(153) Kayser, B., Altman, J., Noth, H., Knizek, J., Beck, W. *Eur. J. Inorg. Chem* **1998**, 1791.

(154) Diallo, A. K.; Daran, J.-C.; Varret, F.; Ruiz, J.; Astruc, D. *Angew. Chem. Int. Ed.* **2009**, *48*, 3141.

(155) Nierle, J., Barth, D., Kuck, D. *Eur. J. Org. Chem* **2004**, 867.

(156) Diercks, R., Armstrong, J. C., Boese, R., Vollhardt, K. P. C. *Angew. Chem. Int. Ed.* **1986**, *25*, 268.

(157) Boese, R., Matzger, A. J., Mohler, D. L., Vollhardt, K. P. C. *Angew. Chem. Int. Ed.* **1995**, *34*, 1478.

(158) Sonoda, M., Inaba, A., Itahashi, K., Tobe, Y. *Org. Lett.* **2001**, *3*, 2419.

(159) Ito, S., Inabe, H., Morita, N., Ohta, K., Kitamura, T., Imafuku, K. *J. Am. Chem. Soc.* **2003**, *125*, 1669.

(160) Anthony, J. E., Khan, S. I., Rubin, Y. *Tetrahedron Lett.* **1997**, *38*, 3499.

(161) Tolman, C. A. *Chem. Rev.* **1977**, *77*, 313.

(162) Bruce, M. I., C. Hameister, Swincer, A. G., Wallis, R. C. (Fackler, J. P., Jr., Ed.), *Inorganic Syntheses*; John Wiley & Sons, **1982**; Vol. XXI.

(163) Bruce, M. I., Wong, F. S., Skelton, B. W., White, A. H. *Dalton Trans.* **1981**, 1398.

(164) Francke, V., Mangel, T., Mullen, K. *Macromolecules* **1998**, *31*, 2447.

(165) Wilson, J. N., Josowicz, M., Wang, Y., Bunz, U. H. F. *Chem. Commun.* **2003**, 2962.

(166) Yu, B. Z., Li, M. K., Lu, M., Li, H. L. *Appl. Phys. A.* **2003**, *76*, 593.

(167) Maruyama, S., Kawanishi, Y. J. *J. Mater. Chem.* **2002**, *14*, 2245.

(168) Dalton, G. T., Rigamonti, L., Babgi, B., Australian National University, Canberra, **2007**.

(169) Cifuentes, M. P., Australian National University, Canberra, **2010**.